

Architectural and Engineering Study of Thin Concrete Membrane Shells

Review of past practices to revive shells into new, innovative, sustainable, and resilient architectural engineering forms

Master-Thesis

A thesis submitted in partial fulfillment
of the requirements for the degree of

Master of Membrane Structures

Submitted to:

Anhalt University of Applied Sciences

Faculty of Architecture,
Facility Management and Geo Information

By:

Pedro R. Munoz

February 7, 1958 – Born in Cartagena, Colombia, South America and currently living in Methuen, MA, USA

Matrikel Number: 4055829

Submission date: February 17, 2018

First Tutor: Prof. Dr.-Ing Robert Off

Second Tutor: Dr.-Ing Switbert Greiner



Statement of Originality:

I, Pedro R. Munoz, hereby declare that I am the sole author of this thesis and the work presented in this Master thesis, entitled:

“Architectural and Engineering Study of Thin Concrete Membrane Shells“

Is entirely of my own creation and that I did not use any sources or auxiliary means other than those referenced and cited in this thesis work. The Author has collected and selected some relevant graphics material and photos presented in the chapters of this thesis which have been reproduced from information widely available in the web-internet and that has been used for illustrative purposes to clarify the subject topic being discussed in this thesis. Citations and references where appropriate are listed in the text of the thesis and in the References section at the end of the thesis.

I herein authorize Anhalt University and the Institute of Membranes and Shell Technologies, IMS to make this thesis available to other institutions, individuals, and researchers for the purposes of scholarly research studies and further advanced studies in the subject of this thesis or any other similarly related topics.

I herein further authorize Anhalt University and the Institute of Membranes and Shell Technologies, IMS to make this thesis available for digital scanning, photocopying, or any other means of digital or mechanical reproductions in total or in part to other institutions, individuals, and researchers for the purposes of scholarly research studies in the subject of this thesis or any other similarly related topics.

Methuen, MA, USA, February 17, 2018

Pedro R. Munoz, Ph.D., P.E.
prmz@att.net



Copyrights © 2018 by Pedro R. Munoz, Ph.D., P.E., All Rights Reserved

The original and copies of this Master Thesis or any parts thereof are copyrighted by Pedro R. Munoz, Anhalt University, and IMS
Reproduction in any form of this Thesis document or any parts thereof is strictly prohibited except by written permission of Anhalt University



TABLE OF CONTENTS

	PAGE		PAGE
ABSTRACT	i		
ACKNOWLEDGMENTS	ii		
PREFACE	iii		
LIST OF FIGURES	iv		
CHAPTER	PAGE		
1 INTRODUCTION	1		
1.1 Natural Forms of Shells	2		
1.2 Ancient man-made Forms of Shells	3		
1.3 Basic Geometrical Conical Shapes	5		
1.4 Types of Thin Shell Structures	6		
1.5 Gaussian Curvature of Shells	9		
1.6 Basic types of Shell Surfaces	11		
2 LITERATURE REVIEW			
2.1 German and Swiss School	18		
2.2 North-American School	20		
2.3 Italian School	22		
2.4 Spanish School	23		
2.5 Latin-American School	25		
3 BASIC ARCHITECTURAL AND ENGINEERING CONCEPTS OF MEMBRANE SHELLS	29		
3.1 Architectural Form, Function, and Forces	30		
3.2 Hyperbolic Paraboloids, Hypar Forms	33		
3.3 Engineering Analysis and Design of Membrane Shells	45		
		3.4 Graphic Statics Analysis for Membrane Shells	58
		3.5 Architectural and Engineering Shell Projects	67
		3.6 Hypar Parabolic Surface Generation using straight lines	83
		3.7 Heinz Isler and Felix Candela Shells	87
		4 FABRIC FORMED MEMBRANE SHELLS, EXPERIMENTAL AND RESEARCH WORK	97
		4.1 Overview of fabric formed concrete shells past work	97
		4.2 Membrane-Concrete Shell Prototype Research Project at IMS	111
		4.3 Prototype Dimensions, Materials, Testing, and Construction	112
		5 FINITE ELEMENT ANALYSIS OF IMS SHELL USING Ix-CUBE 4-10 SOFTWARE	138
		5.1 Finite Element Analysis Methodology	139
		5.2 Non-Linear Analysis of IMS Shell Prototype.	143
		5.3 Finite Element Analysis of IMS Shell Prototype.	151
		6 CONCLUSIONS	191
		7 REFERENCES	194
		8 APPENDICES	203
		APPENDIX A – Notation	203
		APPENDIX B – AutoCAD Lisp and Rhino Python Scripts	206
		APPENDIX C – Drawings of Membrane-Concrete Prototype	208
		APPENDIX D – Datasheets of Materials for IMS Prototype	210
		APPENDIX E – Units Conversion Table	217



The development and construction of thin concrete shell structures dates back to the early 1920's when modern architecture looked for new curvilinear type of free forms of long span, thin, and economical ways to build roof structures that would cover large assembly places, sports arenas, public markets, music halls, and some other similar outdoor and indoor spaces where large number of people could gather under a solid and sound roof structure.

At that time reinforced concrete construction was at its early stages of development and building such thin reinforced concrete shell structures required the use of very sophisticated, complicated, and intricate system of formwork that had to follow the non-traditional curvilinear shape of the newly designed structural form of shells. The mathematical formulations to solve the forces, stresses, and deformations of such slender type of reinforced concrete shell structures were very difficult to solve manually and computers as we have them today did not exist at that time, therefore it was extremely difficult for engineers and designers to arrive to a reliable mathematical solution that could accurately predict the actual behavior of the concrete shells under construction loads and service loading conditions of selfweight of materials, wind, snow, and earthquake environmental effects.

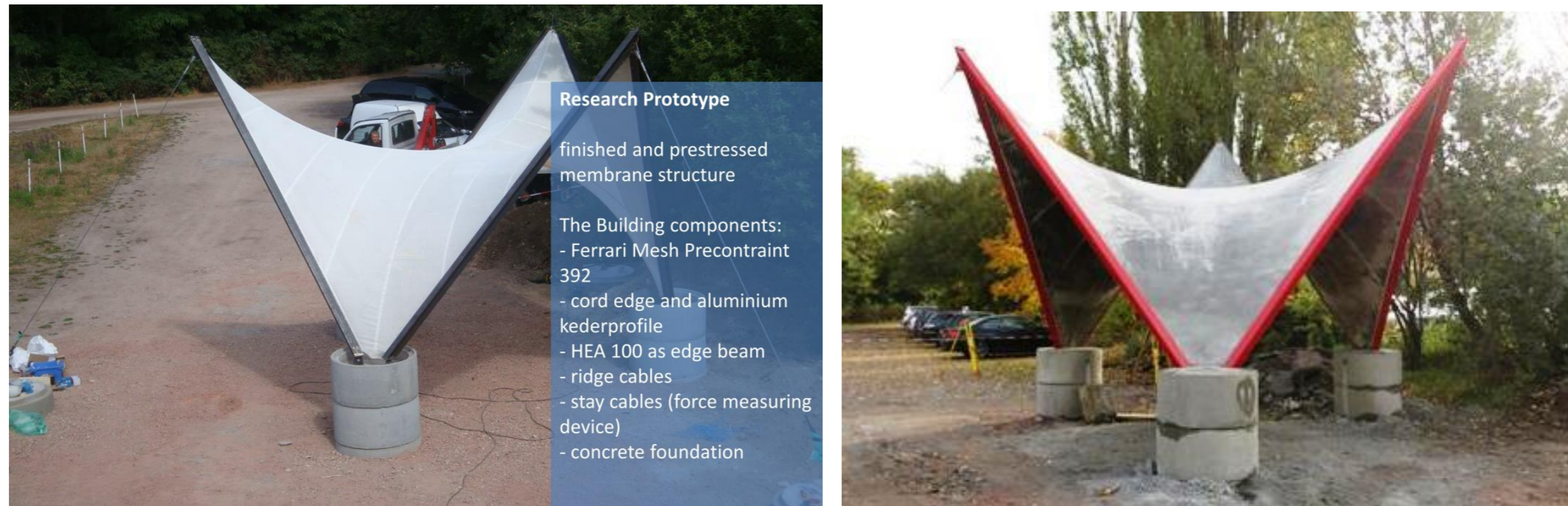
Engineers and builders of those early times of development of concrete shells implemented their own reduced scale models and tested them with some type of proportional loads to the actual size of the structures to be built and developed their own empirical results to extrapolate the expected approximate internal forces, stresses, and deformations on the actual size of the shell structure and check its behavior under service loading conditions. An elaborate system of wooden formwork was used to create the curvilinear form of the reinforced concrete shells. Other builders created their own methods of using the natural ground to create shapes of certain curvilinear forms to then cast the concrete over the ground and then at a later time remove the ground from underneath to achieve the desired shape of the concrete shell structure.

Inflatable forms and other type of tensioned fabric formwork have also been used by builders, architects, and engineers to achieve some type of spherical, cylindrical, and flexible fabric formwork to build walls, beams, columns, precast members, curtain wall façade components, and other type of reinforced concrete shells. The subject of this thesis work is to document some of the past work on reinforced concrete shells, their basic analysis, and in particular to study the use of tensioned fabric as the main formwork to construct a reinforced concrete shell and perform a finite element analysis to validate the results of an experimental prototype.



ACKNOWLEDGMENTS

The Author wishes to express his gratitude and appreciation to Prof. Dr.-Ing. Robert Off, Director of the IMS-Institute of Membrane and Shell Technologies for suggesting the topic of this thesis and for making available the documentation of analysis, building materials, and information of the experimental testing and construction of the prototype of a tensioned fabric-formed reinforced concrete canopy shell structure to the Author for review, study, modeling, and analysis using the IxCube 4-10 and Staad-Pro software. Pictures of the as-built fabric-formed thin concrete shell are shown below.



Prototype of a Fabric-Formed Thin Concrete Shell Canopy structure built at the Bernburg Campus of Anhalt University, Germany, 2013

The Author also appreciates immensely the assistnace of Mr. Henning Dürr for providing the technical information, and input data for the diffrent type of materails that were used to build the prototype thin concrete shell. Special Thanks are due to Gerry D'Anza for permitting the use of the IxCube 4-10 software during the course of the Master studies program and during the modeling and verification of the prototype tensioned membrane shell structure. The Author also appreciates Dr.-Ing Switbert Greiner for the review of the thesis and his valuable comments and feedback.

KEYWORDS: Tensioned Membranes, Thin concrete shells, Flexible Formwork, Fabric-Formed Concrete, Hypars, Form Finding, IxCube 4-10, IMS, Finite Element Analysis, Shotcrete, Photogrammetry, Concrete Testing.



PREFACE

The subject of my Master's Thesis entitled: "Architectural and Engineering Study of Thin Concrete Membrane Shells" is focused on the review of past theoretical and construction work performed on practical applications and implementations of reinforced concrete shells to create architectural and engineering structures for several different type of projects. This study is intended to explore the possibilities to revive the incorporation of thin reinforced concrete shells into main stream building construction practices that will ultimately result into new and innovative sustainable and resilient forms which will be more energy efficient, structurally optimized for strength and stiffness, and that will be much easier to build and maintain than prior similar concrete shell forms.

The topic of this thesis was suggested by Prof. Dr.-Ing. Robert Off, Director of the Institute of Membrane and Shell Technologies (IMS) of the Anhalt University of Applied Sciences as part of an extended investigation of a recently built research project of realization of a tensioned membrane form into a rigid concrete shell. The main focus of this thesis will consist in performing a 3D finite element analysis of the prototype model of the tensioned membrane and the hardened concrete shell that was built using tensioned membrane and shotcrete to achieve the desired thickness of the final shell structure. The FEA study will investigate the distribution of principal stresses that will develop over the entire surface of the hardened membrane shell under the selfweight of the concrete shell and the applicable environmental wind and snow loads and the load combinations of selfweight, initial membrane prestress, wind, snow loads, and some concentrated forces at specific points on the shell surface. In addition to investigating the distribution of shell stresses, this thesis will also include the observations of the displacements of the concrete shell structure at the points of connection of the corners of the membrane shell to the tie-down cables to the ground.

I am very thankful to Dr.-Ing. Robert Off and Dr.-Ing. Switbert Greiner members of my thesis review panel for their guidance and feedback on my thesis work herein presented. Special thanks also to Mr. Henning Dürr of IMS for allowing access to the information of the original research project materials, data, and results of the prototype built at Bernburg Campus of Anhalt University. I would like to thank from the bottom of my heart to my wife Paula Andrea who has being very supportive of my efforts and time studying at IMS and during the time spent on writing my thesis at home.

Pedro R. Munoz, Ph.D., P.E., Methuen, MA, USA, February 17 of 2018



LIST OF FIGURES

- Figure 1.1** - Different forms of Natural Shells: Egg, Skull, Oyster/Mussel, Turtle, Marine Shell, and Amazonian Rose.
- Figure 1.2** - Different forms of Man-made Shells: Dwellings, Tombs, Temples, Caps, and Domes.
- Figure 1.3** – Ruins of ancient building structure having a parabolic type of arched form in the ancient Mesopotamian city of Ctesiphon in Iraq.
- Figure 1.4** – Geometric representation and mathematical formulations of basic conical shapes.
- Figure 1.5** - Four typical shapes of thin shell surface forms: cylindrical, spherical, hyperbolic-paraboloid, and combined free form.
- Figure 1.6** - Different types of shell surfaces with single and double curvature, vaulted, anticlastic, and synclastic shape.
- Figure 1.7** – Basic types of Shell Surfaces based upon their Gaussian Curvature.
- Figure 1.8** – Surfaces of Revolution: Cylindrical, Conical, Spherical, Parabolic, Hyperboloid, and Toroidal.
- Figure 1.9** – Typical Ruled Surfaces, Hyperbolic Paraboloids, Hyperboloids, and Conoids.
- Figure 1.10** – Mathematical expression and typical samples of Hyperbolic Paraboloid Hypar Surfaces.
- Figure 1.11** – Samples of Hyperbolic Paraboloid (Hypar) Roof Projects in Bali, Indonesia, and Poland.
- Figure 1.12** – Physical Models of Hyperboloids and different types of as-built Hyperboloid structures around the world.
- Figure 1.13** – Typical Conoidal Ruled Surface - Experimental Conoidal Roof in San Bartolo, Mexico, by Felix Candela, 1950.
- Figure 1.14** – Church of Christ the Worker, Floor Plan and Exterior Conoidal Reinforced Brickwork, by Eladio Dieste, Atlantida, 1960.
- Figure 1.15** – Church of Christ the Worker Conoidal Brickwork Walls – Conoidal Brick Roof of Gaudi’s School of Sagrada Familia in Spain
- Figure 2.1** – Franz Dischinger and some of his shell structures in Germany.
- Figure 2.2** – Ulrich Finsterwalder and some of his shell structures in Germany.
- Figure 2.3** – Heinz Isler and some of his experimental and built shell structures in Switzerland.
- Figure 2.4** – Anton Tedesko and some of his shell structures in the USA.
- Figure 2.5** – John V. Christiansen and his Kingdome and World’s Fair shell structures in Seattle, WA, USA.
- Figure 2.6** – Eero Saarinen and his TWA Flight Center at JFK Airport in NY and St. Louis Arch in St. Louis, MO.
- Figure 2.7** – Pier Luigi Nervi and some of his work on shell structures in Italy and Europe.
- Figure 2.8** – Eduardo Torroja, Spanish Engineer and his work on reinforced concrete shells.



- Figure 2.9** – Felix Candela and some of his hyperbolic paraboloid shell structures in Mexico and Spain.
- Figure 2.10** – Santiago Calatrava and his outstanding shell structures in Spain and the USA.
- Figure 2.11** – Eladio Dieste and his reinforced brick and shell structures in Uruguay, South America.
- Figure 2.12** – Hilario Candela and his thin reinforced concrete shell structures in Miami, Florida, USA.
- Figure 2.13** – Oscar Niemeyer and his outstanding and elegant curvilinear shell structures in Brazil.
- Figure 2.14** – Max Borges and few of his shell structures in Cuba.
- Figure 2.15** – Eduardo Catalano and his hyperbolic paraboloid shell structure and metal shell sculpture.
- Figure 3.1** - Form, Forces, and Function of Architectural Engineering Structures, Topology Optimization.
- Figure 3.2** – Hyperbolic Paraboloid geometrical representation and mathematical equation in x-y-z coordinate system.
- Figure 3.3** – Single Saddle Vault - Isometric, Picture of sample structure, Plan, Section and Aerial View.
- Figure 3.4** – Groined Vaults - Isometric, Picture of sample structure, Plan, Section and Aerial View.
- Figure 3.5** - Groined Vaults of three intersected Hypars – Plan, Picture of sample structure, Section and Aerial View.
- Figure 3.6** – Multiple polar array of Groined Vaults - Isometric, Picture of sample structure, Plan, Section, and Aerial View.
- Figure 3.7** – Free Standing Inverted Umbrellas - Isometric, Picture of sample structure, Plan, Section, and Aerial View.
- Figure 3.8** – Conoid - Isometric, Picture of sample structure, Plan, Section, and Aerial View.
- Figure 3.9** – Intersecting Gabled Roof Shells - Isometric, Picture of sample structure, Plan, Section, and Aerial View.
- Figure 3.10** – Double Hypar Cantilever - Isometric, Picture of sample structure, Plan, Section, and Aerial View.
- Figure 3.11** – Hyperboloids - Isometric, Picture of sample structure, Plan, Elevations, and Aerial View.
- Figure 3.12** – Generalized curvilinear shell element with internal stress resultants, radius of curvature, and middle surface definitions.
- Figure 3.13** – Basic diagrams of Membrane Shell structure, Radius of Curvature, and Shell external loads and internal forces.
- Figure 3.14** – Anticlastic Saddle type of Shells with double curvatures of opposite signs.
- Figure 3.15** – Synclastic Spherical type of Shells with radius of curvature of same sign and different types of supports.
- Figure 3.16** – Deformations and Buckling Shapes of Arched and Semispherical Shells under external uniform and concentrated loads.
- Figure 3.17** – Geometrical and Mathematical representations of Circle, Parabola, and Catenary curves.



- Figure 3.18** – Suspended Cable Curve of span L , with uniform load w , and simply supported at both ends.
- Figure 3.19** – Graphic Statics Method for a simply supported 2D Parabolic Arch of span L and uniform load w .
- Figure 3.20** – 2D and 3D planar and curvilinear surfaces modeled using the Truss Analogy Method with Struts and Ties.
- Figure 3.21** - Eero Saarinen & Associates, Architects – Ammann & Whitney – 1955; Cambridge, MA – USA; $R = 112$ ft., $t = 3.5''$ – $R/t = 384$.
- Figure 3.22** - Frank Lloyd Wright, Architect – 1956; Milwaukee, WI – USA ; $R = 197$ ft., $t = 3.5''$ – $R/t = 675$.
- Figure 3.23** - Loofburrow Architects; J. Christiansen Engineers – 1990; Yakima, WA – USA; $R = 248$ ft., $t = 3.75''$ – $R/t = 794$.
- Figure 3.24** – Cylindrical Vaulted Shells – Support Conditions and Distribution of internal forces and stresses.
- Figure 3.25** - Louis I. Kahn, Architect; A. Komendant, Structural Engineer – 1972; Fort Worth, TX – USA.
- Figure 3.26** – Felix Candela, Engineer, Architect, and Builder - Conoid Concrete Shell Structures in the 1950's, Mexico.
- Figure 3.27** – Typical Hyperbolic Paraboloid Thin Concrete Shell Roof Structure and Hypar Diagram with straight perimeter edges.
- Figure 3.28** – St. Athanasius Church Hyperbolic Paraboloid Roof Aerial View, Rendering, and Interior view of hypar concrete roof.
- Figure 3.29** – St. Athanasius Church Hyperbolic Paraboloid Roof – Exterior Elevation Views of hypar concrete roof.
- Figure 3.30** – St. Athanasius Church Hyperbolic Paraboloid Roof – Exterior Front and Side Elevation Views of hypar concrete roof.
- Figure 3.31** – Los Manantiales Restaurant and L'Oceanografic Groined Vaulted Roof Shells of F. Candela and S. Calatrava.
- Figure 3.32** – Hyperbolic Paraboloid Roof Shells in the form of Inverted Umbrellas and Intersected Tied Gable Roof Shells.
- Figure 3.33** – Inverted Umbrellas, Warm Mineral Springs Inn Motel, by V. Lundy. Architect & D. Sawyer, Engineer, North Port, FL 1958.
- Figure 3.34** - Zarzuela Hippodrome, by E. Torroja, Architect & Engineer, Madrid, Spain, 1935 – Cantilevered Inverted Hypar Umbrella Shell.
- Figure 3.35** - Hyperboloid Shell of McDonnell Planetarium, by HOK Architects & A. Alper Structural. Engineer, St. Louis, MO, USA, 1963.
- Figure 3.36** – Cantilevered Shells for the TWA Terminal at JFK Airport, by E. Saarinen, Architect, Ammann & Whitney, Engineer, NY 1962.
- Figure 3.37** – Los Manantiales Restaurant in Xochimilco Mexico by Felix Candela, 1958, Plan, Elevations, and Isometrics Models.
- Figure 3.38** – Generation of Hyperbolic Paraboloid (Hypar) Shell Surfaces within three parabolic curves, by Felix Candela.
- Figure 3.39** - Hyperbolic Paraboloid (Hypar) formed by two sets of intersecting straight lines bounded by three parabolic curves, by F. Candela.
- Figure 3.40** – Los Manantiales Restaurant of F. Candela modeled using AutoCAD, Plan and Isometric of solid surface and wireframe model.
- Figure 3.41** – Heinz Isler and Felix Candela type of thin reinforced concrete shells analogy to horizontal and vertical eggs.



- Figure 3.42** – Heinz Isler and some of his constructed thin reinforced concrete shells in Switzerland, Europe.
- Figure 3.43** – Heinz Isler models of shells based upon hardened hanging clothes and inverted shells.
- Figure 3.44** – Heinz Isler thin reinforced concrete shell projects designed and built in Switzerland and Europe.
- Figure 3.45** – Heinz Isler thin reinforced concrete shell projects in Switzerland and Europe, Aerial Views, Elevations and Formwork.
- Figure 3.46** – Felix Candela and Frei Otto, Los Manantiales Restaurant shell in Mexico and the Botanical Garden shell in Norway.
- Figure 3.47** – Felix Candela shell project: Los Manantiales Restaurant built in Mexico and Model built at Princeton University in USA.
- Figure 3.48** – Felix Candela thin reinforced concrete inverted umbrella shell project built in Mexico, Formwork and Elevation View.
- Figure 4.1** – Fabric Formed Beams, by Mark West.
- Figure 4.2** - Pneumatically formed concrete shell, Patented by W. Neff, 1941.
- Figure 4.3** - The TailorCrete Project, “Demonstrator“, Danish Technological Institute (DTI), Design Concept and Completed Sculpture.
- Figure 4.4** - The TailorCrete Project, “Demonstrator“, Danish Technological Institute (DTI), Steel Rebars and Robotic Generated Formwork
- Figure 4.5** - The “Stealth“, Architectural Decorative Sculpture in Atlanta, Georgia, USA., Rebars, Formwork, and completed Sculpture.
- Figure 4.6** - Curvilinear Wave, Hyperbolic and Gaussian Shell Fabric-Formed Concrete experimental prototypes, University of Edinburgh.
- Figure 4.7** – Textile Fibre Reinforced Concrete – “TFRC”, Sample of textile fabric reinforcement, and Bending of Textile Reinforced Plate.
- Figure 4.8** – Thin Shell Composite Hyperbolic Paraboloid Roof, TSC Hypar, built by TSC Global LLC Company for African Nations.
- Figure 4.9** – Geographical location of research project at Anhalt University of Applied Sciences Bernburg Campus in Germany.
- Figure 4.10** – IMS Membrane-Concrete prototype research project location at Bernburg Campus of Anhalt University.
- Figure 4.11** – Conceptual Dimensioned Plan, Elevation, Isometric, and Aerial View of the IMS Membrane-Concrete Prototype Structure.
- Figure 4.12** – Plan View of Membrane-Concrete Prototype Structure with labeled components and experimental testing of Concrete.
- Figure 4.13** – Digital Model of Membrane-Concrete Prototype Structure with Von Mises Stresses, Members, Cables, and Reaction Forces.
- Figure 4.14** – Constructed Tensioned Membrane, Steel Frame, Cables Concrete Bases, Concrete Shell, Anchors, and Footings of Prototype.
- Figure 4.15** – Plots of obtained final concrete shell thickness from 3D scan photogrammetric survey and Deflection of lower shell surface.
- Figure 4.16** – Plots of obtained final concrete shell thickness from 3D scan photogrammetric survey and Deflection of lower shell surface.



- Figure 4.17** – Constructed Tensioned Membrane-Concrete Shell, Steel Frame and Cable Connection Details to Steel Frame.
- Figure 4.18** - Constructed Tensioned Membrane-Concrete Shell, Steel Frame and Tie-down Cable Connection Details to Concrete Bases.
- Figure 4.19** – Plot of variation of tie-down cable forces during the application of shotcrete on the membrane surface.
- Figure 4.20** – Pictures of completed membrane-concrete shell prototype after hardening of shotcrete and finished shell surface.
- Figure 4.21** – Pictures of 1st large scale load tests on the top surface of the membrane-concrete shell prototype.
- Figure 4.22** – Tabulated axial tensile forces recorded at tie-down cables for the four loading increments on the membrane-concrete shell prototype.
- Figure 4.23** – Pictures of 2nd and 3rd large scale load tests on the top surface of the membrane-concrete shell prototype.
- Figure 4.24** – Pictures of 3rd load test of concentrated load and detail to hung weights from the membrane-concrete shell prototype.
- Figure 4.25** – Tabulated axial tensile forces recorded at tie-down cables for the 2nd and 3rd load tests on the membrane-concrete shell prototype.
- Figure 4.26** – Plot of tabulated axial tensile forces recorded at tie-down cables for the 2nd and 3rd load tests on the membrane-concrete shell prototype.
- Figure 4.27** – Laser Scan plots and Nurbs lines of the shell prototype surface to determine the deflection of the shell under loads.
- Figure 4.28** – Laser Scan plots of the shell prototype for loading cases M_4, M_5, and M_6 to determine deflection of the shell surface.
- Figure 4.29** – Laser Scan plots and Nurbs surface lines of the shell prototype surface to determine the deflection for M_4, M_5, and M_6.
- Figure 4.30** – Laser Scan plots in Plan and Elevation of the shell prototype for loading case M_5, Unusual deflections of surface and cables.
- Figure 4.31** – Laser Scan plots and Nurbs surface lines of the shell prototype to determine the deflection from Concentrated Load for M_7.
- Figure 4.32** – Membrane-Concrete Specimen Samples, Geometry for testing, Testing Machine setup. and Specimen after bending test.
- Figure 4.33** – Tabulated bending stress values from 3-point laboratory flexural testing with detailed tabulated stress calculations.
- Figure 5.1** – Conceptual 3D Model of the IMS Membrane-Concrete Shell Prototype – Plan and Isometric Views.
- Figure 5.2** – IMS Membrane-Concrete Shell Conceptual Model and Installed Membrane, Frame, Cables, and Concrete Bases.
- Figure 5.3** – Pictures of the completed IMS Membrane-Concrete Shell Prototype with the entire shotcrete shell surface installed.
- Figure 5.4** – IMS Membrane-Concrete Shell Prototype modeled using Ix-Cube 4-10 software for membrane form-finding and stress analysis.
- Figure 5.5** – IMS Membrane-Concrete Shell Prototype conceptual 3D Model Plan, Elevations, and Isometric using Rhino software.
- Figure 5.6** – Step 1 – Geometrical 3D Model Plan and Isometric of IMS Membrane-Concrete Shell Prototype using Rhino software.



Figure 5.7 – Step 2 – Geometrical 3D Model components of IMS prototype imported from Rhino into IxCube 4-10 software.

Figure 5.8 – Step 3 – Form-finding of the membrane structure with the three high points fixed and the membrane clamped to the steel edge beams.

Figure 5.9 – Step 3 – Form-finding of the membrane structure with the three high points free and the membrane clamped to the steel edge beams.

Figure 5.10 – Step 3 – Axial Forces and Reactions at Support points from the Form-finding Analysis of the tensioned membrane structure.

Figure 5.11 – Step 4 – 3D Model of the Membrane-Concrete Shell Structure with Beams, Cables, and Supports inside IxCube 4-10.

Figure 5.12 – Step 5 – 3D Prototype structure Selfweight Load condition and Membrane Concrete Shell structural components.

Figure 5.13 – Step 5 – 3D Prototype structure with Snow Load condition and Isometric View of the 3D model.

Figure 5.14 – Step 5 – 3D Prototype structure with Wind Loading Condition along X and Y Axis, Cp values for different shell surface regions.

Figure 5.15 – Step 5 – 3D Prototype structure with Wind Loading Condition along V and Z Axis, Cp values for different shell surface regions.

Figure 5.16 – Step 5 – 3D Prototype structure with Seismic Loading Condition along X and Y Axis, Cs values for shell surface regions.

Figure 5.17 – Step 5 – 3D Prototype structure with Seismic Loading Condition along V and Z Axis, Cs values for shell surface regions.

Figure 5.18 – Step 5 – 3D Prototype structure with Selfweight Loading Condition and Evenly Distributed Surface Loads on Shell structure.

Figure 5.19 – Step 5 – 3D Prototype structure with Unsymmetrical Distributed and Concentrated Point Load on Surface of the Shell structure.

Figure 5.20 – Membrane-Concrete Shell Prototype – Summary of Results from Finite Element Analysis – $t = 50$ mm. – High Points Tied Down.

Figure 5.21 – Membrane-Concrete Shell Prototype – Summary of Results from Finite Element Analysis – $t = 10$ mm. – High Points Tied Down.

Figure 5.22 – Membrane-Concrete Shell Prototype – Summary of Results from Finite Element Analysis – $t = 50$ mm. – No Tie Down Cables.

Figure 5.23 – Membrane-Concrete Shell Prototype – Summary of Results from Finite Element Analysis – $t = 10$ mm. – No Tie Down Cables.

Figure 5.24 – Finite Element Analysis Graphical Results for Testing Load P2 – Load Case Combination #3 – $t = 50$ mm. – Tie Down Cables.

Figure 5.25 – Finite Element Analysis Graphical Results for Testing Load P3 – Load Case Combination #4 – $t = 50$ mm. – Tie Down Cables.

Figure 5.26 – Finite Element Analysis Graphical Results for Seismic Load EQY – Load Case Combination #11 – $t = 50$ mm. – Tie Down Cables.

Figure 5.27 – Finite Element Analysis Graphical Results for Snow+1/2 Wind Load V–Load Case Combination #16 – $t = 50$ mm. – Tie Down Cables.

Figure 5.28 – Finite Element Analysis Graphical Results for 1/2Snow+ Wind Load V–Load Case Combination #20 – $t = 50$ mm. – Tie Down Cables.

Figure 5.29 – Finite Element Analysis Graphical Results for Snow+ 1/2 Seismic EQY–Load Case Combination #23 – $t = 50$ mm.–Tie Down Cables.

Figure 5.30 – Finite Element Analysis Graphical Results for 1/2 Snow+ Seismic EQY–Load Case Combination #27 – $t = 50$ mm.–Tie Down Cables.



- Figure 5.31** – Typical Stress-Strain Curves of Normal Weight Concrete samples under Axial Compressive Test, No Steel Fibers.
- Figure 5.32** – Typical Stress-Strain Curves of Steel Fiber Reinforced Concrete samples under Axial Compressive Test.
- Figure 5.33** – Typical 3-Point set-up of Flexural Testing of Concrete samples with Geometrical Design and Strength Parameters.
- Figure 5.34** – Tabulated empirical relationships between Flexural Strength and Compressive Strength of plain concrete by Country Building Codes.
- Figure 5.35** – Experimental 3-Point set-up of Flexural Testing of Concrete samples of IMS Membrane-Concrete Shell Prototype.
- Figure 5.36** – Calculations to check the design and capacity of steel edge beams for axial loads, bending moments, and shear forces.
- Figure 5.37** – Tabulated Safe Loads and Minimum Breaking Strength of Steel Wire Rope Cables – 6 strand x 19 wire (6x19).
- Figure 5.38** – View of completed Membrane-Concrete Shell Structure, edge beams, cables, and concrete bases right after completed construction.
- Figure C.1** – Plan Layout of Concrete Footings, Elevations, Base Plates with Anchor Bolts, Rebar Details and Cables.
- Figure C.2** - General Arrangement, Base Plates, Membrane, Steel Edge Members, and Steel Connection Details.



The study of thin concrete membrane shells can be traced back and framed into two of their predecessor's types of shells that can be found in nature and to those man-made types of shell forms used in ancient times. In this chapter we will review the basic concepts that set up the foundations for the existence of these natural and man-made forms of shells and will correlate the geometrical parameters and concepts that differentiate the types of shells. Every type of shell form can be classified in one group or another depending on the geometrical form, layout in plan and elevations, radius of curvature, thickness and shell dimensions among others, therefore it is very important to have a clear and basic understanding on the different types of curvilinear surfaces that creates one or another type of shell form.

A shell in general terms is a three-dimensional arch-vaulted shaped surface structure which can support and transmit forces and stresses to its supports mainly by compression, tension, and shear actions in single and double curvature of the structure. Very efficient shells have their shape in the form of funicular curves where the resulting forces act either in direct compression or tension along the center line of the shell. Thin shells are defined as those curvilinear surfaces which have their thickness (say in the z-axis) of small dimension compared to their other two dimensions in space (say in the x-axis and the y-axis), either in the Cartesian coordinate system (x-y-z axis) or the polar coordinate system (r- θ -z axis).

This study includes the basic concepts of architectural and engineering aspects of thin concrete shells which we could call archineering of shells. Archineering could be defined as the art and science of integrating architecture and engineering to produce buildings and structural designs that will be buildable, economical, integrated, safe, sustainable, resilient, adaptable, comfortable, and code compliant.

This architectural-engineering study of shells is intended mainly to bring special attention and revive the interest of architects, engineers, designers, developers, and project owners on the subject of practical and relevant applications of thin shell concrete roof structures that could provide efficient, light weight, elegant, strong, durable, resilient, and functionally integrated solutions of concrete shells with other traditional and newly developed roof covering materials that will go well and integrate efficiently with the natural environment.

Thin concrete shells could be designed as continuous solidly built 3D structures or they could also be designed in a 3D grid shell form that will allow the reduction of the total selfweight of the overall shell structure. The void spaces left in a 3D grid shell can be filled with ETFE bubbles or pillows that have very small selfweight and could also be combined with struts and cables in the grid of the shell to improve the compressive and tensile properties of the combined 3D grid shell of heavy weight thin concrete and light weight ETFE films, or PTFE-PVC membranes, just to mention some of the multiple options of combinations that could bring about a light weight and thin composite shell structure.



1.1 - NATURAL FORMS OF SHELLS

The different natural forms of shells shown in Figure 1.1 all have some type of curved surfaces and appear to be of solid form, but in reality they are not totally solid but rather they are composed of some type of cellular or tubular substructures which provides the exterior appearance of the shell natural form. If looked in the microscope one could notice that the internal substructure of the natural shell forms is in reality formed of honey-comb substructures. In summary the structure and substructure of the natural forms of shells are composed of curvilinear surfaces and due to their ratio of thickness to shape dimensions can be cataloged as thin shells.

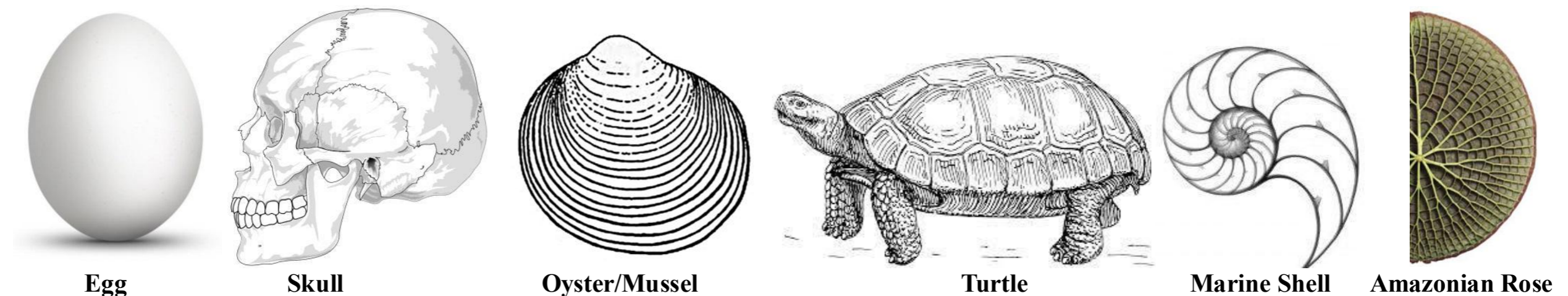


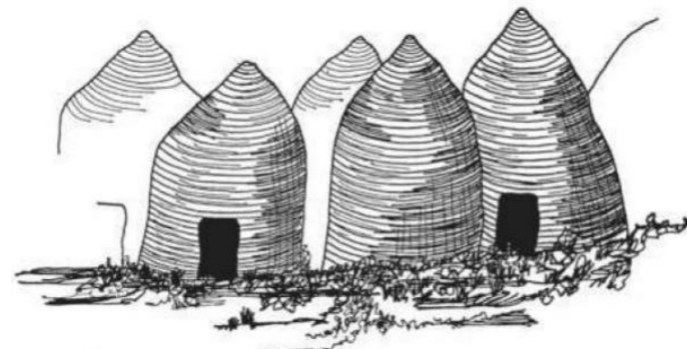
Figure 1.1 - Different forms of Natural Shells: Egg, Skull, Oyster/Mussel, Turtle, Marine Shell, and Amazonian Rose.

It is important to observe very carefully the shape, curvature, ratio of thickness to radius of curvature, composition, and organization of the different parts of natural forms shown in Figure 1.1 so that we can learn from them how these forms perform their intended function in complete conformance with the natural forces that they will be subjected to in the environment and be able to survive or last for the period of time that nature have them to serve their intended purpose in mother earth. It is like applying Bionics to Shell Structures.

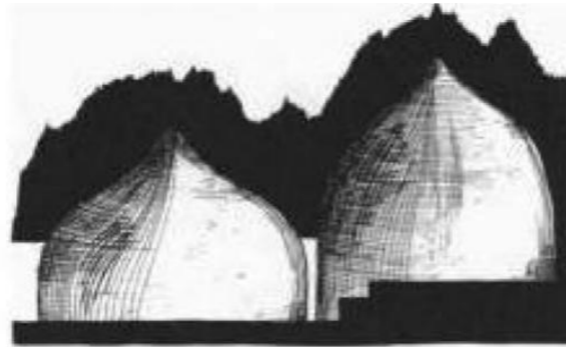
In principle our ancestors looked at natural forms and learned from them how they behaved and survived for short and long periods of time, how fragile and how strong they were, how the configuration of their external shape served a specific function and how they could adapt them to their daily life for certain uses that will help mankind to have shelter, protection, and storage uses among others.



1.2 - ANCIENT MAN-MADE FORMS OF SHELLS



A Qubab Dwelling in a Syrian Village



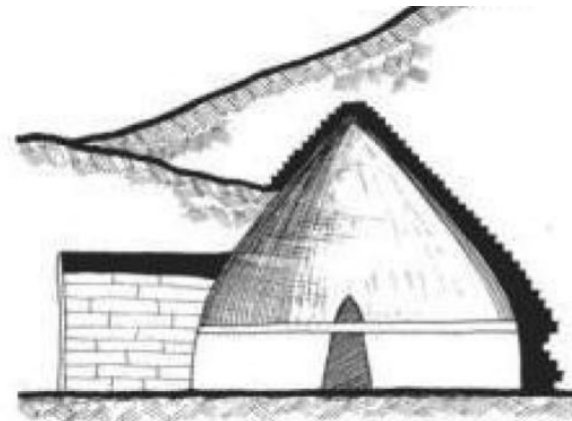
A rock-cut Tomb with a pointed shape; Sicily, Italy



A Building form in a Syrian Temple



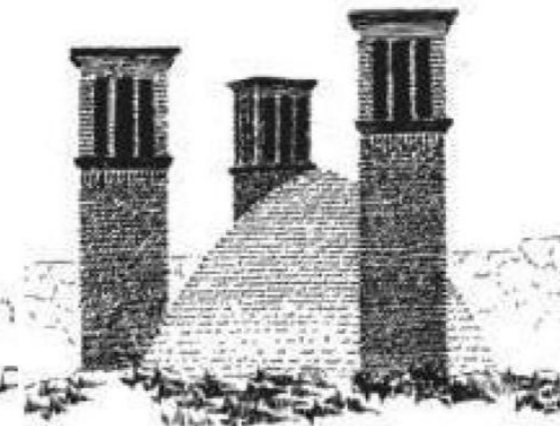
A Domical Pointed Roman Cap



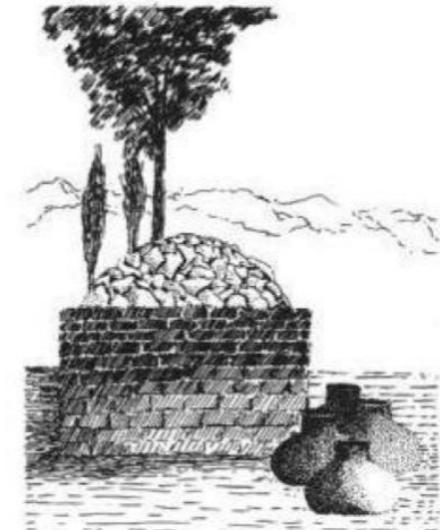
**The Tomb of Agamemnon
Corbeled Mediterranean Dome**



A Sun-dried Dome used as an Ice house in Kerman, Iran



A masonry dome to cover Cisterns of water storage, Iran



Masonry rubble Dome covers kiln in Mexico

Figure 1.2 - Different forms of Man-made forms of shells: Dwellings, Tombs, Temples, Caps, and Domes



Like in ancient times man used pieces of dried skin of animals and trunks of trees and branches to create shelters for nomadic tribes, also at that same time in several different parts of the world man discovered and recognized the conical and arched type of forms that could be created with natural stones and other rigid natural materials to achieve closed spaces for different uses ranging from shelters, temples, storage, protection, and other utilitarian uses for the nomadic and permanent communities, villages, and whole portions of civilization.

It is interesting to notice that man carved portions of caverns and rocks based upon the same principles of achieving some type of conical, cylindrical, semispherical domes, and other types of combined geometrical surfaces and forms of different thicknesses that would allow to support the total weight of natural materials and stored goods as well.

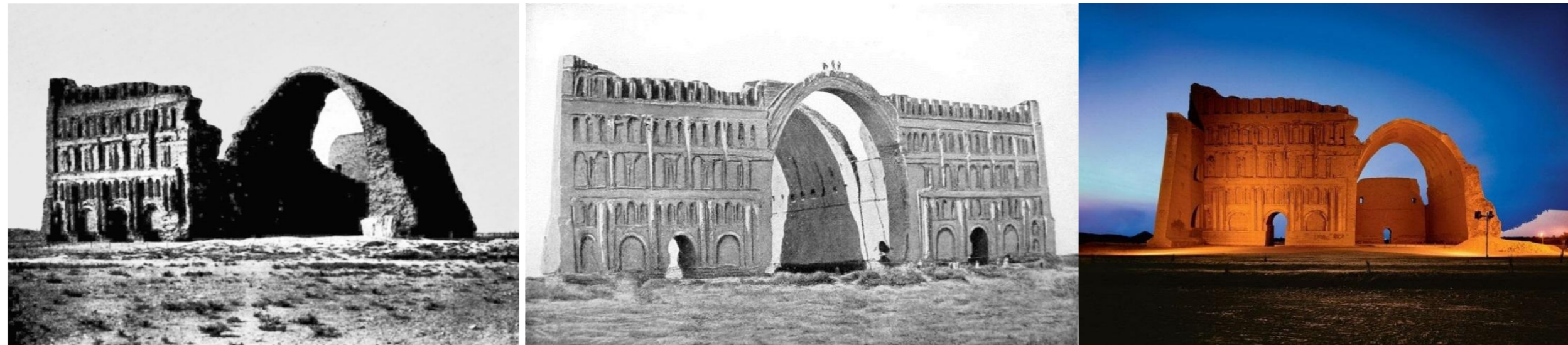


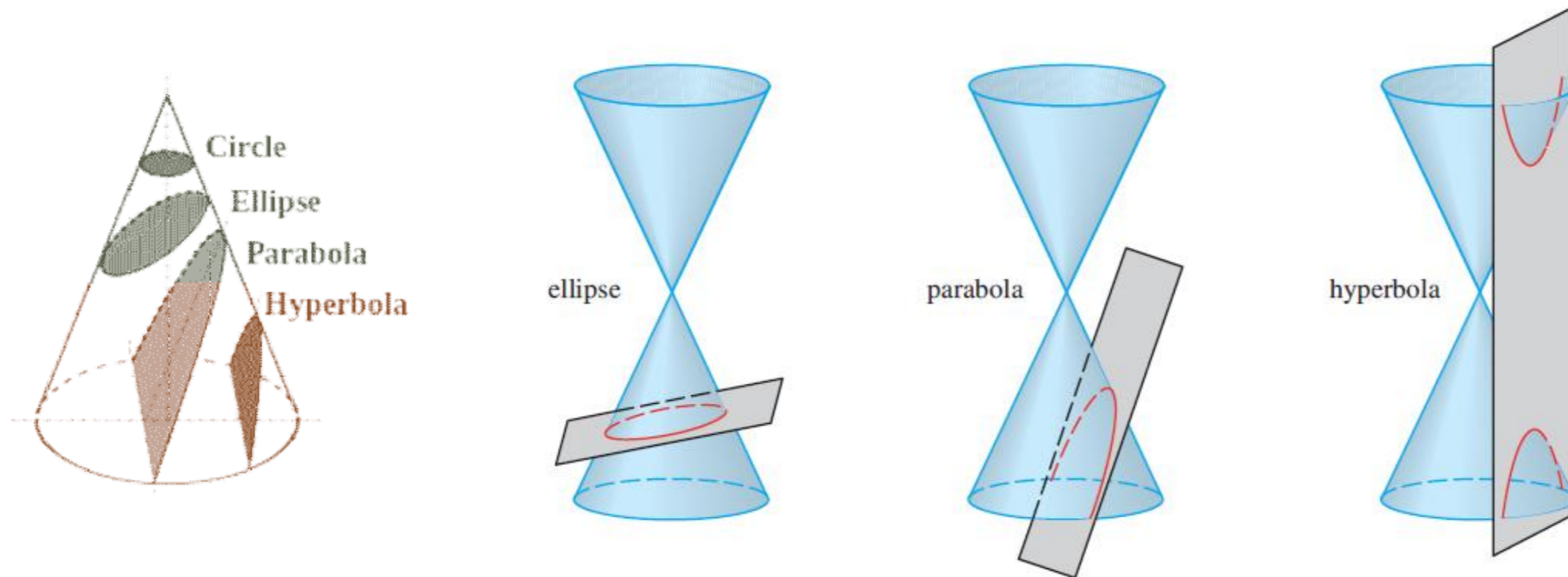
Figure 1.3 – Ruins of ancient building structure having a parabolic type of arched form in the ancient Mesopotamian city of Ctesiphon in Iraq.

As communities grew in size and the number of people increased considerably the need for larger gathering places was required to accommodate the living and meeting necessities of the people. The use of the parabolic shape of arched type of stones created dramatic and grandiose spaces which are evidenced in ruins of ancient temples and buildings. The parabolic curve creates some type of funicular shape where the resultant of the gravity forces from the selfweight of the materials that form the arch and the weights supported by the arch are such that they travel downward following a trajectory that creates mostly compression along the center line of the cross section of the arch structure. Naturally a well-built parabolic or catenary structure appears to be one of the more efficient structural forms to carry loads from top to bottom across a given span.



1.3 - BASIC GEOMETRICAL CONICAL SHAPES

GEOMETRICAL FIGURES



$$x^2 + y^2 = r^2$$

Circle

$$\frac{x^2}{a^2} + \frac{y^2}{b^2} = 1$$

Ellipse

$$y^2 = 4px$$

Parabola

$$\frac{x^2}{a^2} - \frac{y^2}{b^2} = 1$$

Hyperbola

Figure 1.4 - Geometric representation and mathematical formulations of basic conical shapes.

The figures and mathematical formulas shown in Figure 1.4 clearly display the different types of geometrical shapes that can be obtained out of the basic solid conical object. By taking a solid geometric cone and slicing a horizontal plane, an inclined plane intersecting the sides, an inclined plane intersecting the side and the base, and a vertical plane intersecting the side and the base we obtain the basic geometrical shapes of a circle, an ellipse, a parabola, and a hyperbola as shown in Figure 1.4 above.



1.4 - TYPES OF THIN SHELL STRUCTURES

There are four basic types of thin shell structures most commonly found in architectural and engineering projects for a wide variety of buildings and civil engineering applications. They include cylindrical and spherical surfaces with single or double curvature in a synclastic shape having curvature of same sign, the saddle shape surfaces with double curvature with radius of curvature of opposite sign leading to an anticlastic shape typically found in hyperbolic paraboloid (hypars) surfaces, and the free-form combined surfaces that could include both types of synclastic and anticlastic surfaces in the same structural shape. The latest are the most complicated shell surfaces which requires very sophisticated methods of analysis and well defined support conditions to be able to maintain stability for strength, stiffness, global and local buckling.

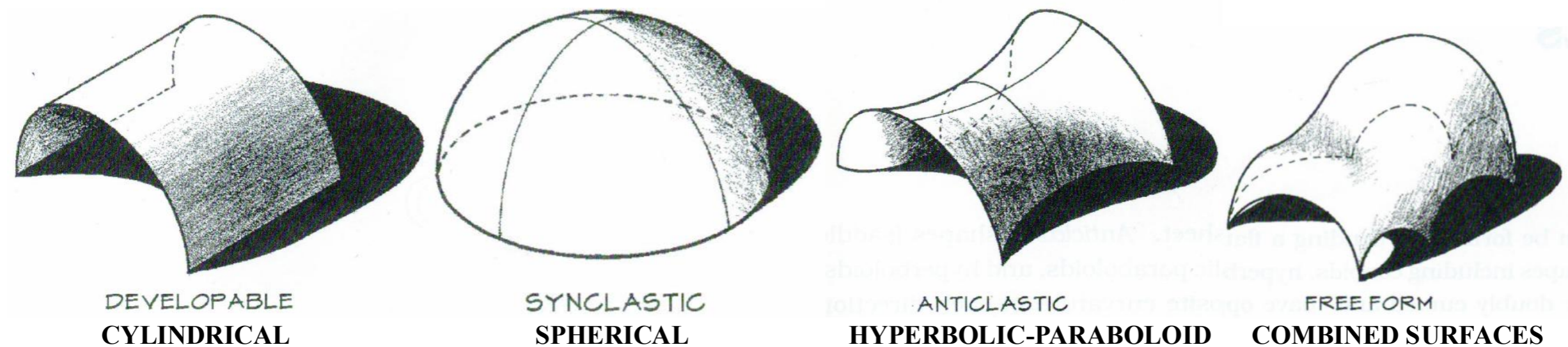


Figure 1.5 - Four typical shapes of thin shell surface forms: cylindrical, spherical, hyperbolic-paraboloid, and combined free form.

Each one of the four typical forms of shell surfaces will have specific and unique values of radius of curvature (r) in either one or two directions and thickness (t) of the shell which will define the ratio of radius of curvature to thickness (r/t) that will influence greatly the overall behavior of displacements, shell bending, axial, shear, and torsional stresses that will develop in the cross section of the shell.

The type of shell under evaluation shall be accurately represented by the shape of the shell, loading, material properties, boundary, and support conditions for analysis and design. It is very important that the shell designer models the shell structure with its loading and support conditions as close as possible to the final as-built conditions to make sure that the shell behavior will closely represent the analysis and final as-built conditions.



By definition in the textbooks of Strength of Materials, a “THIN-WALL VESSEL OR SHELL” refers to a vessel or shell having an inner-radius-to-wall-thickness ratio of 10 or more ($r/t \geq 10$). It has been found from specific analysis that for those vessels and shells having values of $r/t=10$ the results of the thin-wall analysis will predict stresses that are approximately 4% less than the actual maximum stress in the vessel or shell. For those cases where values of r/t are much larger than 10 then this error will be even smaller.

In general when a vessel or shell wall is thin ($r/t > 10$), then the stress distribution throughout its thickness will not have significant variations across the thickness of the member and therefore it can be practically assumed that the stress distribution is uniform or constant across the thickness. Since the thickness of the member is thin or small compared to the other dimensions of the member then it is important to understand that the bending stiffness of the thin member is very small for any external effects in the planes perpendicular to the thickness of the shell. Therefore thin shells have very low or insignificant bending stiffness for out-of-plane loading effects on the shell.

For the purposes of this Thesis study we will be referring mainly to thin shell members. Thin-wall vessels are commonly used for cylindrical and spherical vessels in the industry to serve as boilers or tanks under internal or external pressures. The values of “ r/t ” ratios of 10 given in the strength of materials textbooks will be used mainly as a reference values to have an idea of the proportions of the shell members for distribution of internal axial, compressive, and shear stresses. Torsional and Bending stiffness is very small for thin shell members and can be in principle considered negligible and be ignored for the purposes of their contribution to bending and torsional stiffness.

In reality as-built concrete or timber shells display ratios of radius of curvature to thickness way above the $r/t=10$ noted above, and is not uncommon to see shell members with $r/t > 800$ or 1,000. For every case of shell members it is always recommended that architects and engineers perform a detailed analysis and stress checks to make sure that all the allowable stresses are always below the safe values recommended for tension, compression, shear, and most importantly that the stability check of the thin shell member assures that the shell member will not buckle in global or local modes or any other of the unstable buckling modes due to high slenderness ratios. Commonly designed reinforced concrete shells are in the range of approximately $r/t = 500$.

Membrane shells in simple form can be defined as a thin curved membrane member, plate, or shell surface that resist external forces mainly by its capacity of axial compressive, tensile, and shear stresses, for given values of their corresponding: r = radius of curvature and t = thickness of the member, plate, or shell. Bending in thin membrane shells is mostly avoided at all sections of the member, plate or shell, to be able to minimize and optimize the thickness and weight of the final shell.



Efficient shell forms are those that can effectively transfer the exterior applied loads and selfweight of the concrete shell itself fully in compression or tension along a funicular shape of the shell, where tensile stresses develop within the shell thickness then appropriate amount of steel reinforcement or prestressing steel may be necessary to maintain tensile stresses and strains controlled by the steel reinforcement within the shell thickness, always maintaining a shell shape that will be without excessive bending stresses, which will allow to have a true membrane shell.

Commonly used engineering materials for thin shell members and thin folded plates include but are not limited to conventional wood, timber, plywood, cross laminated timber, latticed plywood, reinforced concrete, cold formed steel and aluminum grid-shells, timber, aluminum, and steel tubular grid shells, and any combinations of the above to form stiff, strong, and stable shells and grid-shells curvilinear surfaces. Thin Concrete Shells present many advantages in the construction of long span roofs due to its competitive costs of materials, reusing of forms for repetitive modular forms, the use of concrete alone as a roof structure presents inherent fireproofing properties and no need for costly waterproofing finishes, only basic waterproofing coatings that can be reapplied every so many years are necessary to maintain the roof structure watertight.

Concrete Shells of very small thicknesses can be achieved for relatively long span structures, for example a 3” thick reinforced concrete shell can cover a roof area of approximately 160 ft. x 40 ft. The minimization of form through the effective design of the curvilinear shape of the concrete shells can be achieved by taking advantage of the contribution of the compressive and tensile strength of the shells due to its radius of curvature. One can say that the Strut-and-Tie model of reinforced concrete structures of the ACI 318 can effectively be applied to the efficient design of thin reinforced concrete grid shells.

A new type of thin reinforced concrete grid shells that can be modeled as a grid or network of struts (compressive portions of concrete) and ties (tensile sections of shell reinforced with rebars or cables) are herein labeled to be part of a new long span structural concrete shell system to be labeled for the first time as: “TENSHELLGRIDITY”. **Tenshellgridity** is herein defined as: “The Art and Science of creating a thin shell concrete structure composed of a grid of reinforced concrete members that intersect each other and follow the surface of a shell structure, acting either as compression strut members or tension tie members (strut-and-tie) forming a synclastic or anticlastic curvilinear surface”.

In principle most of reinforced concrete shell structures built up to date are commonly seen as continuous concrete surfaces of solid thin concrete or as combination of solid concrete shell surface bounded by reinforced concrete ribs or beams. The type of reinforced concrete grid shell described above would allow the optimization of the concrete shell surface by creating holes in the concrete shell which will be bounded by grids of members which will either be in tension or compression (strut-and-tie model), allowing a considerable reduction of the overall weight of the structure.



1.5 - GAUSSIAN CURVATURE OF SHELLS

Shells can take multiple forms and can be built based upon their own geometrical characteristics. Following is a list of just a number of practical shell forms that can be used in the building construction industry: a.) Shell Straight or Curved Walls, b.) Domes, c.) Circular Cylindrical Shells, d.) Translational Shells along curved paths, e.) Shells of Double Synclastic or Anticlastic Curvature, f.) Folded Curvilinear or Plate Shells, g.) Free form curvilinear surfaces having a combination of synclastic and anticlastic sections within the same shell structure.

Shell Designers frequently decide to use one or another type of shell surface, whichever they consider is more suitable for the project design requirements or due to their own personal preference based upon the type of shell they feel more comfortable designing and building. The selection of the type of shell to be designed and build has ramifications on the type of supporting structures and foundations that will carry the total weight of the shell onto the ground. Figure 1.6 below display the basic types of shell surfaces which either have a synclastic or anticlastic shape.

The radius of curvature and the thickness of the final constructed shells are the main parameters that will dictate the overall behavior of the shell under loads and that will determine the level of internal axial, bending, and shear stresses that will develop internally within the shell thickness. Some bending stresses will eventually develop also internally in the shells depending on the level of out-of-plane loads and the conditions of fixity at the points of supports and around the boundary connections of the body of the shell with adjacent structures and supports.

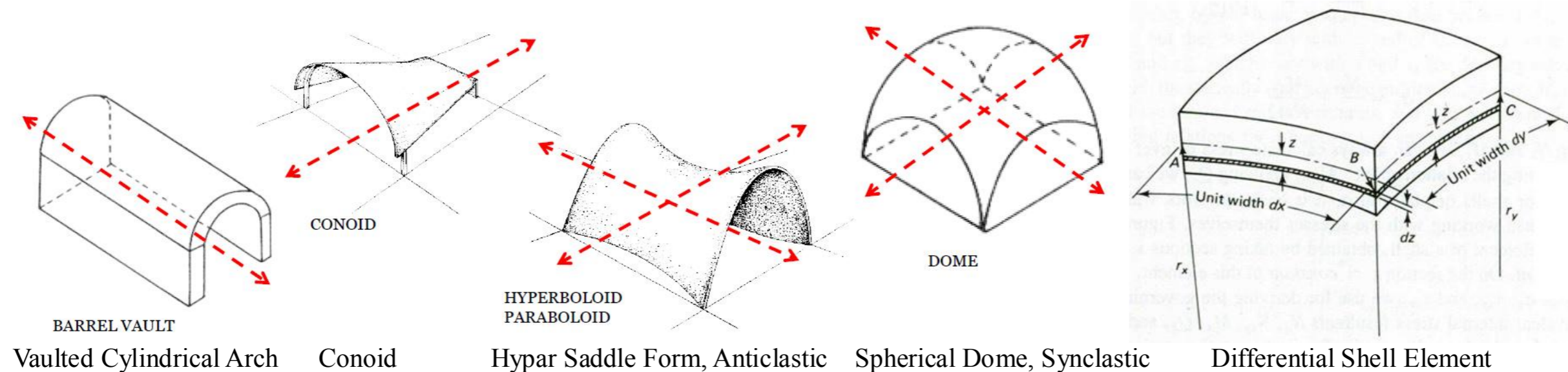


Figure 1.6 - Different types of shell surfaces with single and double curvature, vaulted, anticlastic, and synclastic shape.



Shells that have curvilinear surfaces have their own radius of curvature. Figure 1.6 above shows different configurations of shells having single and double curvature. A small differential element of the shell surface can be taken for any of the types of shells shown in Figure 1.6 and from there the radius of curvature in the x and y directions given as r_x and r_y can be determined. Depending on the orientation of the shell surface, either concave or convex with respect to an x-y plane of the surface we can then identify the sign of the curvature as concave (+) and convex (-) and we then say that for a shell having curvature of the same sign or in the same orientation with respect to the x-y plane the type of shell has a synclastic shape like a dome and on the opposite side for a shell having curvatures of opposite sign or with opposite orientation of the curvatures then the shell has an anticlastic shape like a hyperbolic paraboloid (hypar). The curvature of the shells is directly related to the flow of stresses over its surface.

If we call: $r_x = R_1$ and $r_y = R_2$; then we can find at any point on the surface of the shell the product of the two principal radius of curvature of the shell with their signs which is known as the **Gaussian Curvature, G** . The value of G can be zero, positive, or negative. The expression for the Gaussian curvature is shown in the equation below.

$$G = \left(\frac{1}{R_1} \times \frac{1}{R_2} \right)$$

The shell surface is considered to be a developable surface when the Gaussian curvature is zero as is shown for a Barrel Vault or Conoids of Figure 1.6. In these two cases a straight line can be developed along the path of either a single circular track to generate a cylindrical surface or along one or two curvilinear tracks to generate some type of vaulted conoid.

For a shell having positive Gaussian curvature (G is +) then we say that the shell has a synclastic surface like a dome and if the shell has a negative Gaussian curvature (G is -) then we say that the shell has an anticlastic surface like a hypar.

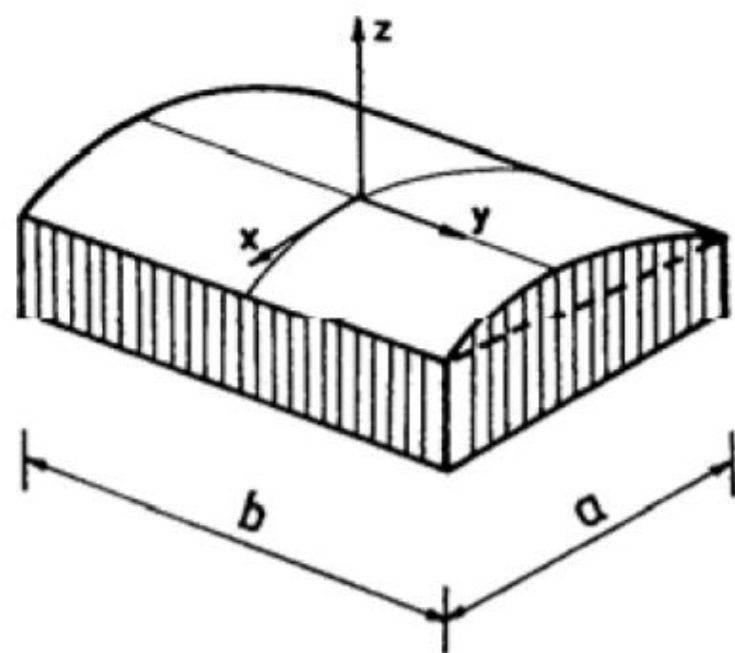
For the two cases of anticlastic and synclastic surfaces, we could notice that an anticlastic surface like the hyperbolic paraboloids (hypars) can be generated by developing a curve of a given curvature along the tracks of another curve having opposite curvature, then generating a shell surface of double curvature. A synclastic surface like a semispherical surface can then be generated by developing a semi-circular arc along the track of another circular curve both having the same positive or negative curvatures.

Curves of other shapes such as parabolas, ellipses, or any other type of nurbs curves can also be used to generate free form surfaces which will yield some interesting designs of synclastic or anticlastic configurations. Organic and futuristic designs of shells have been constructed in the last years both in the research labs of universities, as demonstration projects, and ultimately as actual multifunctional structures and buildings.

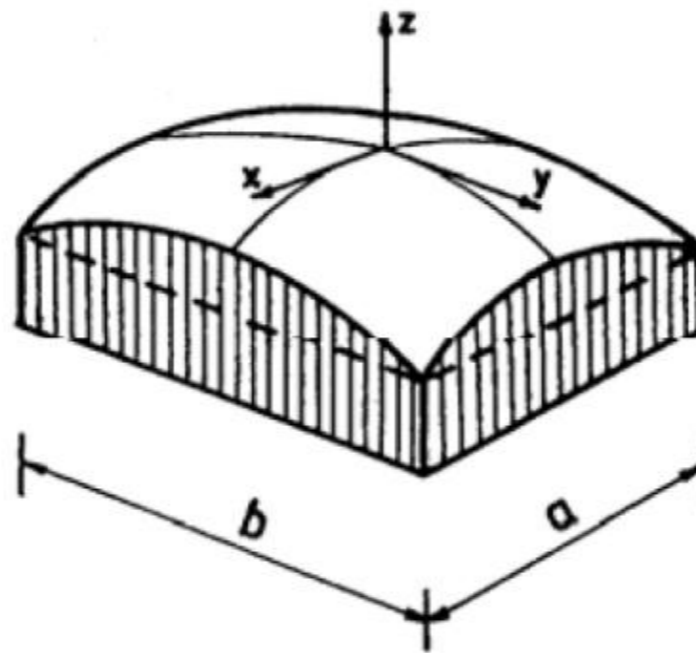


1.6 - BASIC TYPES OF SHELL SURFACES

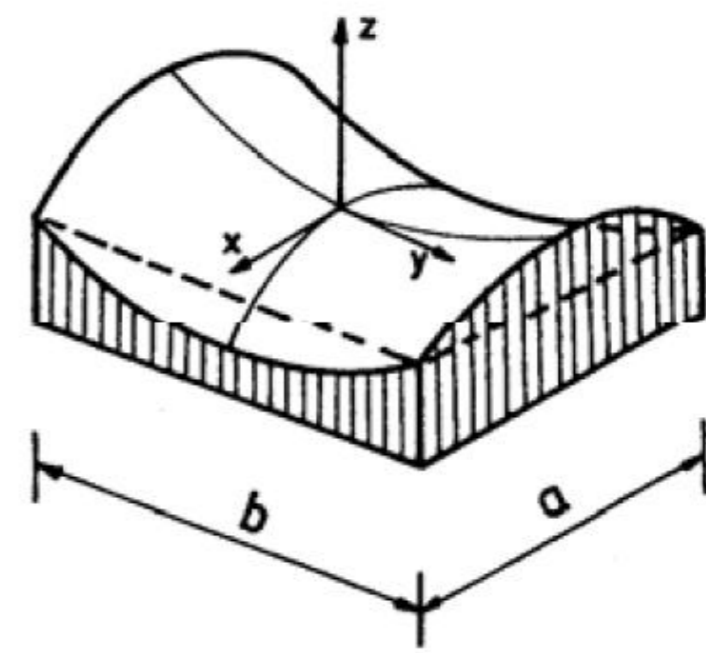
The three basic and most commonly used types of shell surfaces shown in Figure 1.7 can be cataloged based upon their Gaussian curvature described in the previous Section 1.5. We can generate Surfaces of Translation when we use one rectilinear or one curvilinear line and develop this line along another rectilinear or curvilinear line and in doing so generate one of the three types of surfaces shown in Figure 1.7. In figure a) we develop a curvilinear parabolic line along a straight line generating a cylindrical paraboloid with zero Gaussian curvature. In figure b) we develop a curvilinear parabolic line along a curvilinear elliptical line generating an elliptic paraboloid with positive Gaussian curvature. In figure c) we develop a curvilinear parabolic line along another curvilinear parabolic line generating a hyperbolic paraboloid with negative Gaussian curvature.



a) Cylindrical Paraboloid
ZERO GAUSSIAN CURVATURE



b) Elliptic Paraboloid - SYNCLASTIC
POSITIVE GAUSSIAN CURVATURE



c) Hyperbolic Paraboloid - ANTICLASTIC
NEGATIVE GAUSSIAN CURVATURE

Figure 1.7 – Basic types of Shell Surfaces based upon their Gaussian Curvature.

One can notice that the type of curvilinear surfaces generated above are very suitable to cover spaces with long span, such is the case for exhibition and convention centers, hangars, factories, stadiums, gymnasiums, atriums, music halls, and other similar type of architectural and engineering structures where the curvature of the surface provides great advantage for light weight and economical long span roof systems.



A. SURFACES OF REVOLUTION

Three Dimensional (3D) surfaces can be generated by rotating a straight or a curvilinear line around an axis of rotation as shown in Figure 1.8. The surfaces of revolution obtained all have a mathematical expression associated with each one of them and also have an analytical and geometrical way to draw and build them. Typically we recur to Analytic Geometry to obtain the equations that allows us to create the graphics of the surfaces of revolutions shown below. Each one of the surfaces of revolution has a unique mathematical equation which can be plotted for a given of parameters in the x-y-x or the r- θ -z coordinate systems by using any of the widely used graphics software. One very useful software tool to generate geometrical graphics for mathematical functions that represent different type of surfaces is “GeoGebra”, <https://www.geogebra.org/home> , which is a graphing calculator software to generate parabolic and other geometrical functions, shapes, curves, surfaces, solids, algebra, calculus, statistics, and 3D math. GeoGebra is user friendly, applicable to solve multiple mathematical and geometrical problems. It can be found at the website noted above.

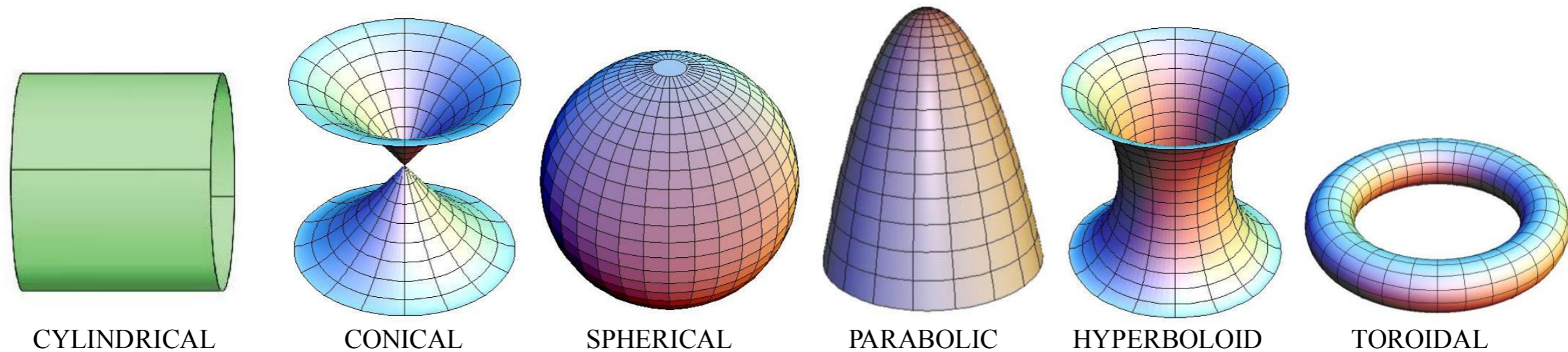


Figure 1.8 – Surfaces of Revolution: Cylindrical, Conical, Spherical, Parabolic, Hyperboloid, and Toroidal.

Architectural forms inspired by mathematics were built many centuries ago. The link between math and architecture goes back to ancient times, when the two disciplines were virtually indistinguishable. Great Pyramids and Ancient Temples were some of the earliest examples of mathematical inspired monumental structures built centuries ago when computers and CAD software were not available and were unthinkable at the time. Observations of natural forms and different trials of building structures with materials that were readily available in the environment lead to the achievement of monumental buildings that have lasted for centuries and that are still standing up.



B. DEVELOPABLE RULED SURFACES AND HYPERBOLIC PARABOLOIDS – HYPARS

As it has been discussed in previous Sections 1.5 and 1.6, ruled surfaces can be generated by developing a straight or curvilinear line along another rectilinear or curvilinear line. Three typical forms shown below in Figure 1.9 are the Hyperbolic Paraboloid (Hypar), the Hyperboloid (Hypoid), and the Conoid. Pictures of realized project will be shown in the following Sections below.

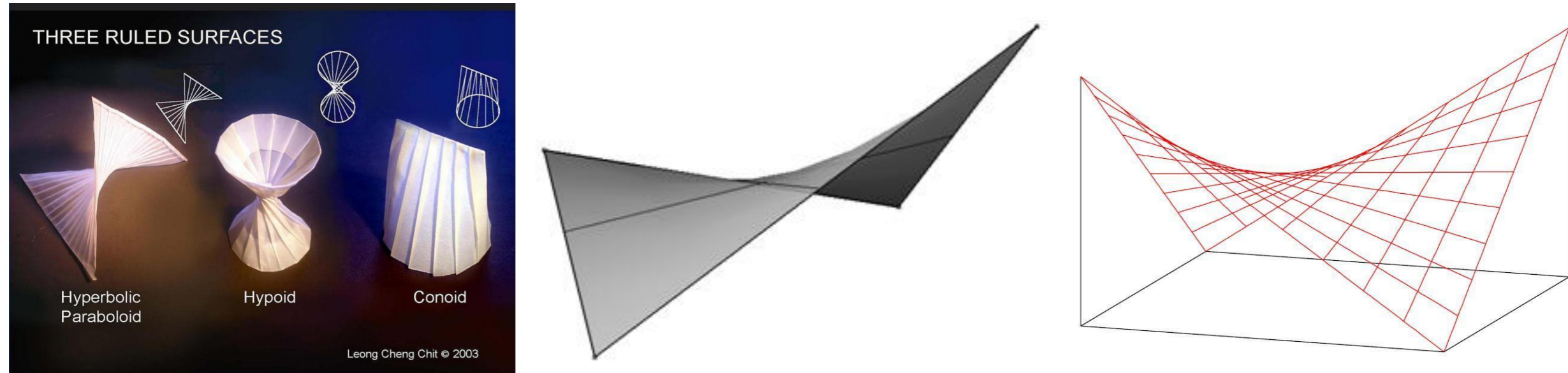


Figure 1.9 – Typical Ruled Surfaces, Hyperbolic Paraboloids, Hyperboloids, and Conoids.



Figure 1.10 – Mathematical expression and typical samples of Hyperbolic Paraboloid Hypar Surfaces.



C. DOUBLE CANTILEVER HYPARS

The Hyperbolic Paraboloid Hypar surface could have curvilinear or straight edges along the boundaries of the surface, typically they are built with two high and two low points at opposite corners of the surface. Samples of double cantilever Hypars are shown in Figure 1.11, where we can see a Hypar built with Bamboo for a Green School in Bali, Indonesia, another highly steeped Hypar built for the Waikikian Hotel, by G.J. Wimberly, in 1960, and a shallow slope Hypar built for the Warsaw Ochota Railway Station, Warsaw, Poland, in 1962.



Figure 1.11 – Samples of Hyperbolic Paraboloid (Hypar) Roof Projects in Bali, Indonesia, and Poland.

D. HYPERBOLOIDS

A hyperboloid of one layer is a doubly ruled surface of straight lines revolving around two circular end sections top and bottom. It can be generated by two sets of families of straight lines as shown below in the working models and the real built hyperboloid structures. Figure 1.12 shows some same samples of hyperboloids. The physical models show two doubly ruled surfaces generated by two families of straight lines. The picture at the center of Figure 1.12 shows three reinforced concrete cooling towers for a Power Station in UK, the next photo shows an elevated structure for a Toroidal Tank in Poland, and the last picture shows a tall Kobe Port Tower in Japan, which is one example of a tall hyperboloid steel tower of a double ruling set of straight lines of steel members. The concept of hyperboloids has been introduced recently into the construction of tall buildings with unusual exterior facades that appear to be turning around the center core of the buildings.



Hyperboloids are commonly built using solid surfaces of reinforced concrete or post-tensioned concrete for the majority of the height of the towers leaving the bottom section with openings for air circulation and access to the hyperboloid towers. When the hyperboloid tower does not need to have completely solid sections then it is customary to use some type of interlaced grid of members which will follow the typical pattern of the double ruling sets of straight lines that will form the hyperboloid structure.



Figure 1.12 – Physical Models of Hyperboloids and different types of as-built Hyperboloid structures around the world.

E. CONOIDS

Conoids are formed by ruled surfaces that are generated by linear segments connecting points of two curves running along the two ends of the straight lines. The shape of the two curves at the ends of the straight lines could be virtually of any type of curvilinear shape and the basic condition is that the two curves are divided into the same number of segments to be able to connect the straight lines along the curves in a uniform manner.

Conoidal surfaces can be used very effectively as roof and wall structures, due to their curvature that is created by developing a straight line along one or two curvilinear end tracks, the resulting surface presents geometrical properties that will provide much higher section modulus (S in in.^3) and moment of inertia (I in in.^4) than a planar surface. The thin surface with its curvilinear profile will provide large bending strength and stiffness which very effectively will support heavy gravity loads due to the selfweight of the structure or high lateral wind or seismic forces perpendicular to the curvilinear surface. Actual roof and wall structures built in the 1950's and 1960's are shown in Figures 1.13, 1.14, and 1.15.



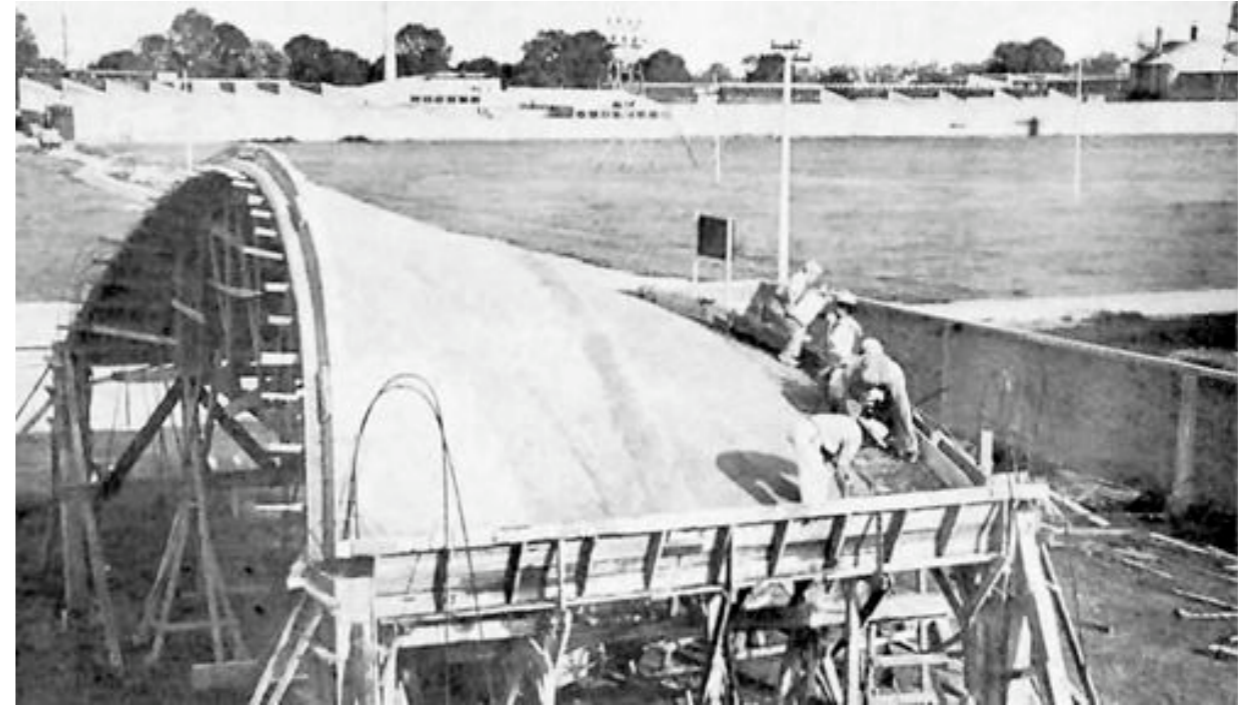
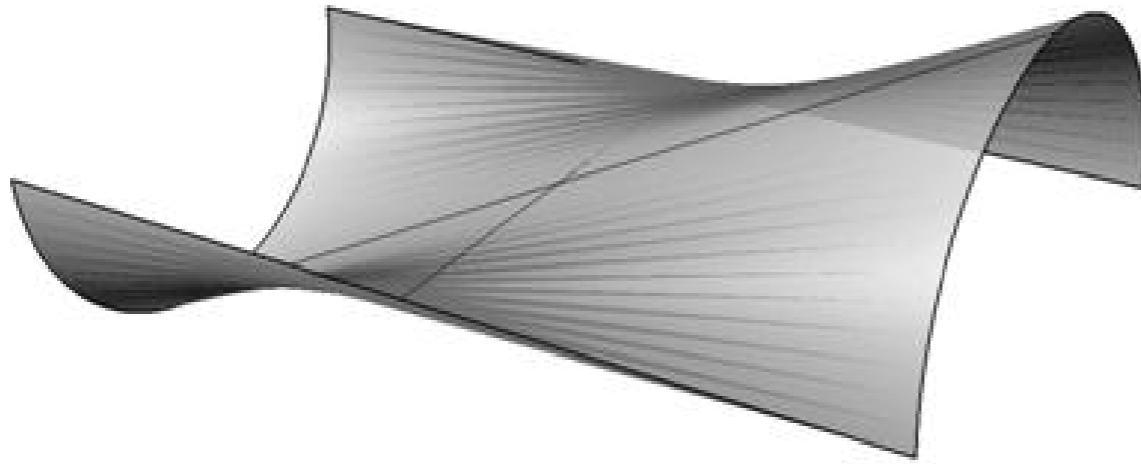


Figure 1.13 – Typical Conoidal Ruled Surface - Experimental Conoidal Roof in San Bartolo, Mexico, by Felix Candela, 1950.

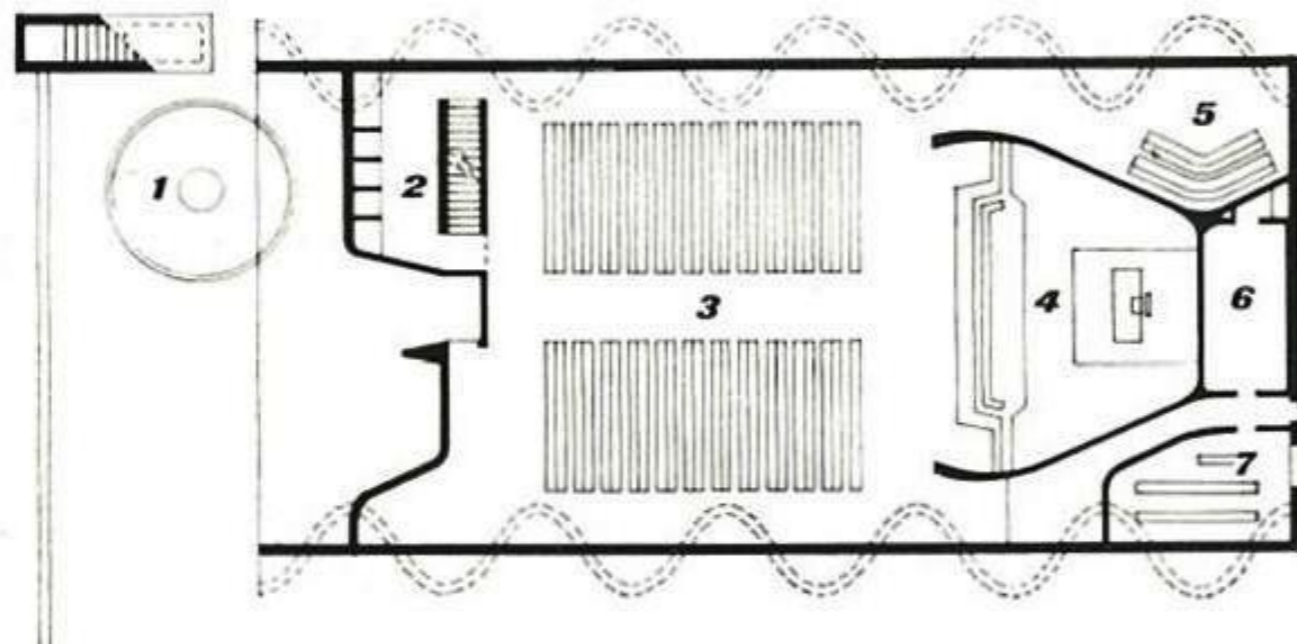


Figure 1.14 – Church of Christ the Worker, Floor Plan and Exterior Conoidal Reinforced Brickwork, by Eladio Dieste, Atlantida, 1960.





Figure 1.15 – Church of Christ the Worker Conoidal Brickwork Walls – Conoidal Brick Roof of Gaudi’s School of Sagrada Familia in Spain.



CHAPTER 2 - LITERATURE REVIEW

2.1 - GERMAN AND SWISS SCHOOL

Franz Dischinger, German Civil Engineer; 1887-1953 - A Pioneer German Engineer, In 1922, designed the **Zeiss Planetarium** in Jena with Walther-Bauersfeld, using a thin-shell concrete roof in the shape of a hemisphere. Their system was subsequently patented in 1922.

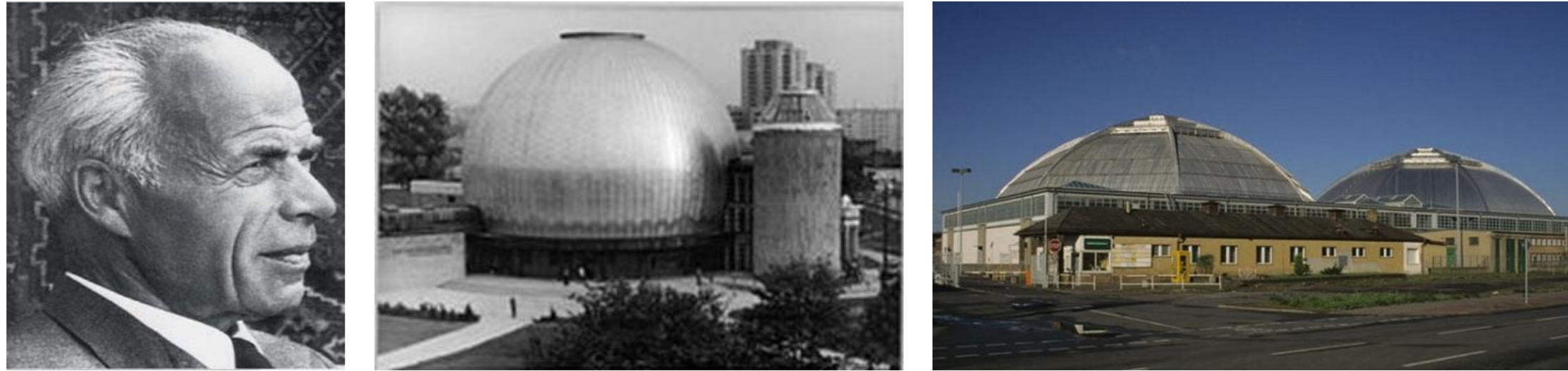


Figure 2.1 – Franz Dischinger and some of his shell structures in Germany.

Ulrich Finsterwalder, German Architect & Engineer; 1897-1988 - First published formulas supporting barrel shell design in 1933. His Theory is called the “Membrane Theory” used extensively in shell design, ignores bending in shells. Worked together with Franz Dischinger at the same firm.



Figure 2.2 – Ulrich Finsterwalder and some of his shell structures in Germany.



Heinz Isler, Swiss Structural Engineer; 1926-2009 – Swiss Engineer notable and famous for his thin concrete shells and innovative designs. Left a legacy of more than 1,000 elegant thin concrete shell forms all over Europe. The most notable are the roofs for a complex of sports halls and a swimming pool at the Norwich Sports Village (1987-1991). Isler demonstrated three methods of shaping: through using earth mounds, inflated rubber membranes, or hanging cloths.

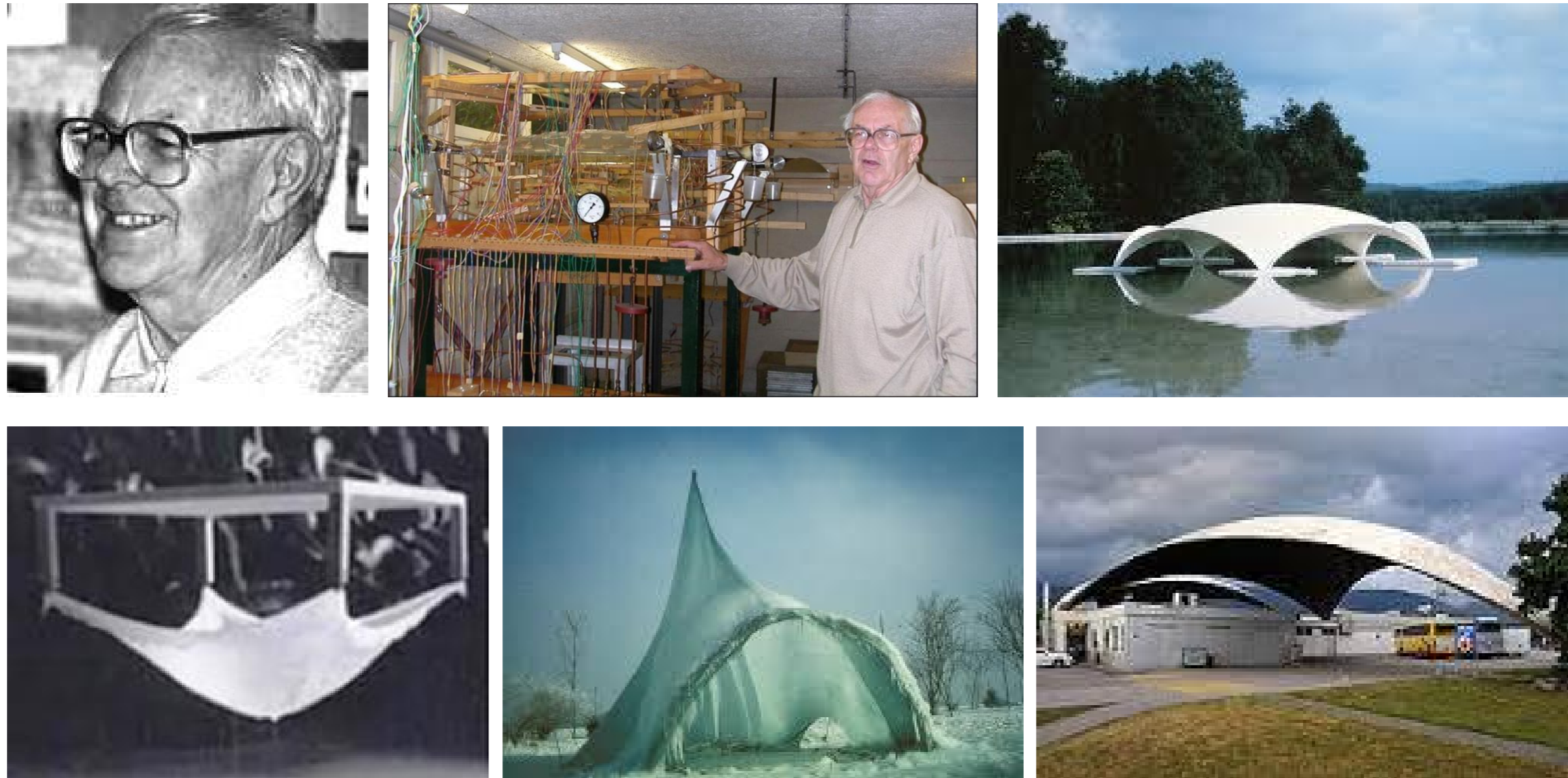


Figure 2.3 – Heinz Isler and some of his experimental and built shell structures in Switzerland.



2.2 - NORTH-AMERICAN SCHOOL

Anton Tedesko, Born in Germany, Raised in Austria, and lived in the USA; 1903-1994

Attributed with much of the success of thin-shell concrete structures in the USA. The first shell of the Z-D system built in the United States was Tedesko's design for the 1934 Hayden Planetarium dome in New York (81 ft. diameter, 3 in thick). The 1936 Hershey Arena roof in Pennsylvania (222 ft. span, 3.5 in thick) was the first short barrel shell in the USA and represented a significant departure from German practice. Anton Tedesko introduced the thin shell concrete roof construction to the United States and was responsible for the design of over 60 shells during his career. His engineering design approach relied on a balance of theory, experience with full-scale structures and close collaboration with contractors.

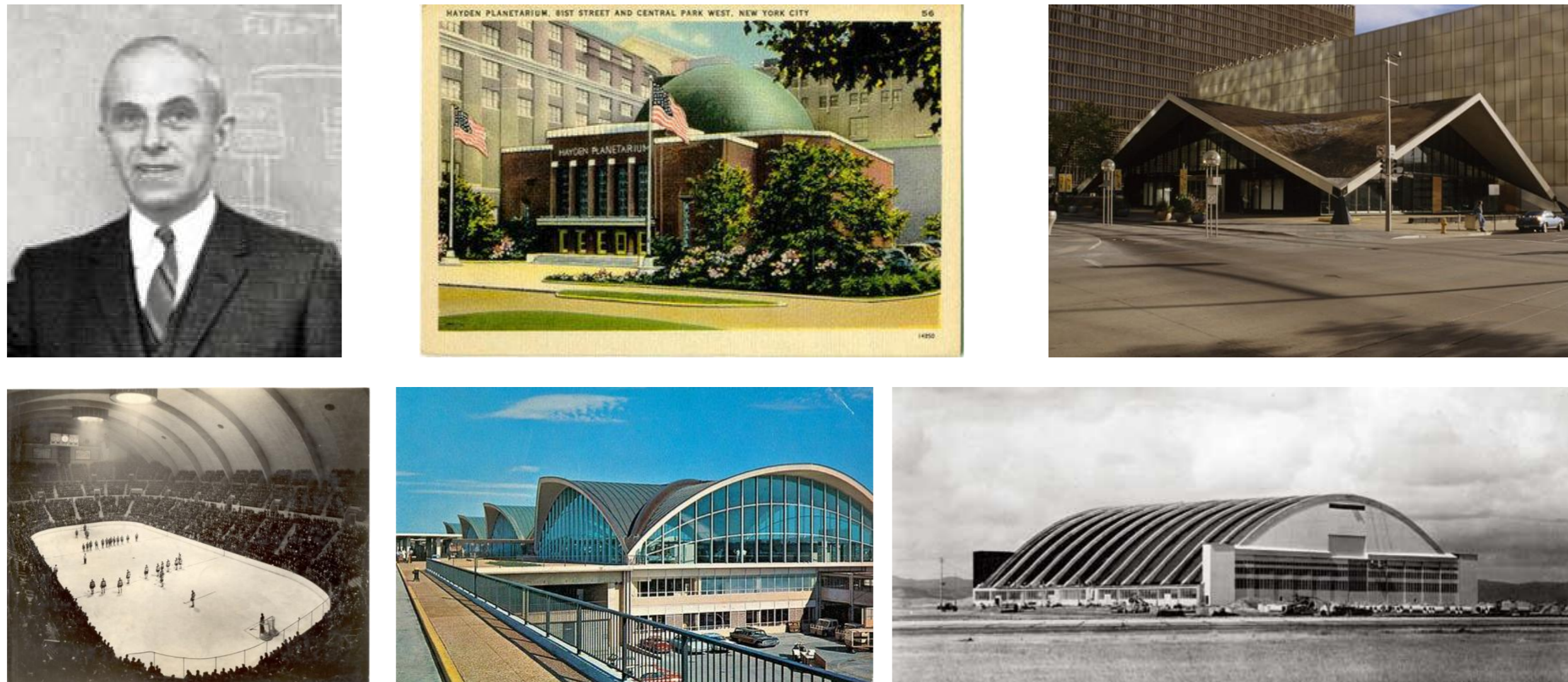


Figure 2.4 – Anton Tedesko and some of his shell structures in the USA.



John “Jack” V. Christiansen, Born in Chicago, 1927- 2017 - Jack’s work with thin-shell concrete brought him credit as one of the world’s top thin-shell concrete designers. Used Hyperbolically Curved Concrete Shell sections in between stiffening rib arched beams. The Kingdome, in Seattle, WA, 1976 at 661 ft. The largest clear span concrete dome in the world. The Kingdome shell structure was demolished in March 26 of 2000.



Figure 2.5 – John V. Christiansen and his Kingdome and World’s Fair shell structures in Seattle, WA, USA.

Eero Saarinen, A Finnish American Architect, 1910-1961 - An architect and industrial designer of the 20th century famous for shaping his neofuturistic style known for designing the TWA Flight Center Shell in New York City and the Gateway Arch in St. Louis, Missouri.



Figure 2.6 – Eero Saarinen and his TWA Flight Center at JFK Airport in NY and St. Louis Arch in St. Louis, MO.



2.3 - ITALIAN SCHOOL - Pier Luigi Nervi, Italian Engineer-Shell Designer, 1891-1979

He is widely known as a structural engineer, builder, and for his innovative use of reinforced concrete, ferrocemento, and his focus on Aesthetics.



Figure 2.7 – Pier Luigi Nervi, Inventor of Ferrocemento and some of his work on shell structures in Italy, Europe, and USA.



2.4 - SPANISH SCHOOL - Eduardo Torroja, Spanish Architect-Structural Engineer; 1899-1961

Notable as a pioneer in the design of concrete-shell structures. The book "The Structures of Eduardo Torroja", by Torroja y Miret, 1958, contains a review of the designs and works of Torroja using reinforced concrete shells. Eduardo Torroja designed the thin-shell water tower in Fedala and the roof of the "La Zarzuela" racetrack in Madrid in the form of a hyperboloid.



Figure 2.8 – Eduardo Torroja, Spanish Engineer and his work on reinforced concrete shells.

Felix Candela, Spanish Architect-Engineer; 1910-1997 - A student of Eduardo Torroja, Felix Candela, was born in Madrid, Spain and lived in Mexico where he developed most of his outstanding experimental, design, and construction work on shells. Spent the last part of his life in the USA.



Figure 2.9 – Felix Candela and some of his hyperbolic paraboloid shell structures in Mexico and Spain.



Santiago Calatrava, Spanish Architect-Engineer; 1951 - A Spanish neofuturistic architect, structural engineer, sculptor and painter. Calatrava said: “I am always looking for more light and space”. Most of his outstanding shell structures are close to the water for great visual and natural contrast.



Figure 2.10 – Santiago Calatrava and his outstanding shell structures in Spain and the USA.

Ildefonso Sanchez del Rio, Spanish Engineer; 1898-1980 - Is one of the most respected Spanish engineers of the generation called: Generation of the 1927's” (“Generacion del 27”), including Jose Entrecanales, Eduardo Torroja, y Carlos Fernandez Casado who were all educated as engineers at the School of Engineers of Madrid. His most notable achievement in shells includes the Oviedo Sports Pavilion built between 1961 to 1975. He invented many reinforced concrete systems including the type of undulated reinforced concrete long span shell structures. “The Engineer with a soul of an Artist”.



2.5 - LATIN-AMERICAN SCHOOL - Eladio Dieste, Uruguayan Architect & Engineer; 1917-2000 - A Uruguayan Engineer and Builder who spent his long career designing arched and vaulted shell structures mainly made of reinforced concrete and reinforced brick masonry in Uruguay.



Figure 2.11 – Eladio Dieste and his reinforced brick and shell structures in Uruguay, South America.

Hilario Candela, Cuban Born Architect; 1935 - A distant cousin of Felix Candela. Designed the Miami Marine Stadium completed in 1963. Educated at Georgia Tech, USA, practiced most of his life in Miami, Florida, USA. The Marine Stadium still exists with its shell structure still good.



Figure 2.12 – Hilario Candela and his thin reinforced concrete shell structures in Miami, Florida, USA.



Oscar Niemeyer, Brazilian Architect; 1907-2012 - Is thought to be an important name in worldwide modern architecture. Was a pioneer in using curvilinear reinforced concrete forms for buildings and shell structures which often have a lot of empty space and elegant shapes.



Figure 2.13 – Oscar Niemeyer and his outstanding and elegant curvilinear shell structures in Brazil.

Max Borges Jr., Cuban Architect; 1918-2009 - Borges' style was highly influenced by his work with Spanish structural engineer Félix Candela. Borges invited Candela to work with him in Cuba, and they both developed extraordinary projects in the island of Cuba.



Figure 2.14 – Max Borges and few of his shell structures in Cuba.



Eduardo Catalano, Argentinian Architect; 1917-2010 - Inventive Argentinian architect and teacher whose work was eye-opening modern. A student of Walter Gropius and Marcel Breuer, the Buenos Aires-born architect was considered a modernist visionary whose massive concrete edifices attempted to redefine the relationship between structure and space. Catalano was a Faculty Professor of Architecture at MIT up to 1977.



Figure 2.15 – Eduardo Catalano and his hyperbolic paraboloid shell structure and metal shell sculpture.

It is important to mention here that to this date the pioneering designers of reinforced concrete shells in most parts of the world have passed away and we only now rely on the documentation that has been left by them and that have been passed on to those that have had the privilege to have learned directly from one of the pioneers mentioned above.

Nowadays the widespread use of large-scale computers and powerful workstations with sophisticated Finite Element Analysis software makes the task of analysis and design of complex concrete shell structures more manageable and easier to perform as compared to the more complex and laborious partial differential equations that had to be solved either manually or by means of tabulated parametric values of very limited cases of shells with specific boundary conditions and specific ratios of dimensions and thickness. Therefore it is now possible to verify the designs that were done several decades ago and which were built and proved to work satisfactorily until those structures were demolished or simply deteriorated beyond practical repairs.



Thin shell concrete structures had a rapid evolution since the time they were successfully built and their tremendous load capacity had been realized and verified by the strength, stiffness, stability, and longevity of the accomplished designs. The shells evolved from simple cylindrical and spherical surface forms to more sophisticated and efficient hyperboloids cooling towers.

A very popular type of shell that gained a lot of attention and was highly favored by architects, owners, and engineers is the Hyperbolic Paraboloid (Hypar) that can be very easily constructed by using the development of simple straight lines crossing each other from two opposite sides of a square, rectangle, or rhomboid four-sided shape.

As the use of concrete shells became more widespread around the world, it was always imperative that the designers maintain a careful level of quality control on the design phase of the structures, particularly with the thickness of the concrete shell, the radius of curvature in either one or two directions in relation to the total span of the structure to maintain overall stability and avoid premature localized or global buckling of the thin concrete shell structure.

Recognizing the fact that concrete shells can develop either tensile or compressive stresses over the thickness of the shell in the directions corresponding to the principal stresses, designers shall always maintain the appropriate levels of allowable stresses that will keep the structures safe and stable under the expected loading conditions of the structure always keeping in mind to stay within the safe allowable stresses of the concrete and steel reinforcement to avoid excessive compression or undesirable tensile or bending stresses that could cause cracking in the concrete.

Reinforced concrete shell structures also undergo creep effects which are the axial deformation of the concrete thickness under sustained effects of axial compressive forces. At the same time those sections of reinforced concrete shells that will be under the effects of tensile stresses during the life time of the structure could also undergo some level of axial tension in the concrete portions of the reinforced shell that may cause cracking at partial section of the shell thickness.

The Author wishes to recognize that the Literature Review and the documentation of the few outstanding architects and engineers briefly presented and discussed above, that had done work on thin concrete shells represent only some of the many personalities which have influenced the developments and achievements of constructed concrete shell structures in different parts of the world. The literature review written in this Section of the Thesis does not necessarily include all the architects and engineers from other parts of the world which may have also made a great contribution to the developments and constructions of thin concrete shell structures, particularly from other continents such as Asia, Africa, and Australia due to limitations on information widely available in commonly published textbooks, the internet, and the web.



The bibliography, photos, graphics, and documentation on the work of the pioneers of shell structures presented in this Section and other parts of this Thesis have been obtained from public information available in websites and publications posted in the web at Wikipedia, Structurae Magazine, and other internet sites that can be searched in Google and with other search engine tools. The intent of this Thesis is to highlight the immense work done by a select group of notable pioneers of shell structures listed above. There are other shell designers and shell builders throughout the world which are not mentioned here but have already contributed to the development of shell structures in their regions and native countries.

The immense architectural and engineering work on thin concrete shells done by the personalities presented in this Section inspires us to look at their work as a testament to originality, courage, and vision to see beyond the limits of what we can be able to achieve when we recognize the intrinsic behavior of structural systems, understand the material properties used, and ultimately find the most ingenious ways to build these amazing and outstanding structural shell systems.

We will pass away one day, but the new generations could always look back and learn from what others were able to do and leave behind for the advancement of science and technology and for the wave of young architects and engineers to undertake in the future to create new and better structural systems that could be adaptable and flexible to the needs of humanity.

CHAPTER 3 - BASIC ARCHITECTURAL AND ENGINEERING CONCEPTS OF MEMBRANE SHELLS

In this Chapter the Author will present an overview of the basic architectural and engineering concepts related to shells emphasizing on thin reinforced concrete shells. The influence of architectural forms and the function of the structures being designed have an intrinsic relationship with the flow of forces within the main structural components that support the final shape of the buildings and structures. Certain geometrical shapes in 2D and 3D space present particular advantages over others in the way the selfweight of the materials and the environmental forces acting on the supporting structures are carried down from their points of support to the ground and their foundations.

Hyperbolic Paraboloids surfaces and geometrical forms will be reviewed including some graphical and parametric methods to generate their surfaces of doubly curvature using straight lines bounded by three parabolic curves, the basics of the engineering analysis and designs of different forms of shells will be discussed, graphical and computer methods to study funicular forms will be briefly presented, some samples of architectural and engineering projects realized using reinforced concrete shells will be displayed, and finally part of the work of two pioneers of shell structures,



Heinz Isler and Felix Candela will be presented to highlight the basic experimental, mathematical, and graphical methods that were used to achieve such magnificent thin shell reinforced concrete structures in the past.

3.1 - ARCHITECTURAL FORM, FUNCTION, AND FORCES

The architecture of shells is inspired by geometrical forms and mathematics. Ancient Pyramids and Temples are testament of the link that existed between the basic architectural forms and their intimate relationship with the mathematical formulations that expressed their existence in 3D space. The key in lightweight structural design relies on removing weight from the structure without reducing its strength.

For a given solid member, part, or structural component subject to external forces applied on the exterior surface of the body, there are always different paths for the forces to flow from the point of application of the forces to the points of supports. The distribution of internal forces and stresses will follow the lines of the principal stresses that will result from the combination of axial stresses in two or three perpendicular planes across the main geometrical axis of the structural components.

Ultimately the external forces will need to travel from point of origin to the given supports or boundary conditions of the structural members, the entire portions of the member are not all subjected to the same magnitude of principal stresses, and there will always be portions of the members which literally are subjected to zero values of principal stresses, therefore those portions of the member under zero stresses can be removed or be left out without compromising the structural integrity of the member.

The process of finding an efficient structural form that will perform its intended architectural or engineering function and carry the external applied forces in a safe and appropriate manner is called “Topology Optimization”, where we start with an original solid member and we end up with a final structural shape that may have configurations which are somewhat different than the original solid shape, may have somewhat the similar boundary configurations, but its internal layout of the solid component may have holes and a layout of solid pieces that can be arranged in a manner similar to struts and ties which will allow the component to be in equilibrium and carry the loads in a safe and stable manner.

Figure 3.1 below has been reprinted from an article published by contributing editor Lawrence S. Gould on optimizing automotive parts to achieve lightweight designs. The software ParetoWorks from SciArt Company is a plugin for SolidWorks that allows the optimization process of parts to reduce costs, reduce materials, reduce weight, and increase quality for stronger and stiffer parts which are the product of innovative design process that allows the efficient flow of forces through the network of optimized portions of the whole member under loads.



Similar design process can be applied to the thin shell reinforced concrete structures, where the designer could optimize the final shape of the shell structure based upon the flow of forces along the path of the principal stresses through the shell structure.

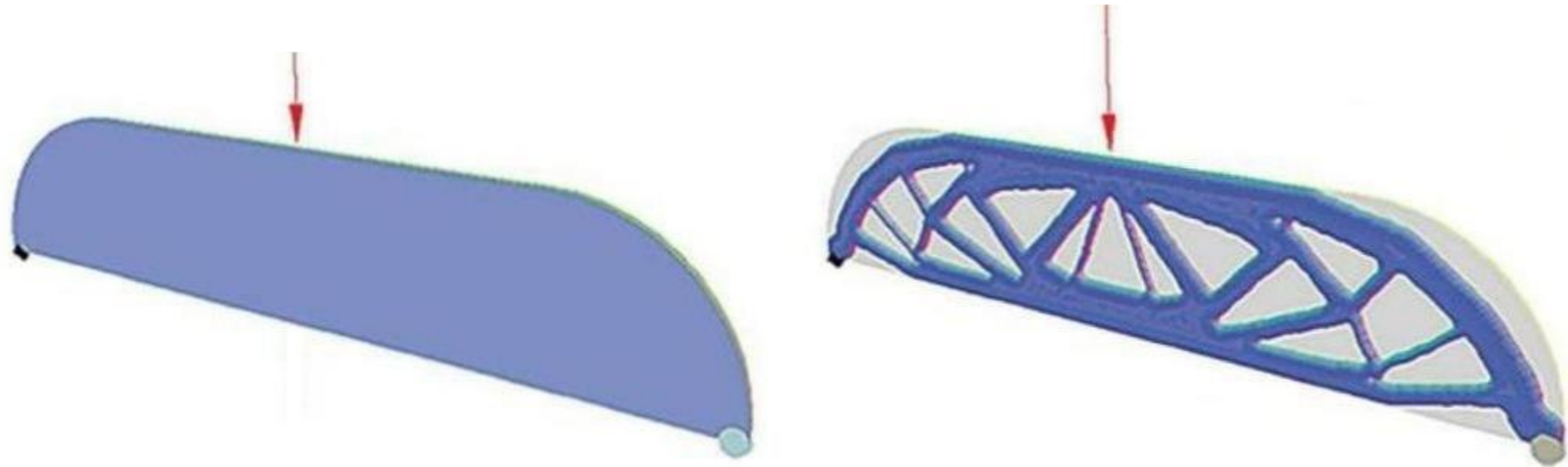


Figure 3.1 – Form, Forces, and Function of Architectural Engineering Structures, Topology Optimization.

In practice solid shell structures are built of continuous curvilinear surfaces of different forms, such as cylindrical, spherical, hyperbolic paraboloids, hyperboloids, conoids, and other similar geometrical surface forms. In principle the relatively low cost of materials and the high cost of labor advocates for simplicity and speed of construction which has taken preference over the optimization and lower weight of shapes.

The economies and construction methods in the world are constantly changing and evolving, the same happens with the materials and labor costs, therefore the concepts of optimization, sustainability, and efficiency must be incorporated into new practical methods of designs and buildability of structures which could lead into a favorable effect and renewed interest in the revival or thin shells and grid shells designs and constructions into the main-stream building industry.

The shapes and forms that we observe in nature have evolved over time and for centuries and have been naturally tested to be optimal in form and efficient load resistant structural shapes. Therefore one could obviously ask the question: “Why numerous shapes and forms existing in nature are ignored or neglected to be used more often in practical designs of new architectural and engineering structures and buildings ?”, this is an absolute



mystery and a big unknown fact among many design professionals that do not embrace nature into their designs of new buildings. Perhaps we have forgotten the lessons of the natural forms that have endured the test of environmental effects throughout centuries and for the longest times.

“The resistant virtues of the structure that we make depend on their form; it is through their form that they are stable and not because of an awkward accumulation of materials. There is nothing more noble and elegant from an intellectual viewpoint than this; resistance through form”. By: *Eladio Dieste, Uruguayan Architect Engineer, 1917-200.*

Structures which are based or inspired on nature or natural forms tend to adapt their shapes to efficiently and effectively support and resist the environmental forces that exist in nature and also the superimposed forces from meteorological and human effects following certain paths which are more efficient when they follow the lines of gravitational forces or what is called funicular paths.

Therefore it is very important to understand first how forces flow in nature and how they are more efficiently supported along their boundaries and points of support so that they can apply those basic principles of form, function, and forces to the design of our architectural and engineering buildings. Shell structures because of their natural forms are ideal and optimal shapes that provides both superior strength and economy of material due to their inherent natural distribution of its own components.

In thin concrete membrane shells the distribution of axial stresses are commonly considered to be distributed uniformly across the thickness of the shell and they tend to flow along the axis of the curved members or along the curvature of the shell in a funicular form following the lines of a catenary curve or approximately that of a parabolic curve where the stresses will be either in pure compression or pure tension along the funicular curve. When the thin concrete shells carry the external forces and pressures in pure compression or tension without significant bending stresses then it is said that the member behaves and can be analyzed based upon the principles of the Membrane Theory which will be reviewed in Section 3.3.

For thin concrete membrane shells then the Graphical Analysis Method (GAM) is suitable to determine the equilibrium of forces for the funicular form that will be adopted for the parabolic or catenary curves of the membrane shells or cables either fully in compression or tension axial forces. If we were to think of thin reinforced concrete membrane shells as a rigid or solid body composed of multiple small interconnected pieces of members that will form some type of discretized truss then we could model and analyze a shell as a hybrid body of struts (compression members) and ties (tension members) which will be in equilibrium under external forces. We could basically apply the principles of Tensegrity to thin reinforced concrete shells, some type of Truss Analogy to the continuous and solid curvilinear shell surface.



The Graphical Analysis Method was the dominant method of structural analysis of statically determinate systems until the early 1900's. It is said that the catenary shell form is perhaps “the most time enduring shape or form known to humankind”. Graphical Analysis Methods can be used for two-dimensional and three-dimensional structural systems as long as the system is statically determined in the 2D and 3D spaces. More details of Graphical Methods will be discussed next in Section 3.4

The ACI 318-14 Building Code has recently incorporated in Chapter 23 the Strut-and-Tie Models which is a method for analysis of structural members based upon a Truss Analogy Method (TAM), where the whole structural member can be modeled as a Truss system composed of struts and ties members interconnected at nodes capable to transfer the external loads applied to the structure onto the supports. The struts and ties will be then designed to support the compression and tension forces corresponding to each one of the truss members based upon the dimensions of the struts and the size of the reinforcement provided for the ties.

Thin Reinforced Concrete Shells can certainly be analyzed using the Strut-and-Tie Model (STM) of the ACI 318-14 Code. Concrete Shells can then be modeled as a grid or mesh of interconnected members which will form the curvilinear form or shape of the anticlastic or synclastic surface of the shell. The shell designer will have to model the surface of the shell in the form of a Truss Model that will more closely represent the actual shape of the shell, using a layout of members that will act as struts or ties depending on the configuration of the shell, its support conditions, its edge or boundary conditions and the applied loads on the shell surface.

3.2 - HYPERBOLIC PARABOLOIDS - HYPAR FORMS

Hyperbolic Paraboloids also known as “Hypars” are surfaces of translation that can be generated by moving a parabola curve along the path of another parabola curve that is of an opposite curvature of the first one creating what is commonly known as a “Saddle-shaped” surface. The type of surface that is generated has what is called a negative Gaussian curvature. Hypars can also be generated by the translation of straight lines along two straight or curvilinear lines that will ultimately create some type of double curved surface. This property of hypars makes them very suitable for numerous types of applications of thin concrete shell structures that can be constructed solely based upon the use of straight lines along other straight or curved edges.

An equation to define the three dimensional surface of a hyperbolic paraboloid (hypar) with straight rectilinear edges along the four sides and of height h from the low to high points of the two opposite corners of the hypar is shown below, for $a = b = 1$, then $c=h/w^2$:



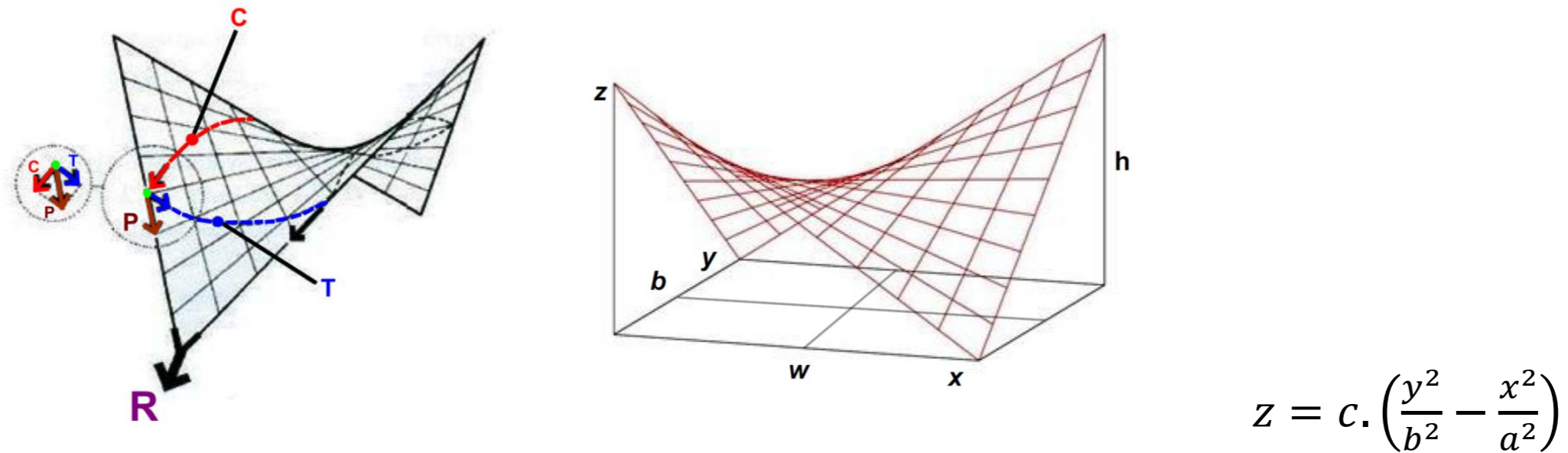


Figure 3.2 – Hyperbolic Paraboloid geometrical representation and mathematical equation in x-y-z coordinate system.

Hyperbolic Paraboloid surfaces can also be generated by a double set of straight lines within three parabolic curves of specific parametric dimensional relationships. This concept was widely used by Felix Candela to create most of his outstanding thin reinforced concrete shells in Mexico. Some examples of projects built by Felix Candela are shown in Section 3.5. The Author will discuss in Section 3.6 some of the techniques that can be used to generate the type of Hypar surfaces done by Candela by using some specific dimensional relationships and layout of the parabolic curves that will allow the creation of two sets of perfectly straight lines in two directions joining opposite sides of the parabolic curves that will then create an anticlastic surface with two grids of intersecting straight lines. This concept can be used to generate different type of hyper shell configurations such as the ones achieved by Candela. The method is called: Hyperbolic Paraboloid Grid Shells (HPGS) and is inspired by Felix Candela.

Hyperbolic Paraboloids in the form of thin reinforced concrete shells have been built since the early 1900's and there has always been innovations in experimental laboratory and physical models, construction methods, materials, analysis methodologies, and computational techniques that permitted the realization of amazing thin shell structures which will be described in the following sections of this chapter. The samples of shell projects built and shown in this Thesis cover a great variety of type of shells, such as concrete vaults, domes, arches, corbeled and voussoir types of shell constructions which could be subjected to in-plan and out-of-plane environmental loads and pressures. The type of supports for shells have to go in conformance with the type of reaction forces generated at the boundaries and supports of the shells at the ground level or at elevated points of the shell structures.

Several Textbooks, Structural Handbooks, Ph.D. Dissertations and Master Thesis, Technical Papers and Articles in Structural Journals, Magazines, and Engineering Publications have documented well the advancement of thin reinforced concrete, prestressed, and posttensioned concrete shells which have paved the way for architects, engineers, and constructors to more efficiently and confidently analyze and design different types of thin concrete shells.

One of the key components of the building process of shell structures is the “FORMWORK”. Depending on the final shape of the thin reinforced concrete shell and the type of either single or double curvature of the shell surface, builders face the big challenge to find the most appropriate, efficient, economical, practical, and feasible method to install a formwork which will be suitable and strong enough to achieve the desired three-dimensional curvilinear surface of the desired shell structure. Therefore the selected FORMWORK is key for the success of installation of shell structures.

Hyperbolic Paraboloids have been built using materials other than plain or reinforced concrete. Late Dr. Donald L. Dean, in 1956 then an Associate Professor of Engineering at the University of Kansas School of Architecture and Engineering with the help of his senior students designed and constructed a three-bedroom house located south of the Kansas University campus. This unique hyperbolic paraboloid house in Lawrence, Kansas, is composed of cross laminated wood lattice with high and low points supported only at three concrete bases at ground level. This type of construction proved to be economically feasible and the labor and materials costs for this roof system was kept down.

Hyperbolic Paraboloids with straight boundary edges that connect the high and low points of the shell surface can be designed to have very thin edges which will make the final shape of the shell to look very elegant and lightweight, but in many situations where the edge members attract large axial, bending, and shear forces, then the edge members of the Hypar can become of very large size. It is then necessary to take into account all the axial, shear, bending, torsional and out-of-plane stresses that may develop along the free edges of Hypars, when necessary the shell designed could devise ways to provide and design curvilinear bending active perimeter members that can take advantage of their curvature to minimize the shear and bending effects along the boundaries of hypar shells.

Melaragno M. in his textbook: “An Introduction to Shell Structures” refers to the Modern Symbolism of Hyperbolic Paraboloids (Hypar) indicating that this relatively modern geometric form stimulated mystical feelings in Antonio Gaudi (1852-1926) who apparently saw “The Holy Trinity” in the generation of a surface depending on three straight lines, the generatrix and two directrices. Gaudi apparently visualized the Father and the Son in the two infinite straight lines constituting the directrices, and apparently saw the Holy Spirit in the straight line generatrix.



Several forms of hyperbolic paraboloids can be developed based upon the shape and curvature of the edges of the surface and the lines or curves that delineate the grids formed within the boundary edges. The following figures describe the many types of hypar forms possible.

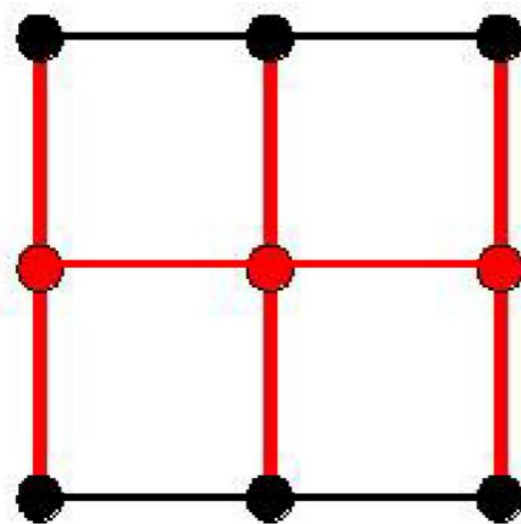
A. - SINGLE SADDLE VAULT



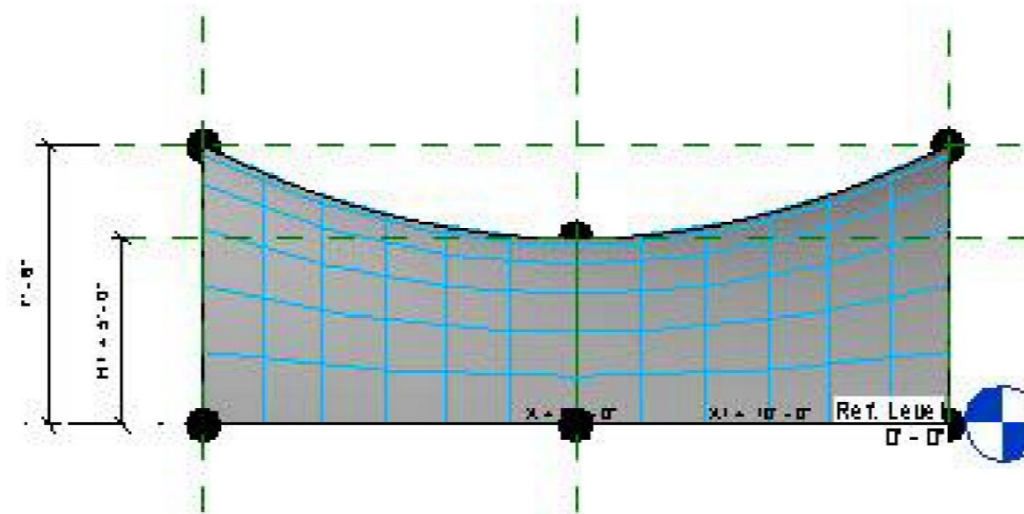
ISOMETRIC VIEW



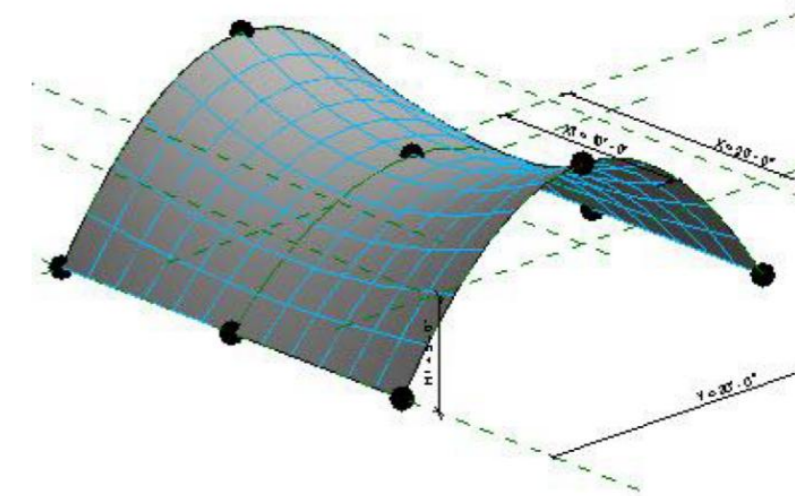
Cosmic Rays Laboratory, Mexico, 1951 – by F. Candela



PLAN



SECTION



AERIAL VIEW

Figure 3.3 – Single Saddle Vault - Isometric, Picture of sample structure, Plan, Section and Aerial View.



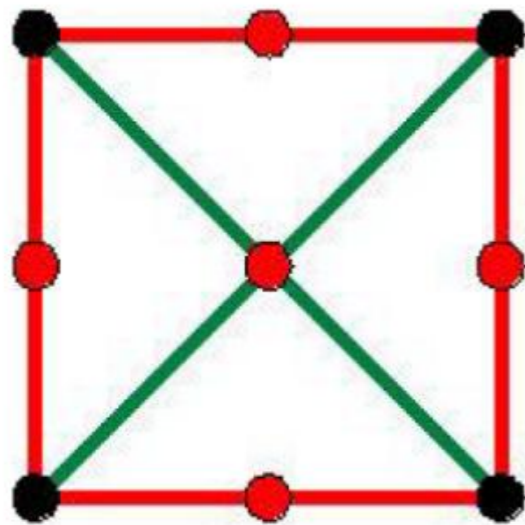
B. - GROINED VAULTS - TWO CURVED HYPARS INTERSECTED AT RIGHT ANGLES, (CATENARY VAULTS).



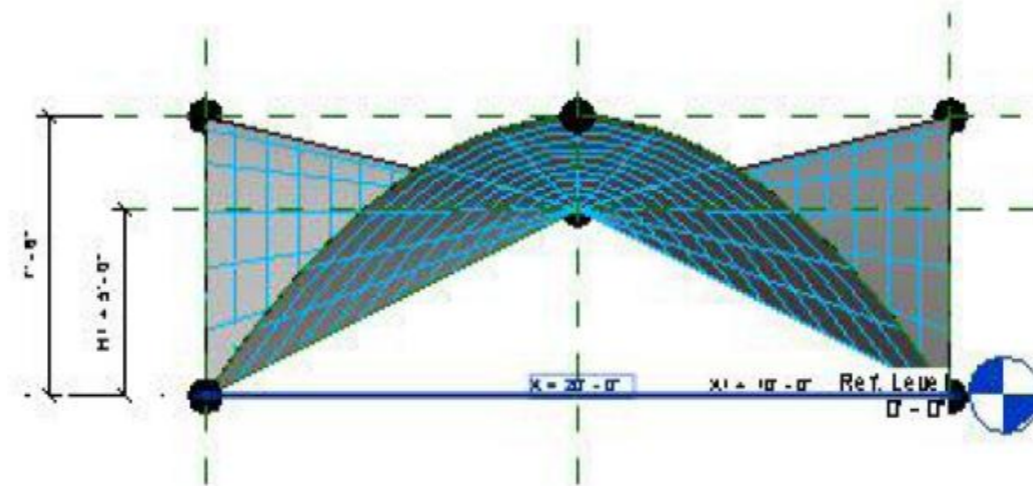
ISOMETRIC



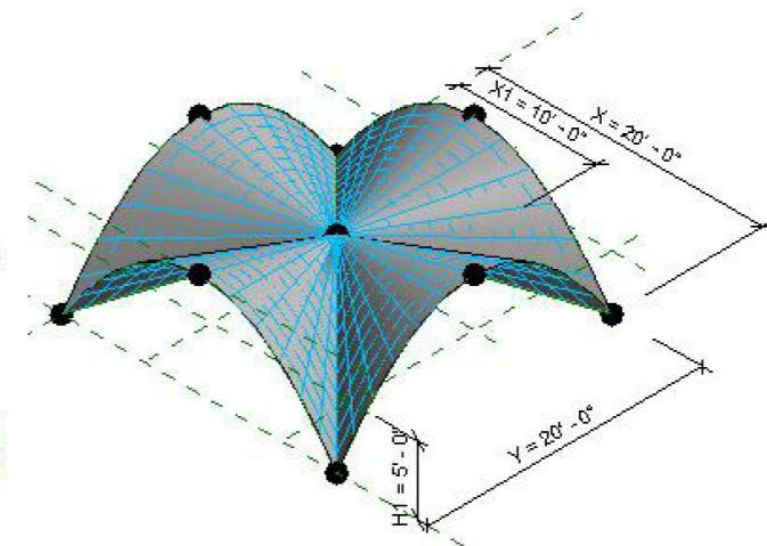
Bacardi Rum Factory, Puerto Rico, 1960 – by Candela



PLAN



SECTION

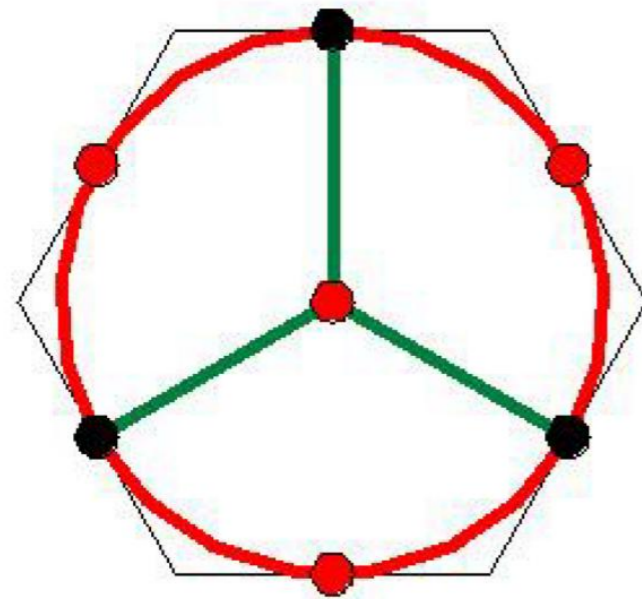


AERIAL VIEW

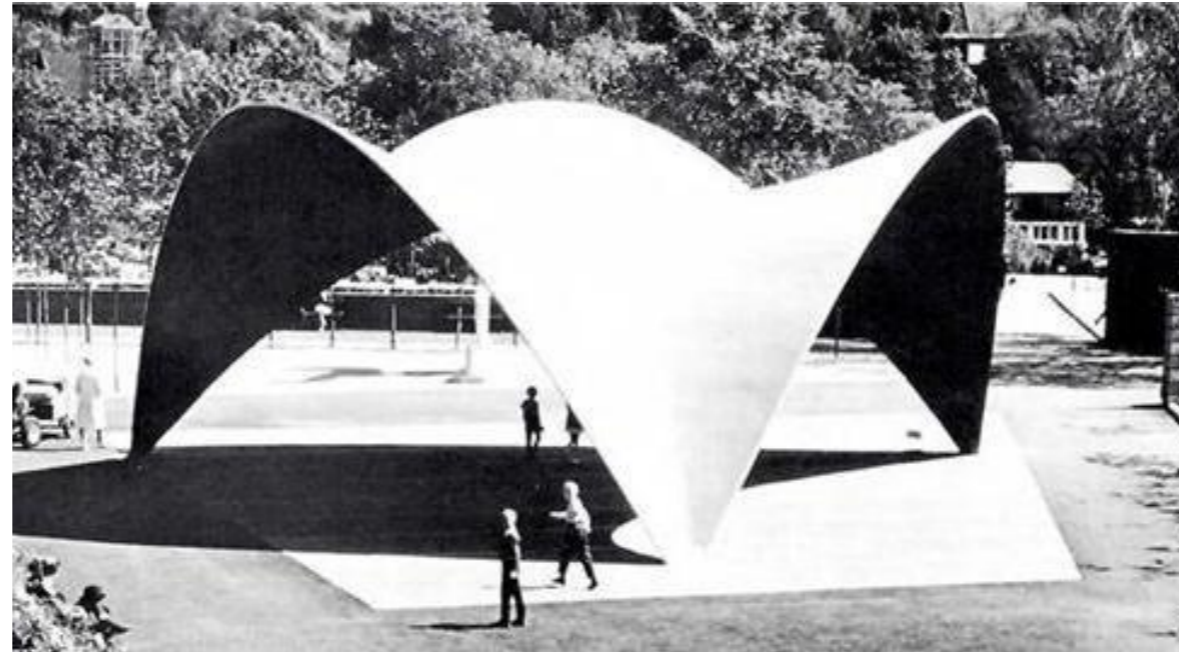
Figure 3.4 – Groined Vaults - Isometric, Picture of sample structure, Plan, Section and Aerial View.



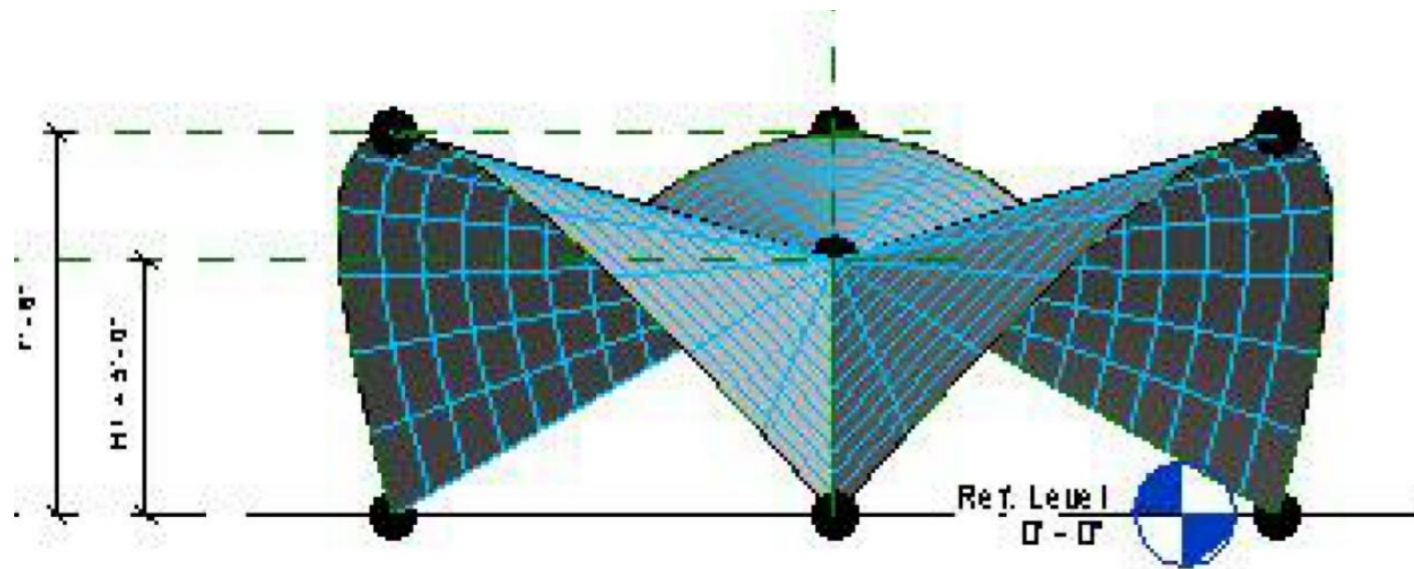
C. - GROINED VAULTS OF THREE INTERSECTED CURVED HYPARS, TRIPLE CANTILEVER HYPARS.



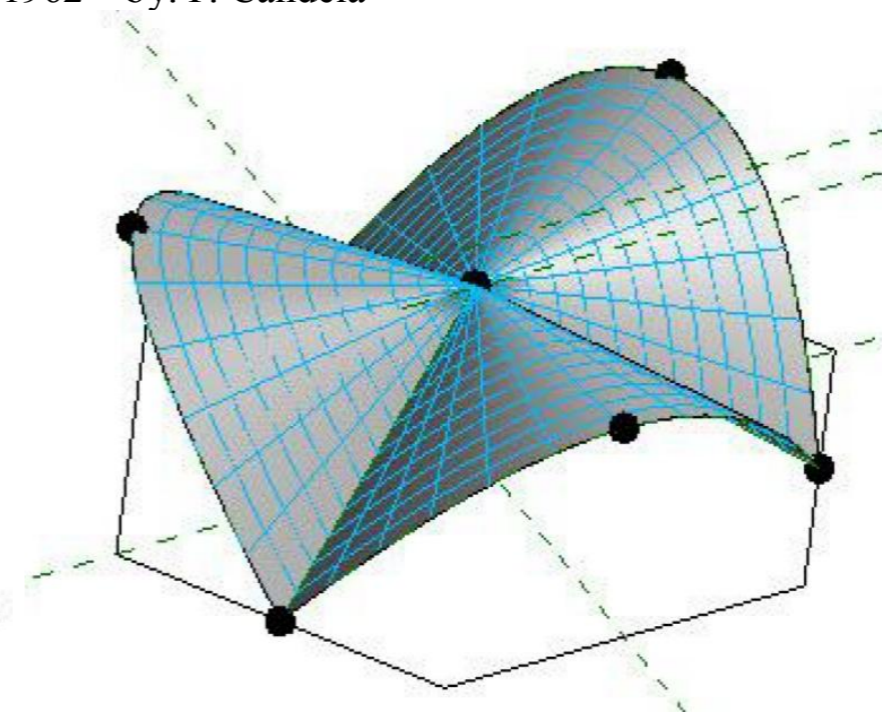
PLAN



Botanical Garden, Oslo, Norway, 1962 – by: F. Candela



SECTION

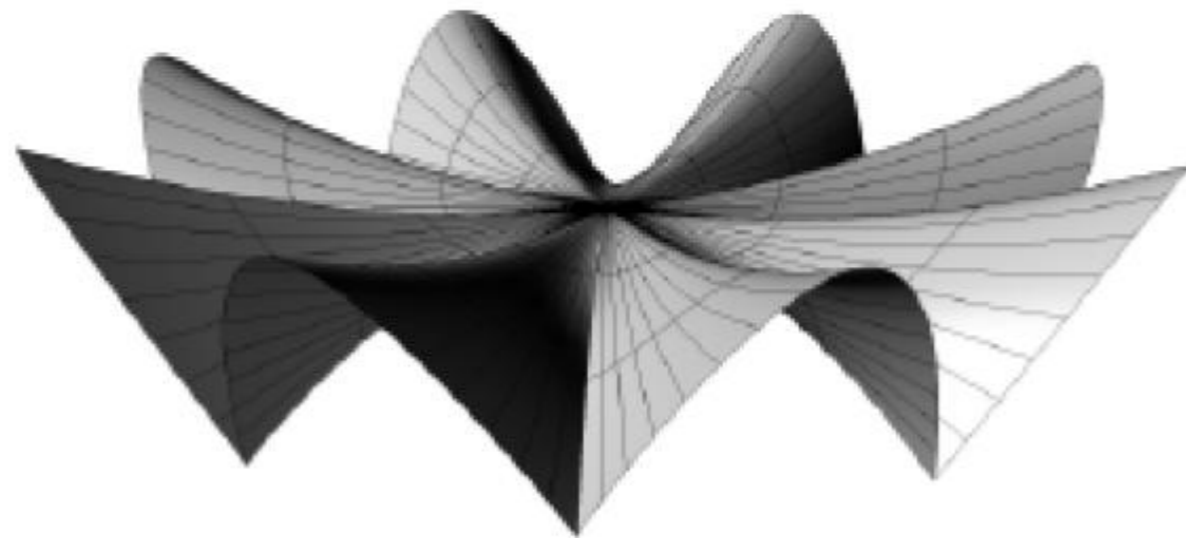


AERIAL VIEW

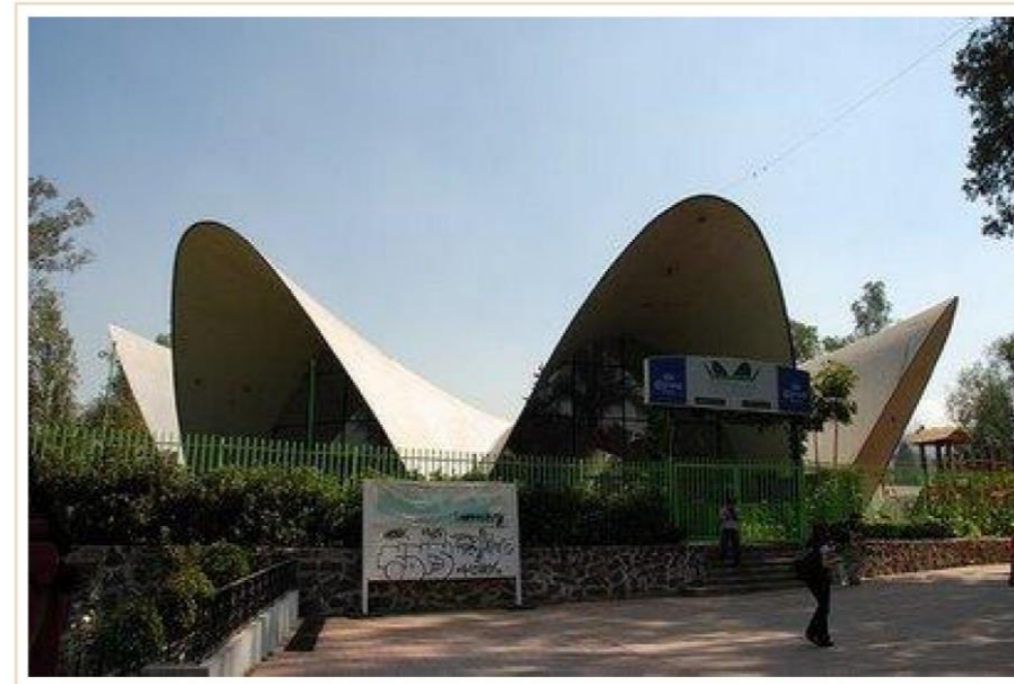
Figure 3.5 - Groined Vaults of three intersected Hypars – Plan, Picture of sample structure, Section and Aerial View.



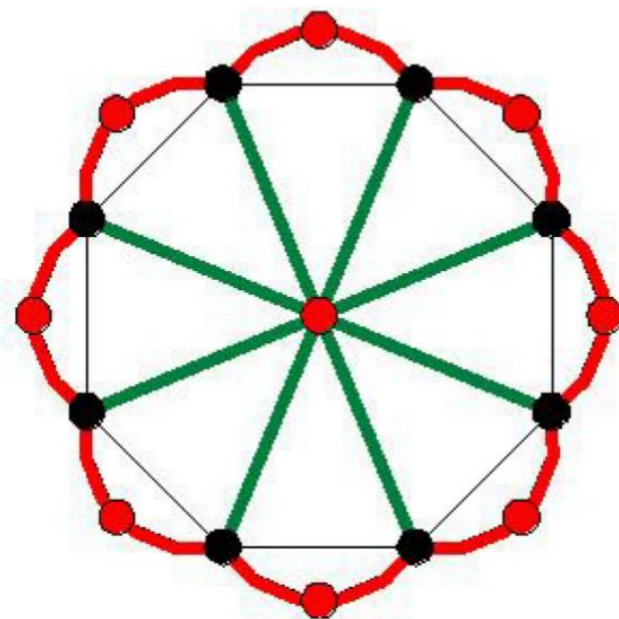
D. - MULTIPLE POLAR ARRAY OF GROINED VAULTS.



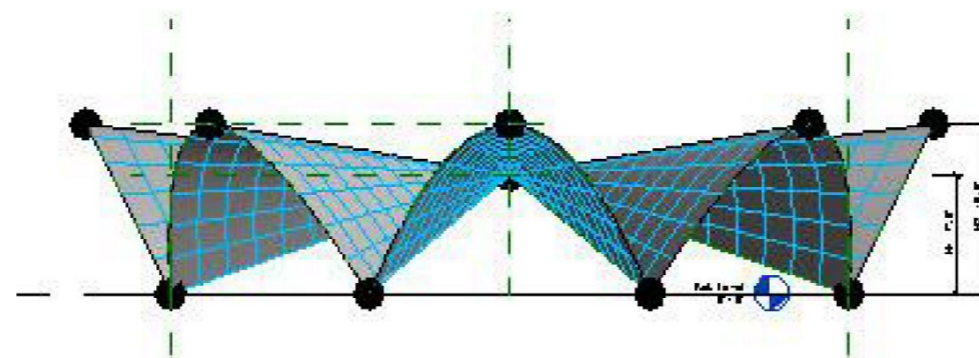
ISOMETRIC



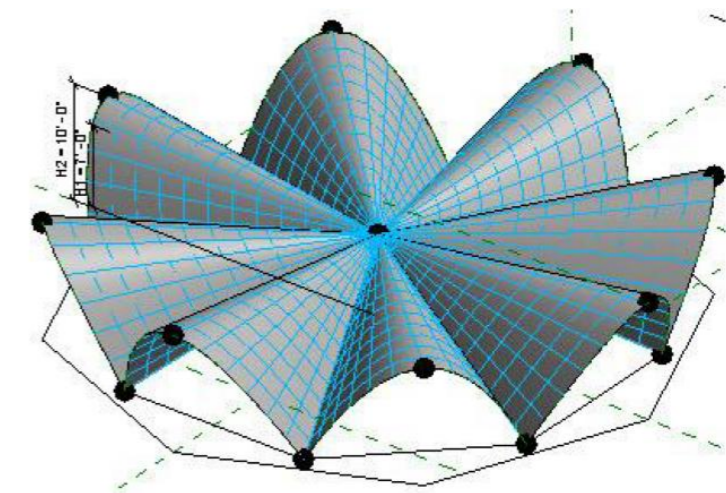
Los Manantiales, Xochimilco, Mexico, 1958 – by: F. Candela



PLAN



SECTION

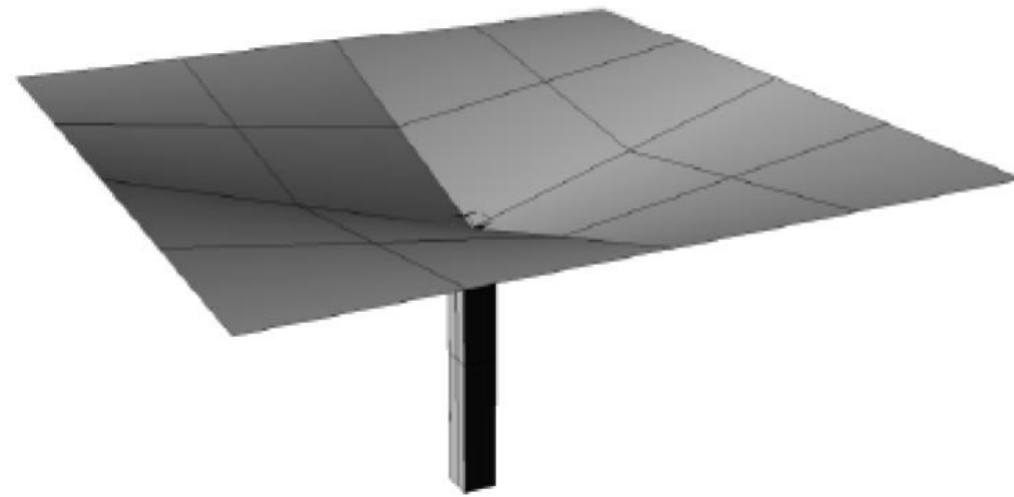


AERIAL VIEW

Figure 3.6 – Multiple polar array of Groined Vaults - Isometric, Picture of sample structure, Plan, Section, and Aerial View.

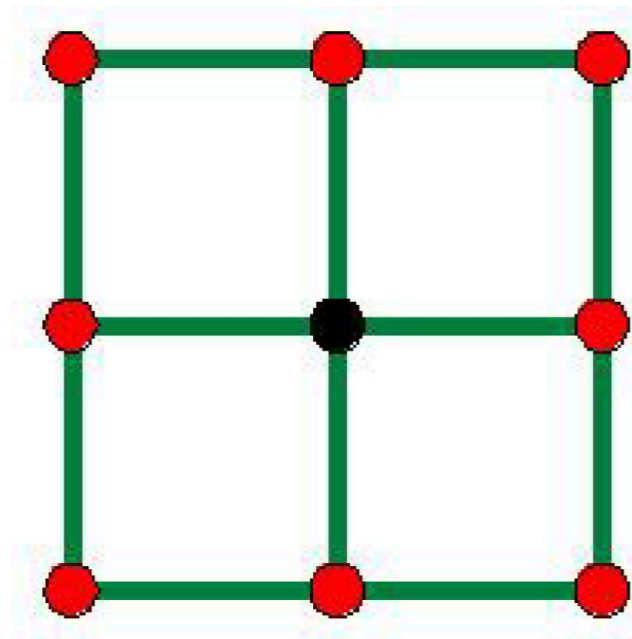


E. - FREE STANDING INVERTED UMBRELLAS

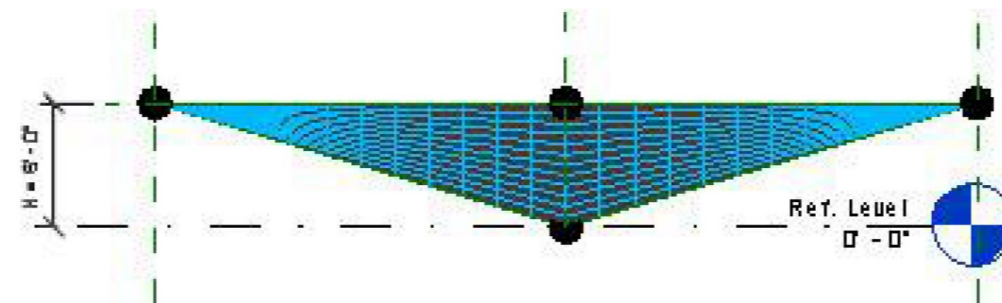


Warm Mineral Springs Inn Motel, North Port, FL, 1958– by Candela, Today Demolished.

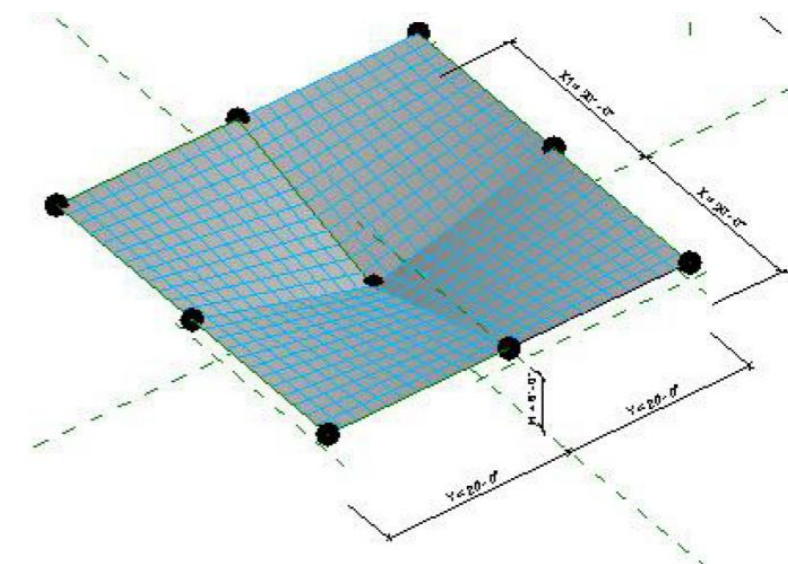
ISOMETRIC



PLAN



SECTION

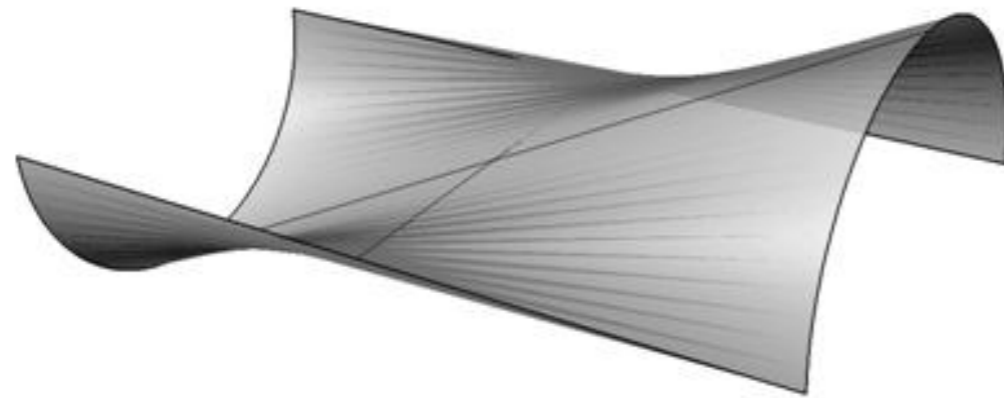


AERIAL VIEW

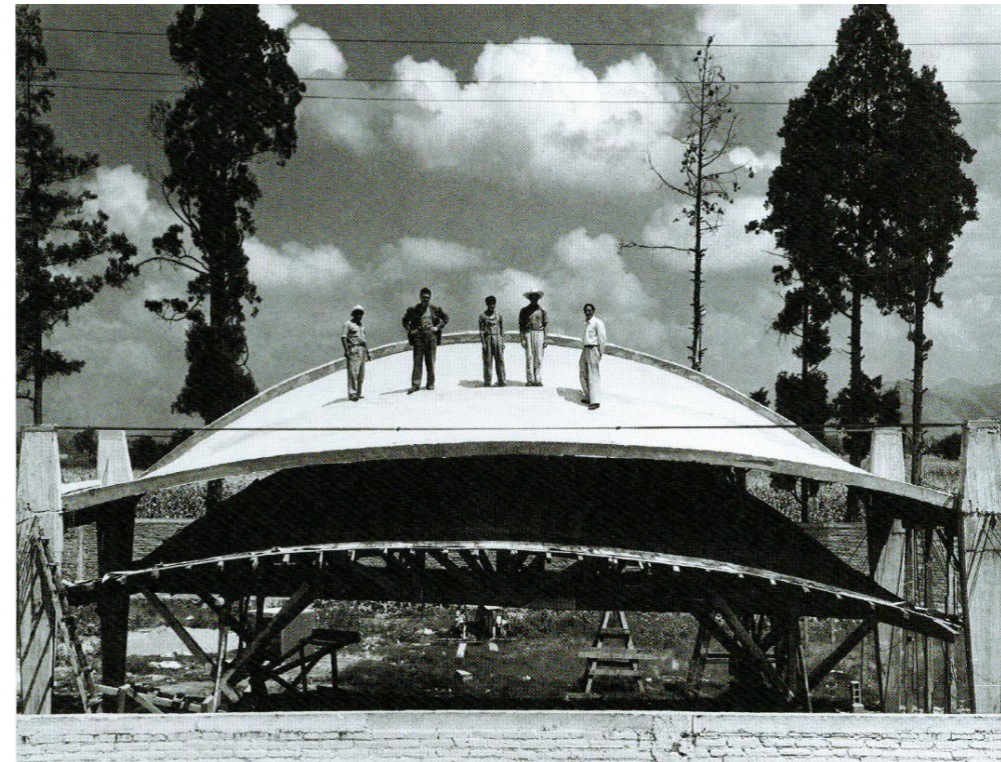
Figure 3.7 – Free Standing Inverted Umbrellas - Isometric, Picture of sample structure, Plan, Section, and Aerial View.



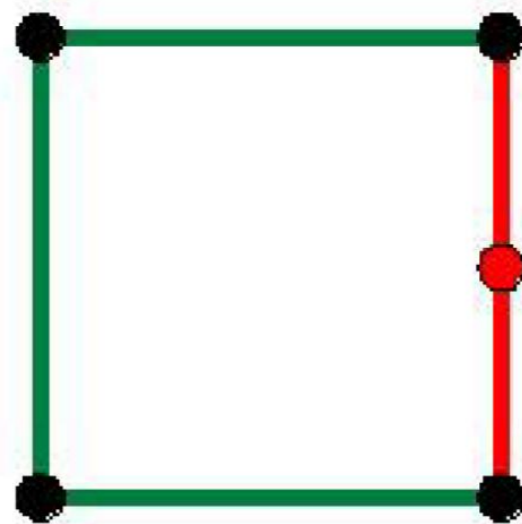
F. - CONOID



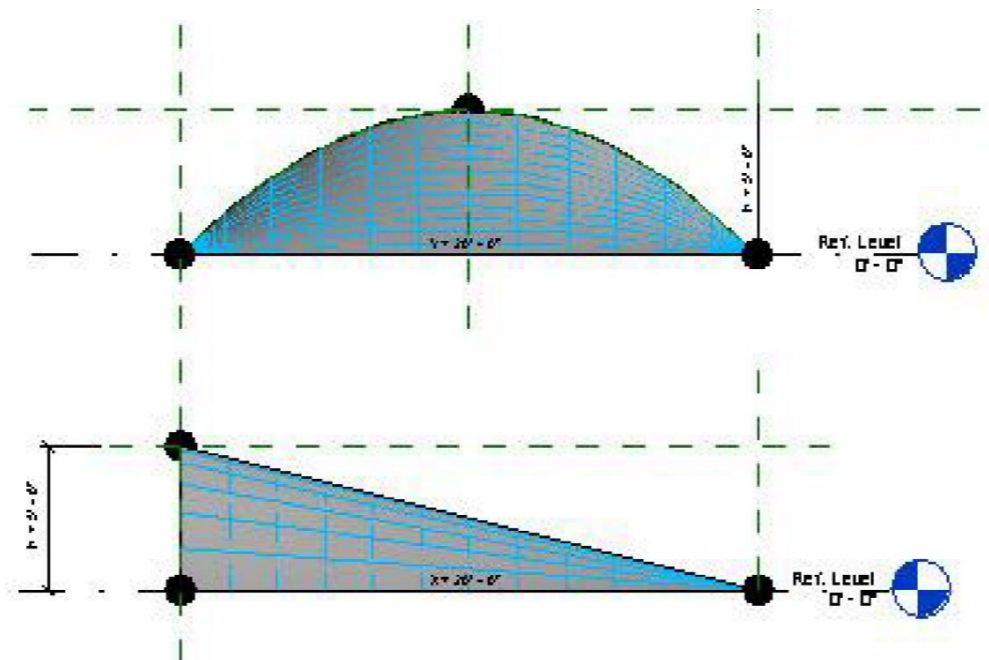
ISOMETRIC



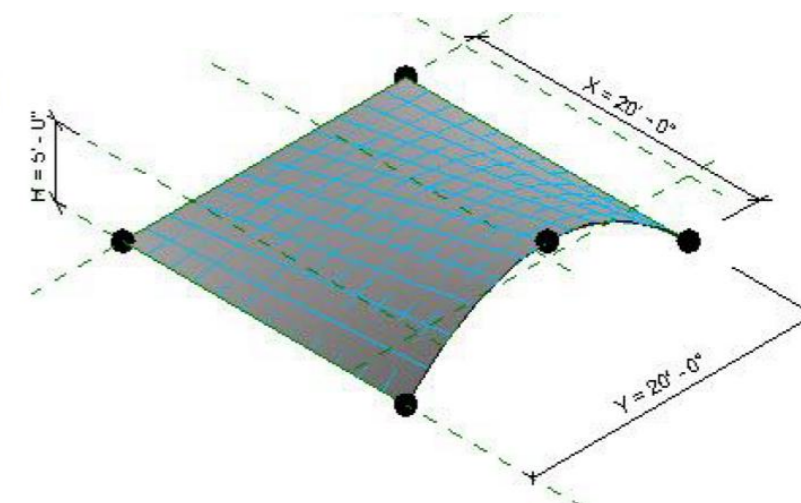
Experimental Conoid, Mexico City, 1950 – by F. Candela



PLAN



SECTION

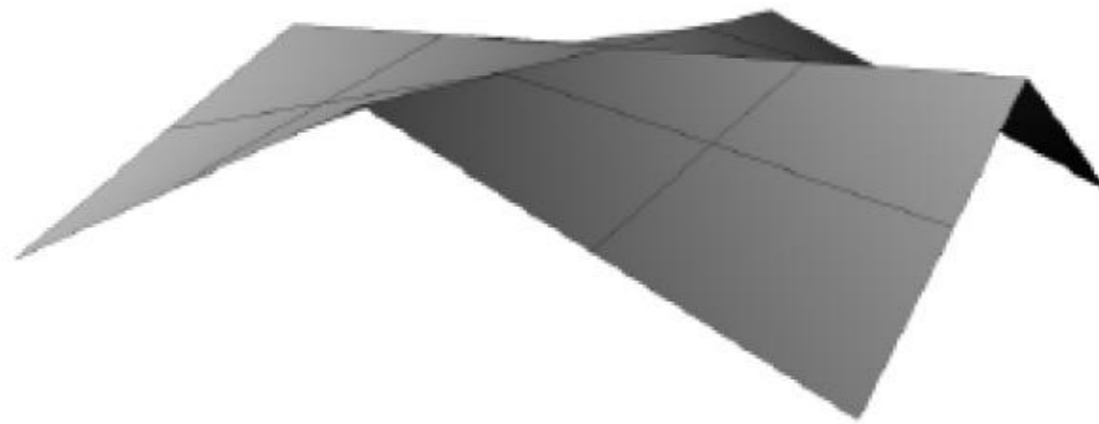


AERIAL VIEW

Figure 3.8 – Conoid - Isometric, Picture of sample structure, Plan, Section, and Aerial View.



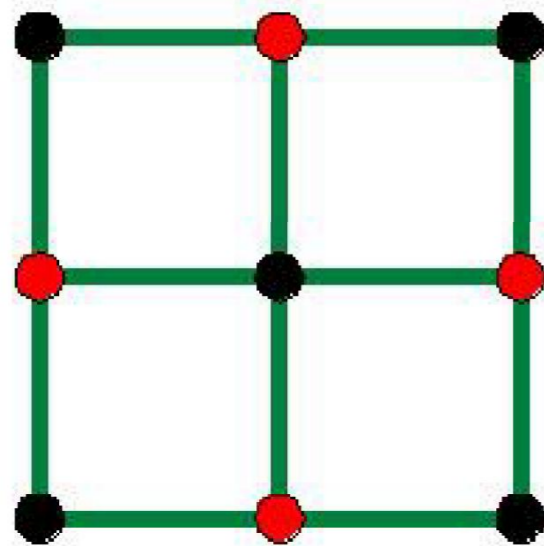
G. - INTERSECTING GABLED ROOF SHELLS



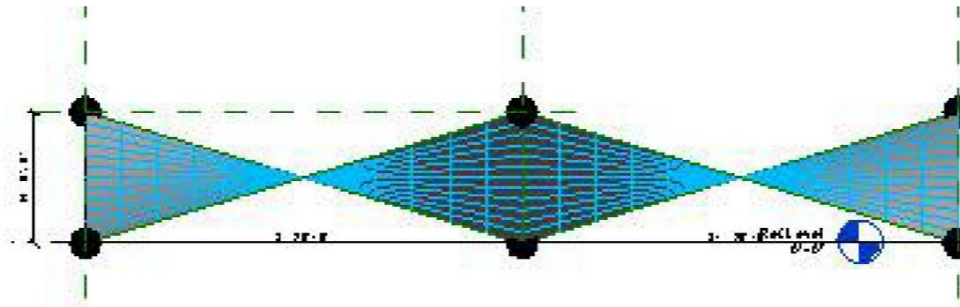
ISOMETRIC



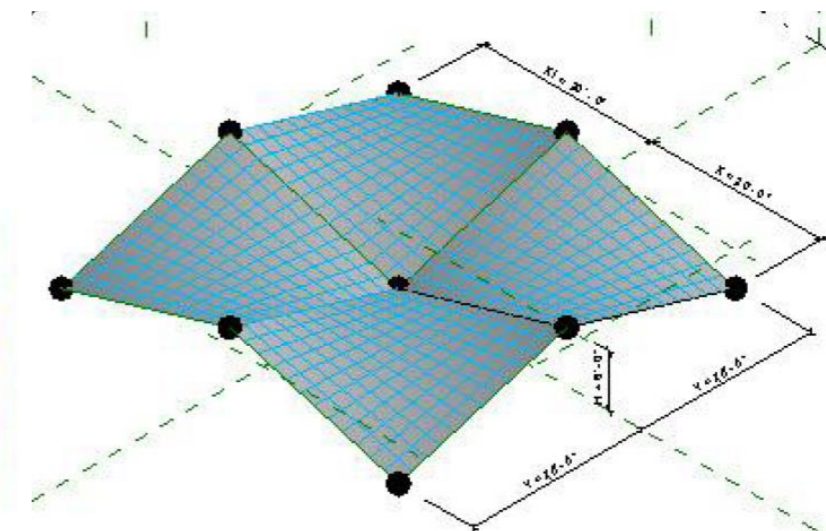
Denver Courthouse Square, Denver, CO, 1958 – by: A. Tedesko “Demolished in 1996”



PLAN



SECTION

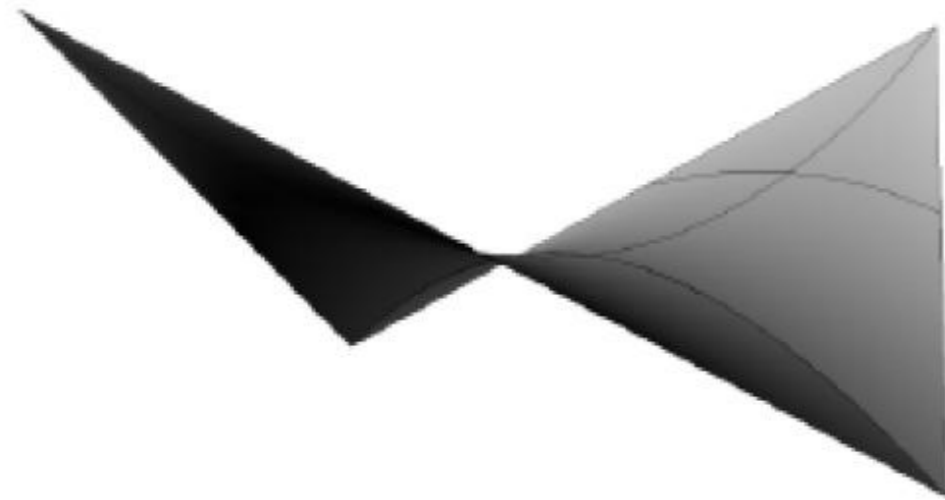


AERIAL VIEW

Figure 3.9 – Intersecting Gabled Roof Shells - Isometric, Picture of sample structure, Plan, Section, and Aerial View.



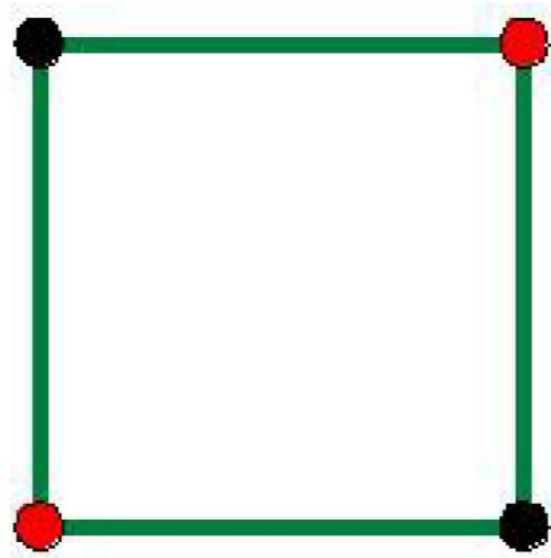
H. – DOUBLE HYPAR CANTILEVERS



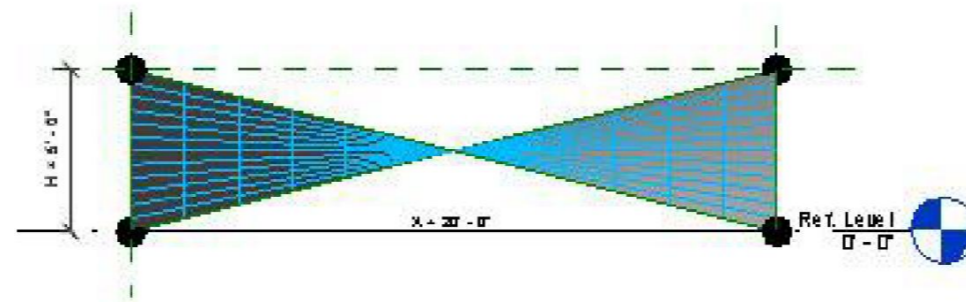
ISOMETRIC



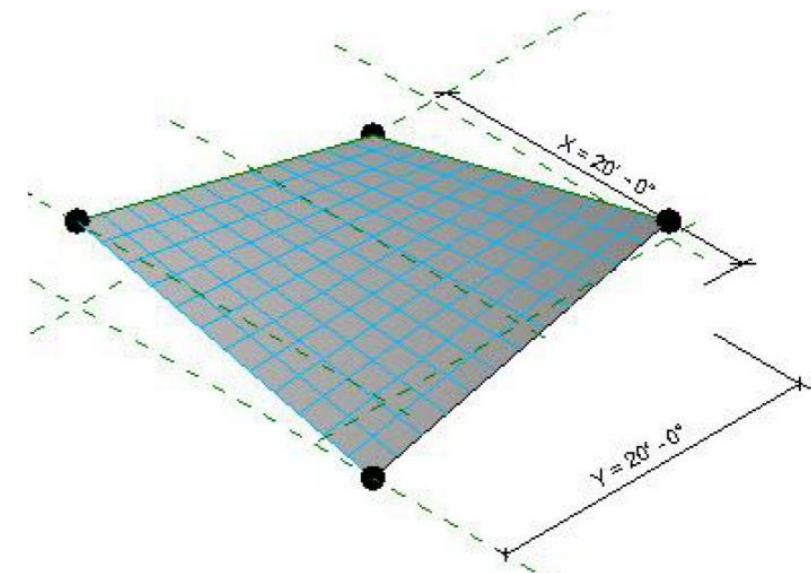
El Altillo Chapel, Mexico City, 1963 – by: F. Candela



PLAN



SECTION



AERIAL VIEW

Figure 3.10 – Double Hypar Cantilever - Isometric, Picture of sample structure, Plan, Section, and Aerial View.



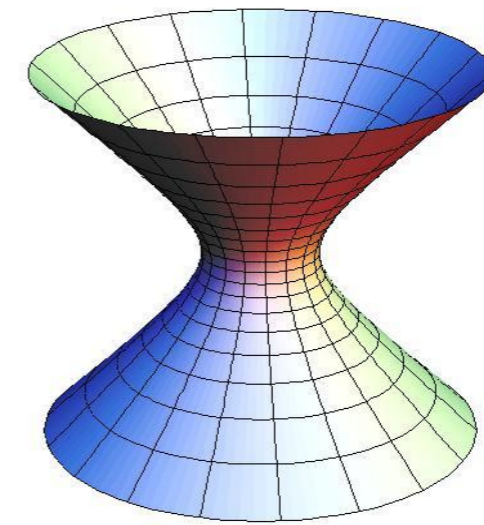
HYPERBOLOIDS



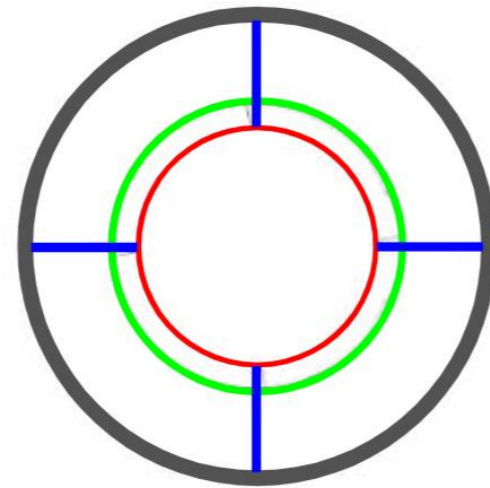
ISOMETRIC



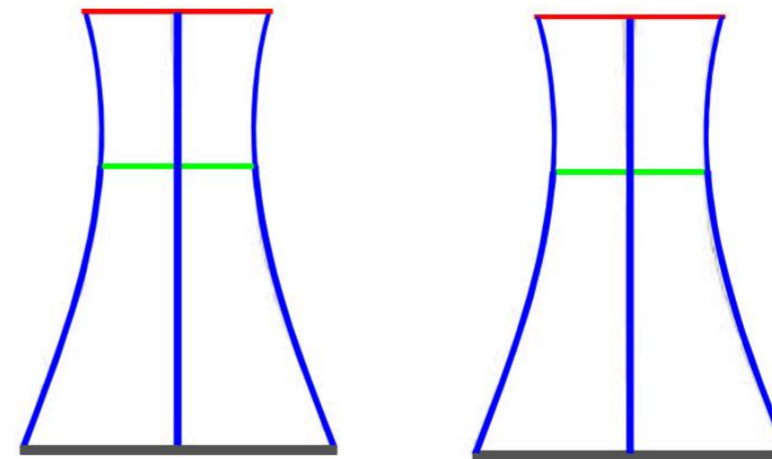
Cooling Towers, Europe



AERIAL VIEW



PLAN



ELEVATIONS

Figure 3.11 – Hyperboloids - Isometric, Picture of sample structure, Plan, Elevations, and Aerial View.



3.3 - ENGINEERING ANALYSIS AND DESIGN OF MEMBRANE SHELLS

ENGINEERING ANALYSIS OF SHELLS - Membrane Shells in general terms are defined as those curvilinear surfaces that support the external forces, pressures, and environmental effects by means of developing internal forces which are mostly axial tension, compression, bending, and shear stresses in the plane of the curved surface. Fig. 3.10 below describes the simplified analytical formulation of external forces and internal forces in curved surfaces.

The bending and torsional moments in thin membrane shells theory are mainly neglected and may be considered to be zero for the purposes of the high-order differential equations formulation needed to solve the thin membrane shell equations of equilibrium and compatibility of displacements. The membrane theory is a reduced form of the more generalized bending theory where the effects of bending and torsion are included in the overall system of partial differential equations.

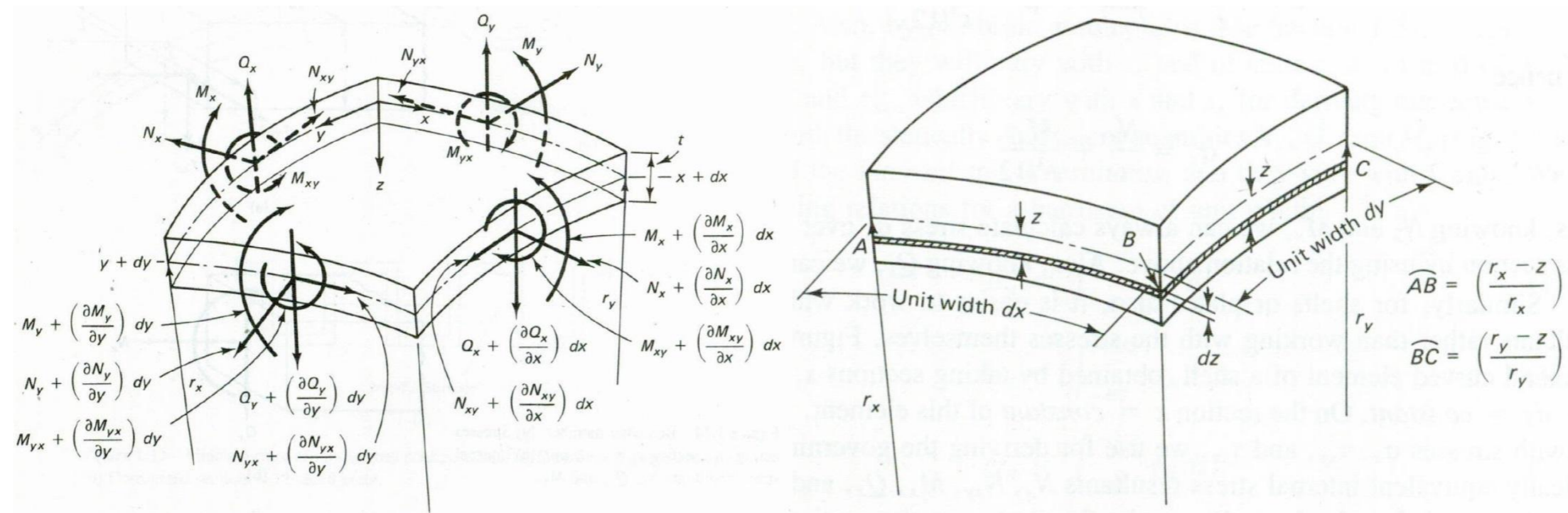


Figure 3.12 – Generalized curvilinear shell element with internal stress resultants, radius of curvature, and middle surface definitions.



Following is a description of the terminology commonly used in the mathematical formulations of the generalized shell element internal stress resultants, forces, unit width of the shell element dx , dy , and the radius of curvature for the solution of the partial differential equations:

- $N_x, N_y =$ Axial Tensile or Compressive Stresses in the x and y axes of the shell element.
 $Q_x, Q_y =$ Shear Bending Stresses in the faces perpendicular to x and y axis of the shell element.
 $M_x, M_y =$ Bending Moments along the x and y axes of the shell element.
 $N_{xy}, N_{yx} =$ Shear Torsional Stresses in the faces perpendicular to x and y axis of the shell element.
 $M_{xy}, M_{yx} =$ Torsional Moments along the x and y axes of the shell element.
 $r_x, r_y =$ Radius of Curvature of the curvilinear surface with respect to x and y axis of the shell element.

Generally the internal stress resultants noted above vary across the thickness of the cross section of the shell elements. For each particular case of a shell structure there will be a set of corresponding partial differential equations which can be solved to determine the internal stress resultant forces, the corresponding displacements of the free nodes of the shell elements in space, and the corresponding support reactions at the boundary points of the shell structure. For the shell structure to be stable and produce an acceptable solution, the partial differential equations shall be resolved to satisfy the following conditions:

- a. Equilibrium of forces in x , y , and z directions shall be satisfied for all nodes of the shell structure.
- b. Compatibility of deformations shall be maintained throughout the entire surface of the shell structure.
- c. Support Reactions shall be compatible with the boundary conditions at the points of support of the shell structure.
- d. Material Properties of the shell elements represented by their corresponding stress-strain curves in tension and compression shall be defined.

The middle surface of the thin shell passes through the centroid of the thickness of the shell which is the plane where the internal stresses noted above are assumed to act in the shell structure. In reality the stresses and internal forces vary across the thickness of the shell but due to the small thickness dimension (along the z axis), compared to the other two shell surface dimensions along the x and y axis normal to the z axis, then for all practical and simplified purposes it can be considered that the internal stresses and forces for thin shells are uniformly distributed across the thickness of the shell.

The basic assumption is that the external forces will produce internal stresses and forces which pass thru the center line of this three-dimensional middle surface defining the centroid of the thin concrete shell.



Therefore for thin concrete shells we work with the internal stress resultants rather than with the distribution of the internal stresses across the thin concrete section, which for practical purposes of design are given in terms of internal stress per unit length along the x and y axis of the shell surface, very similar to what is done with tensioned membrane structures, where the tensile stresses in the fabric/membrane are given in terms of force per unit length of the membrane surface in the warp and weft directions of the curvilinear shape of the membrane surface.

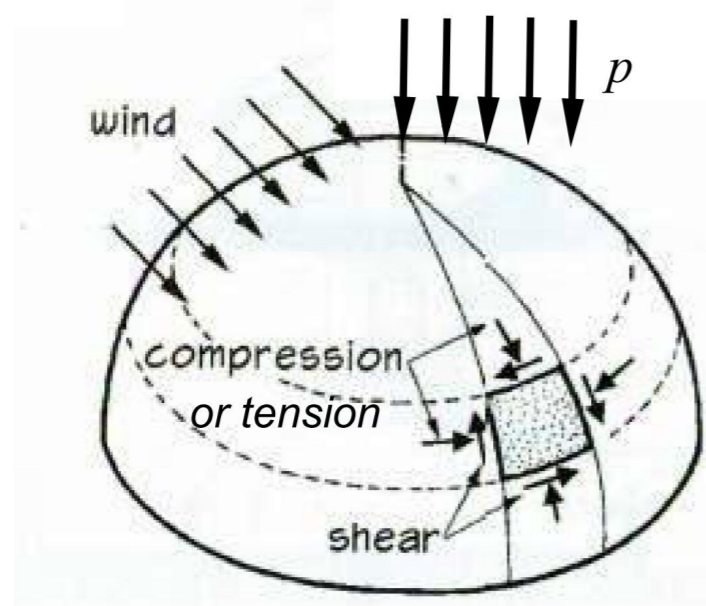
Having the bending and torsional moments be zero, then the system of equations can be tremendously simplified leading to more simplified system of equations that can be more easily solved by the principles of basic equilibrium of forces and simple boundary conditions of the supports in the form of pinned ends.

p = External Pressure

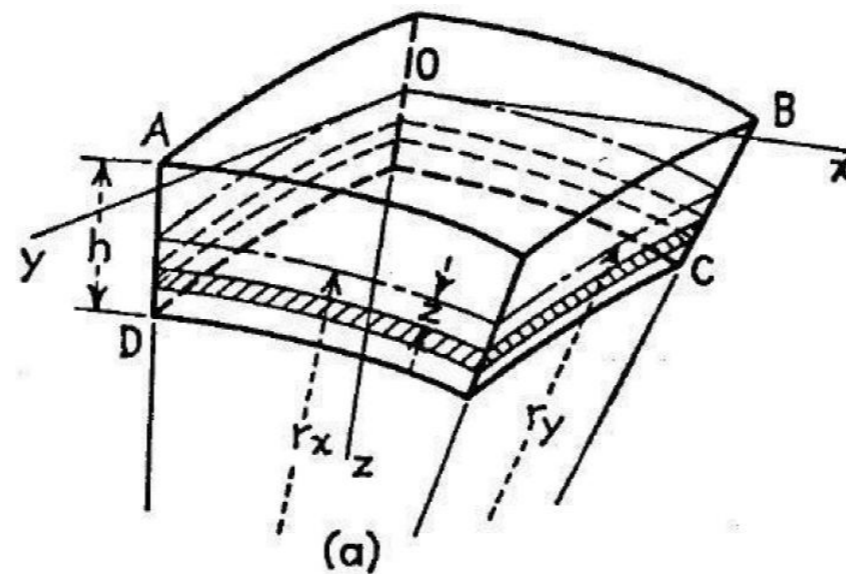
t = Thickness = h ; r = Radius of Curvature

N_x , N_y , and N_{xy} membrane forces

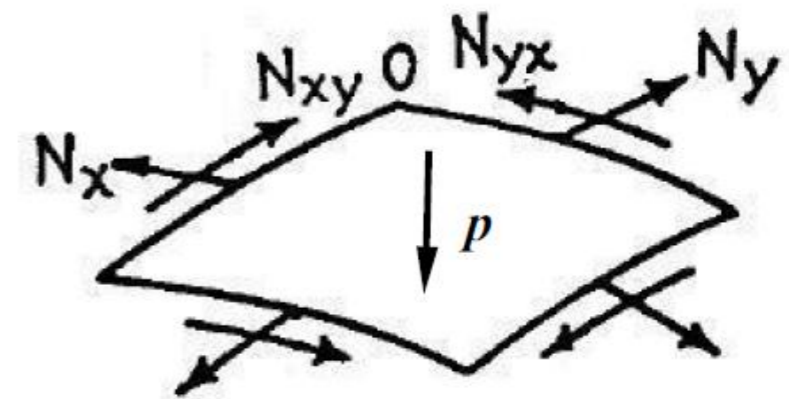
$$\sigma = \text{Membrane Stresses} = p \cdot (r/t)$$



Semispherical Shell



Synclastic Curvature: $r_x (+)$ and $r_y (+)$



Membrane Forces in small shell element

Figure 3.13 – Basic diagrams of Membrane Shell structure, Radius of Curvature, and Shell external loads and internal forces.



Based upon the basic thickness dimension of the shell itself and its plan dimensions and curvature, synclastic and anticlastic shells have been built in the past years, displaying an ample variation of radius of curvature to thickness ratios which can be found to vary in the range of: $20 < (r/t) < 1000$. A typical value of ratio of shell thickness to Span of shell (t/L) of 1/500 is commonly considered to be a thin concrete shell.

Materials used to build shells can be of a variety of different engineering products commonly found in the civil, mechanical, and aeronautical structures. For buildings in the civil construction industry we could find the use of timber and conventional wood-plywood, cross laminated timber (CLT), and reinforced concrete among others, in the mechanical industry we could find the use of metal and steel for pressure vessels, liquid storage tanks and containers, among others, in the aerospace industry we could find the use of aluminum, fiberglass, honeycomb composites, grid-shells and latticed fuselages and composites to form light weight and strong shell forms.

It is important to mention in this section that every shell designer shall identify and select the most appropriate material properties and design parameters to be used for both the analysis and design process of the shell structure. Stress-strain relationships, modulus of elasticity, poisson's ratio, tensile, compressive, and shear limit strength values, shear modulus, ductility limit values are some of the key analysis and design parameters to have available during the shell design process.

Membrane shells are well suited to extend and cover long span of building spaces such as roof structures due to the advantage of being able to carry loads with small thin members and minimum of deflections. These long span thin curved surfaces can be assimilated to those of soap-film membranes built with internal air pressure that will cover long span areas with extremely small thicknesses, or can also be assimilated to eggshells which are able to resist high external pressure in spite of being of very small thin thickness. These curvilinear synclastic or anticlastic surfaces which have their thicknesses small compared to their other two curvilinear spatial dimensions are commonly labeled to be Thin Shells. The subject of thin concrete folded plates are outside the scope of this study and will not be part of this Thesis.

The engineering analysis of different forms of membrane shells under a variety of external loading condition and supported at their boundaries by either pinned or fixed supports can be accomplished by three very distinctive and separate methods that can be identified as follows:

- A. Mathematical closed formed solutions have been derived based upon specific governing differential equations for given equilibrium of forces, boundary, loading conditions, material stress-strain relationship, and elastic stability. Extensive derivations and formulations are available in the textbooks of Theory of Plates and Shells and Elastic Stability of Timoshenko and other authors given in the References.



The analysis of buckling of bars, plates, and shells plays a key role in the overall performance of thin shells, since the small thickness and the long span of shell structures make them prompt to overall buckling failure and local buckling instability.

To understand the complexity of the mathematical analysis of a generalized form of shells, one has to start by recognizing that a shell structure of any given form subjected to certain loading conditions could always be analyzed and its internal values of normal axial stress, bending, shear, and torsional stresses, and their corresponding deformations could be solved by finding the solution to the general equations of three-dimensional Theory of Elasticity. The equations being solved are very complex and are solvable for only certain specific and idealized cases of loading and support conditions.

Therefore for a majority of practical shell structures that may deviate from the specific mathematical cases being formulated and solved, the mathematical closed formed solutions are not always suitable to be applied to the specific practical shell designs and other different simplified theories for different categories of specific shell structures have to be established which will only be applicable to the cases being formulated.

For the case of bars, beams, shafts, cables, and other linear structures that can be represented by straight or curved lines, which had dimensions in one direction that were very large compared to the other two directions, then the simplified “theory of lines” was described by a second order differential equation which were solved for most practical linear problems and produced results that were in general agreement with the experimental observations and advanced theoretical computations performed on this linear structures.

For the case of linear beams which are intended to resist the external loads mainly in bending and shear there is a “theory of beams” where the internal stresses and deflections along the length of the beam can be found by solving a fourth-order differential equation.

For the case of plates and shells where the structures are represented by a surface which may be plane or curved and where the loads are applied perpendicular to these surface planes, simplified mathematical theories have also been developed and labeled, “theory of plates” and “theory of shells”. For the more generalized case of shells that will be subjected to loadings both normal and tangential to their surfaces and they will develop and resist the loadings by means of internal in-plane normal stresses as well as by bending and shear stresses, then we will have the more generalized case of an eight-order partial differential equation in terms of the deformation and the x and y coordinates over the surface of the shell.



In general terms the derivations of the governing partial differential equations to solve the plates and shells problems follow the same basic steps that were implemented to derive the differential equations for bars and beams in Strength of Materials with the corresponding adjustments of boundary conditions, loadings, and support assumptions. Kelkar and Sewel in their book “Fundamentals of the Analysis and Design of Shell Structures” listed in the References provide the mathematical derivation of governing differential equations and its solutions for some limited cases of practical applications of thin shell concrete structures such as circular cylindrical, barrel vaults, spherical, hyperbolic paraboloids, and surfaces of revolution with axisymmetrical loading and support conditions.

- B. Approximate and simplified analysis methods which are based upon the principles of mechanics, must include the following principles: a) the equilibrium of forces, b) compatibility of deformations, c) stress and strain relationship of shell material, and d) flow, and distribution of forces, and e) the support conditions. In the past, Isler and Candela developed and implemented the analysis and design of small-scale prototypes of reinforced concrete thin shell structures. Particularly early shell designers rely on small scale models that were built to scale of the large size structures to be built and were tested under extreme loading conditions to prove the strength and stability of the design of their shells. Felix Candela built and tested many of his early hyperbolic paraboloid (Hypars) reinforced concrete shells in Mexico. In Europe Heinz Isler also experimented with thin shell structures. Samples of the tested models are included in other sections of this Thesis and are also included in some of his Technical Articles included in the References section at the end of this Thesis.

For those cases where the closed form mathematical solutions based upon the partial differential equations described above in Section A become impractical or very difficult to accomplish, then it is possible to divide the shell structure into two or more primary structures in two or three dimensional sections which do have mathematical solutions that satisfy the boundary conditions, loading conditions, and supports of the overall shell structure. The overall shell structure is sectionalized along points of discontinuity of displacements to create substructures that are in themselves statically stable and do have compatibility of deformations and satisfy the boundary conditions and supports along the points of connectivity. The substructures can be discretized and a formulation based on the Flexibility or Stiffness analysis methods can be applied to each substructure, maintaining always the deformations and support compatible conditions between the substructures and the overall structure.

The Flexibility and Stiffness methods are matrix formulations that can be solved for the selected number of discrete segments of the substructures, very similar to a Finite Element Analysis which will be discussed in Chapter 5. For the particular cases of the substructures,



the forces and displacements that occur at the interface of the junction of the substructures need to be compatible and must be in equilibrium, a matrix solution process takes place which is done in the formulation of the flexibility and stiffness methods. This procedure is very similar to what is commonly applied to the solution of statically indeterminate cases of beams and frames. Compatibility of displacements, deformations, and equilibrium together with the stress-strain material relationships for the shell structure must be maintained at all times with the boundary and support conditions. Appropriate coefficients of flexibility and stiffness terms shall be established for the matrix formulation.

In summary either the Flexibility or the Stiffness methods can be formulated as approximate solutions to shell structures with different loading, supports, shell dimensions, and material properties. Computer programs can be used to obtain solutions of shell configurations with varying thicknesses by dividing the different sections of the shell into a number of elements that can have different thicknesses. The shell designer must always verify the results obtained by any given selected approximate method of analysis to make sure that the internal stresses, forces, support reactions and shell displacements make sense and are realistic with the applied loading and boundary conditions.

Candela and Isler type of shells that are shown in Chapters 2 and 3 can be analyzed using the simplified method of subdividing the overall shell structure in individual substructures composed mostly of funicular parabolic curved arches that will support the discretized elements of the shell structure and transfer the total selfweight of the structure and the applied external forces onto the supporting foundations of the shell structure.

The analysis and design of thin concrete shells can also be accomplished by using tabulated solutions for some specific and straightforward commonly type of shells of revolution cylindrical, spherical, conical, barrel vaults, and folded plates that have been produced by several recognized institutions dedicated to the subject of reinforced concrete structures, thin shell structures, and civil engineering projects. In the USA (United States of America) Tables have been published in the past by the ASCE (American Society of Civil Engineers), ACI (American Concrete Institute), and PCA (Portland Cement Association). In Europe the EUROCODE 2 and the IASS (International Association for Shell and Spatial Structures) Working Group No. 5 has published recommendations for the design and construction of reinforced concrete shells and folded plates. In Asia the Indian Standards Institution (ISI) and Codes also provides specific recommendations for the analysis, design, and detailing of reinforced concrete shells.



The Tables published by the ASCE, ACI, PCA, and some other ones published by researchers such as Parme and Conner among others and listed in the references provide tabulated stress parameters and internal stress resultants of shear and bending moments that can be used for preliminary and basic designs for some specific types of reinforced concrete shell structures such as spherical, semispherical, cylindrical barrel vaults, and circular arch vaults. It is important to point out here that those Tables do not provide generalized solutions for all types of reinforced concrete shells, therefore their use is strictly limited to those cases for which the specific tabulated solutions were developed and the shell designer is alerted to be extremely careful when using the tabulated values to make sure that the boundary and loading conditions, edge and support conditions for the shell under consideration matches those parameters for which the solutions are presented in tabulated form. The use of Tables therefore is very limited and it does not always apply to all shell configurations.

Kelkar and Sewel in their textbook of Analysis and Design of Shell Structures present some examples for applications of using the Tables of ASCE and Parme and Conner for cylindrical shells and multibarrel shells.

The IASS publication listed in the References include specific and detailed recommendations for the thickness of reinforced concrete shells for roof structures, minimum percentages or ratio of steel reinforcement to cross sectional area of the shell, spacing and placing of the steel reinforcement, minimum cover of the steel reinforcement, and the size of the recommended steel reinforcing bars of the concrete shell that will satisfy the demand of the external forces producing the internal stresses and forces for the proper design for longitudinal, transverse, bending, shear, and shrinkage and temperature reinforcement of the shell. . The items noted above are of paramount importance for the appropriate long term behavior of reinforced concrete shells. Similar recommendations are also provided in the American Concrete Institute (ACI), Eurocode (EC), Japan Concrete Institute (JCI), and Indian Standards Institution (ISI).

- C. Computer Programs to solve both the partial differential equations and the simplified methodologies to obtain the internal stresses, force resultants, and shell displacements can be implemented to allow for a much easier and practical solution to the different types of thin concrete shells that would like to be solved. Once the equations that represent the solutions to the partial differential equations and to the simplified methodologies of analysis of shells have been obtained, then it is possible to make use of several commercially available computer software such as EXCEL, MATHCAD, MATHLAB, VISUAL BASIC, and other similar programs that allow for a quick and accurate solution of the established solutions of the partial differential equations and the simplified approximate methodologies.



The ACI 318-14 Building Code has recently incorporated the “STRUT-AND-TIE MODEL” (STM) for analysis and design of structural members in Chapter 23 of the Code. This methodology is some type of “TRUSS ANALOGY” method which allows the discretization of large structural members into a system of two-dimensional or three-dimensional truss members composed mainly of STRUTS and TIES. The ACI 318 Code defines Strut-and-Tie model as: “A truss model of a structural member or of a D-region in such a member, made up of struts and ties connected at nodes, capable of transferring the factored loads to the supports or to adjacent B-regions”.

In Chapter 23 the ACI 318 Code indicates that: “Strut-and-tie model design procedure shall be permitted to design structural concrete members or D-regions in such members, by modeling the member or region as an idealized truss. The truss model shall contain struts, ties, and nodes as defined in Section 23.1. The truss model shall be capable of transferring all factored loads to the supports or adjacent B-regions. Furthermore: “The strut-and-tie model shall be in equilibrium with the applied loads and the reactions. In determining the geometry of the truss the dimensions of the struts, ties, and nodal zones shall be taken into account.

As per ACI 318 Code Chapter 23: “In a three-dimensional strut-and-tie model, the area of each face of a nodal zone shall not be less than that given for a two-dimensional nodal zone, and the shape of each face of the nodal zones shall be similar to the shape of the projection of the end of the struts onto the corresponding faces of the nodal zones”.

Finite Element Analysis (FEA) computer programs codified on the basis of the traditional stiffness method provide a more generalized type of solution for a variety of shell structures of configurations which are not the traditional circular arches, cylindrical, spherical, barrel vaults, and other similar ones that can be analyzed using the partial differential equations. The FEA allows for the analysis of shells with irregular boundary, supports, and edge conditions, symmetrical and unsymmetrical loading conditions, varying thickness over different sections of the shell surface, and other different geometrical conditions and material properties. The stress-strain relationships for the type of shell material can be easily modeled using the FEA method. The type of 2-dimensional or 3-dimensional type of shell element can also be specified using either planar or curved type of elements.

In summary the main objective when performing the analysis of shells by any of the three methods described in sections A, B, or C above, is to determine for a given type of shell structure, either of anticlastic or synclastic curvatures as shown in Figures 3.12, 3.13, and 3.14 below, the internal stress resultants along the principal axes of the shell elements, variations in the distribution of stresses along the discontinuities of the shell edges and supports, forces along the edges of the shell, local and global deformations of the shell nodes, buckling modes of the overall shell structure



depending on the shell thickness and radius of curvature, magnitude of major bending stresses at points of high localized concentrated forces on the shell surface, and any other major stress concentrations that can occur on the shell surface due to openings and cutouts of the shell under consideration.

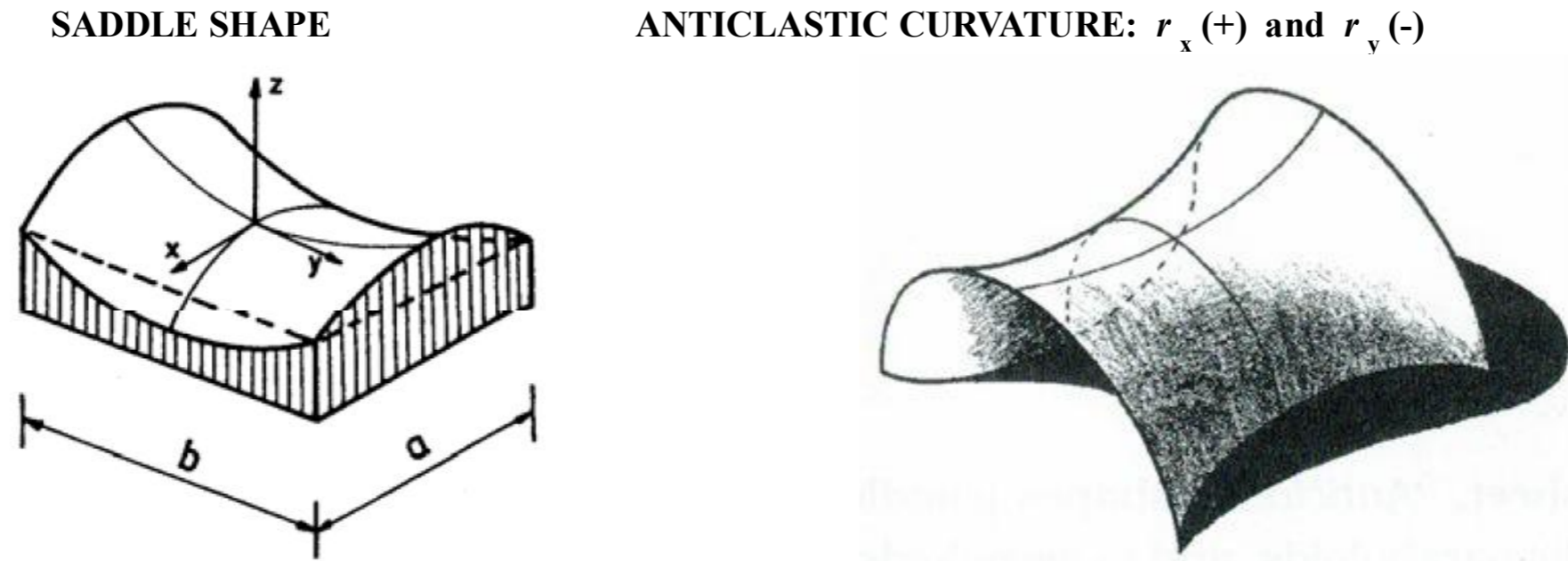


Figure 3.14 – Anticlastic Saddle type of Shells with double curvatures of opposite signs.

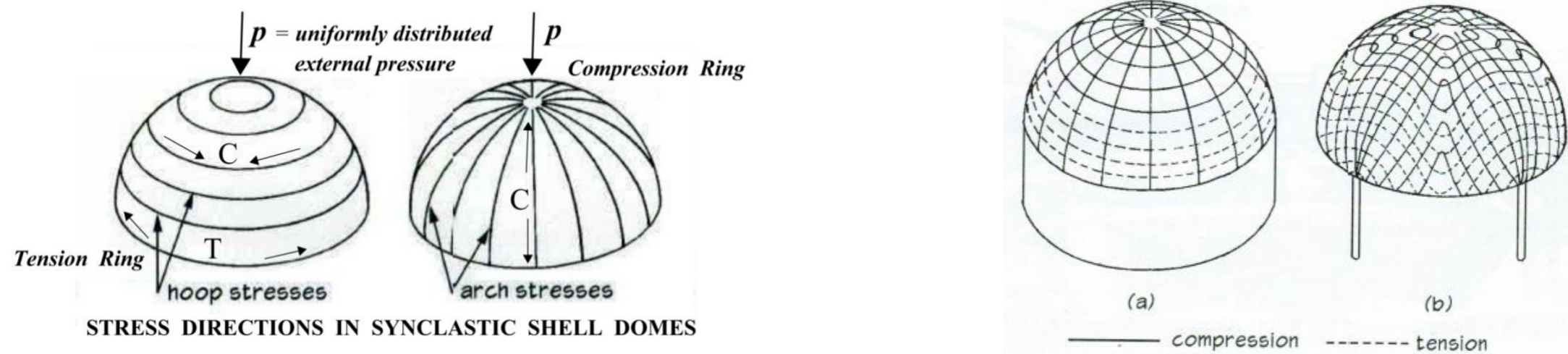


Figure 3.15 – Synclastic Spherical type of Shells with radius of curvature of same sign and different types of supports.

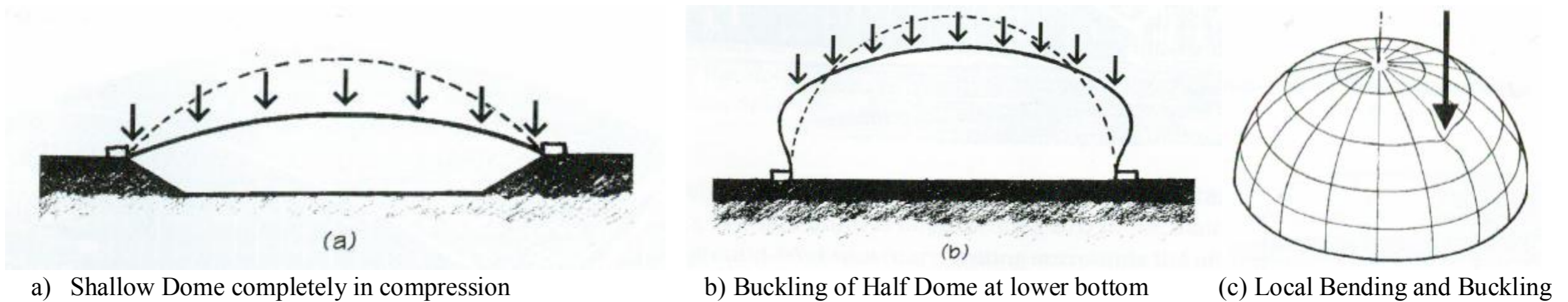


Figure 3.16 – Deformations and Buckling Shapes of Arched and Semispherical Shells under external uniform and concentrated loads.

There is a misconception that the adequacy of thin concrete shells is determined only by its capacity to adequately resist axial compressive stresses on the concrete section alone, the thickness of the shell plays an important and key role in the overall stability of the shell structure. The higher the ratio of the radius of curvature of the shell to its thickness (r/t) the more critical is the stability of the shell to support the buckling stresses produced by the externally applied forces on the surface of the shell. Therefore having a reinforced concrete shell with internal axial compressive and tensile stresses which have been obtained from a first order static analysis does not necessarily mean that the three-dimensional shell will be stable and strong enough when it is actually built.

The overall stability and strength of the thin concrete shells is controlled primarily by its capacity to resist internal stresses produced by the different modes of buckling of the thin concrete shell. Therefore for the most part BUCKLING controls the final design of thin reinforced concrete shells with single or double curvature.

ENGINEERING DESIGN OF SHELLS - After the engineering analysis of thin shells have been completed, the engineer or shell designer will then proceed to provide the appropriate design for the selected type of shell materials. For reinforced concrete shells, the design shall include among others: the compressive strength of the concrete, f'_c , the diameter and spacing of the reinforcement bars selected for the main longitudinal, transverse, and temperature reinforcing bars all in conformance with the applicable building code of the locality where the reinforced concrete shell will be built. The reader is referred to the References chapter of this thesis for the applicable standards and codes pertinent to the design of shells.

In the USA, the ACI 318 Building Code, Chapter 19 - “Shells and Folded Plate Members” has a dedicated section specifically for the design and detailing of reinforced concrete shells. The ACI 318 Code in Sections 19.1.1 and 19.1.2 indicates that: “Provisions of Chapter 19 shall apply to thin shell and folded plate concrete structures, including ribs and edge members”, also states that: “All provisions of the ACI Code not specifically excluded, and not in conflict with provisions of Chapter 19, shall apply to thin-shell structures”. Additionally in Section 19.1.3 defines Thin Shells as: “Three-dimensional spatial structures made up of one or more curved slabs or folded plates whose thicknesses are small compared to their other dimensions. Thin shells are characterized by their three-dimensional load-carrying behavior, which is determined by the geometry of their forms, by the manner in which they are supported, and by the nature of the applied load”. In Section

In Europe, EUROCODE 2 (EC2) shall be used. In India, the Indian Standards Institution (ISI) shall be used, and in Japan, the Japan Concrete Institute (JCI) shall be used.

The reader is advised to always look for the latest and most current version of the applicable standards for the design of shells for the corresponding region where the shell will be built. This thesis is not intended to present all the specific design requirements for reinforced concrete shell structures, but to guide the reader to the applicable standards and codes. For other regions and countries not covered by the listed standards, the reader is advised to consult their own country to see which local or regional standards are of common use in their country.

For other materials such as timber, steel, or aluminum, the shell designer will then select the appropriate member sizes (width and depth of cross section), thicknesses or any selected square or rectangular tubes for grid-type trussed shells, and any specific bracing requirements that the shell structure will require for strength, stiffness, and stability.

In summary at the end of the engineering analysis process for a given concrete shell structure, the engineer shall obtain the following internal stresses and forces corresponding to the following actions over the cross section thickness of the shell structure:

- a) axial tension and compression, b) bending and torsional moments, c) transverse shears from bending and torsion,
- d) displacements of the shell surface free nodes in the x, y, and z directions, and e) support reactions.

The results listed above shall be valid to be used for engineering design of the shell structure only if the displacements of the free nodes of the shell surface are in stable equilibrium, the shell itself will not buckle under the external loads, and the stresses of the shell material will be below the allowable and ultimate strength of the materials for every internal type of stresses listed above. Therefore the shell designer shall first review carefully the results obtained from the engineering analysis of the shell structure before proceeding to perform a suitable engineering design.



Once the engineering analysis of the shell structure is completed and it has been verified that the shell will be stable, will not buckle, and will have internal stresses which will be below the allowable safe and ultimate strength of the shell material, then the shell designer can proceed to design the appropriate steel reinforcement for the axial loads, bending moments, shrinkage and temperature, and any required additional reinforcement for shear and torsional effects that may be significant in the shell structure.

Special attention shall be given to the appropriate and recommended thickness of concrete cover over the interior and exterior layers of steel reinforcement. Cracking of the thickness of the shell shall be avoided at all times to avoid moisture and water penetration into the inner parts of the concrete shell which may cause rusting and corrosion of the steel rebars.

The design of the reinforced concrete shell structure can be accomplished by applying either the elastic design method or the strength ultimate design methods with the applicable load and materials factors specified in the applicable building code for the locality of the shell structure. The selected reinforcement to satisfy the internal stresses and forces of the shell structure could be either small size high tensile strength reinforcing bars, wire mesh, and when appropriate depending on the shell dimensions and thicknesses, fiber reinforcement.

Depending on the applicable Building Code for reinforced concrete design of the country where the shell will be built, the shell designer shall recognize the fact that bending moments could develop at locations of the shell structure that may experience some restraining support conditions and alternate transitional positive and negative bending moments at changes of curvature of the shell surface. Therefore it is highly recommended to consider the placement of longitudinal and transverse reinforcement in two layers near the top and bottom surfaces of the shell to make sure that any bending moment is captured by the internal bending resistance of the steel rebars and concrete shell sections in compression.

At the end of the analysis and design process the shell engineer shall perform one final review of the overall shell structure to make sure that the provided shell configuration, dimensions, thickness, profile, curvature, span, and overall appearance that will satisfy the project specifications, performance requirements, functionality of the space covered by the shell, and the aesthetic curvilinear form dictated by the architect that will be compatible with the flow of forces and owner requirements.

Textbooks that contain extensive Analytical and Design procedures for thin reinforced concrete shells have been published and are recommended to be reviewed by shell designers to become familiar with the most appropriate steps for the specific type of shell structure being designed. Mathematical solutions to the most complicated shapes and free forms of synclastic or anticlastic type of reinforced concrete shells are not always possible due to the complexity of the partial differential equations, boundary and loading conditions.



Billington, Varguese, Farshad, Kelkar, and Sewel among other Authors have published academic textbooks listed in the References Section of this Thesis which contain detailed analytical equations and step by step design procedures for some of the most commonly found type of shell structures that had been built to date. Discussions on the subjects of partial differential equations, simplified methods, and use of Tables of ASCE, ACI, PCA and those of individual researchers are presented in the different textbooks of the Authors noted above.

3.4 - GRAPHIC STATICS ANALYSIS FOR MEMBRANE SHELLS

Hanging Cables and suspended Shells simply supported at their ends and under their own weight tend to take the shape of catenary curves that project the flow of their own selfweight of forces in a funicular form towards the supports. For small radius of curvature of hanging cables and shells the catenary curve can be approximated to the shape of a parabolic curve which for uniformly distributed weights or forces along the projected length of the span of the shell approximates very well to the catenary curve. Therefore for simplification and practical purposes a catenary curve can be approximately expressed as a parabolic curve, opening either upward or downward depending on the behavior of either a hanging tensile cable or a funicular compression shell. If we take the funicular or catenary shape of a hanging cable and we invert it and make it a solid surface in the form of a hardened curvilinear shell then the flow of tensile forces is inverted becoming compression forces over the shell thickness.

Samples of some architectural and engineering shell projects will be presented in Section 3.5 and Examples of concrete shells of small and large curvature which were built by Isler and Candela will be discussed in Section 3.7. It is interesting to observe the distinctive profiles of the type of low profile concrete shells designed and built by Isler in Europe and in contrast the high profile type of concrete shells built by Candela in Mexico. The higher the ratio of the shell sag to the span of the shell, the lower the horizontal reaction forces at the supports. Therefore it is very important that shell designers recognize these critical parameters when designing the overall structure of the shell and its supporting foundations.

It is then very important to study the basic mathematical equations to describe the geometrical forms of a circle, a parabola, and a catenary curve, that will best and accurately represent the type of hanging cables or funicular shells which are presented below. The relationship of the x and y coordinates can be calculated based on the mathematical expressions and can be graphically plotted in the x and y axis as shown in Figure 3.17.

A suspended cable that is subjected to a vertical uniformly distributed load along the length of the cable will form a catenary curve, with the parameter: $a = w/T_0$, where w is the magnitude of the uniformly distributed vertical load along the length of the cable, and T_0 is the horizontal tension

in the cable at its lowest point. Circle, $R = \text{Radius}$, $x^2 + y^2 = r^2$ Parabola, $p = \text{focal length}$, $y^2 = 4px$ Catenary, $y = (\cosh(ax) - 1)/a$; $a = w/T_0$



When a circle is inscribed in a section of a parabola of height d and width c , as shown in Figure 3.17, then some basic relationships between a circle and a parabola can be established and are presented below.

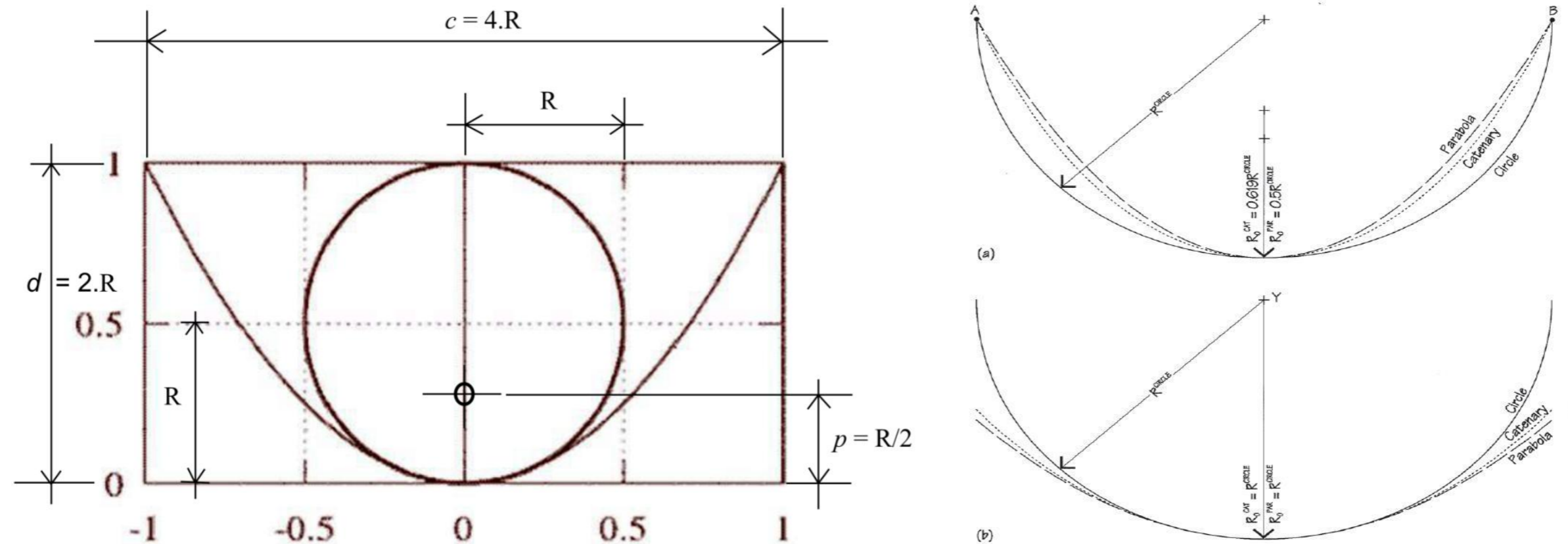


Figure 3.17 – Geometrical and Mathematical representations of Circle, Parabola, and Catenary curves.

$$p = \text{focal length of the parabola} = \frac{c^2}{16.d} = \frac{(4.R)^2}{16.(2R)} = \frac{16.R^2}{16.R.2} = R/2$$

The radius of curvature of the parabola at the vertex is twice the focal length p ; $R = 2.p$

The width of the parabola c at top of circle is four times the Radius of Circle; $c = 4.p$

The height of the parabola d at center of circle is twice the Radius of Circle; $d = 2.R$



From the traces of the lines of the circle, parabola, and catenary curves shown in Figure 3.17, one can notice that depending on the value of the radius of curvature of a given circle, parabola, and catenary curves, for smaller values of radius of curvature the three curves tend to approximate to each other. The two curves that present closer approximation to each other for a given value of radius of curvature are the parabola and catenary, therefore for practical representations and easier solutions of the mathematical equations the designers can make good use of the parabolic curves in lieu of the most complicated mathematical solutions of the catenary curves.

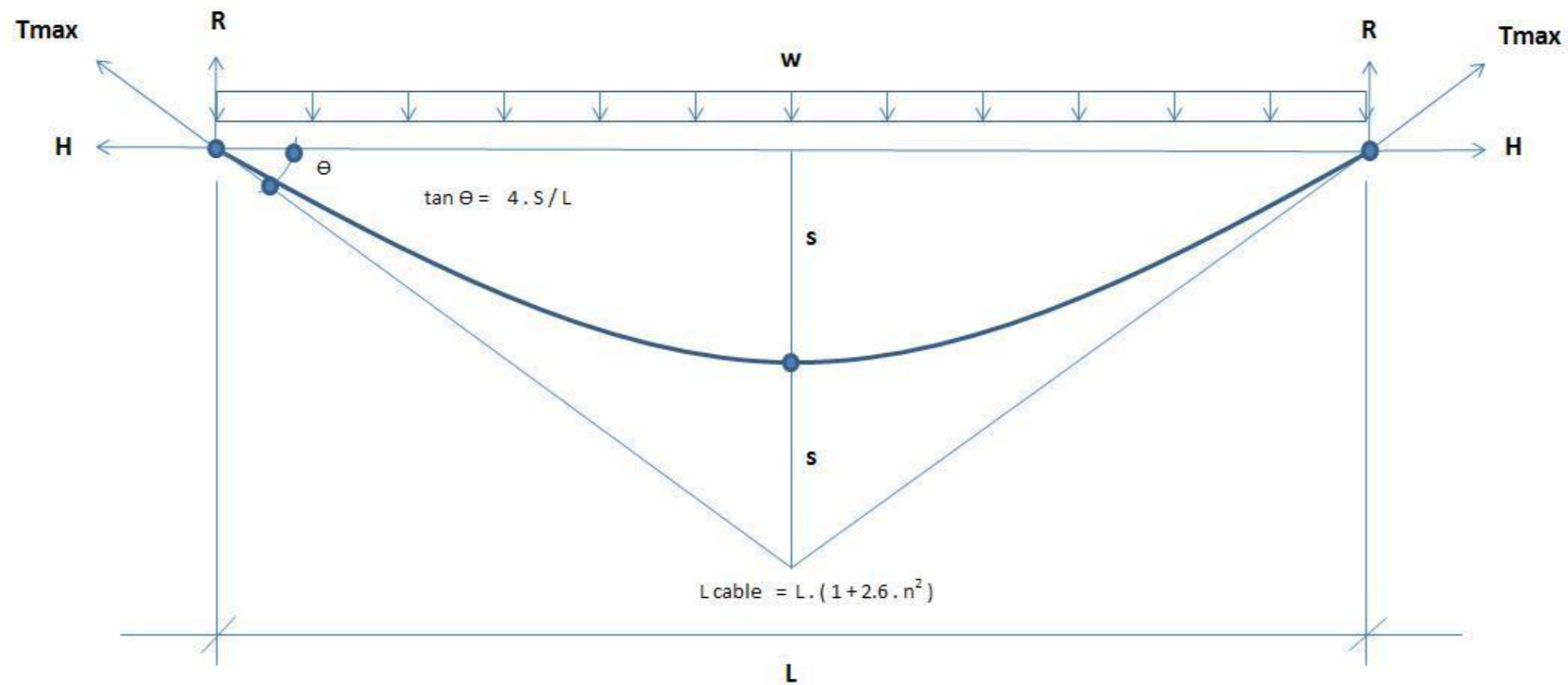


Figure 3.18 – Suspended Cable Curve of span L , with uniform load w , and simply supported at both ends.

The study of parabolic curves will apply very similarly for both: cables under tension and shells under compression. Therefore we can focus on studying first the case of a suspended cable supporting a uniformly distributed load along the projected length of the span of the suspended cable.

Figure 3.18 above shows the basic parameters involved in the study of a parabolic suspended cable under a uniform load w , sag s , span L , and cable length $l_p = L_{cable}$ along the parabolic curve. The parameter n is the sag to span ratio which can be used in the mathematical expressions of Equations 3.1, 3.2, and 3.3 noted below to estimate the approximate length of the parabolic curve of a suspended cable under uniform load w . The parameter α can be defined as a function of s , l_p , and L as noted below.

Since the expressions used to calculate the approximate length of parabolic or catenary curve of the cables are approximate and based upon mathematical solutions of differential equations, it is noted that as the value of n or s increases then the calculated length of the curved cable length starts to diverge from the actual parabolic or catenary curved length of the cable when using Equations 3.1 and 3.2.

$$n = \frac{s}{L} ; \quad l_p = L_{cable} ; \quad \alpha = f(s, l_p, L) ; \quad \alpha = \frac{3}{8.n^2} \cdot \left(\frac{l_p}{L} - 1\right) ; \quad n = \sqrt{\frac{3}{8.\alpha} \cdot \left(\frac{l_p}{L} - 1\right)} ; \quad a = s ; \quad b = L$$

Equations 3.1 and 3.2 are approximate solutions of the differential equation of the catenary curve based on a summation of series of values of the sag ratio n , span L , and coefficient α . The tabulated list of values noted below were calculated for different values of sag ratio n from 0.00 to 1.00 and for a given suspended cable span $L=20$ ft. The approximate length of the catenary curve of the cable is estimated to be given by the values of l_p listed below. From the results one can observe that the values of α above $n=0.20$ start to diverge and become lower than 0.90, which indicates that any calculated values of the length of cable based upon Equations 3.1 and 3.2 for values of n larger than 0.20 are not that accurate.

Equation 3.3 is another solution of the catenary equation based upon natural logarithmic expression that provides a more accurate solution for values of sag $s = a$ and span $b = L$. The expressions for the length of cables listed as Equations 3.1, 3.2, and 3.3 can be found in most of textbooks of Statics and Structural Analysis, some of which are listed in the References. These equations are rare to see in the most recent textbooks of Statics, Strength of Materials, and Elementary Structural Analysis where the subject of solutions to Cable supported structures is not given much attention as it was done in prior years. It is very important to be able to calculate or estimate the length of suspended cables for given values of sag ratio n and span L .

A similar concept can be applied by inverting the cable and treating the shape of the curve of the cable as a shell under compression. For both cases either cable under tension or shell under compression, this length l_p will allow the designer to estimate the selfweight along the curve.



n	L	s	lp	α	lp/L
0.00	20	0.0	20.00	1.00	1.00
0.05	20	1	20.13254454	0.994084085	1.006627227
0.1	20	2	20.52121261	0.977273641	1.02606063
0.15	20	3	21.14231877	0.951932307	1.057115938
0.2	20	4	21.96460168	0.920907035	1.098230084
0.25	20	5	22.95587149	0.886761448	1.147793575
0.3	20	6	24.08694214	0.851446278	1.204347107
0.35	20	7	25.33309372	0.816289855	1.266654686
0.4	20	8	26.67410806	0.782122039	1.333705403
0.45	20	9	28.09370884	0.749417485	1.404685442
0.5	20	10	29.57885715	0.718414286	1.478942858
0.55	20	11	31.1190942	0.689200054	1.55595471
0.6	20	12	32.7059913	0.66177038	1.635299565
0.65	20	13	34.33271172	0.636067088	1.716635586
0.7	20	14	35.99366928	0.612002651	1.799683464
0.75	20	15	37.6842648	0.589475493	1.88421324
0.8	20	16	39.40068293	0.568379383	1.970034146
0.85	20	17	41.13973523	0.548609046	2.056986761
0.9	20	18	42.89873829	0.530063386	2.144936914
0.95	20	19	44.67541858	0.5126472	2.233770929
1	20	20	46.46783762	0.496271955	2.323391881

$$l_p = L \cdot \left(1 + \frac{8}{3} \cdot n^2\right); l_p = L \cdot \left(1 + \frac{8}{3} \cdot \alpha \cdot n^2\right) \quad (\text{EQ. 3.1})$$

$$l_p = L \cdot \left(1 + \frac{8}{3} \cdot n^2 - \frac{32}{5} \cdot n^4 + \frac{128}{7} \cdot n^6 - \frac{512}{9} \cdot n^8\right) \quad (\text{EQ. 3.2})$$

$$l_p = \frac{1}{2} \cdot \sqrt{b^2 + 16 \cdot a^2} + \frac{b^2}{8a} \cdot \ln\left(\frac{4a + \sqrt{b^2 + 16a^2}}{b}\right) \quad (\text{EQ. 3.3})$$



The Graphic Statics Method that has been extensively documented in educational textbooks, technical papers, and publications on the subject of Statics and Elementary Structural Analysis can be used to resolve 2D parabolic arches that form thin reinforced concrete shell structures. Figure 3.17 shows a simplified solution of a parabolic arch using the graphic statics method. Several textbooks and technical papers on this subject of graphic statics are presented in Chapter 7, References section of this Thesis.

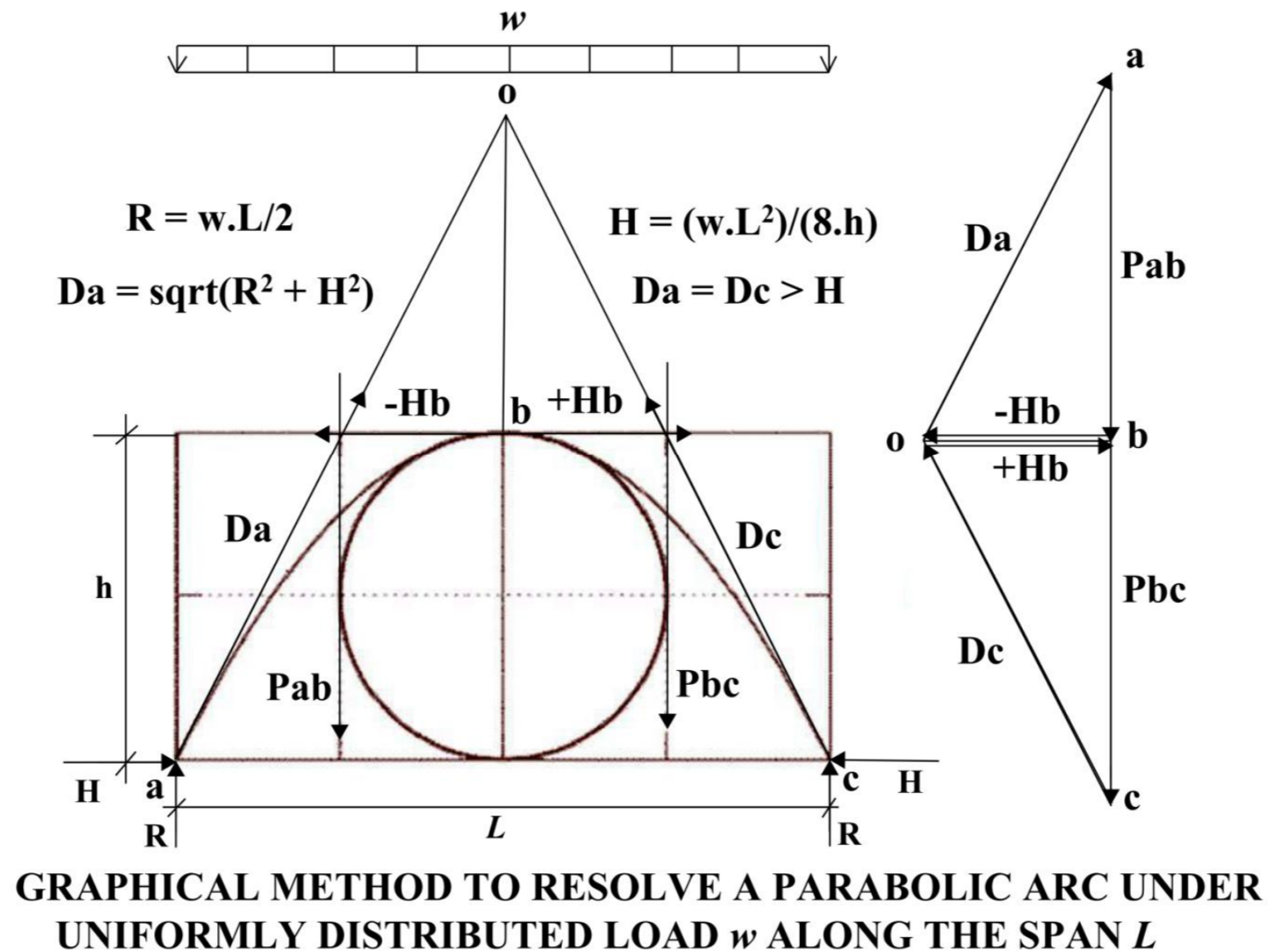


Figure 3.19 – Graphic Statics Method for a simply supported 2D Parabolic Arch of span L and uniform load w .



This method was widely used in the past to obtain graphical solutions of different types of statically determinate structural forms under external forces to solve for the reaction forces at the support points that will allow for a closed form solution of the vectors of forces and reactions that will provide static equilibrium.

The majority of shell structures can be modeled in a very simplified way by simply understanding that their overall 2D or 3D structure can be discretized as an assembly of interconnected set of straight beams and curvilinear arches and catenaries that will form an entire shell structure in equilibrium. In essence shell structures achieve their overall strength, stiffness, and stability mainly by their curvilinear form, which will provide the most efficient structural shape to support the external loads and carry them over through the boundary edges to their supports.

GEOGEBRA listed in the References is a very practical and intuitive computer program software that allows the generation and graphics of parabolas and other geometric shapes, curves, surfaces, solids, and mathematical functions.

The 2D Graphic Statics Method can also be extended to the 3D space for statically determinate 3D structural systems. 3D Graphic Statics method may be used as long as the system of external forces and the support reaction forces can be concurrent in space to form a closed formed vector solution. The 2D and 3D Graphic Static Methods may be used for both a grid of compression shell members and a grid on tensile cable members.

The main requirement for either a 2D or 3D graphical method solution for shells or cable systems is that the complete set of vectors of external forces, internal member forces, and support reaction forces provide a closed loop solution of the set of all vector forces. For structural grid systems with nodes where no more than three members come together are considered to be determinate system where the system of vectors of forces can be determined and will close to be in equilibrium. Indeterminate systems will require the use of some other type of computer methodologies involving the use of force density or dynamic relaxations methodologies to be able to solve the indeterminacy of the system.

In Recent years a group of researchers at the Computer Science and Architecture Departments of MIT have developed special-purpose software that uses the particle-spring systems to create physical simulations of 2D and 3D networks of linear members and particles to obtain the form finding of structural systems in equilibrium of axial or compression forces only.

Killian and Ochsendorf of MIT and other students of the Computer Science and Architecture Departments of MIT have implemented Java and C++ scripts and a software tool called “CADenary” to model hanging models under their own weight which will produce a tension only network of members and particles at intersecting nodes of members.



RhinoVAULT software by Matthias Rippmann (Rippmann@arch.ethz.ch) is a Plug-In App for Rhinoceros that allows to perform the Funicular Form Finding of vaulted shell structures. It is noted by Rippmann in the website of food4Rhino that this Plug-In App for Rhino emerged out of a research project exploring the structural form finding of shells using the Thrust-Network-Approach (TNA) implemented by the Block Research Group (BRG) a team of architectural and engineering students led by Professor Phillip Block of ETH in Switzerland working together to develop highly efficient and sustainable structures.

Block and Ochsendorf in 2007 published a Technical Article in the Journal of IASS where they describe a method to generate compression-only vaulted surface structures and network of elements under compression called: Thrust Network Analysis. This TNA methodology is based on a graphical and intuitive method that uses projective geometry, duality theory, and linear optimization for the analysis of vaulted historical unreinforced masonry or new vaulted type of compression-only structures.

The TNA methodology permits the analysis of compression-only structures. Using reciprocal diagrams it provides an intuitive fast method that has the same advantages of techniques used in the 2D Graphical Statics Methods but allowing the extension of this methodology to 3D structures. It is a graphical form finding computer methodology to determine form and forces for curvilinear 3D funicular surfaces under compression. The approach is noted to be an interactive bidirectional design methodology to explore the stability and final form of funicular networks (grids) of compression-only vaulted shell structures. In essence the TNA is a 3D extension of the traditional 2D Graphic Statics method well known for centuries and which was done graphically by hand when the computers did not ever existed.

This TNA method can also be called “3DGS” that stands for: Three Dimensional 3D Graphic Statics” that is based upon the traditional Graphic Statics Method (GSM) for design and analysis of form and forces of structures based on 2D Geometry and Drafting. The 3DGS methodology uses a Structure Grid, a Force Diagram applied over the structure grid, and determines the Form Diagram of the final funicular structure in static equilibrium of forces. For both the TNA and 3DGS methods the structural stability of the system is achieved by carefully adjusting the flow of forces within the structural members to maintain a closed loop of forces at all joints and members of the structure.

Recently with the adoption of the Strut-and-Tie Model (STM) for analysis of reinforced concrete structures, published in Chapter 23 of the ACI 318-14, and with the appropriate adaptations of the basic concepts of the definitions of struts, ties, and nodes of reinforced concrete members to the case of highly curvilinear synclastic or anticlastic thin concrete shells then it is possible to model the entire surface regions of concrete shell structures as a 2D or 3D truss system and be analyzed as such. This method is herein defined and called: “Truss Analogy Method (TAM)”.



TRUSS ANALOGY METHOD – TAM

The Truss Analogy Method (TAM) herein proposed by the Author consists in modeling a 2D or a 3D planar or curvilinear surface as a grid or mesh of intersecting lines that will form a 2D or 3D truss composed of members that will act mainly either in Tension (ties) or Compression (struts), and will follow the curves or lines of principal stresses of a planar or curvilinear surface under external forces which will be distributed over the member surface mainly in the form of membrane stresses. At the plane where the principal stresses on elements are located the shear stresses are zero.

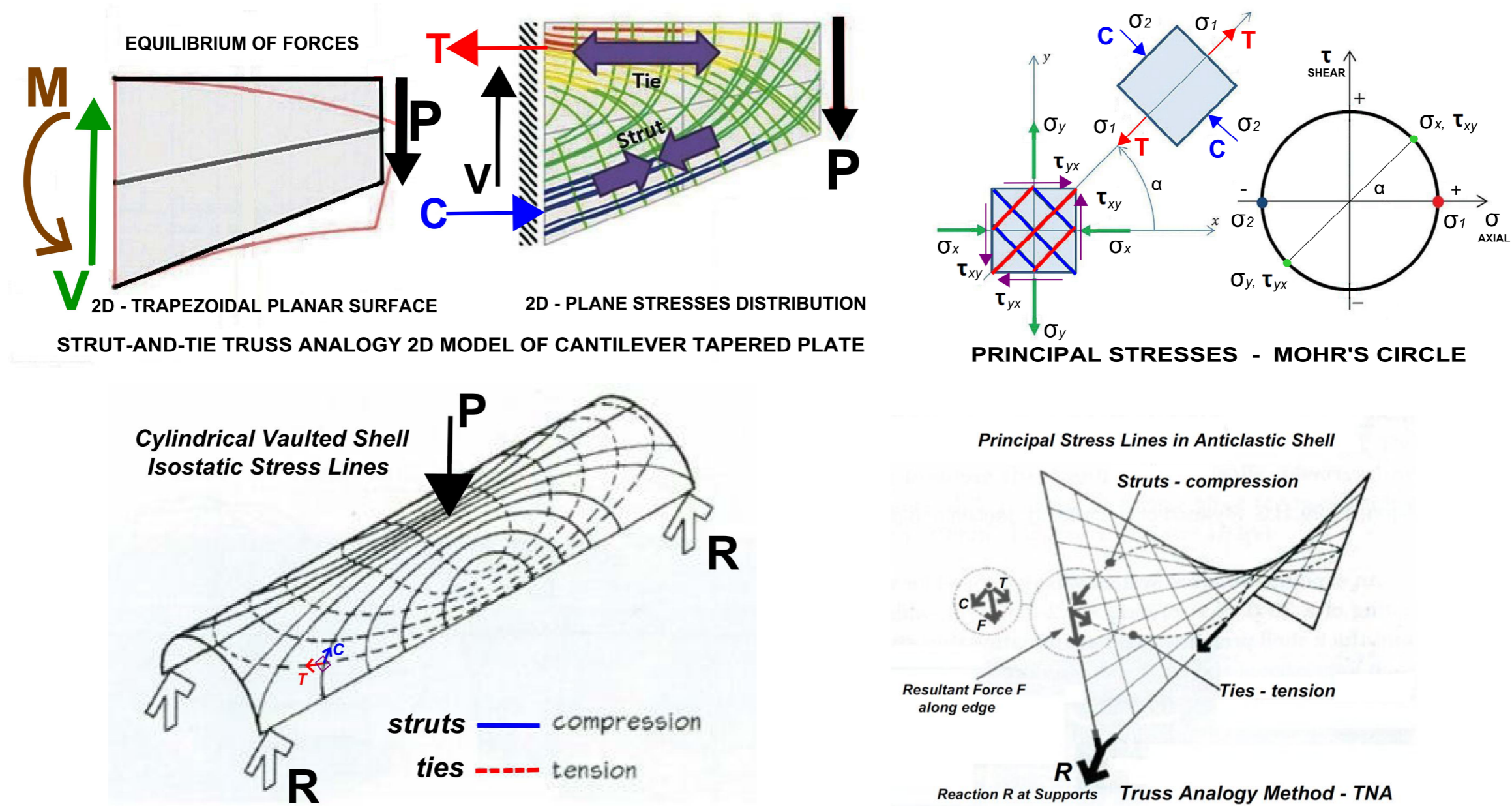


Figure 3.20 – 2D and 3D planar and curvilinear surfaces modeled using the Truss Analogy Method with Struts and Ties.



3.5 - ARCHITECTURAL AND ENGINEERING SHELL PROJECTS – Following are a selected sample of as-built reinforced concrete thin shell structures that have been built mainly in the USA and Mexico. Just to show few of classical examples of thin shell realizations.

A. MIT KRESGE AUDITORIUM, Cambridge, MA-USA

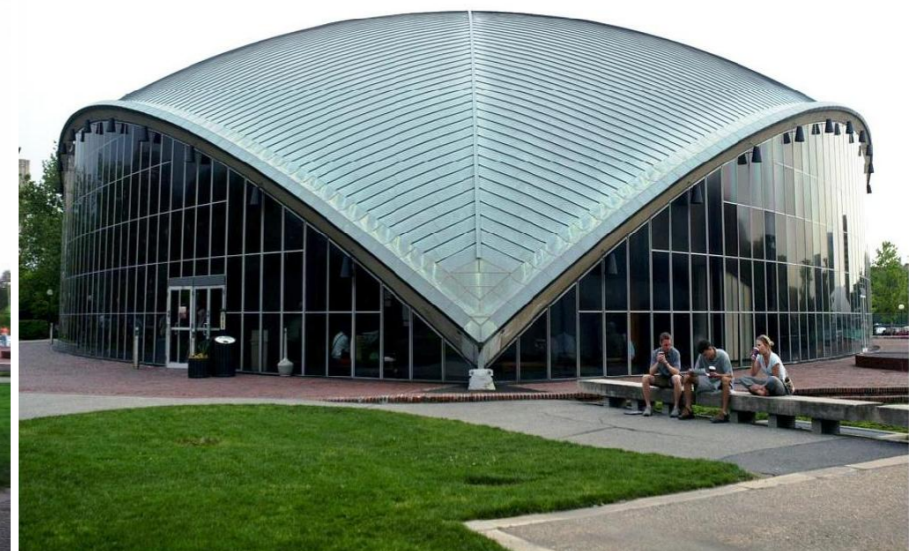
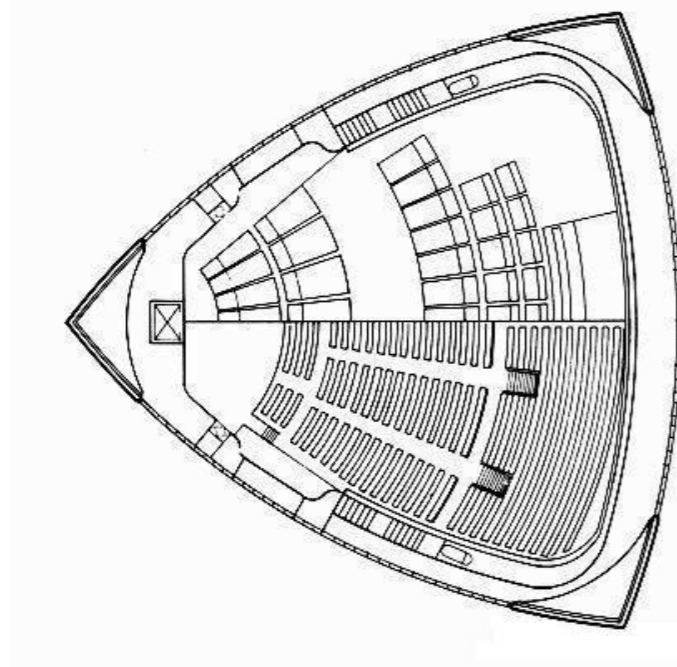
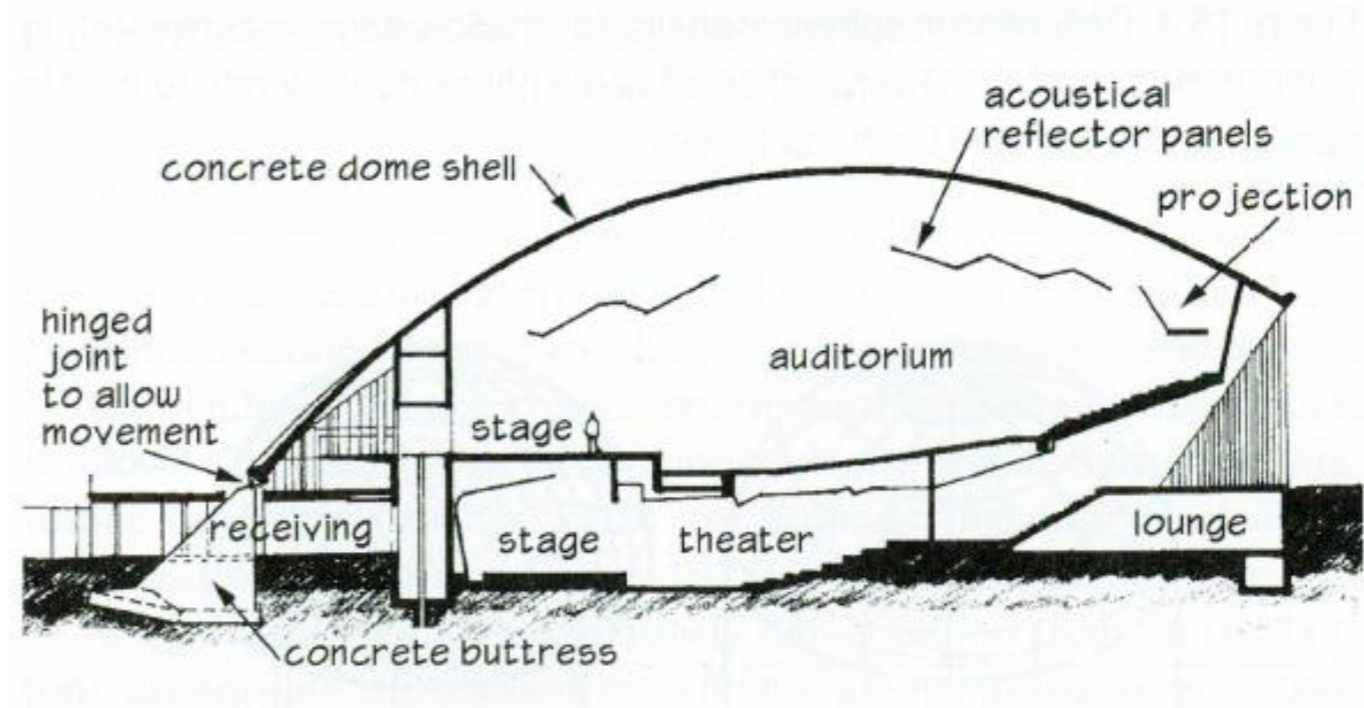


Figure 3.21 - Eero Saarinen & Associates, Architects – Ammann & Whitney – 1955; Cambridge, MA – USA; $R = 112 \text{ ft.}$, $t = 3.5''$ – $R/t = 384$.



B. GREEK ANNUNCIATION ORTHODOX CHURCH, Milwaukee, WI, USA

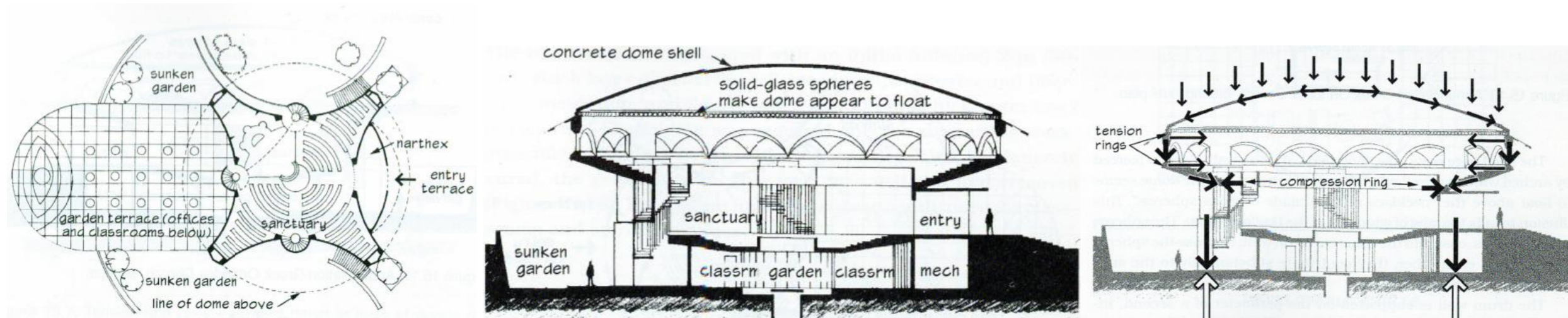


Figure 3.22 - Frank Lloyd Wright, Architect – 1956; Milwaukee, WI – USA ; $R = 197$ ft., $t = 3.5''$ – $R/t = 675$.



C. SUNDOME MULTIPURPOSE STADIUM, Yakima, WA, USA

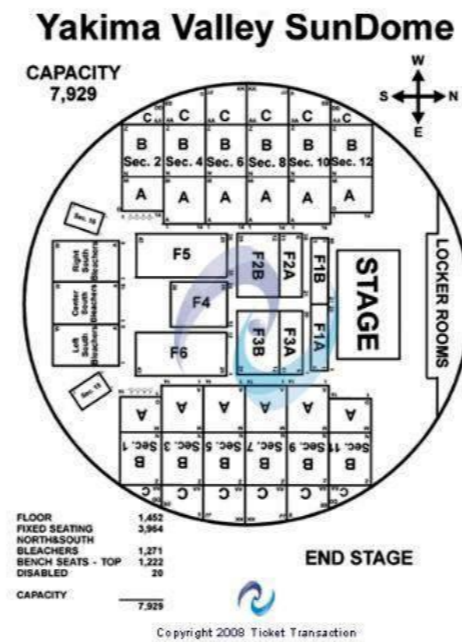
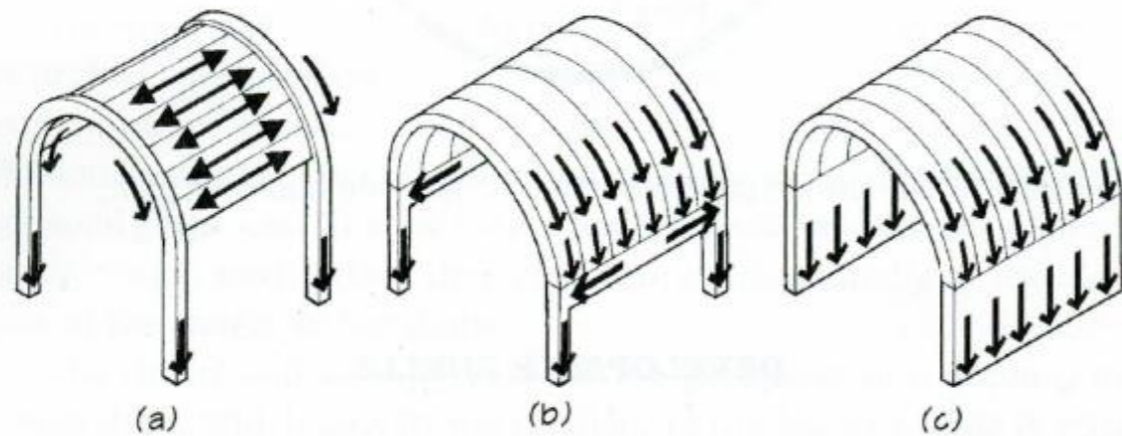


Figure 3.23 - Loofburrow Architects; J. Christiansen Engineers – 1990; Yakima, WA – USA; $R = 248$ ft., $t = 3.75''$ – $R/t = 794$.



D. CYLINDRICAL VAULTED SHELLS

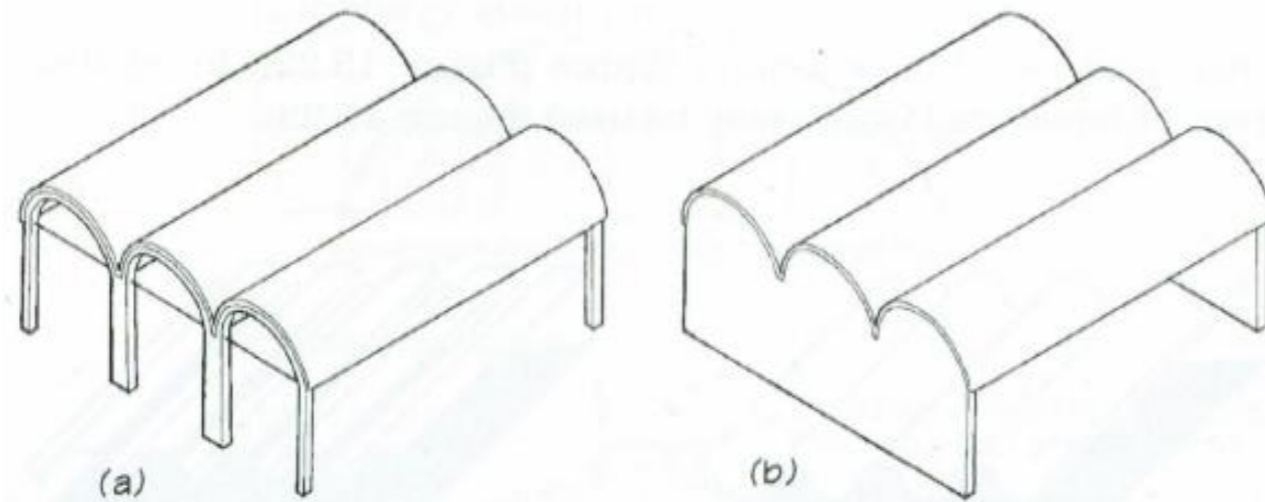
SHORT VAULTED SHELLS



END ARCHES

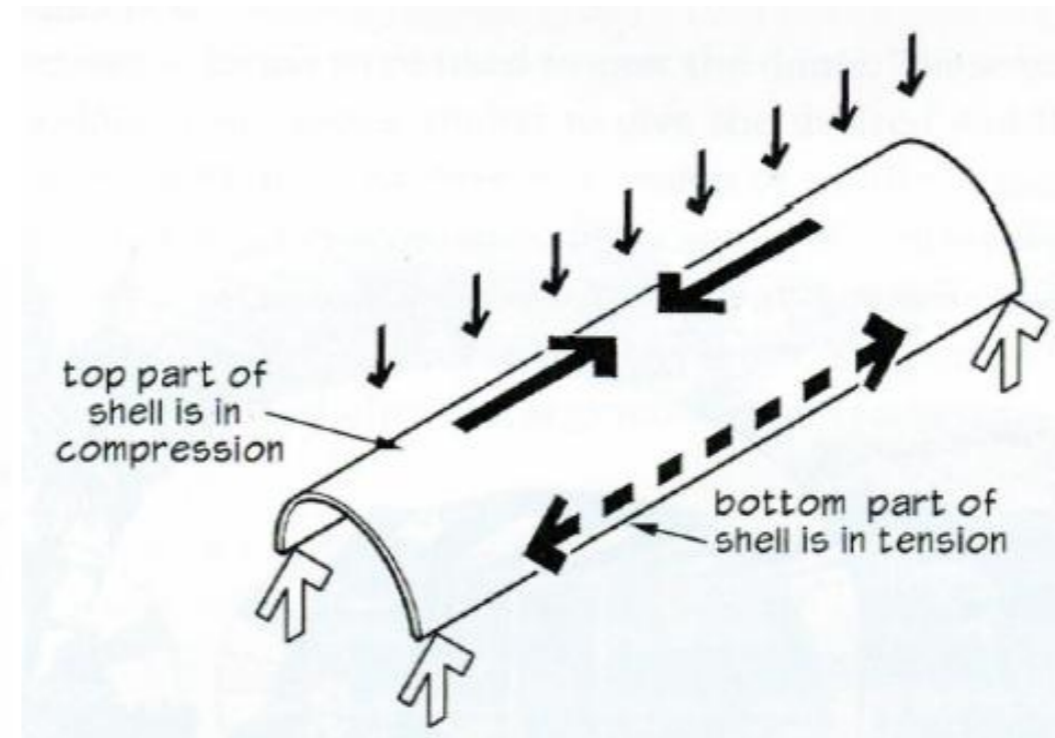
END BEAMS

END WALLS

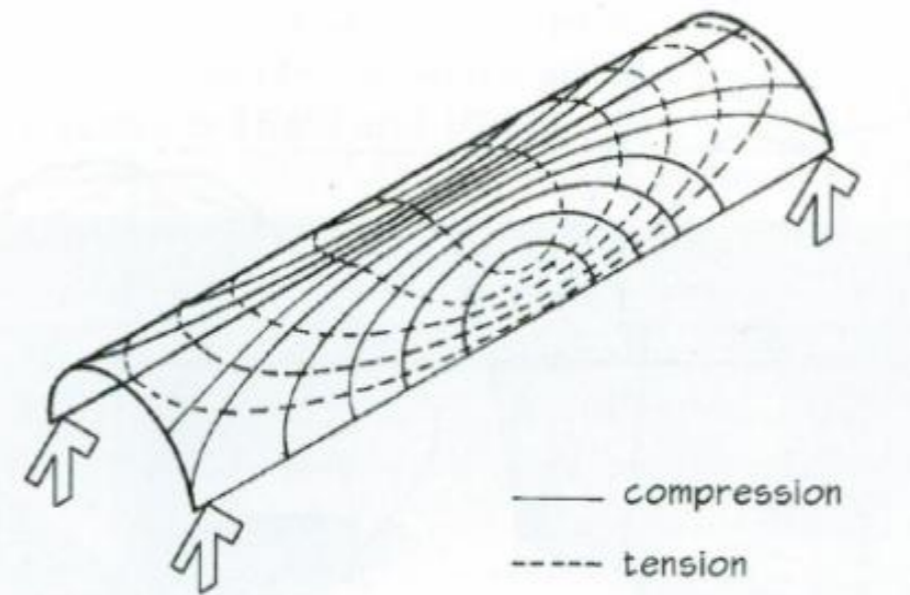


ENDS TIED TO ABSORB THRUST AND MAINTAIN FORM

LONG VAULTED SHELLS



Thickness of Shell, $t = \text{Depth/Span Ratio} \sim 6 \text{ to } 10$ by Code



STRESS DIAGRAM Compression and Tension stresses are Perpendicular

Figure 3.24 – Cylindrical Vaulted Shells – Support Conditions and Distribution of internal forces and stresses.



E. KIMBELL MUSEUM, Forth Worth, TX, USA

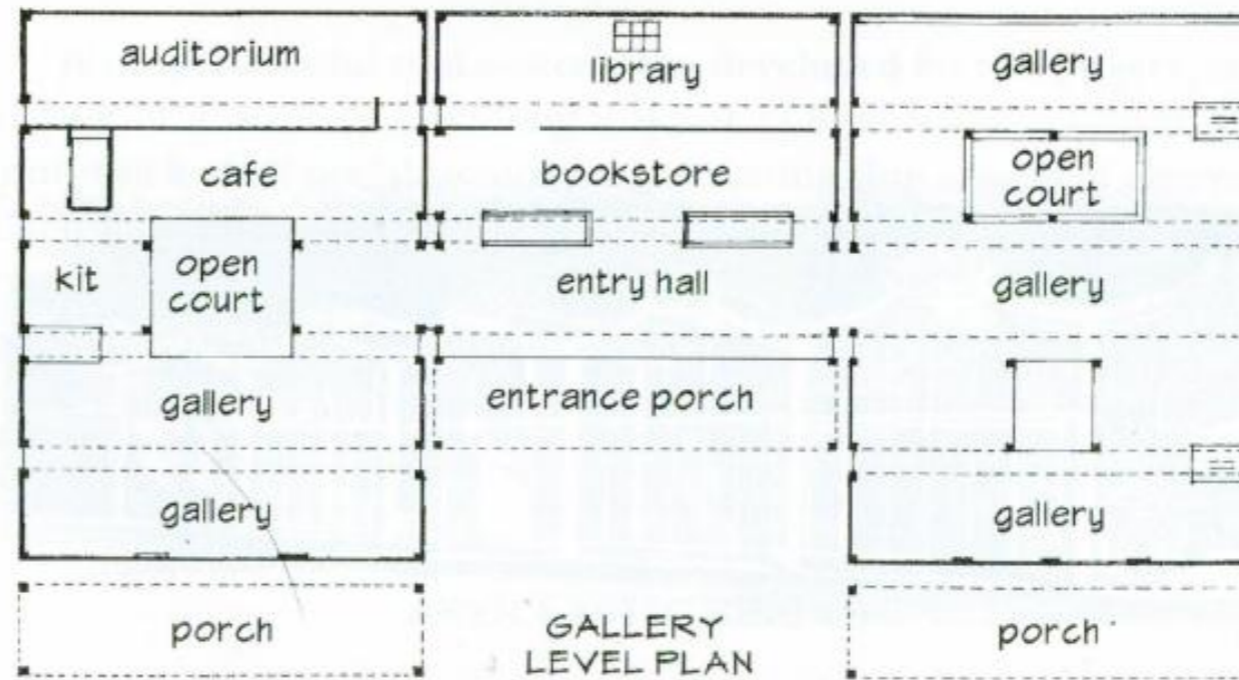
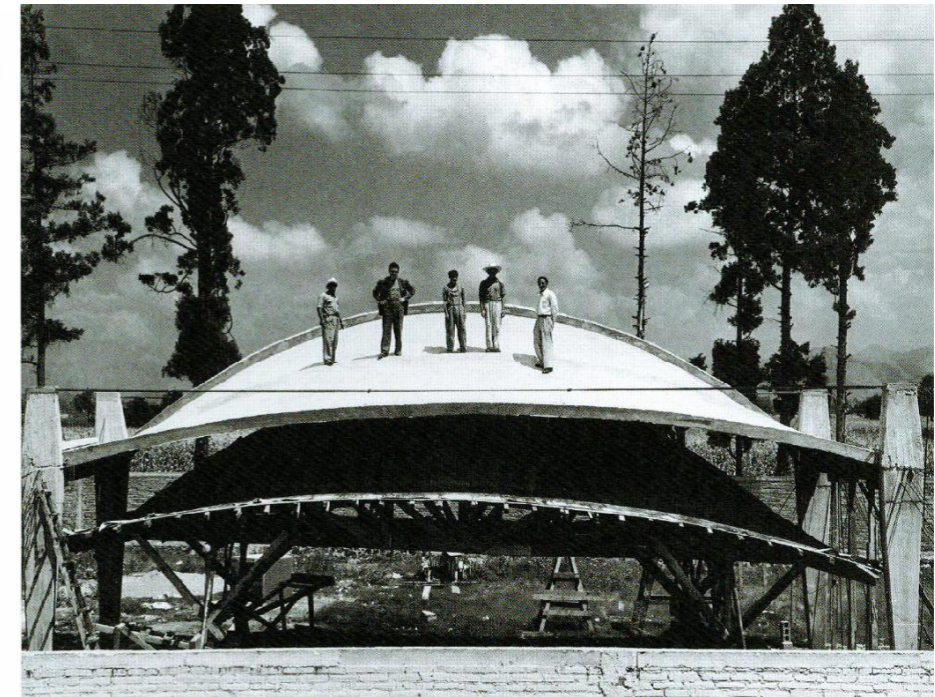
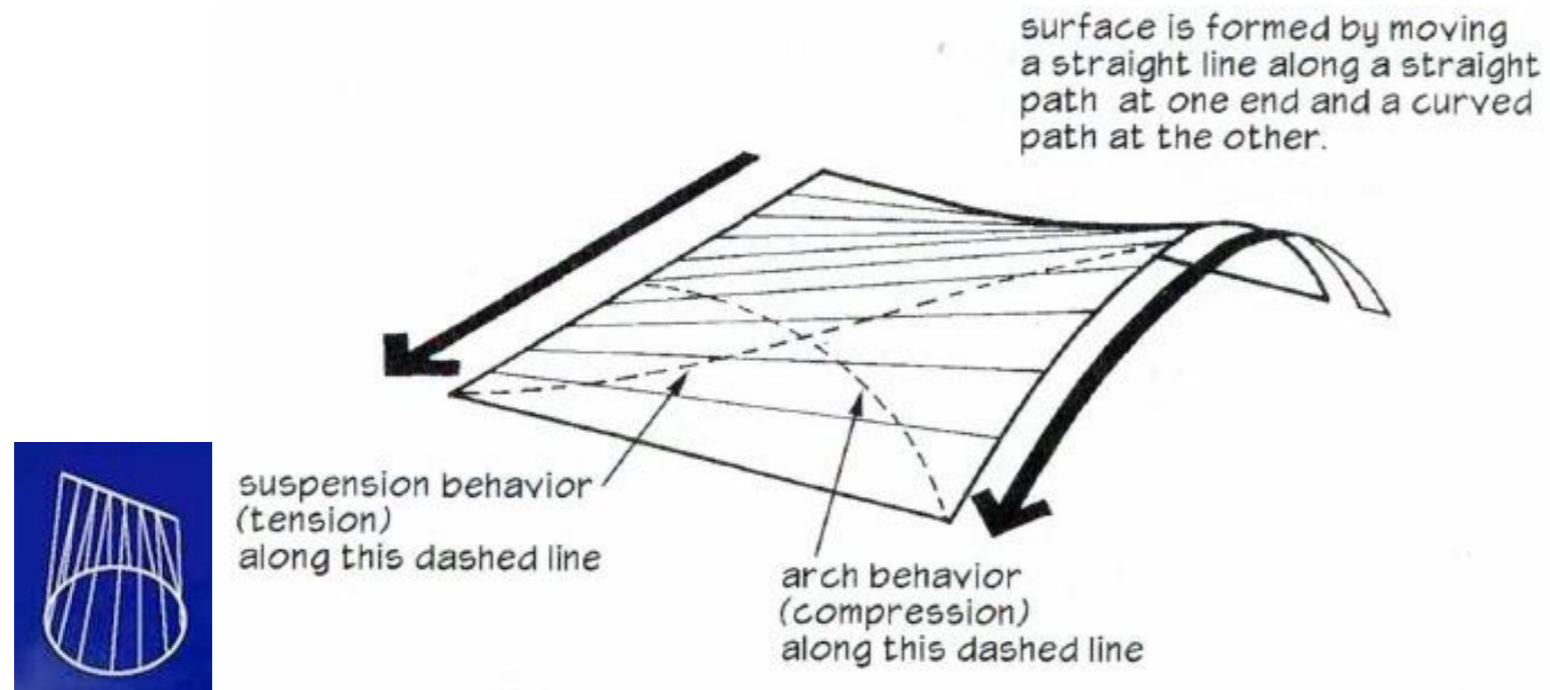


Figure 3.25 - Louis I. Kahn, Architect; A. Komendant, Structural Engineer – 1972; Forth Worth, TX – USA.

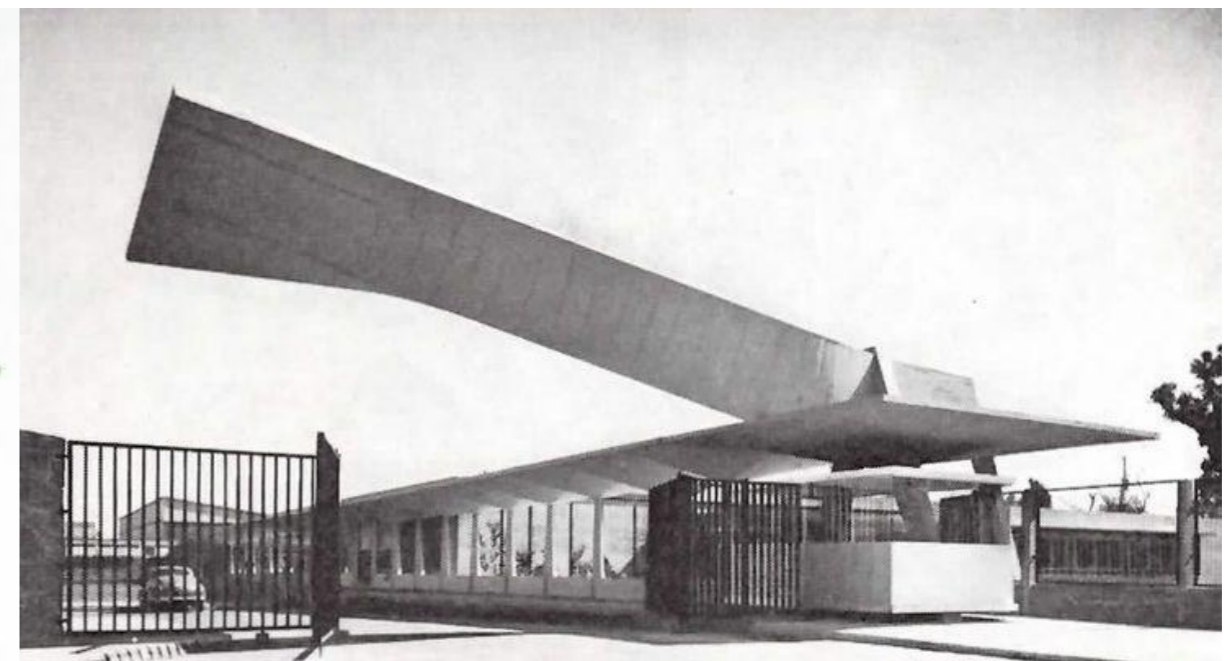
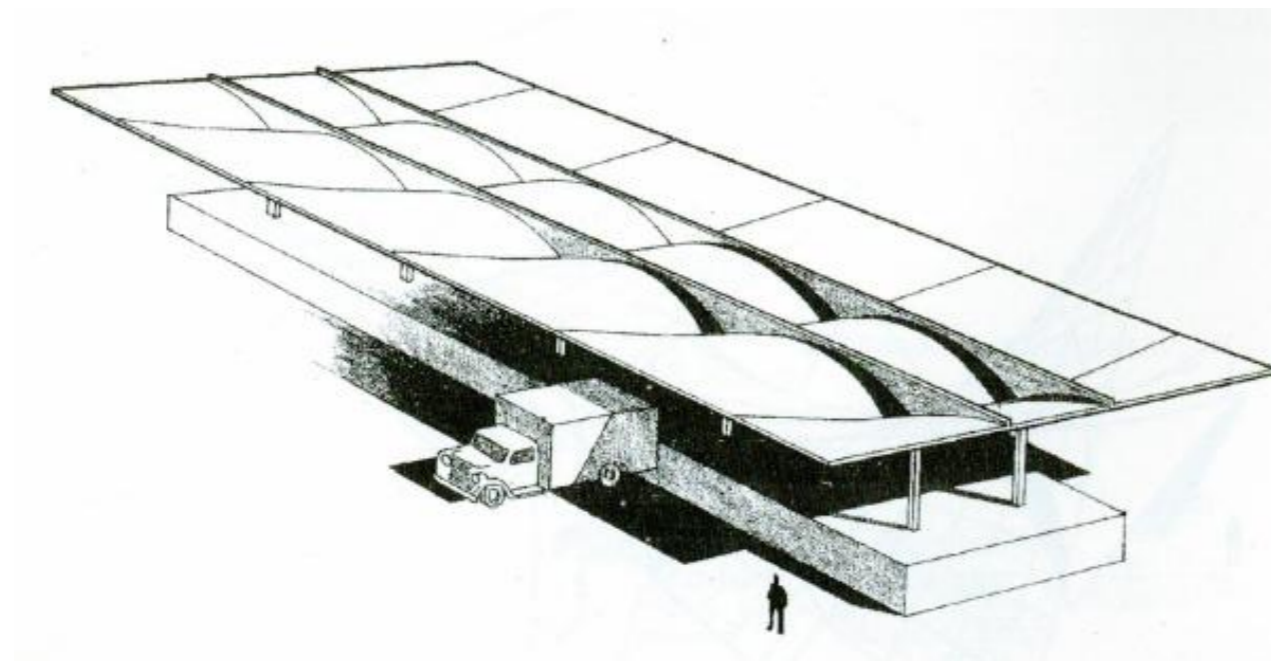


F. ANTICLASTIC SHELLS - CONOIDS



Surface Generation of a Conoid

Experimental Roof Shell in San Bartolo, Mexico, 1950



Lecheria Ceimsa Loading Dock, by Candela & Recamier, Mexico 1952

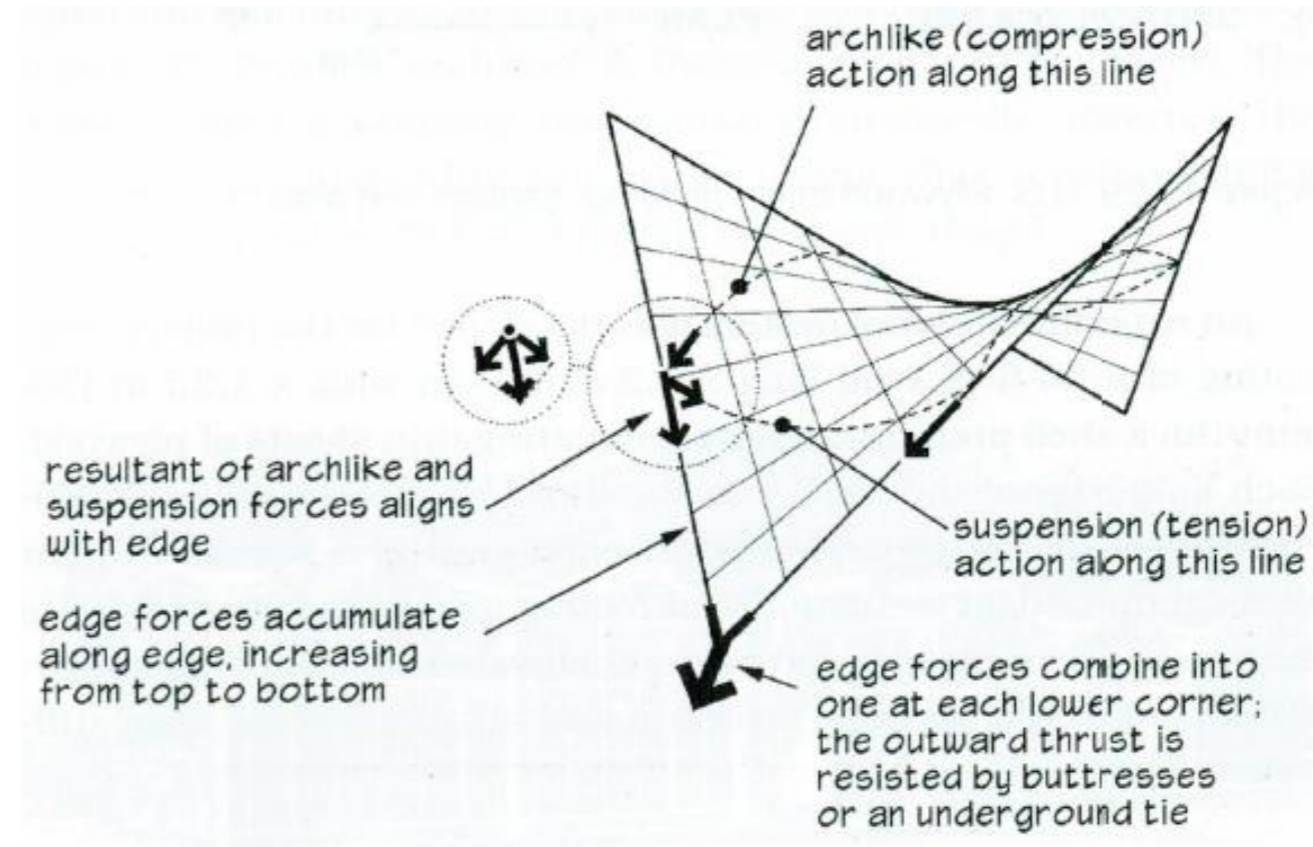
Entrance to the Lederle Laboratories Factory, Mexico City, 1956

Figure 3.26 – Felix Candela, Engineer, Architect, and Builder - Conoid Concrete Shell Structures in the 1950's, Mexico.



G. ANTICLASTIC SHELLS – HYPERBOLIC PARABOLOIDS, HYPARS

The hyperbolic paraboloid (hypar) with straight perimeter edges along the four exterior sides of the shell has been one of the most widely used shapes of anticlastic surface used by architects, engineers, and researchers throughout the world. It has the unique characteristic of forming arch-like sections of the shell which will support shell loads in compression and hanging sections of the shell which will support shell loads in tension. The two lines of arches and hanging sections of shell have radius of curvatures of opposite signs as it is noted in Figure 3.26 below.



Surface Generation for Four Straight Sides – Double Cantilever

Figure 3.27 – Typical Hyperbolic Paraboloid Thin Concrete Shell Roof Structure and Hypar Diagram with straight perimeter edges.

When reviewing the literature of hyperbolic paraboloids (hypars) one can notice that the form shown above in Figure 3.26 is one of the most commonly built forms of hypars for buildings of multiple uses and also in the research laboratories of universities throughout the world using different materials for the formwork and for the actual components of the shell structure, such as reinforced concrete, ferrocemento, cross laminated timber, grid shells of steel, aluminum, cold formed steel, and combinations of different type of materials for form the shell surface.

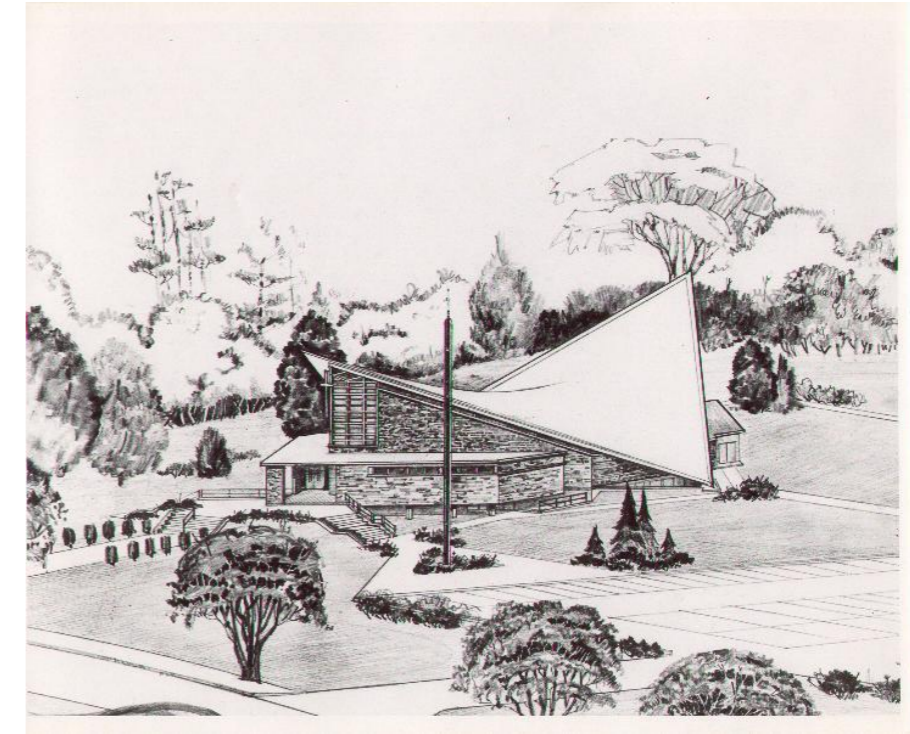


H. HYPERBOLIC PARABOLOID SHELL WITH STRAIGHT EDGES IN THE USA.

The St. Athanasius Church in Reading, MA was designed in 1959 and completed in 1960, was then the largest concrete thin shell (3'') Hyperbolic Paraboloid in the Western Hemisphere. A rhombus in plan ~120' x 155', Seating 800 people, casting of the reinforced concrete roof was completed in One Day. Designed by: Louis A. Scibelli and Daniel F. Tulley, 1959-1960 - Tully International Inc. www.tullyinternational.com



Google Aerial Photo: March 12, 2015



Rendering from James Hundt, Architect, www.jameshundt.com

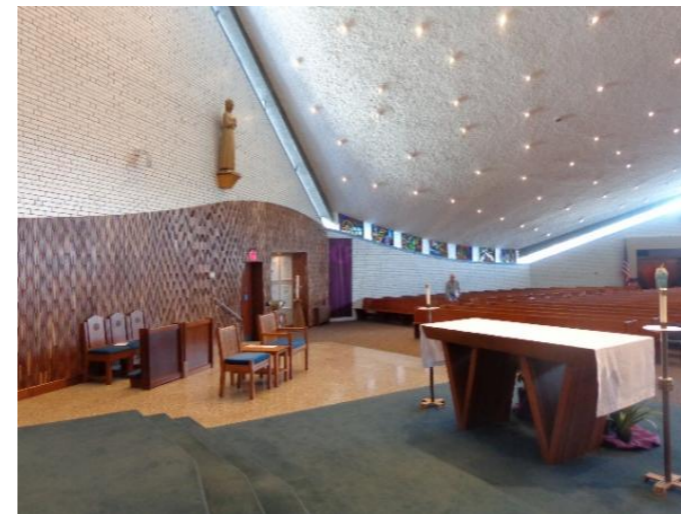
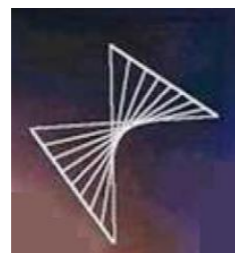


Figure 3.28 – St. Athanasius Church Hyperbolic Paraboloid Roof Aerial View, Rendering, and Interior view of hyper concrete roof.





Figure 3.29 – St. Athanasius Church Hyperbolic Paraboloid Roof – Exterior Elevation Views of hyper concrete roof.



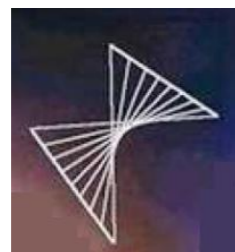
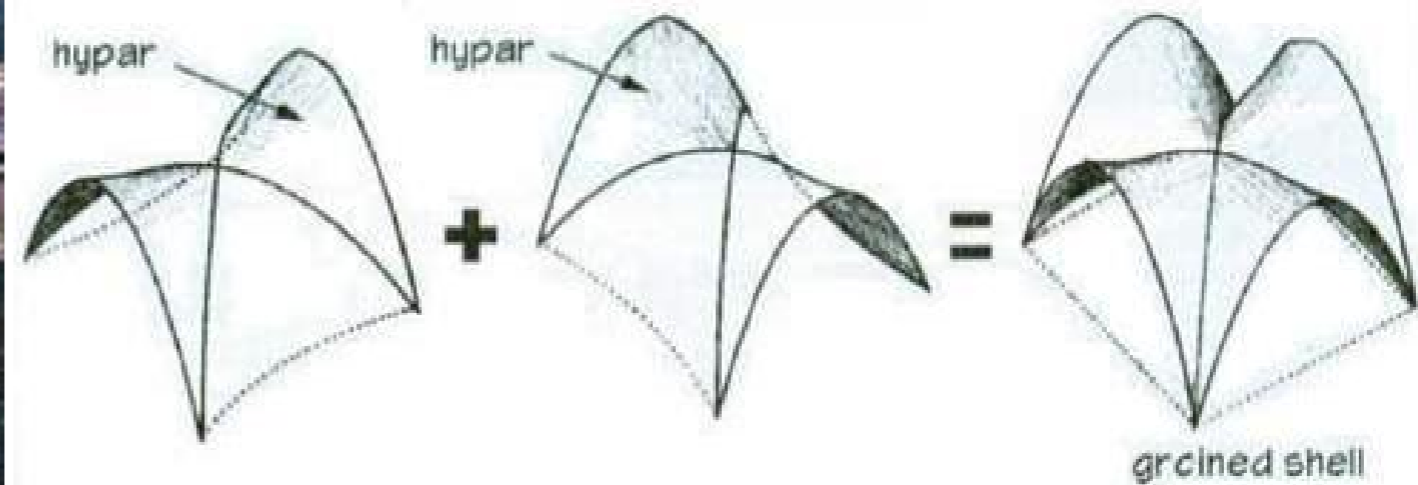


Figure 3.30 – St. Athanasius Church Hyperbolic Paraboloid Roof – Exterior Front and Side Elevation Views of hyper concrete roof.



I. HYPERBOLIC PARABOLOID SHELLS WITH CURVED EDGES AND GROINED VAULTS.

Hyperbolic Paraboloids can be built with groined vaults and forming a circular array to obtain very valuable real state space. Los Manantiales thin shell structure of Felix Candela is an example of a clever way to maximize the use of space in plan with ample space for natural lighting.



Los Manantiales of Felix Candela, Mexico



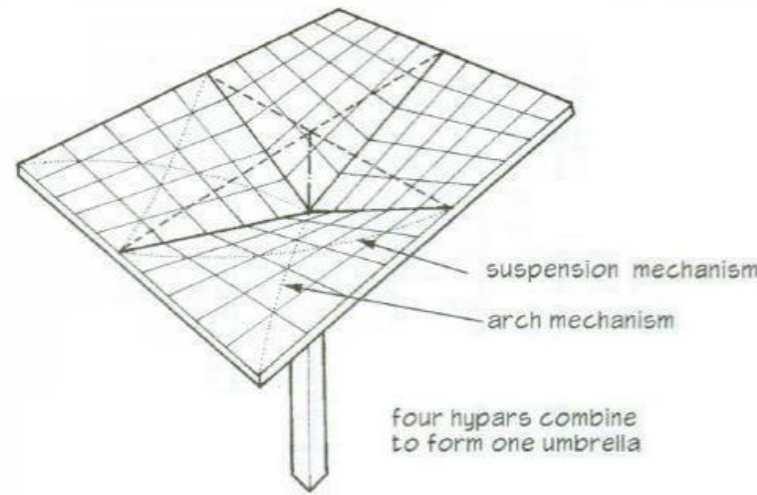
L'Oceanografic, Valencia, Spain

Figure 3.31 – Los Manantiales Restaurant and L'Oceanografic Groined Vaulted Roof Shells of F. Candela and S. Calatrava.

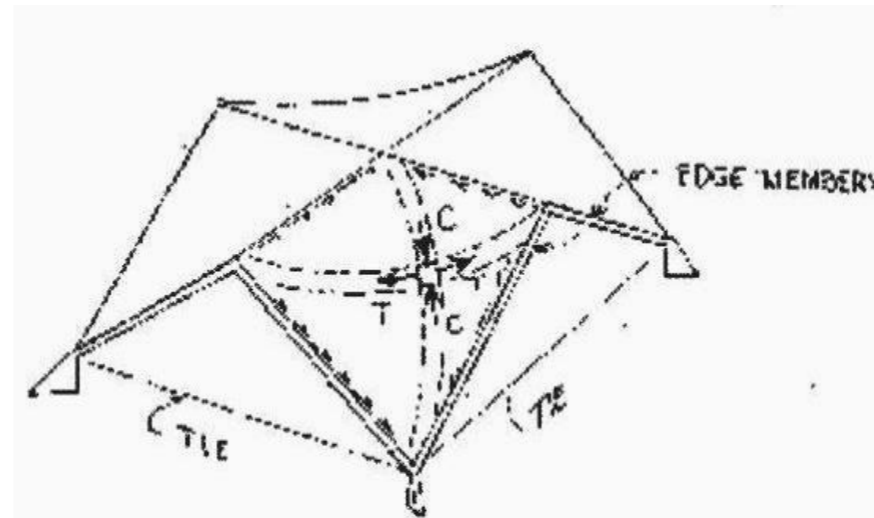


J. HYPERBOLIC PARABOLOID INVERTED UMBRELLA SHELL AND HYPAR DOME/GABLE SHELLS

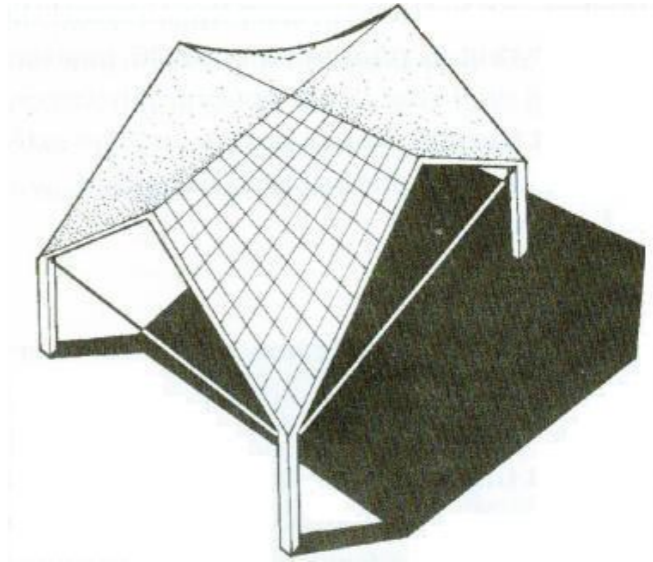
Sections of hyperbolic paraboloid (hypars) could be built one next to the other creating modules that can be repeated in two perpendicular directions to achieve large covered spaces for different uses such as Market Halls, Factories, etc. This concept of inverted umbrellas and intersecting gable hypar roof has been used extensively throughout the world. Below in Figure 3.31 some samples of hypars built by F. Candela in Mexico.



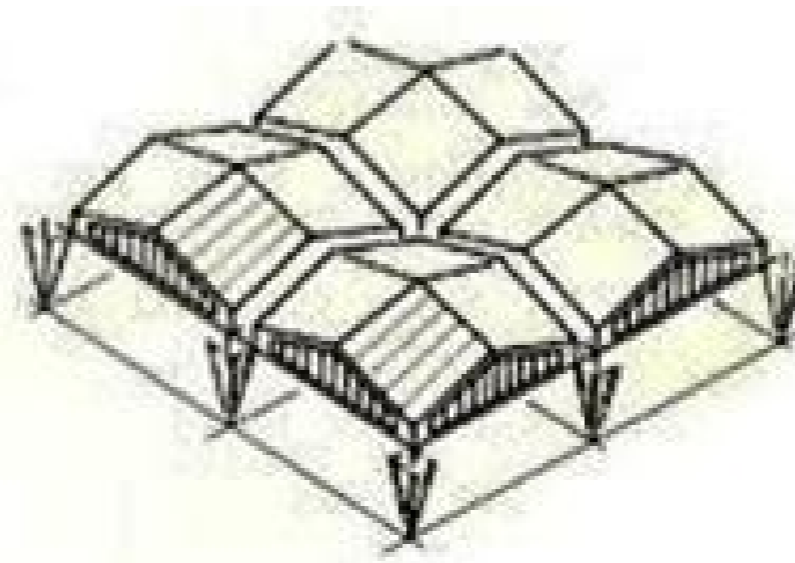
Free Standing Hypar Inverted Umbrella Shell



Four joined Hypars with columns at four corners



Coyoacan Market in Mexico, 1955 by F. Candela, Architect, Engineer, and Builder.



Herdez Plant Gable Hypar Roof in Mexico, 1958

Figure 3.32 – Hyperbolic Paraboloid Roof Shells in the form of Inverted Umbrellas and Intersected Tied Gable Roof Shells.



K. FREE-STANDING HYPAR INVERTED UMBRELLA SHELLS, FOUR HYPARS WITH CENTER COLUMN

A series of inverted umbrellas of 14.4 ft. square and 2” thick reinforced concrete were used to cover the floor plan of a Motel in Florida.

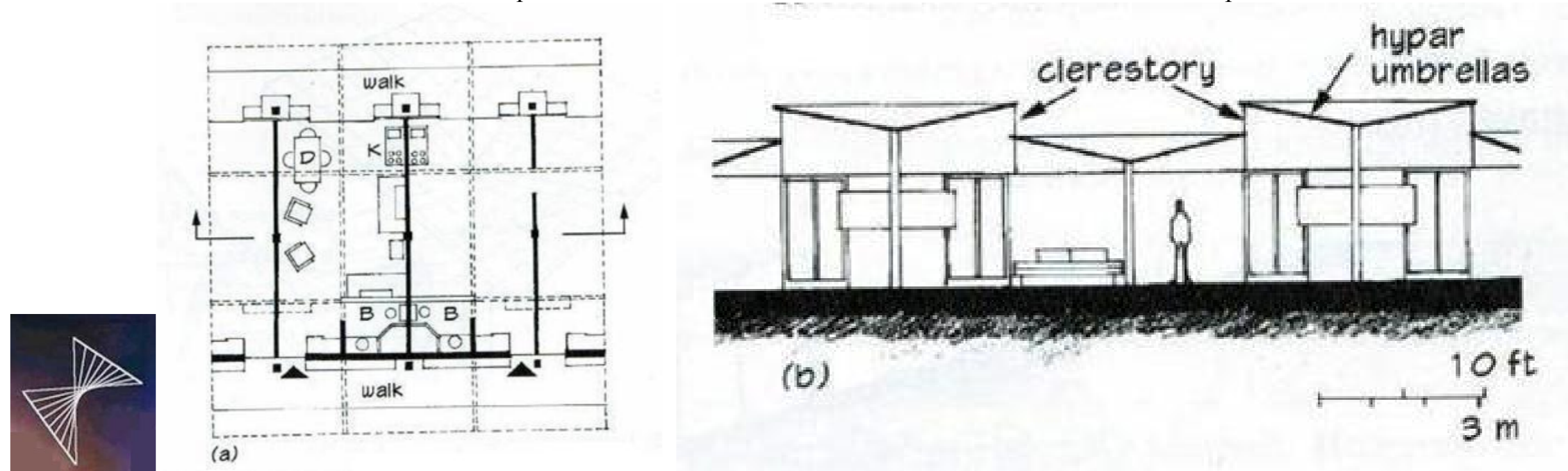


Figure 3.33 – Inverted Umbrellas, Warm Mineral Springs Inn Motel, by V. Lundy, Architect & D. Sawyer, Engineer, North Port, FL 1958.

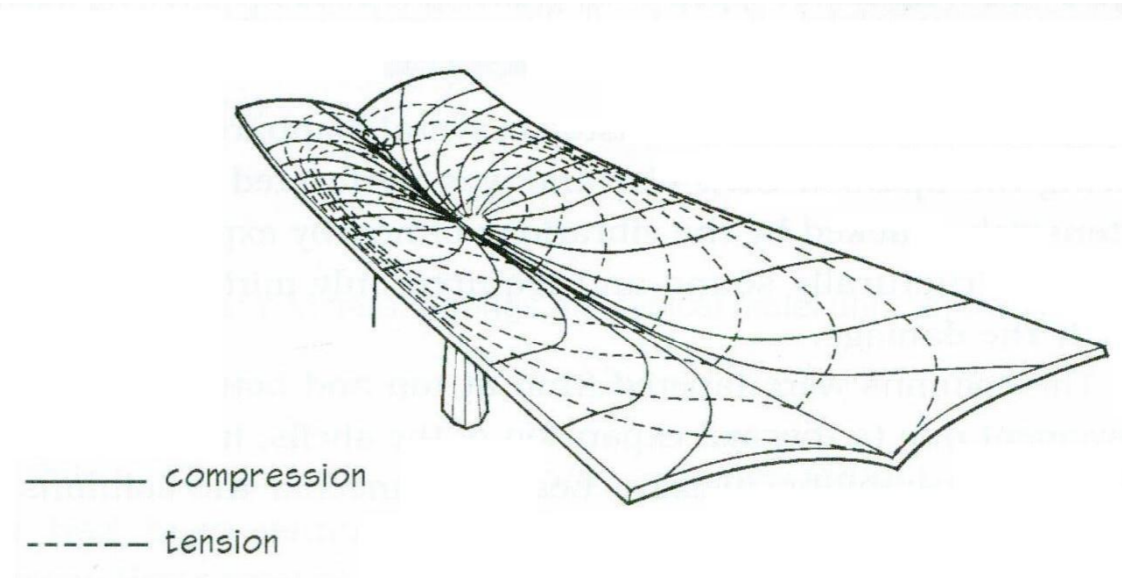


L. ANTICLASTIC CANTILEVERED HYPERBOLIC PARABOLOID THIN CONCRETE SHELLS

Corrugated thin reinforced concrete shells can be used very effectively to produce long span cantilevered structures for roof covered spaces.

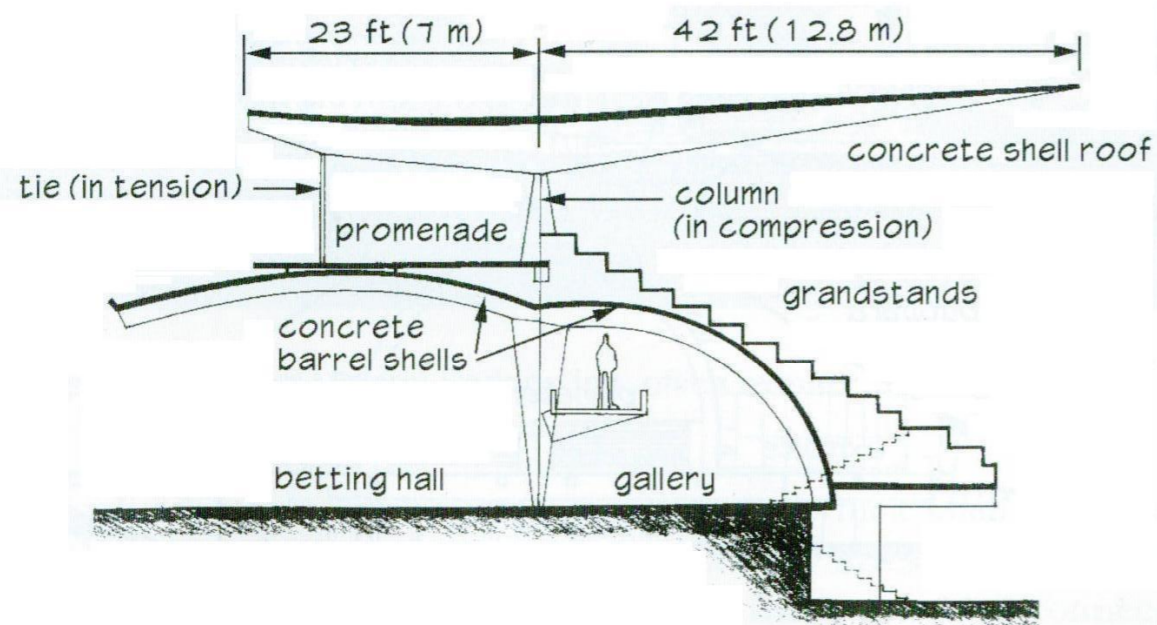


Thickness varies from 2" (50 mm.) to 5.5" (137 mm.)

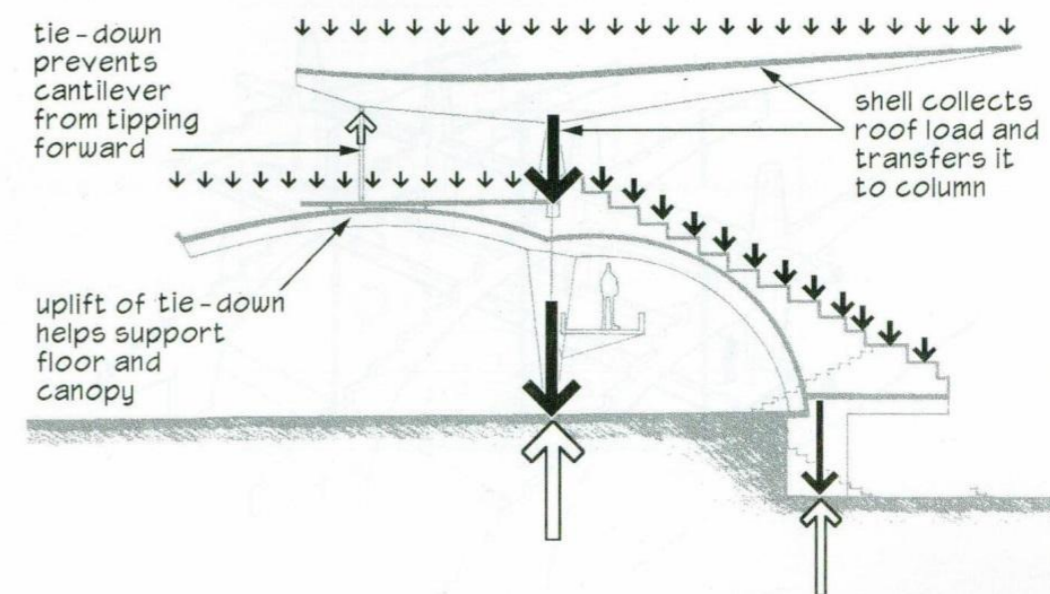


Zarzuela Hippodrome, shell canopy stress contours.

A full-scale prototype was built and tested until failure – 3 times stronger



Zarzuela Hippodrome, section.



Zarzuela Hippodrome, load path diagram.

Figure 3.34 - Zarzuela Hippodrome, by E. Torroja, Architect & Engineer, Madrid, Spain, 1935 – Cantilevered Inverted Hypar Umbrella Shell.



M. HYPERBOLOIDS - ANTICLASTIC SHELLS

The McDonnell Planetarium in St. Louis, MO was built as a Hyperboloid Shell of 160 ft. (49 m.) diameter, 3" thick reinforced concrete shell.

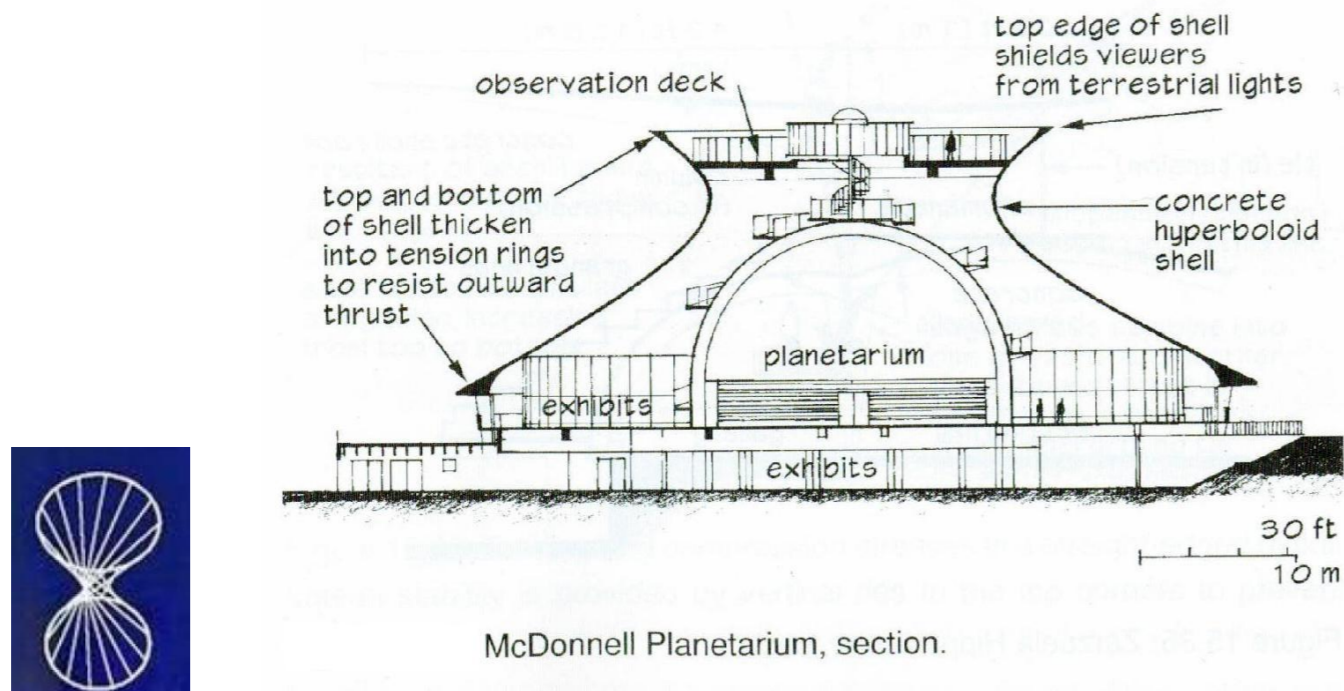
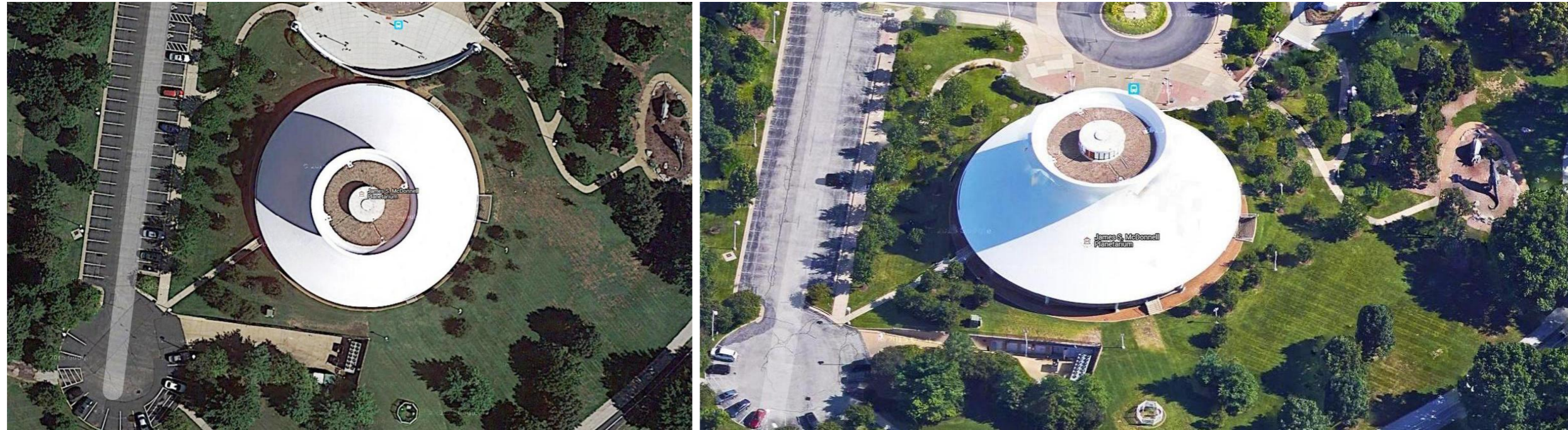


Figure 3.35 - Hyperboloid Shell of McDonnell Planetarium, by HOK Architects & A. Alper Structural. Engineer, St. Louis, MO, USA, 1963.



N. LONG SPAN CANTILEVERED REINFORCED CONCRETE SHELLS OF IRREGULAR FORM

Reinforced Concrete Shells can be built of many configurations and forms that ultimately have to be properly designed and supported.

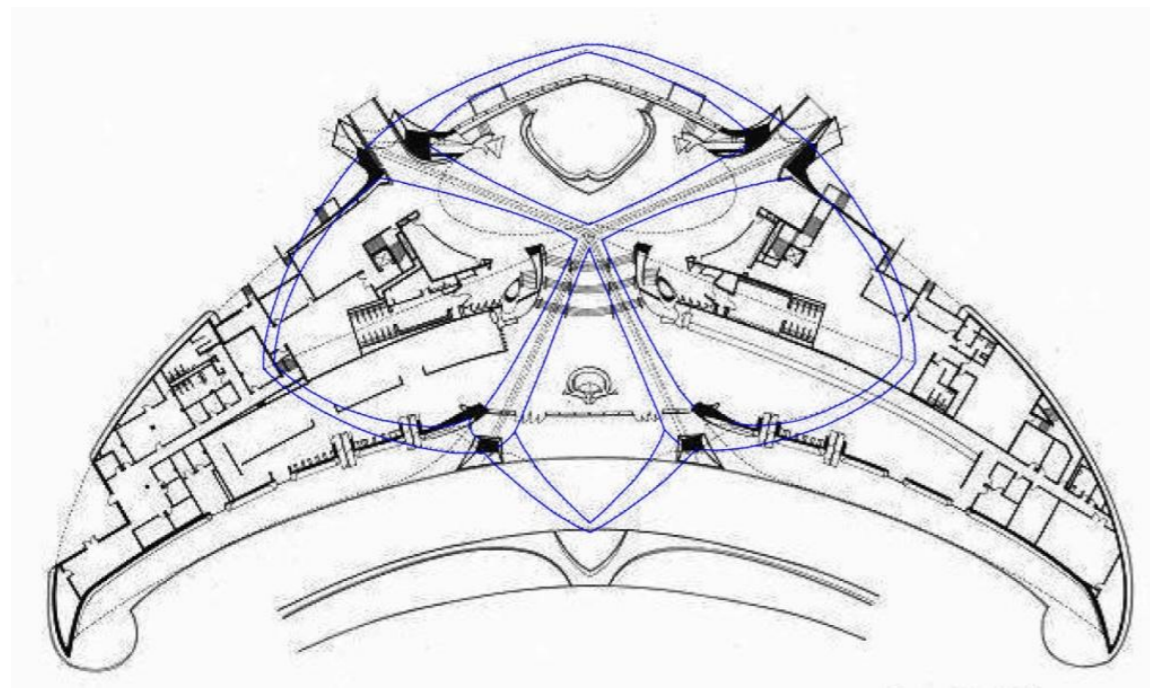


Figure 3.36 – Cantilevered Shells for the TWA Terminal at JFK Airport, by E. Saarinen, Architect, Ammann & Whitney, Engineer, NY 1962.



3.6 – HYPERBOLIC PARABOLOID (HYPAR) SURFACE GENERATION USING STRAIGHT LINES

Hypars formed within curved edges can also be generated using sets of intersecting straight lines between two opposite curves as it is demonstrated by the hyperbolic paraboloid shell structures designed and built by Felix Candela in Mexico and shown in Figures 3.37 to 3.39 below.

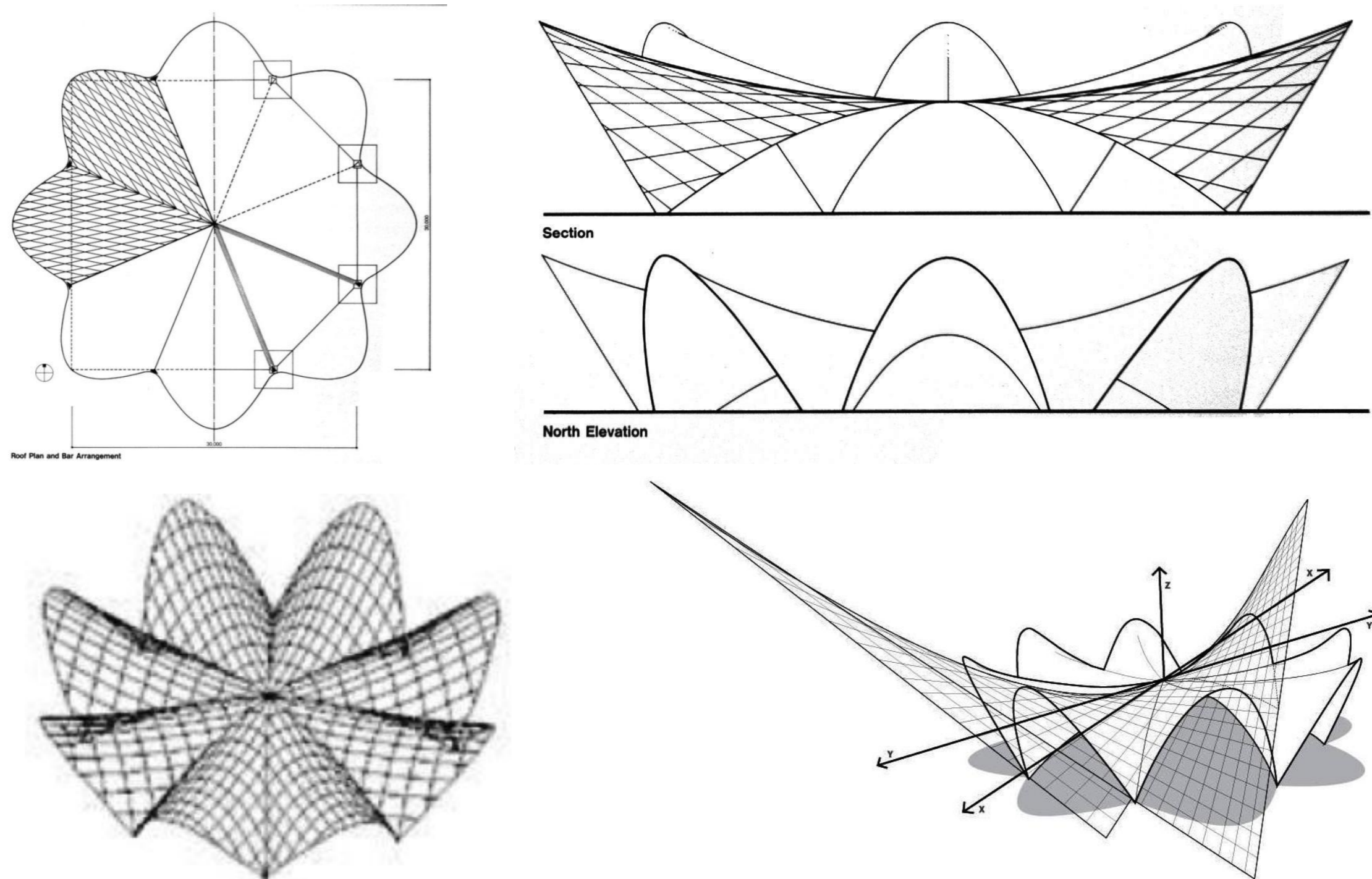


Figure 3.37 – Los Manantiales Restaurant in Xochimilco Mexico by Felix Candela, 1958, Plan, Elevations, and Isometrics Models.



A curvilinear 3D surface to cover a square floor plan can be formed by the intersection of four vaulted conical surfaces which will form what is called Groined Vaults. If we take half of each one of the four intersecting conical surfaces we will have a three dimensional triangular type of surface bounded by three parabolic curves as shown in Figure 3.37. The three parabolic curves are labeled as 1, 2, and 3 and each one of them is divided by $1 \times 5 = 5$, $2 \times 5 = 10$, and $3 \times 5 = 15$ segments of the parabolic curves having equal segments of x and y dimensions in the projected x-y plane.

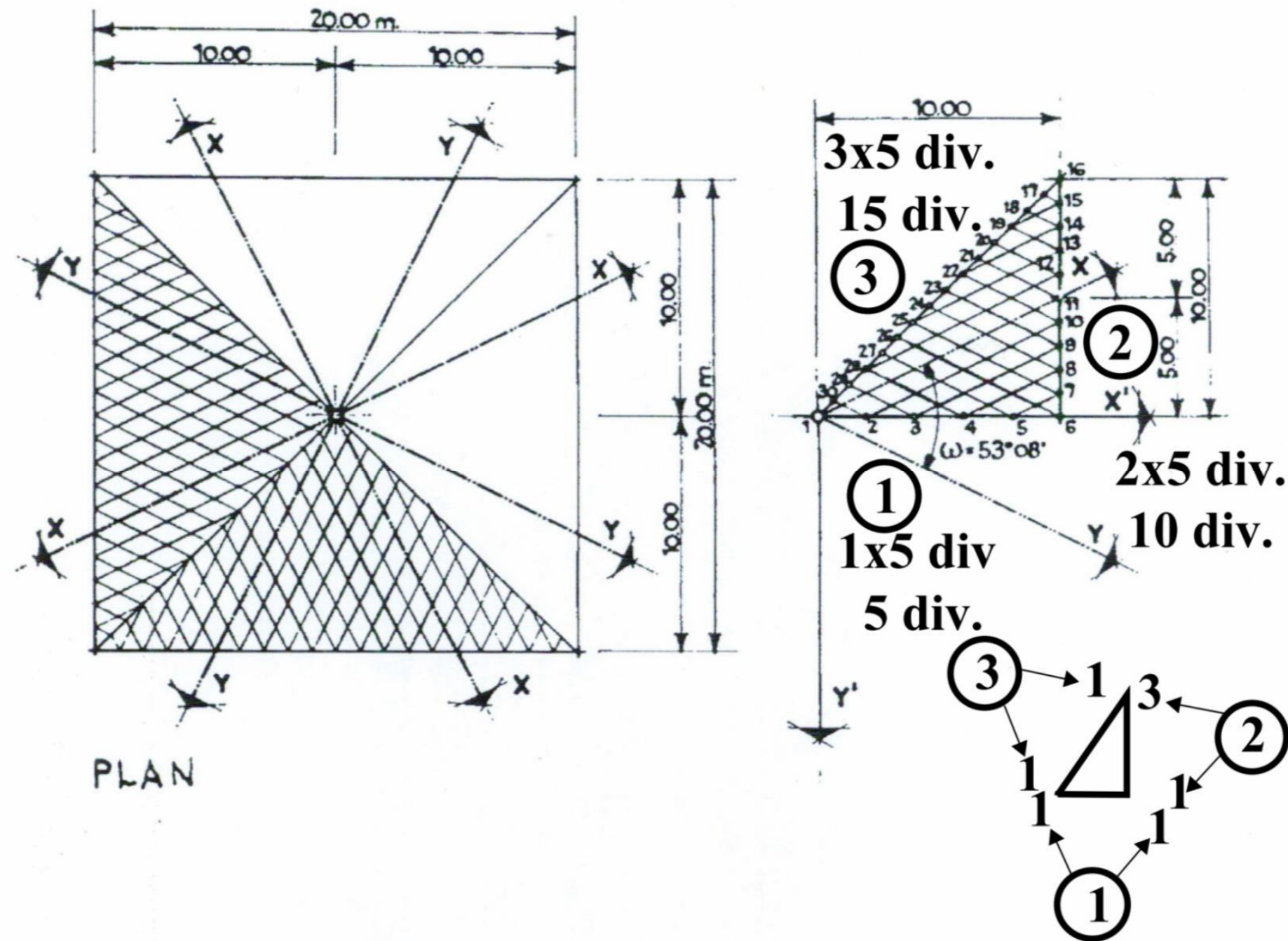


Figure 3.38 – Generation of Hyperbolic Paraboloid (Hypar) Shell Surfaces within three parabolic curves, by Felix Candela.



We can then generate one set of straight lines joining each point of parabolic curves 1 and 2 with the corresponding points along the parabolic curve 3, and another set of straight lines joining each point of the parabolic curve 2 with each point of curve 1 and each other third point of curve 3. The intersection of the two sets of straight lines will form an anticlastic 3D Hypar surface as shown in Figure 3.38.

In October of 1960, Felix Candela published a technical paper in the Journal of the ACI titled: “General Formulas for Membrane Stresses in Hyperbolic Paraboloidal Shells”, where he presented a set of general formulas for reinforced concrete hyperbolic paraboloidal shells and a numerical example to solve a groined vault with a square plan. By joining the intersection points of the two sets of straight lines along parallel planes to the curvilinear parabolic lines 1 and 2 one can clearly obtain two sets of opposite curvature which will define the anticlastic surface of the hyperbolic paraboloid. The set of lines parallel to curve 1 define a surface in tension (ties) and the set of lines parallel to curve 2 define a surface in compression (struts). Candela in this paper noted: “Every point of the surface is the intersection of two straight lines contained in the surface”.

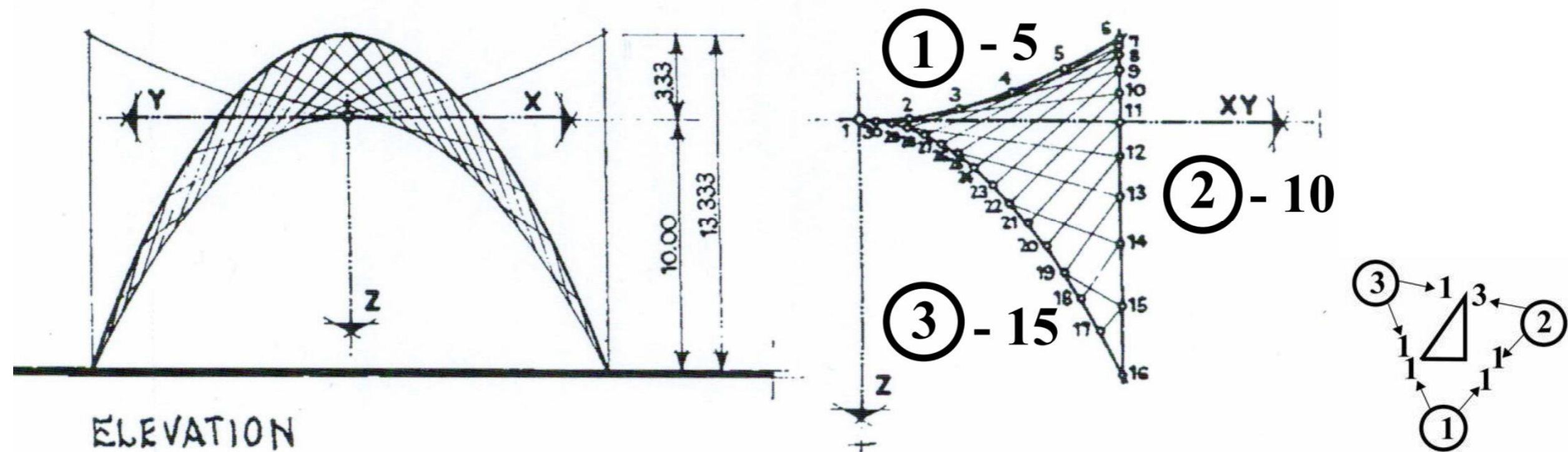


Figure 3.39 - Hyperbolic Paraboloid (Hypar) formed by two sets of intersecting straight lines bounded by three parabolic curves, by F. Candela.



Below in Figure 3.40 is an AutoCAD model of the shell structure of Los Manantiales Restaurant by F. Candela that was generated using the concept noted above of two sets of intersecting straight lines within three curvilinear parabolic lines.

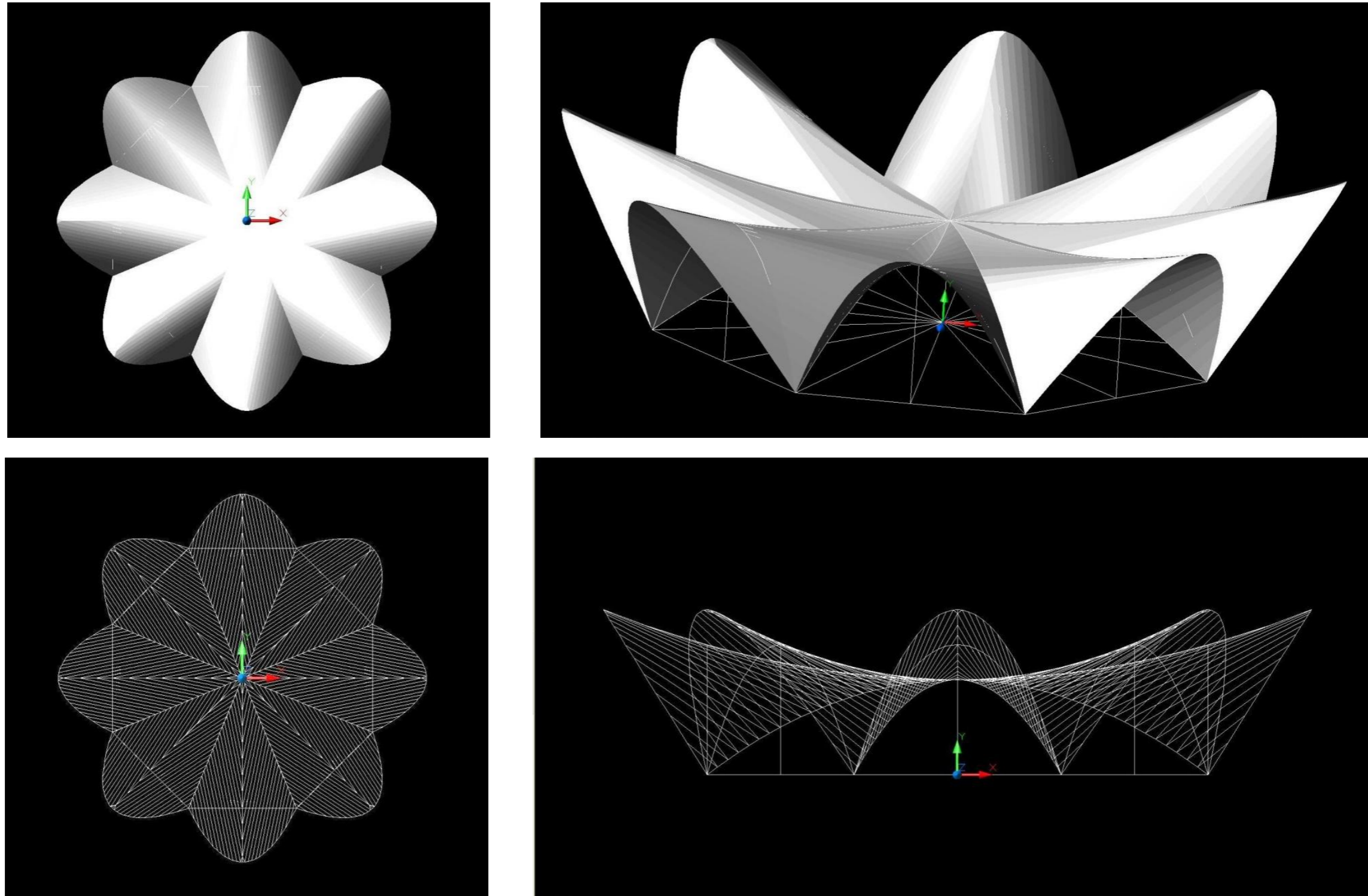


Figure 3.40 – Los Manantiales Restaurant of F. Candela modeled using AutoCAD, Plan and Isometric of solid surface and wireframe model.



AutoCAD, Rhino, and other general purpose 3D CAD software can be used to generate the curvilinear shapes of the parabolic surfaces that are used to form and construct the type of shell structures that will describe the hyperbolic paraboloids (hypars) geometrical surfaces as shown in Figures 3.37 to 3.40. The parabola and catenary curves are the most commonly used geometrical curves to describe the funicular shapes of shell structures under compression and the suspended cables under tensile forces. In Appendix B the Author presents the AutoCAD LISP and Rhino Python Scripts that can be used to generate segmental parabolic curves by selecting three points along the parabolic curve and a given number of segments.

Fuller Moore in his book “Understanding Structures” listed in the References noted that: “The ability of shells to resist tension as well as compression, allows for much greater freedom of form”. Therefore it is very important to understand the actual internal distribution of axial tension, compression, shear, bending, and any torsional stresses in a structural member to be able to design their final dimensions, thickness, and form.

Felix Candela understood very well this concept at his time and recognizing the fact that curvilinear arches and funicular forms due to their curvature can take external forces and following the parabolic or catenary lines carry the forces fully either in compression or tension to their supports virtually eliminating any type of bending stresses. This leads to the principle of Membrane Structures where the shell elements are free of bending stresses. When free curvilinear edges follow the lines of parabolic or catenary curves, then the edge stresses can be minimized which allows having a shell structure without the need of stiffening edge members.

3.7 - HEINZ ISLER AND FELIX CANDELA SHELLS

The exemplary experimental and construction work of the Master Builders of thin concrete shells such as Heinz Isler and Felix Candela among others that contributed to the widespread design and building of concrete roof shells up to the 1970’s left behind a legacy of magnificently built thin shell concrete structures which are to be admired. So many of those concrete shells built by Isler and Candela survive today and can be observed and studied for durability and strength.

John Abel and John Chilton published in the Journal of IASS of September of 2011 a paper entitled: “Heinz Isler – 50 Years of New Shapes for Shells”, where they present a concise summary of the work done by Isler with thin concrete shells.

The Isler type of shells present a typical low profile curvilinear form very much similar to the forms presented by an egg in a horizontal position as shown in Figure 3,41. On the other hand the Candela type of shells presents a typical parabolic form which has a very pronounced height much larger than the horizontal span of the curved surfaces very similar to an egg standing in a vertical position as shown in Figure 3.41.





ISLER TYPE OF SHELLS

CANDELA TYPE OF SHELLS

Figure 3.41 – Heinz Isler and Felix Candela type of thin reinforced concrete shells analogy to horizontal and vertical eggs.

It is important to note that Felix Candela made use of symmetrical configurations or repetitive configurations in rectangular and polar arrays of shells to form the type of groined vaulted structures that identify his work on shells. He noted in his technical paper of ACI, 1960 that: “Symmetrical arrangements of several hypars may lead to simplifications of the necessary support conditions”.

For groined vaults Candela noted: “At the groins of any symmetrical groined vault there remain only forces contained in the plane of the groin, since forces normal to this plane cancel each other with those proceeding from the contiguous surface.

The legacy of Isler and Candela cannot be forgotten and left accumulating dust anymore by today’s architects and engineers. This Thesis is intended to be a document that could spark the interest on this subject and that could serve as a guideline for the “Revival of Shells”. Isler has been considered by many authorities in the field of thin concrete shells as: “a Structural Artist”, due to his sensitivity for the artistic look of his designs of curvilinear concrete shells of mostly low profile height with respect to the shell span, such as the Heimberg Tennis Center, Swiss Bern and many others well documented in the thin concrete shells papers of the IASS.

In the following pages the Author will display some of the multiple numbers of thin reinforced concrete shell structures that were designed and built by Heinz Isler and Felix Candela throughout their professional career in several parts of the world.



A. ISLER SHELLS

Heinz Isler was a prolific shell designer and builder, from initial concept to actual building completion. He based most of his designs on experimental models that he built himself in this private laboratory following some basic proportional dimensions from hanging models of shells.



Figure 3.42 – Heinz Isler and some of his constructed thin reinforced concrete shells in Switzerland, Europe.



From the experimental models that Heinz Isler built from hardened hanging clothes, he noted: “The model has an answer to nearly everything”.

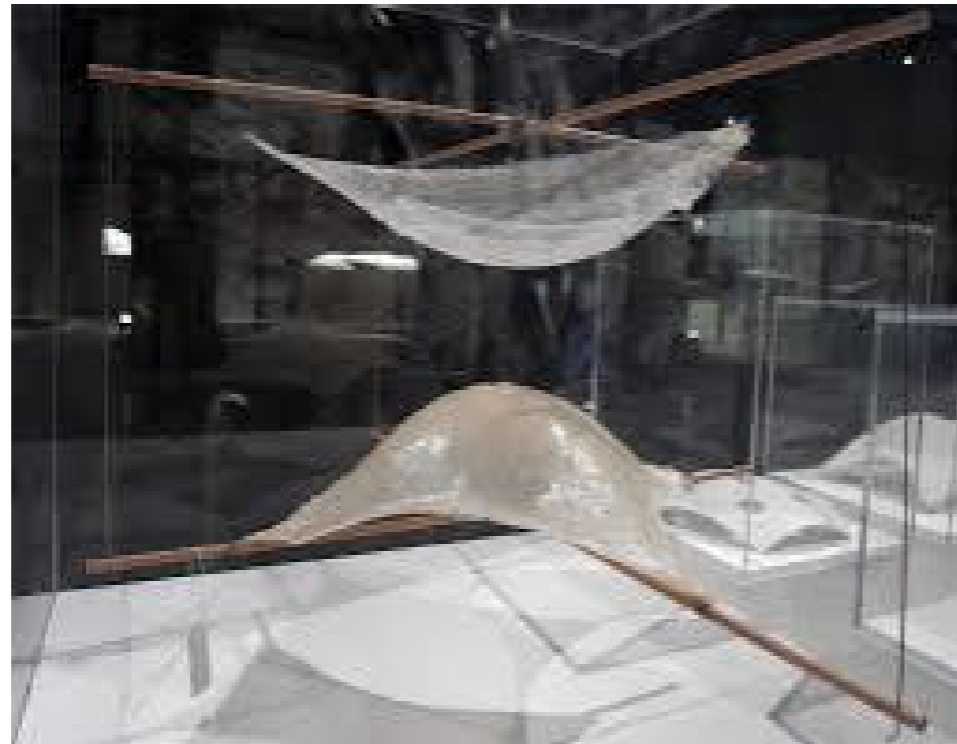


Figure 3.43 – Heinz Isler models of shells based upon hardened hanging clothes and inverted shells.



Some of the shell projects designed and built by Heinz Isler includes: Wyss Garden Center, Solo Thurn, Switzerland, in 1961, The Indoor Tennis Center, Heimberg, Switzerland, in 1979, and the Sicli Company Building, Geneva, Switzerland, Switzerland, in 1969. Photos of these projects are shown in Figures 3.41, 3.43, and 3.44. Heinz Isler understood very well the behavior of shallow height of his shells and provided thickness to the sections of the shells at its supports to make sure that the overall weight of the shell could be properly supported at each point of support. Isler used the undulation and corrugation of the edges of the shells to properly support the axial and any bending forces-stresses along the edges of the shells.



Figure 3.44 – Heinz Isler thin reinforced concrete shell projects designed and built in Switzerland and Europe.



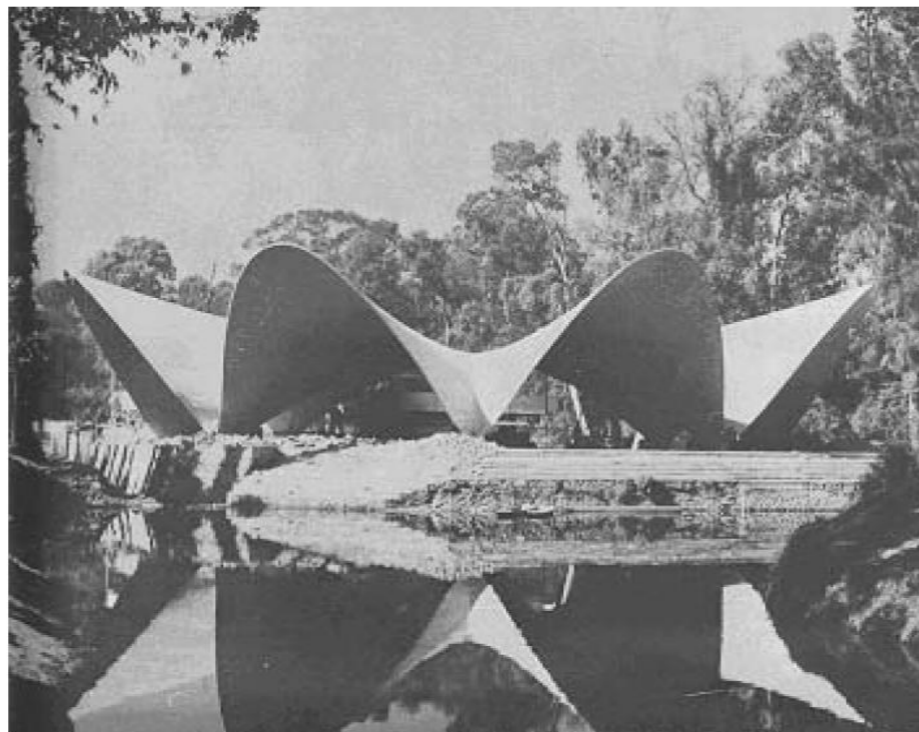
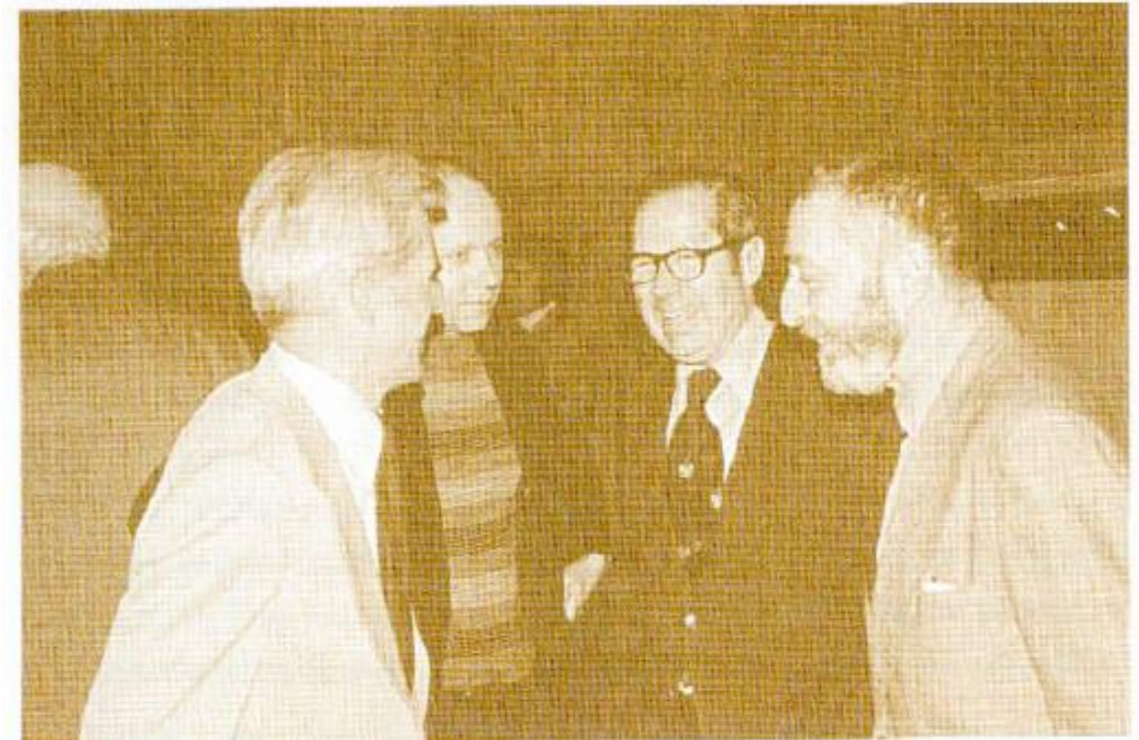
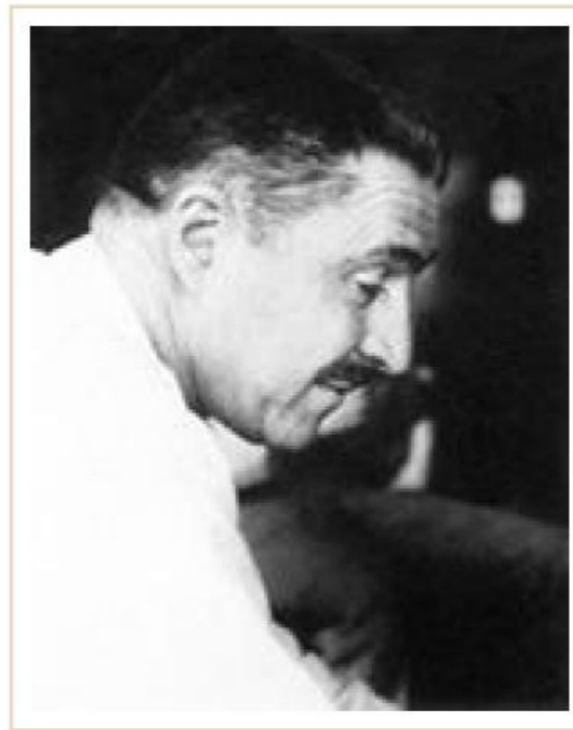
Heinz Isler and Antonio Gaudi experimented and used hanging chains and hanging fabrics to visualize the natural shapes of the forms created by the hanging chains and fabrics to then extrapolate those basic forms into real shell structures.



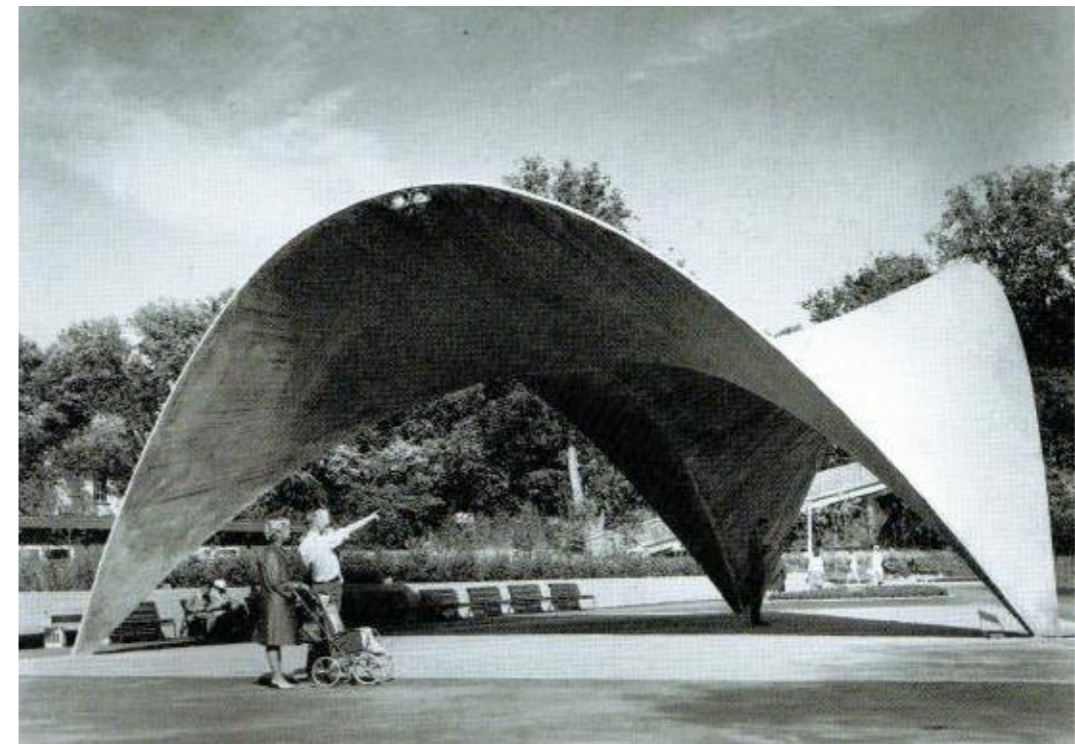
Figure 3.45 – Heinz Isler thin reinforced concrete shell projects built in Switzerland and Europe, Aerial Views, Elevations and Formwork.



B. CANDELA SHELLS



Los Manantiales Restaurant in Mexico



Botanical Gardens in Oslo, Norway, 1962, by Felix Candela

Figure 3.46 – Felix Candela and Frei Otto, Los Manantiales Restaurant shell in Mexico and the Botanical Garden shell in Norway.



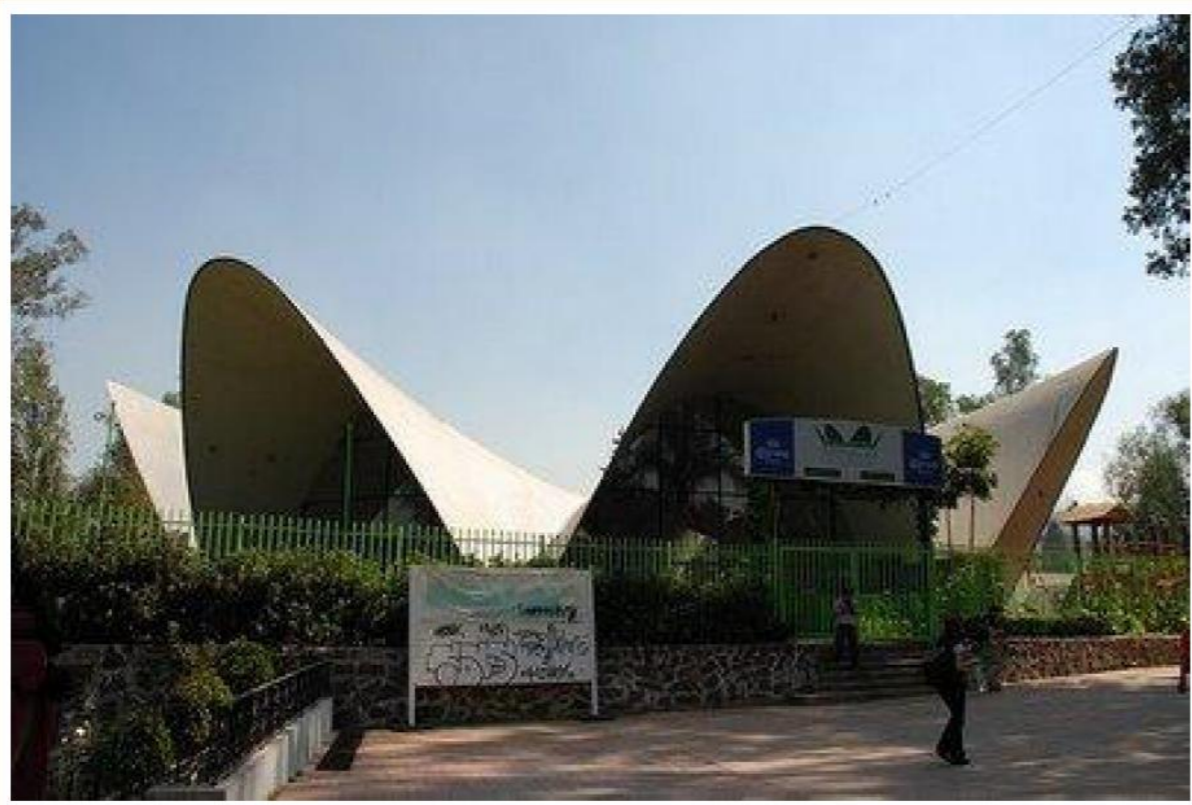


Figure 3.47 – Felix Candela shell project: Los Manantiales Restaurant built in Mexico and Model built at Princeton University in USA.



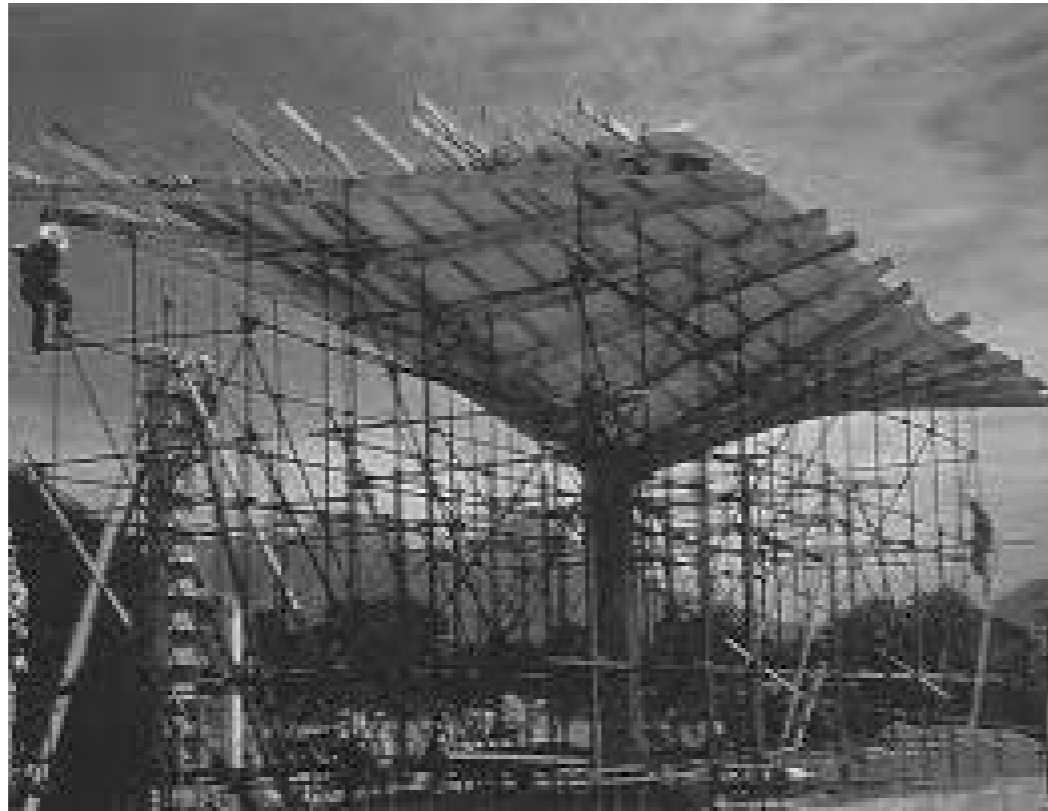


Figure 3.48 – Felix Candela thin reinforced concrete inverted umbrella shell project built in Mexico, Formwork and Elevation View.

As the builders of shells such as Candela and Isler in different parts of the world experimented and started to build new forms of shells and pursued to achieve greater spans with thinner and lighter shell cross sections a great variety of shell forms were realized and built up to the point where the limited strength, stiffness, and stability of the shells reached their maximum feasible spans to thickness ratios (L/t). As the shell span to thickness ratio (L/t) increases then the capacity and stability of the shells become limited mainly by the BUCKLING capacity of the shell section to resist the internal axial compressive forces that will develop in the relatively thin member section. Therefore some modifications to the edge boundaries of the shells are necessary to control buckling of the thin sections of the shell that will be subjected to axial compression and shear stresses.

After studying the multiple shapes and forms of architectural and engineering shell structures that have been built in the past years and when reviewing what is being done currently worldwide at several research institutions by ways of experimental models and demonstration projects it is clear that arched, parabolic, catenaries, spherical, vaulted, domed, and thin shell structures of a variety of forms are there waiting to be rediscovered and also to be reinvented in some new and innovative adaptive forms and practical modern application using new technologies and adaptive new materials. We must use our own intuition to project new scientific ways to adapt current technological methods of construction.



It is important to recognize that a prominent group of leading architects, engineers, builders, and pioneers conceived, envisioned, designed, and constructed outstanding shell structures which are still standing today. Several different type of shell forms were achieved as it is shown in Section 3.3 where multiple projects using reinforced concrete thin shell structures accommodated a variety of multifunctional architectural use of the covered spaces and the structural engineering of the shell forms allowed the efficient use of the reinforced concrete as the main building material.

The mathematical formulations and solutions of the differential equations to describe shell structures in general terms can be very complicated and not always can cover all cases of shells with different curvatures, edge, boundary, support, materials, and loading conditions, therefore at the time those shell structures were designed and build the architects, engineers, and builders had to rely on small scale models of the shell structures to observe their behavior and constructability issues that may arise under the projected service loading conditions.

In the 1940's in Italy, Pier Luigi Nervi experimented extensively and build shell structures using a new type of structural element that he called "FERRO-CEMENTO" which is an extremely thin plate of concrete made of layers of small diameter wire mesh covered thoroughly with cement mortar with wet sand used as the binder. Using ferro-cemento he built an experimental storehouse for his own company in Rome. Nervi introduced two ingenious ingredients to create thin shell structures; first the use of multiple layers of thin wire mesh distributed throughout the surface of the shell and second the elimination of wood formwork to cast the thin concrete shell structures.

Thin shell concrete structures can be exposed to a combination of compression, tension, and shear internal stresses and in some cases depending on the boundary and support conditions to bending out-of-pane stresses, therefore it is critical that well distributed number of steel reinforcement oriented in at least two major perpendicular directions are placed in the cross section of the thin shell to accommodate the tensile stresses that may develop and that cannot be properly absorbed by the weak concrete components under tensile stresses.

Today very sophisticated and powerful computer systems and special purpose software allow the architects, engineers, and builders to experiment multiple options of geometrical forms with different shapes, thicknesses, configurations of curvatures in different directions, and with a mix of materials that will allow for optimized, efficient, and economical final shell structures. Also it is possible to model shell structures using flexible formwork that can be made part of the final shell structure using high tensile fabric materials. The use of software with graphical scripts using Rhino, Grasshopper, and other parametric pre-processor and post-processor routines allows for a fast and intuitive modeling of thin shell concrete structures that are adaptive to the final intended use of the architects, engineers, and builders. 3D printing today allows for a quick review of models before they are actually build, simplifying the experimental building of small scale physical prototypes.



CHAPTER 4 - FABRIC FORMED MEMBRANE SHELL, EXPERIMENTAL AND RESEARCH WORK

4.1 - OVERVIEW OF FABRIC-FORMED CONCRETE SHELLS PAST WORK

Concrete is an ancient man-made construction material that dates back to Roman times. Its ability to take virtually any possible shape provides the construction industry a unique opportunity to achieve an imaginable variety of forms which are tremendously difficult to achieve with any other current building materials. Concrete can be cast-in-place or can be precast at a factory off site. Advances in new technologies to produce high quality concrete have led to the use of several new ways of producing final forms of concrete which can be identified as: self-compacting concrete (SSC), fiber reinforced concrete with a variety of carbon, fiberglass, steel, and other types of ferrous and synthetic fibers, flexible fabric-formed and cable-net formed concrete structures, sprayed concrete and shotcreting (additive fabrication of concrete) processes.

For very small scale experimental laboratory models, stretchy flexible textile such as “Spandex” can be used to simulate the behavior of fabric membranes, and this tensioned fabric mould can then be covered with latex modified cement mix or with some type of Cement of Paris to achieve a casting over the flexible formwork to form a shell-like structure.

Fabric-formed concrete structures can be defined are those where the main formwork used to cast concrete is some type of flexible fabric or membrane which will hold the cast-in-place or precast concrete in place until it hardens to its final form. Diederick Veenendaal in Chapter 2 of the “Fabric Formwork Book” presents a documented description of the history of Fabric Formwork, here we learn how Gustav Lilienthal (1849-1933) born in Anklam (at the time part of Prussia) and today Germany invented the first fabric-formed floor system (fireproofed ceiling) for which obtained a patent in September 8, 1897. This is the first and earliest known case of fabric formwork consisting of wire netting, paper, or other suitable fabric, and screed covered by concrete and used to create a combined fireproofed ceiling-floor system. Lilienthal used the flexible fabric without internal prestress, the fabric was not tightly strained, but it was simply allowed to hang freely under its selfweight creating a catenary formwork between the beams.

A technical article authored by Veenendaal, West, and Block in 2011 presents a well-documented and comprehensive history and overview of the evolution of flexible formwork using fabrics for casting concrete from the mid 1800’s through the early 1900’s and up to 2011 when the article was published. Inflated or pneumatically formed concrete structures have also been achieved in the past as it is documented in this technical paper.



Good portions of the history of Fabric Formwork documented by Veenendaal were incorporated into Chapter 2 of the “Flexible Fabric Formwork” book recently published by Mark West and listed in the references. We also learned from this technical article that early examples of flexible fabric formwork was done using pieces of Burlap and Hessian made from organic fibers which is what was widely available at that time.

At ETH in Zurich, Switzerland, Philip Block leads BRG (Block Research Group) which has been involved in a series of academic and practical research projects using a reusable cable-net and tensioned fabric to form thin shell concrete prototype models. A highlight of their research work is the NEST HILO roof project which is noted to be a ultra-lightweight and super integrated thin concrete doubly curved (anticlastic) shell canopy structure to be built at the top of an apartment building as a penthouse for visiting faculty of Swiss Federal Research Institutes Empa and Eawa in Dubendorf, Switzerland. Details of this project have been published by Veenendaal, Bakker, and Block in a recent article in the Journal of the IASS (March 2017) listed in the References.

In this same technical article noted above, the authors (Veenendaal, West, and Block) highlight how James Waller (1884-1968) noticed that: during war times, ”cement dust blown onto a wet tent rendered the canvas amazingly strong“. Waller is credited with inventing the “Nofrango” system which was a built by using a hessian fabric stretched over a wood or timber frame that was plastered with cement mortar. At the time, Waller also created some type of Hen House (Chicken House) using this same similar system. Waller also created some type of roof construction that followed the shape of an inverted catenary arch with the shape of the roof surface taking the form of a corrugated cross section that will provided substantial stiffness to the shell roof structure to go long spans. Waller labeled his parabolic shaped roof system, the “Ctesiphon Shell System”.

Spanish architect Miguel Fisac (1913-2006) studied at the “Escuela Superior de Arquitectura”, he explored the possibility of using fabric-formwork to achieve aesthetic characteristics of building facades and to achieve structural efficiency and stiffening of building members following the shape of the bending moments of the member under loads, by following the interesting organic and bone-like shapes that were achieved using posttensioned beams. Fisac used smooth and flexible polyethylene type of membranes hanging from rigid frames to be the formwork of the structural members.

Other names of people that contributed to the development of flexible formwork such as Richard Fearn, Dennis Farrar, Guruvayur Ramaswamy, Karl Billner, Haim Heifetz, Bindhoff, Hillen, Lamberton, Turzillo, Scales, Gebhandt, and others paved the way for the current state of flexible fabric formwork building technologies.



Sidney Parker in 1971 patented several floor systems that permitted to lower their construction cost due to the parabolic shape of the formwork that will follow the shape of the bending moment of the floors along the span. Other companies such as Fab-Form Industries have also contributed to the development of different forms of flexible formwork technologies and building systems.

Architect Mark West of Canada and Kenzo Unno of Japan have performed substantial research and have built prototype of fabric-formed concrete members which are used as main structural members of building and as architectural facade members, beams, columns, and other types as well. The use of woven synthetic fabrics as flexible formwork is very attractive in the construction industry due to its relatively inexpensive cost and its very strong tensile properties. Mark West in his recent book “The Fabric Formwork Book” pointed out that: “Living Things are made with Membranes under Pressure” therefore we have a long way to learn from nature and living organisms, including our own body where we could find all type of membranes and forms which could give us the clue on how we could create innovative structures and building forms that can mimic or recreate the efficiency and intelligence already built into nature and living things to advance the technologies for new architectural and engineering structural forms. Bionics and Biomimicry are then two technological areas that deserve great attention for future adaptive building developments.

Robert P. Schmitz completed his Master’s Thesis in 2004 at the Milwaukee School of Engineering titled: “Fabric Formed Concrete Panel Design” focusing his research in the development of a FEM (Finite Element Method) procedure to analyze and design a fabric cast concrete wall panel. Schmitz wrote a technical article in April of 2016 (<http://www.forconstructionpros.com/article/12184038/is-there-a-future-for-fabric-formed-concrete-structures>) titled: “Is there a Future for Fabric-Formed Concrete Structures?”, where he discusses the use of flexible fabric formwork to contain the fluid concrete and form it into final members for structural and geotechnical applications. In this article Schmitz quotes Professor Remo Pedreschi who says: “We should not see fabric formwork as a replacement but a new “disruptive technology” that offers us the opportunity to design formwork in a new way”. The International Society of Fabric Forming (ISOFF) is an association of individuals and institutions from around the world dedicate to study and advance all aspects of flexible forming from concrete to glass and to perform research looking for the most efficient designs and observe the behavior of flexible fabric formed structures. ISOFF has organized congress, seminars, and presentation of flexible forming structures.

Kyle Sturgeon, Chris Holzwart, and Kelly Raczkowski students of Architecture at the University of Michigan in 2010 completed an experimental project of building a very primitive organic form called Fatty-Shell where they used flexible rubber mould filled with concrete to create a very irregular bulging web-like structure that resembles internal human fatty tissues.



This type of structure-sculpture was produced using high-tech fabrication techniques and involving a robotic arm to cut pieces of rubber that were then stitched together to create the overall mould. Detailed information and pictures of this project can be found in this link: <http://k-sturgeon.com/portfolio/fatty-shell-2>.



Figure 4.1 – Fabric Formed Beams, by Mark West

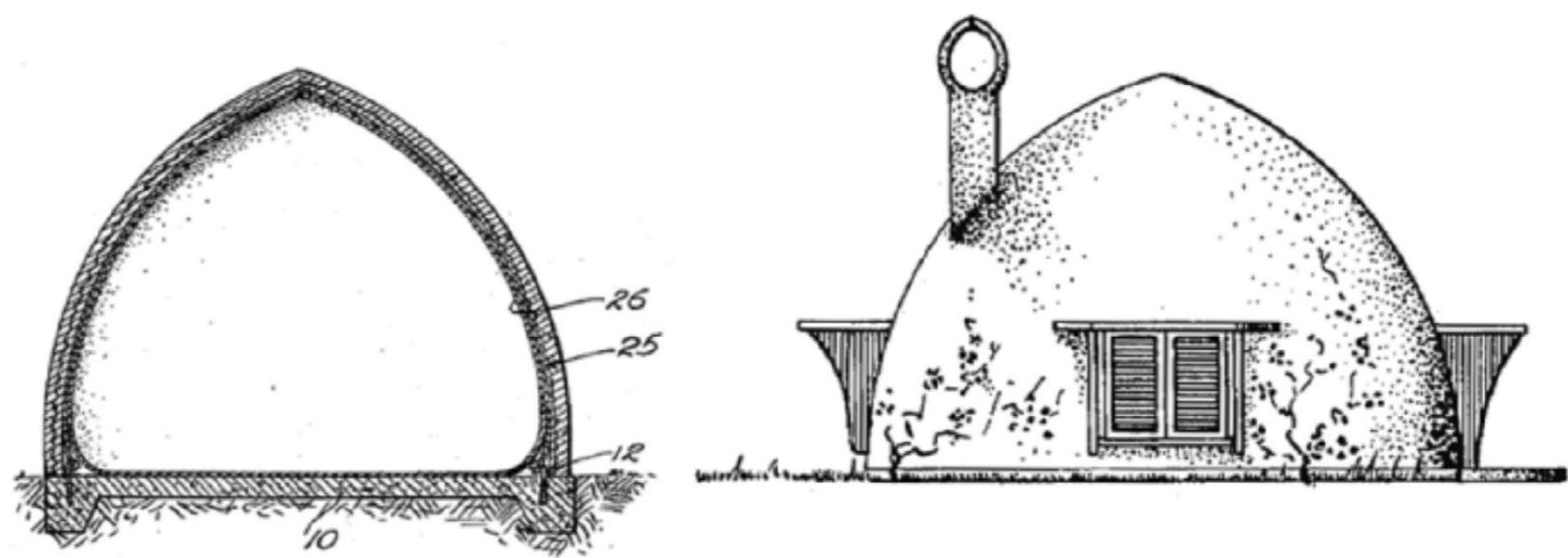


Figure 4.2 - Pneumatically formed concrete shell, Patented by W. Neff, 1941

Wallace Neff in 1941 patented a pneumatically formed shell as it is shown in Fig. 4.2. Neff is credited with pioneering the use of pneumatically formed or inflated domes as formwork for concrete bubbled houses.

Dante Bini later expanded the work of Neff and created what he called the “Binishells” which are widely built now in USA and around the world in different shapes and configurations. Some types of PVC coated fabrics which have very close mesh configuration are well suited as flexible formwork base material.

One of the key findings of researchers working in this field of flexible-fabric-formed concrete is that “excess water escaping through the open spaces of the meshes of fabric, led to unusual higher concrete strength“ than conventional concrete members cast-in-place with traditional rigid formwork made of wood or steel, high quality finish of the concrete surface is also a key characteristic of fabric-formed concrete members achieving improved hardness of concrete surfaces and reduced porosity due to the final water-cement ratios after water escapes from the moulded concrete.



New technologies in concrete construction, recent advancements, and implementation of new technologies in 3D additive manufacturing to build shells of variable cross section thickness, Robotics, 3D printing of concrete, 3D subtractive fabrication, hybrid flexible membranes with rigid thin concrete shells, optimization and highly efficient lightweight structural systems open the doors for new more architectural expressive building forms. All the above can certainly push the envelope and provides new avenues to achieve concrete structures that will satisfy the engineering parameters of strength of materials and the architectural requirements of functional and efficient building forms that will be compatible with the flow of forces to the supports of the concrete structure.

For more complicated curvilinear and non-standardized concrete structures including sculptural free-form architectural concrete for artistic expressions or decorative architectural concrete monuments there have been some recent publications of realized and built concrete shell sculptures. The Danish Technological Institute (DTI) coordinated and executed the construction of a full-scale sculptural architectural concrete structure called the “Demonstrator“, as part of The TailorCrete project located in Aarhus, Denmark. For this project the DTI introduced new novel and cost-effective ways to fabricate non-standardized formwork to cast concrete of very unusual and free form surfaces. Digital three dimensional (3-D) modeling using advanced computer-aided design (CAD) software as well as digital robotic fabrication of formwork and reinforcement rebar cages and complex rebar fabrications to enable the realization of very complex digital architectural surfaces. The use of a flexible membrane to cover over the machined milled EPS (Expanded Polystyrene) type of Styrofoam help to deliver a smooth concrete surface while making sure to reuse and recycle the waste material.



Figure 4.3 - The TailorCrete Project, “Demonstrator“, Danish Technological Institute (DTI), Design Concept and Completed Sculpture.



For this project it is interesting to note that sometimes the same heavily reinforcement cages that are detailed and installed as the main reinforcement of the sculptural structure can also be used to support some type of membrane or fabric that will allow the use of shotcrete over top and bottom faces of the fabric used as part of the formwork. With the appropriate number of layers of shotcrete it is also possible to achieve the same level of thickness of the concrete sculpture and the finished surfaces. Detailed information on this project can be found in the March 2016 issue of the Concrete International-CI Magazine of the ACI.



Figure 4.4 - The TailorCrete Project, “Demonstrator“, Danish Technological Institute (DTI), Steel Rebars and Robotic Generated Formwork.

A 36 ft. high decorative architectural concrete sculpture titled “Stealth“ was built in midtown Atlanta, GA, USA. It features a carbon-black, polished monolithic concrete sculpture of very sharp curvilinear edges and shape. The team that build it, Formations Studios, created a three-dimensional (3-D) parametric model to construct the complex formwork in which the carbon black concrete would be cast by using a hybrid combination of digital manufacturing technologies and manual craftsmanship. Again here a heavy reinforcement cage forms an integral part of the overall inner part of the sculpture. One can argue that here a flexible fabric could have been applied over the complex curvilinear three-dimensional surface of the sculpture and layers of shotcrete could have been used to achieve the final shape. An intricate a very detailed curvilinear formwork had to be devised to achieve the curvilinear formwork around the inner portions of the heavy reinforcement. Detailed information on this project can be found in the March 2016 issue of the Concrete International-CI Magazine of the ACI, dedicated to Decorative Architectural Concrete.





Figure 4.5 - The “Stealth“, Architectural Decorative Sculpture in Atlanta, Georgia, USA., Rebars, Formwork, and completed Sculpture.

”The expression: Less is More”, goes along well with the concept of achieving thinner concrete structures that will be strong enough to serve the functional purposes of architectural and engineering applications of concrete for exterior building facades, short and long span roof and space covering structures, interior designs, and sculptural concrete forms.

Textile Reinforced Concrete (TRC) is a hybrid composite material where an open mesh flexible fabric is cast together with fine-grained concrete to achieve a lightweight concrete structure capable to handling both compressive and tensile stresses for an efficient thin concrete structure with minimal concrete cover.

A technical note from the Teknologisk Institut, NICE Fremtidens Nordiske Betonarkitektur, presents a review of trends and general overview of new advanced and automated solutions in the concrete industry focusing on the different types of non-traditional formwork systems that have been recently introduced into the concrete industry to build more expressive, economical, and efficient short and long span concrete building systems.

Flexible fabric-formed concrete has recently being the subject of a research project at Massachusetts Institute of Technology (MIT) where Namjoo Kim a doctoral candidate performed an experimental research project on ”Latex Formwork: Concrete wall panel construction method (www.holcimawards.org/projects/latex-formwork)“, investigating the practical applications of thin concrete shells to building facades.



The curvilinear wall panels consist of a substructure made of a flexible wire mesh and the flexible formwork made of a latex sheet which faceted form determined the final form of the wall panel. The flexible formwork is reusable and recyclable. The proposed wall panel construction using flexible fabric-formed concrete is thin, lightweight and very adaptable to modular facades with special and attractive architectural expressive form.

Thin concrete structures and shells under service loading conditions can be subjected to high axial compressive and tensile stresses in combination with substantial bending stresses due to the continuity and rigid nature of the shell member. Realizing the brittle characteristics of thin concrete structures then the introduction of steel fiber reinforcement to a special type of new class of cementitious composite mix of concrete at low water cement ratios in the order of 0.25 and optimized gradation of the granular constituents produces an Ultra-High-Performance Concrete (UHPC) which has proven to provide mechanical properties of compressive strength greater than 21.7 ksi (21,700 psi) and sustained post-cracking tensile strength greater than 0.72 ksi (720 psi).

According to extensive investigations, and field reports of the Federal Highway Administration (FHWA) of the USA the UHPC has an inherent discontinuous pore structure that reduces liquid ingress to the finished structure, which significantly enhances the durability of structures built with UHPA as compared to conventional normal weight concrete.

It is important to highlight the role that new materials and new technologies play into the achievement of production of thin fabric-formed concrete structures and shells in the construction industry today. A news short article of the Industry FOCUS section of the ACI Concrete International magazine of March 2014, pp. 10, reports that the SGL Group (<http://www.sglgroup.com>), The Carbon Co. (Wiesbaden, Germany) and V. Frass Solutions in Textile GmbH (Helmbrechts, Germany) have developed a 3-D carbon fiber reinforcement grid product that can be used as reinforcement to allow the production of concrete (UHPC) facade panels of only 26 mm. (1 inch.) thickness. The new 3-D textile reinforcement based on SGL's SIGRAFIL C carbon fibers can also be manufactured in large dimensions to accommodate the production of a variety of sizes of concrete panels to be used at exterior facades of buildings.

Another interesting new type of reinforcement material that can be used with ultra-high-performance-concrete (UHPC) is "solidian" (www.solidian.com) which is a non-metallic reinforcement that comes in the form of grids and rebars made of alkali-resistant glass, basalt, or carbon fibers which possess non-corrosive material properties and very high tensile strength that allows the achievement of thin, slender, lightweight, and durable construction of concrete panels. Other type of fabrics such as "SAERTEX", a 3D woven carbon fiber are available for high tensile capacity.



The total volume of concrete can be greatly minimized due to the high tensile strengths of the mesh of approximately 508 ksi, some 8 times higher than conventional high strength steel reinforcement of 60 ksi. Solidian products available in the market are Solidian GRID Q142/142-CCE-38 rigid mesh and Solidian GRID Q62/62-AAS-30 flexible mesh that can allow the production of precast concrete panels in the range from 0.39 inches To 1.18 inches.

Madeo and Novi reports that researchers at the University of Edinburgh have experimented and produced prototypes of full-scale architectural elements of curvilinear and shell forms. Below are some pictures of the shapes that were built at the university labs showing the complexity of the forms and the quality of the obtained finished concrete surface of the members using the flexible fabric formwork. Researchers at the University of Bath in England have also experimented building concrete structures using fabric formwork.

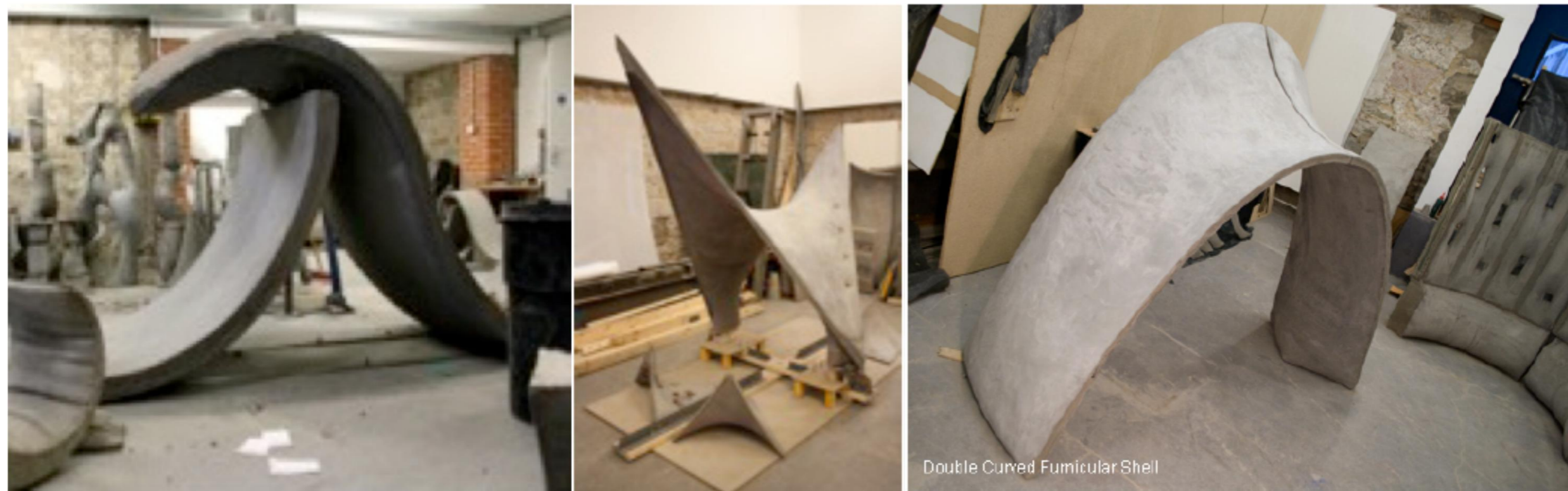


Figure 4.6 - Curvilinear Wave, Hyperbolic and Gaussian Shell Fabric-Formed Concrete experimental prototypes, University of Edinburgh.

A Technical Paper describing the experimental testing and construction techniques used to build four fabric-formed concrete beams specimens of variable cross section geometry was presented by Orr J, Derby A., Ibell R., Evernden M., and Otlet M. of the Department of Architecture and Civil Engineering of the University of Bath, UK. In this paper the Authors indicate that “Flexural elements are fundamentally inefficient and it is in the design of shell structures that real material saving may be found“.



Certainly fabric-formed concrete members of variable cross section built using some type of woven polyester fabric as formwork can achieve reductions in total weight compared to similar prismatic rectangular cross sections and the quality of the finished surface due to the use of a permeable mould is found to be of much better and high quality. Optimized cross sections can be achieved that will ultimately translate into reductions in overall costs of materials, production, installation, and foundations to support the total dead loads of the buildings with reduced weight variable cross section fabric-formed concrete members. Real advantages can be obtained when the fabric-formed concrete members are built as precast units under factory controlled quality conditions and are built in a repetitive manner using and reusing molds of flexible fabric formwork.

It is recognized from the study of current flexural elements that they are fundamentally structurally inefficient since they are built with excess material such as concrete which is cast in a rectangular moulds and reinforced with rebars that not necessarily follow the contour lines of principal stresses. At the opposite side of the spectrum of structural forms we have the curvilinear concrete shell structures which can achieve impressive thin cross sections and are able to carry external forces of high magnitude, providing then a structural form where the real material savings can be realized.

Another type of Fabric Formed Concrete Shell can be created by using 3D Printing of grid shells (using the Additive Manufacturing Process - AMP) of any imaginable synclastic or anticlastic curvilinear surface to serve as the three-dimensional formwork that can then be covered with some type of tensioned fabric membrane that will then receive the uniform or non-uniform thickness of concrete which will form the type of desired shell structure.

The type of membrane grid shells described above can be called: “Discrete Flexible Formwork (DFF)”, which basically can serve two purposes, one to serve as a tensioned grid of support of a layer of membrane formwork that will receive concrete and two to be a grid of reinforcement that can be placed on top of a tensioned layer of flexible fabric formwork and be cast with concrete to have a flexible fabric reinforced concrete shell.

It is also possible to add some layers of textile fabric and embed them into fine grained concrete to form what is called: “TFRC – Textile Fibre Reinforced Concrete” which is an innovative composite concrete system that can be used to create thin reinforced composite concrete shells. The layers of textile fabric embedded or placed as external tensioned formwork can be used as reinforcement of thin concrete shell structures to add tensile strength to the composite member in addition to the randomly embedded fibres that can also contribute to absorb some of the tensile in the matrix.

Figure 4.7 shows a sample of the typical textile fibre reinforced concrete member, a sample of the typical textile fabric mesh, and a sample of a highly ductile thin concrete member under experimental testing. Soranakom and Mobasher at Arizona State University of USA developed a Flexural Analysis and Design Method of Textile Reinforced Concrete.



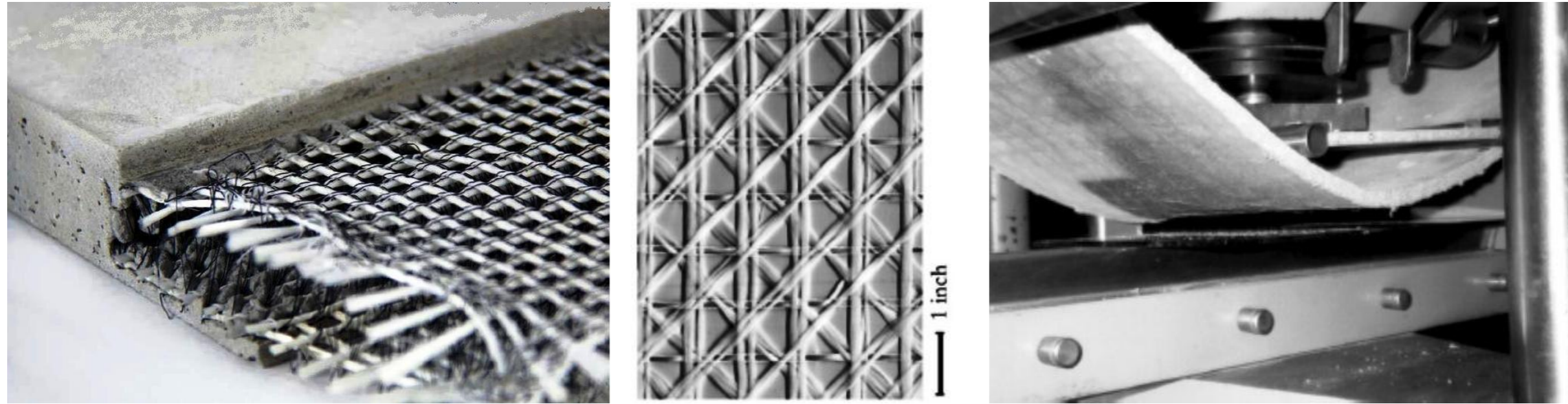


Figure 4.7 – Textile Fibre Reinforced Concrete – “TFRC”, Sample of textile fabric reinforcement, and Bending of Textile Reinforced Plate.

Lepenies and other researchers of the Technical University of Dresden in Germany together with Professor C. Meyer of Columbia University presented a Special Report of ACI, SP 244-7 entitled: “Modeling of Load Transfer of AR-Glass-Rovings in Textile Reinforced Concrete, where they highlight the great benefits of the AR-Rovings to increased stiffness and enhance the ductility of the composite concrete slab reinforced with filaments (continuous fibers) of AR-glass. Figure 4.7 shows a picture presented by Lepenies of a thin concrete slab undergoing large displacements under applied vertical load.

Textile-reinforced concrete (TRC) is an innovative composite material taking advantage of the non-corrosive nature of high strength textiles and fiber materials such as alkali-resistant glass (AR-glass), carbon, or aramid layers of textile-like materials embedded into a matrix of fine grained concrete for designing slender and filigree structural elements. Compared to short-cut fibers, textile reinforcement provides a higher degree of effectiveness because the fiber bundles are arranged in the direction of the main tensile stresses and are continuous along one, two, three, and multiple different directions. The applications of TRC and TFRC extend to a wide range of civil, architectural and engineering building projects including thin reinforced concrete shell structures. Information on this workshop can be found at: www.masterbuilder.co.in/ICI/TRC-Brochure.pdf.

Recently the Indian Concrete Institute Tamilnadu Centre organized an International Workshop on Textile Reinforced Concrete (TRC) Systems dedicated to Professor Wolfgang Brameshuber. The 2nd K P Pradeep Symposium on Pioneering Science and Development for Construction was to take place the 4th of September of 2017 in Chennai, India.





Figure 4.8 – Thin Shell Composite Hyperbolic Paraboloid Roof, TSC Hypar, built by TSC Global LLC Company for African Nations.

TSC Global LLC Company has developed and showcased what they called the Thin Shell Composite Hyperbolic Paraboloid Roof, or TSC Hypar, which is reported to be a roof building technology that has the potential to revolutionize the construction of low cost roofing for the most impoverished and remote countries of the world. Figure 4.8 shows samples of TSC Hypar roof modules built for a number of African nations.

Glen Meyers in his article titled “TSC Global Showcases ‘Roofs for the World’ Demo, published in the Green Building Elements newsletter of July 23, 2010, presents a picture of a typical TSC Hypar roof built at the ground level and raised to their final position at the top of load bearing walls level all around the bottom of the roof. <https://greenbuildingelements.com/2010/07/23/tsc-global-showcases-roofs-for-the-world-demo/>. The TSC Hypar roof is constructed by applying acrylic cement based composite mix over an arched hyperbolic paraboloid shaped cloth that is stretched across a four-sided pyramid type of framework using wood, timber, or bamboo.

William S. Carlton in his Master’s Thesis of 2013 listed in the References cited George Nez as the pioneer of thin Hypar roofs in the 1960’s when he worked for the United Nations on an emergency housing project in the African Nation of Ghana where they required to build some 14,000 new homes in a period of time of less than 18 months. Figure 4.8 above shows the 20’x20’ thin hypar concrete shell roofs that were built at ground level and then lift into their final position by several people without need of cranes or heavy lifting equipment other than human hands.



Thin shell reinforced concrete structures can also be built using wood formwork or some other type of fiberglass or metal formwork, or can also be built without formwork at all. This special case of thin shell reinforced concrete structures were built in the early to mid-1900's by Pier Luigi Nervi using his innovative method of "Ferrocemento" which is a system of reinforced mortar or plaster (cement, sand, and water) thoroughly applied over one or several layers of wire mesh or metal mesh, woven expanded metal, or metal-fibers on closely spaced thin steel rods like steel rebars.

The early inventors of ferrocement are the Frenchmen Joseph Monier and Joseph-Louis Lambot who called the system: "ciment armé" or armored cement who patented their system in the mid 1800's. It was Pier Luigi Nervi who used his "ferrocemento" system widely in large scale building of thin shell corrugated structures in Italy and other parts of the world. The ferrocemento has relatively good strength and high resistance to impact. It behaves well under tensile stresses, having the unique characteristic of displaying good bonding of the mortar to the closely spaced layers of wire mesh which makes it less prone to cracking.

The type of TFRC (Textile Fibre Reinforced Concrete) and TRC (Textile Reinforced Concrete) systems widely used nowadays are some of the derivatives of the early FRC (Ferrocemento) which was widely used by Pier Luigi Nervi in a very ingenious way to achieve long span thin shell reinforced concrete structures in Italy and Europe. Ferrocemento has a unique characteristic of being able to undergo large deformations under load without displaying significant signs of cracking on the faces of the cement exposed to high tensile stresses. Primarily due to the fact that the mix of cement, sand, and water when it hardens it will bond very well to the layers of wire-mesh or fiber mesh set inside the thickness of the member.

It was customary to build sections of Ferrocemento with a multiple number of wire-mesh layers to be able to achieve high ductile behavior of the combined mix of cement plaster and several layers of reinforcement. C. Greco in a technical article titled: "The FERRO-CEMENTO" of Pier Luigi Nervi, published by the University of Rome provides an excellent description of the new material used for the creation of thin shell reinforced mortar structures which will not require the need of any wooden formwork.

The use of closely spaced and multiple layers of steel meshes allowed the direct application of mortar first within the spaces of the mesh and then finishing on both sides, requiring no formwork at all. In this technical article Greco provides a picture of the archive of Antonio Nervi where a very thin sample of slab built with ferrocemento is being tested and undergoes large vertical displacement under external loading without noticeable cracking until the loads reached high concentrated load at the center of the span.

Hanskat, C.S. in a technical article titled: "Shotcrete Placed in Multiple Layers does NOT Create Cold Joints" published in the December 2014 issue of the ACI Concrete International Magazine indicates that the proper placement method of shotcrete ensures consolidation and bond.



Additionally in this paper Hanskat recommends that: “When the placement of shotcrete consists of several layers, concrete delivery should be scheduled so that each layer is placed while the preceding one is still plastic to avoid cold joints”. Hanskat also reports in this paper several interesting facts related to bond between multiple layers of shotcrete: a) “It has been verified with laboratory testing that properly placed shotcrete is very well-consolidated and has excellent strength and durability”. b) “Because shotcrete is placed using high-velocity impact on a receiving surface, it generates an abrasive blast that opens up and thoroughly forces fresh paste into contact with that surface. As a result, shotcrete exhibits excellent bond to previously shot layers and existing concrete surfaces and does not produce a “cold joint” as defined by ACI. Hanskat concludes in his technical paper that: “the items noted above have been confirmed by testing as well as visual inspection of numerous cores taken through multiple layers of shotcrete, where it is often impossible to identify where one layer stops and the other starts”.

The key and main issue for the success of installation of multiple layers of shotcrete is “BOND”, Hanskat in his paper emphasizes and points out that: “Designers and Inspectors often incorrectly confuse the interfaces between shotcrete layers with cold joints experienced in cast-in-place concrete construction. This confusion can lead to needless delays and unwarranted testing”. Therefore it is very important that anyone that uses shotcrete to build thin reinforced concrete shell structures recognizes the facts stated by Hanskat in his paper, so that there is a good understanding of how bonding of multiple layers of applied shotcrete will allow a seamless final section of reinforced concrete shells.

We can learn from nature to attempt to incorporate some of the efficient bio-structural flexible fabrics and membrane components of plants, animals, flowers, trees, fishes, shells, and other natural forms which will provide us some type of hybrid solutions to new sustainable and efficient building structures which can contribute to maintain and reduce pollution and the carbon footprint in the environment. At the same time we shall recognize the new technologies to build more efficient shell structures taking advantage of robotics, digital production of modular parts, ingenious connection details to assemble prefabricated components, innovative installation equipment and other adaptive technologies to better mimic and implement lightweight and optimized shell structures.

In next Section 4.2 the Author will present a narrative to describe the experimental work to build a membrane-concrete shell prototype structure using a flexible tensioned fabric material to serve as only formwork to support the selfweight loads from an anticlastic shell structure constructed using a mix of multiple layers of shotcrete reinforced with steel fibers. The flexible fabric, a Ferrari type Preconstraint 392 S2 fabric mesh is prestressed and clamped along the edges of wide flange steel beams that in turn are supported by tie-down cables at three high points and to three low points on concrete bases set with tops above grade level. The experimental work was directed by Professor Robert Off and Henning Dürr of IMS.



4.2 – MEMBRANE-CONCRETE SHELL PROTOTYPE RESEARCH PROJECT AT IMS

The main subject of this Thesis work is to perform a Finite Element Analysis of a recently built prototype of a membrane-concrete shell structure built at the Bernburg Campus of Anhalt University by a research team of the Institute of Membrane and Shell Technologies, Building and Real Estate (IMS e.V.) led by Dr. Professors Ing. Robert Off and Henning Dürr. The IMS (www.ims-institute.org) is an associated institute of the Anhalt University of Applied Sciences in Dessau, Germany. The focus of the research project was to evaluate the feasibility to build a concrete shell using a flexible membrane as a formwork and as reinforcement to achieve the curvilinear hyper surface of a tensioned membrane stiffened by several layers of shotcrete applied over the surface of the membrane. The main goal of the project is to demonstrate the applied research on flexible membrane as formwork material and the technology to apply shotcrete to stiffen the membrane to a final tensioned hyper concrete shell.

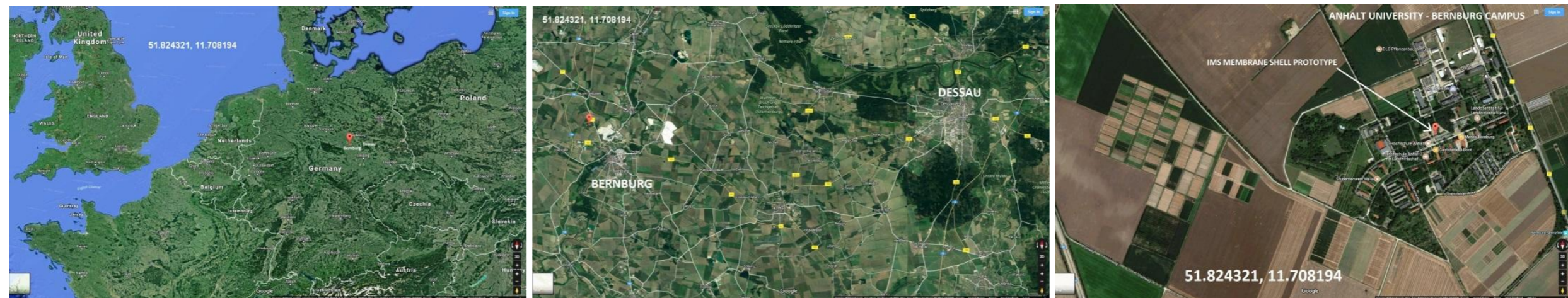


Figure 4.9 – Geographical location of research project at Anhalt University of Applied Sciences Bernburg Campus in Germany.

The project was funded by the Federal Ministry for Economic Affairs and Energy from the AiF (German Federation of Industrial Research Associations) and the site of the project is located in Bernburg, Germany at some 48 kms. (~30 miles) west of Dessau. Figures 4.9 and 4.10 show the geographical global and local site of the IMS membrane-concrete shell prototype project. A report on this project was published in the Nr. 27 issue of TensiNews of September 2014 where Dr. Robert Off, Director of IMS describes the procedure to develop a new method to harden mechanically prestressed membrane structures by spraying them with shotcrete over a tensioned fabric that is used as main reinforcement and as flexible formwork at the same time. IMS formed an interdisciplinary team and partnered with a company for the membrane fabrication (Stegmaier Zelte) and with another one for the application of shotcrete (Lenz & Mundt) to plan, design, detail, construct, and monitor the completion of the building of the tensioned membrane-concrete prototype that is herein reviewed. The realization of this research project took place from August of 2011 to October of 2013.





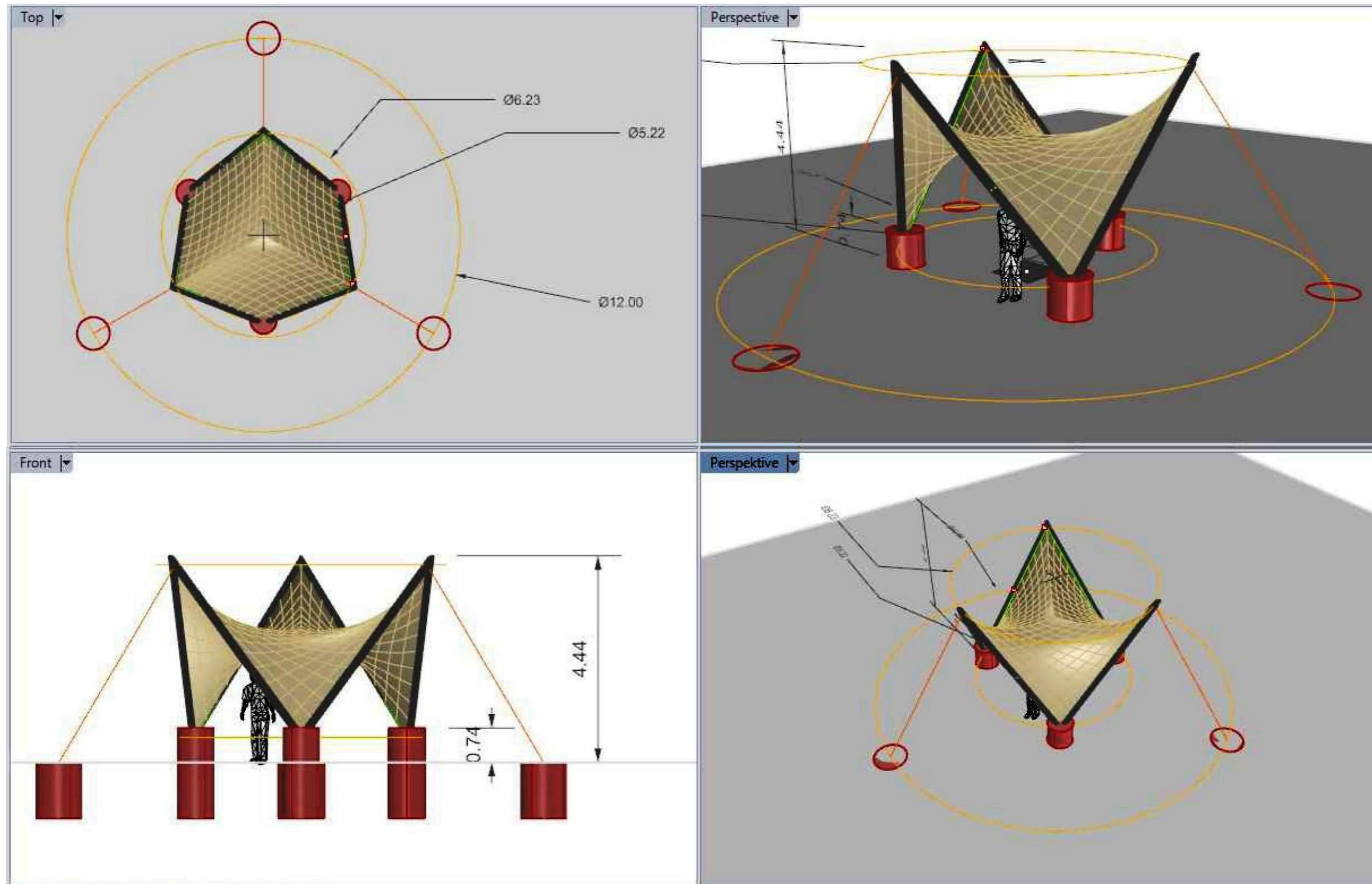
Figure 4.10 – IMS Membrane-Concrete prototype research project location at Bernburg Campus of Anhalt University.

4.3 – PROTOTYPE DIMENSIONS, MATERIALS, TESTING, AND CONSTRUCTION

The prototype structure is geometrically described as a hexagonal anticlastic curvilinear surface bounded by six straight rigid edges forming three high and three low points that creates three ridge lines and three valley lines within the surface of the prototype. The intersection of the lines joining each one of the three high points with each one of the three low points respectively locates the center point of the circles that form the end points of the prototype structure.

The basic dimensions of the key points of the prototype are described as follows: the three low points of the rigid frames are supported on concrete bases set with their tops at some 0.74 m. above the ground level forming a circle of 5.22 m. diameter, the three high points of the rigid frames are set at some 4.44 m. above the ground level and they form a circle of 6.23 m. diameter. The three high points of the rigid frames are tied-down with cables to three concrete bases with their tops set at ground level and forming a circle of 12.0 m. The designed thickness of the completed membrane-shell was set to be 50 mm. (~2"). Figure 4.11 shows the conceptual model of the prototype structure with Plan, Elevation, and Isometric views to illustrate the basic dimensions, heights, and general arrangement of the membrane, edge supports, cables, and concrete foundations.





Concrete Pier Footings – Short, $h=100$ cm., $d=100$ cm. ; High, $h=200$ cm., $d=80$ cm.

Figure 4.11 – Conceptual Dimensioned Plan, Elevation, Isometric, and Aerial View of the IMS Membrane-Concrete Prototype Structure.



An Aerial Plan view of the membrane-concrete prototype with each one of the major components labeled is shown in Figure 4.12 together with a three-point-flexural-tension experimental testing of a concrete sample of the design mix to be used to build the prototype. The research team paid special attention to the preliminary evaluation of the material properties of each one of the components to form the final membrane-concrete shell prototype, particularly different type of cement, additives, maximum grain size of concrete mix, concrete strength, fabric type of material with its physical properties, chemical resistance, different type of yarn materials, coatings, size of the fabric mesh openings, and weaving types were all evaluated and assessed prior of building the prototype. Several concrete samples were tested for compressive, splitting tensile and flexural-tensile strength. The workability and fluidity of the concrete mix was of primary importance due to the steep slope of the tensioned membrane of the prototype and the final method of application of the different layers of the concrete on the membrane. Shotcrete was used to spray the layers of concrete mix on the entire surface of the tensioned membrane. The initial state of uniaxial and biaxial prestress forces to be introduced into the fabric prior of applying the layers of shotcrete was carefully evaluated to maintain adequate support of the hardened layers of concrete and avoid ponding of the membrane-concrete shell prototype.

As part of the preliminary design process a digital model of the membrane-concrete prototype with the fabric tensioned between the edge steel beams supported at three concrete bases and anchored with tie-down cables to three concrete footings into the ground was analyzed to determine the level of prestress necessary to maintain the fabric properly tensioned and the whole structure in static equilibrium. Figure 4.13 shows the results of the preliminary form-finding analysis of the membrane and the axial tensile and compressive forces in the ridge cables, tie-down cables, and edge steel beams respectively. The axial compressive downward reaction forces at the three low points of the prototype are also shown in Figure 4.13.

The spraying process of the concrete over the membrane was planned to be done in the form of spraying shotcrete in layers. Some preliminary spraying trials were done with actual physical mock ups to evaluate the real spraying process and to adjust some parameters such as: type of spraying, pressure, water-cement ratio, distance and angle of the gun nozzle to the surface of the membrane. The samples tested in the laboratory and the samples tested in the field show some differences which were identified and corrected for the final concrete mix proportions and mix parameters for the actual spraying process to build the prototype. Prior to building the membrane-concrete shell prototype shown in Figure 4.14, an initial trial prototype consisting of a 4-point sail with two high and two low points and four edge cables (3m. x 3m.) was built in the laboratory. The initial 4-point sail prototype is shown in Figure 4.15. The flexibility of the overall membrane and cables of this trial sail proved to be of inadequate prestressed level to prevent ponding of the sprayed concrete and uneven thicknesses of the final membrane-concrete shell.



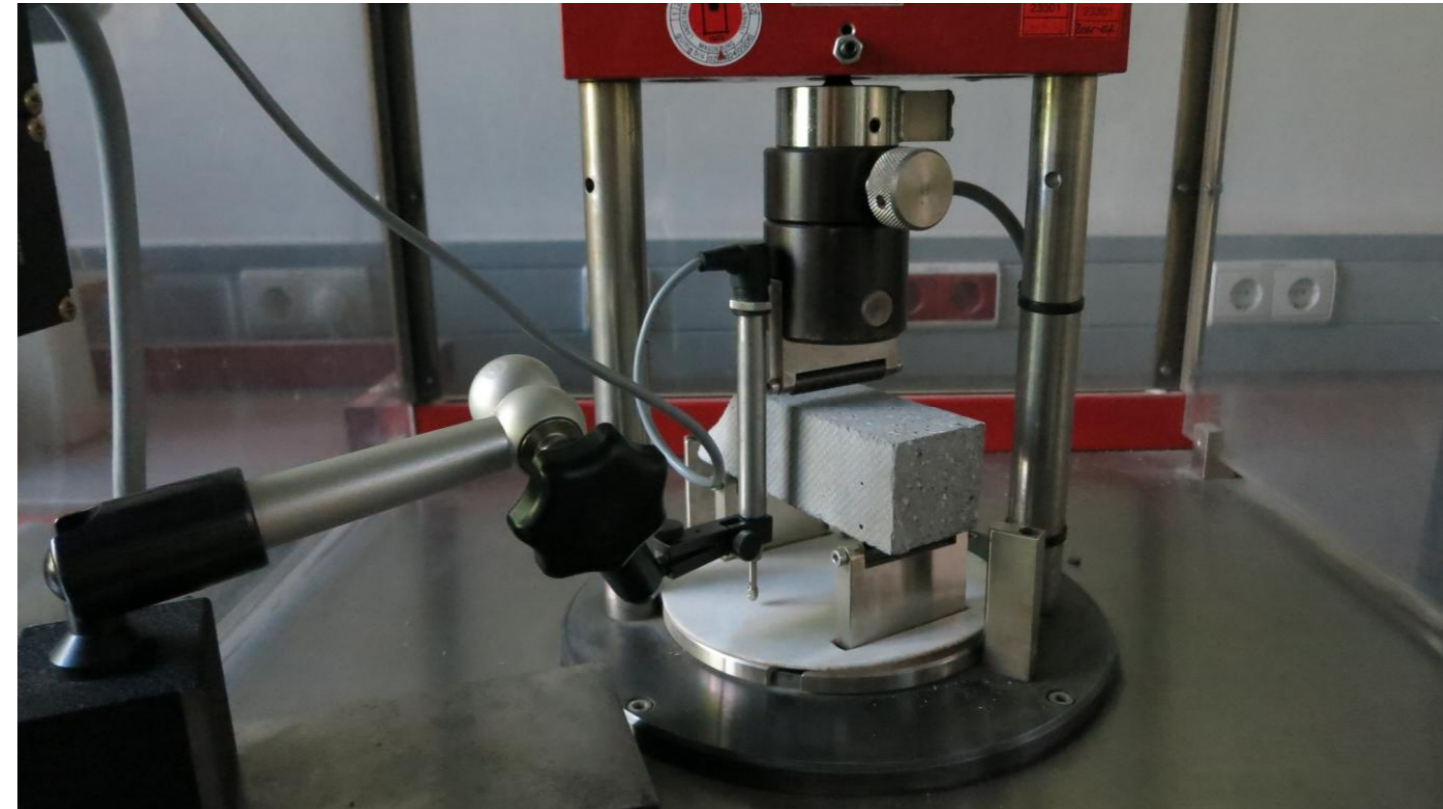
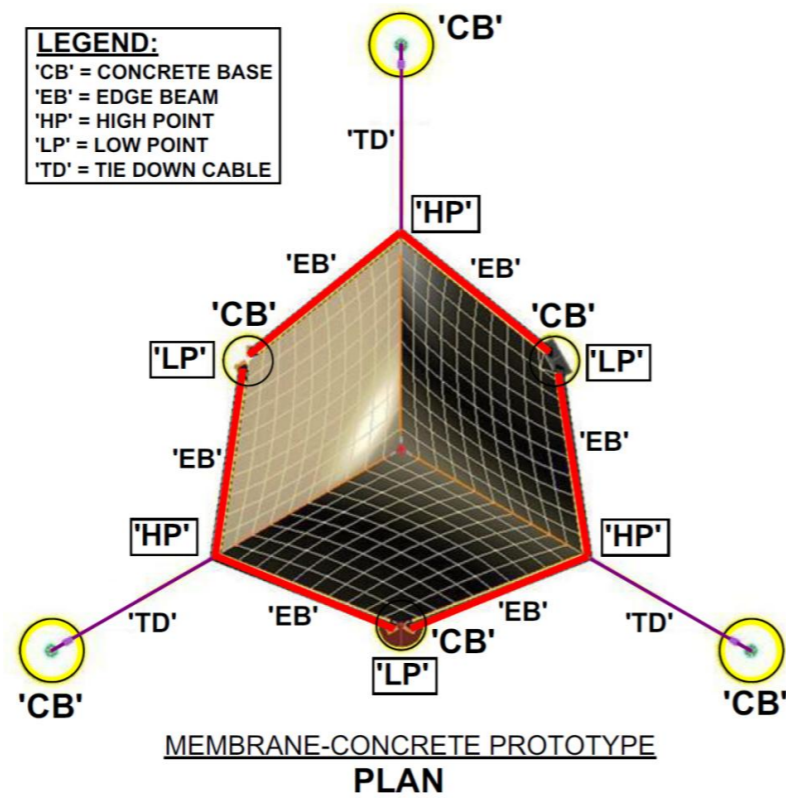


Figure 4.12 – Plan View of Membrane-Concrete Prototype Structure with labeled components and experimental testing of Concrete.

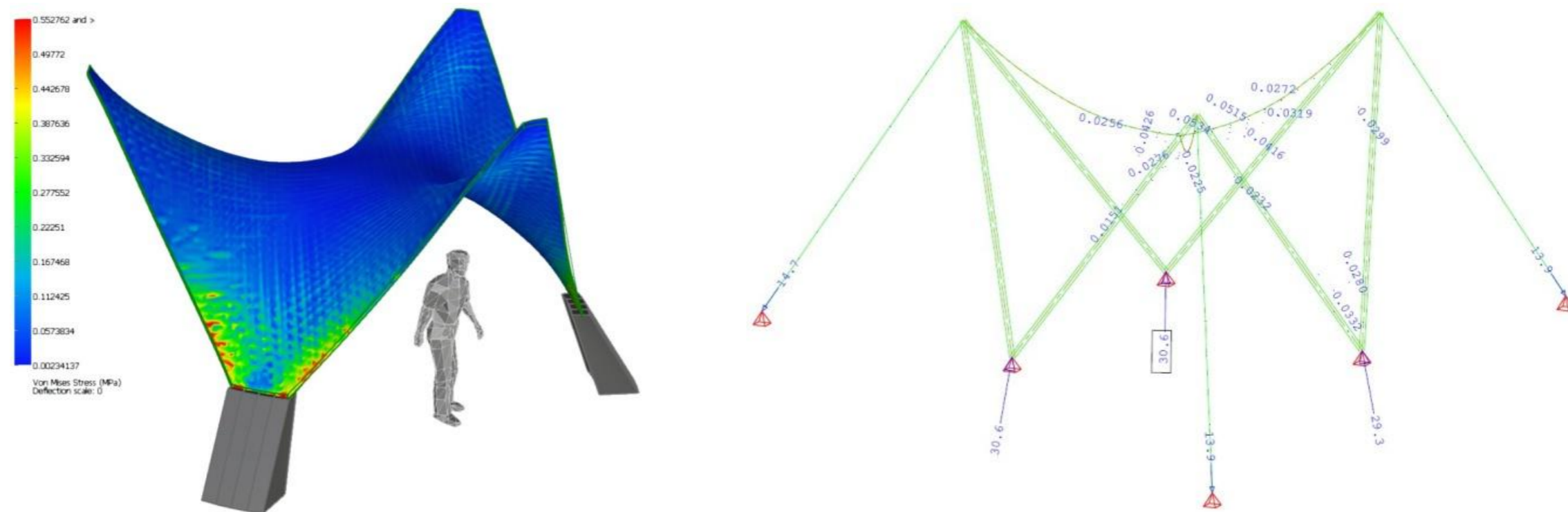


Figure 4.13 – Digital Model of Membrane-Concrete Prototype Structure with Von Mises Stresses, Members, Cables, and Reaction Forces.



The actual construction of the membrane-concrete shell prototype is shown in Figure 4.14. The prototype was built using the following basic components: a) A flexible PVC fabric mesh material, type Ferrari Preconstraint 392 clamped along six sides to steel beams, b) Six straight rigid steel I-beams (HEA 100) rigidly connected (welded) in pairs (forming three A-frames) at three high points and supported at the bottom by circular concrete bases at their corresponding low points, c) Three steel wire ridge cables (Pfeifer PG5) all rigidly connected at the center point of the membrane surface at one end and to the top points of the intersecting steel edge beams at the three high points of the prototype, d) Three steel wire tie-down cables (Pfeifer PG10) with load cells and tensioning fitting devices to connect the ends of the three pairs of steel beams at their high points down to the steel plates anchored to three concrete bases cast into the ground, and e) Three circular reinforced concrete (concrete: C20/25, steel rebars: BSt 500S) bases set into the ground (1.00 m. diameter x 1.00 m. total height) with their top close to the ground to anchor the three tie-down cables and Three circular reinforced concrete (concrete: C20/25, steel rebars: BSt 500S) bases set into the ground (0.80 m. diameter x 2.00 m. total height) with their top high above the ground to support the lower points of the six straight edge steel beams, and finally f) The sprayed on concrete commonly known as Shotcrete which was designed as a mix of Sakret SSM4P and Harek steel fibres.



a) Prototype with Tensioned Membrane, Steel, Cables, and Footings



b) Constructed Membrane-Concrete Shell Prototype – March 2014

Figure 4.14 – Constructed Tensioned Membrane, Steel Frame, Cables Concrete Bases, Concrete Shell, Anchors, and Footings of Prototype.



The steel frames were connected at the top to the tie-down cables and at the bottom to the top of concrete bases with hinged connections that will allow movement of the ends of the steel frames. The steel cables were installed with tensioning devices and load cells to control and monitor the level of prestress forces to be induced into the tie-down cables to maintain the overall level of prestress in the membrane of the prototype.

The final construction materials of the membrane-concrete prototype included an open mesh PVC fabric and a concrete mix with steel fibers that was sprayed on as shotcrete on the surface of the pre-tensioned membrane in several layers. First a thin layer of shotcrete is sprayed on to give the structure enough stiffness to allow workers to walk on the hardened surface, the second shotcrete layer is intended to provide the structure the desired rigidity and stiffness of the composite membrane-concrete shell. The third and final shotcrete layer will provide the structure the final surface of the shell. After the three layers of shotcrete had been completed then a finish layer done by hand provided a smooth surface to seal the concrete shell and prevent water and dirt to stick to the final surface. To achieve optimal bonding and adhesion between the shotcrete layers, each layer was sandblasted prior of applying the next layer of shotcrete.

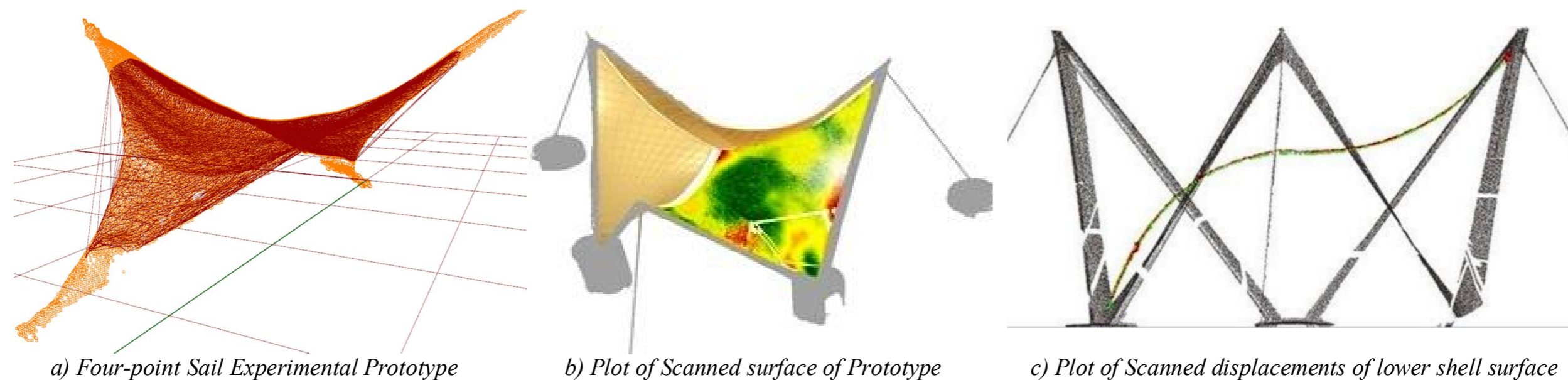
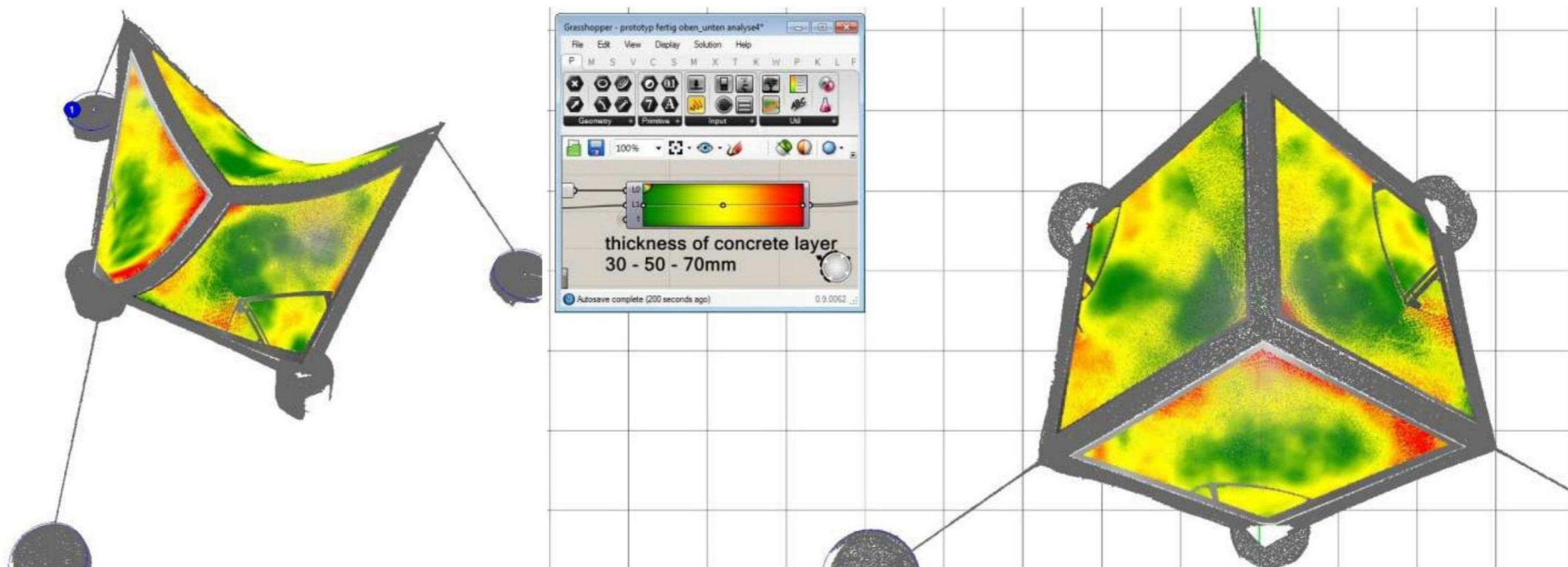


Figure 4.15 – Plots of obtained final concrete shell thickness from 3D scan photogrammetric survey and Deflection of lower shell surface.

During the building process of the membrane-concrete prototype shown in Figure 4.14 the research team performed a series of 3D scanning survey of the top and bottom surfaces of the finished concrete shell structure to evaluate the geometry and displacements of the finished shell surfaces to compare the completed build structure with the initial digital model used to design the prototype.

Figure 4.15 shows the graphics of the 3D scans obtained and plotted by the research team to document the structural behavior of the prototype and digital model. Tensioning of the fabric, concrete spraying, and cable forces were also closely monitored during the construction process as well. Samples of the concrete sprayed using the shotcrete process were also taken for testing to compare the actual values of the prototype with the values of the testing samples done in the laboratory.

The evaluation of the final constructed shell thickness is reflected in Figure 4.16. The research team set up a measurement system consisting of two digital scans, one to survey the top surface and the other one to survey the bottom surface. The scanned survey information was post-processed using the combined Rhinoceros and Grasshopper software



Evaluation of the concrete layer thickness (green = 30 mm to red= 70 mm)

Figure 4.16 – Plots of obtained final concrete shell thickness from 3D scan photogrammetric survey and Deflection of lower shell surface.

Two sets of nurbs surfaces were generated from the upper and lower scanned points, from there the distances between the cloud points of the upper and lower nurbs surfaces were obtained to determine the thickness of the concrete shell at each one of the upper and lower points of the scanned surfaces. The results of the shell thickness reveal that the thickness of the concrete layers varies from 30 mm. to 70 mm. throughout the entire surface of the membrane concrete shell excluding the areas directly along the six edge beams and the three ridge cables.

One of the most challenging tasks to build the membrane-concrete prototype was the application of the shotcrete in a way that will guarantee that a uniform distribution of the sprayed concrete will permit to achieve approximately the same thickness of concrete throughout the surface of the shell. The shape of the steel I-beam with the fabric clamped to the bottom flange of the beam permitted to have a well-defined thickness of the shell along the six edges of the prototype. The final thickness of the shell away from the edges and towards the center of the prototype had to be closely monitored by the skilled craftsmen who had to manually adjust the final thickness of the shell as they progressed throughout the surface of the membrane. At the end the top and bottom surfaces of the completed membrane-concrete shell were scanned to obtain and evaluate the variation of the thickness over the entire surface of the prototype.

Figure 4.17 shows pictures of the completed membrane-concrete prototype details of the main connections (bolted clamping) of the membrane to the steel frames, ridge and tie-down cable connections to the high points of the steel A-frames, and the connection detail of the three ridge cables to the center point of the prototype under the membrane.



Figure 4.17 – Constructed Tensioned Membrane-Concrete Shell, Steel Frame and Cable Connection Details to Steel Frame.



Figure 4.18 show pictures of the completed membrane-concrete prototype details of connections of the edge steel frame members and tie-down cables to the top of the reinforced concrete bases set into the ground. It is noted that three concrete bases with the tie-down cables are set with their tops close to the ground level and the three other concrete bases supporting the low points of the A-frames are set with their tops elevated some 0.74 m. above the ground level.



Figure 4.18 - Constructed Tensioned Membrane-Concrete Shell, Steel Frame and Tie-down Cable Connection Details to Concrete Bases.

The entire membrane-concrete prototype structure and all the components that form the prototype which have been described in this Chapter were built based upon detailed drawings and computer models of the form-finding, patterning, cutting, weldment, and clamping of the membrane, CAD drawings of the general arrangement and geometry of the entire structure, ridge and tie-down cables, steel edge rigid frame beams, connection details of steel beams to cables, reinforced concrete bases with the shop drawings of the rebars, placement of steel base plates, weldment plates, anchor bolts, bolting and clamping connection details of the membrane to the steel beams are shown in a set of eight drawings in Appendix C.

The structural and statics analysis, design, detailing, membrane patterning, steel, cables, concrete foundations, manufacturing, installation and construction of the entire prototype structure was directed by Prof. Dr. Ing. Robert Off in coordination with M.Eng. Wolfgang Warisch, Ingenieurburo fur Membranbau und Tragwerksplanung of Bobingen, Germany in 2013 who certified the structural integrity of the designs of the prototype.

The tie-down cable forces were closely monitored and recorded during the spraying process of the shotcrete being applied in three layers over the tensioned membrane. Three AST load cells were installed at the ends of the tie-down cables to record the tension forces at each cable with recording data logger load device Almemo type.



Figure 4.19 shows a plot of the measurements taken at the three load cell devices KMD1, KMD2, and KMD3 during the prestressing process of the tensioned membrane and the final stage of spraying of the shotcrete layers performed during September 12 and 13 of 2013. The plot is a graphical representation of the variation of the tension axial force in the tie-down cables from the time the membrane was initially prestressed until the time after the 3rd layer of shotcrete was sprayed on the tensioned membrane.

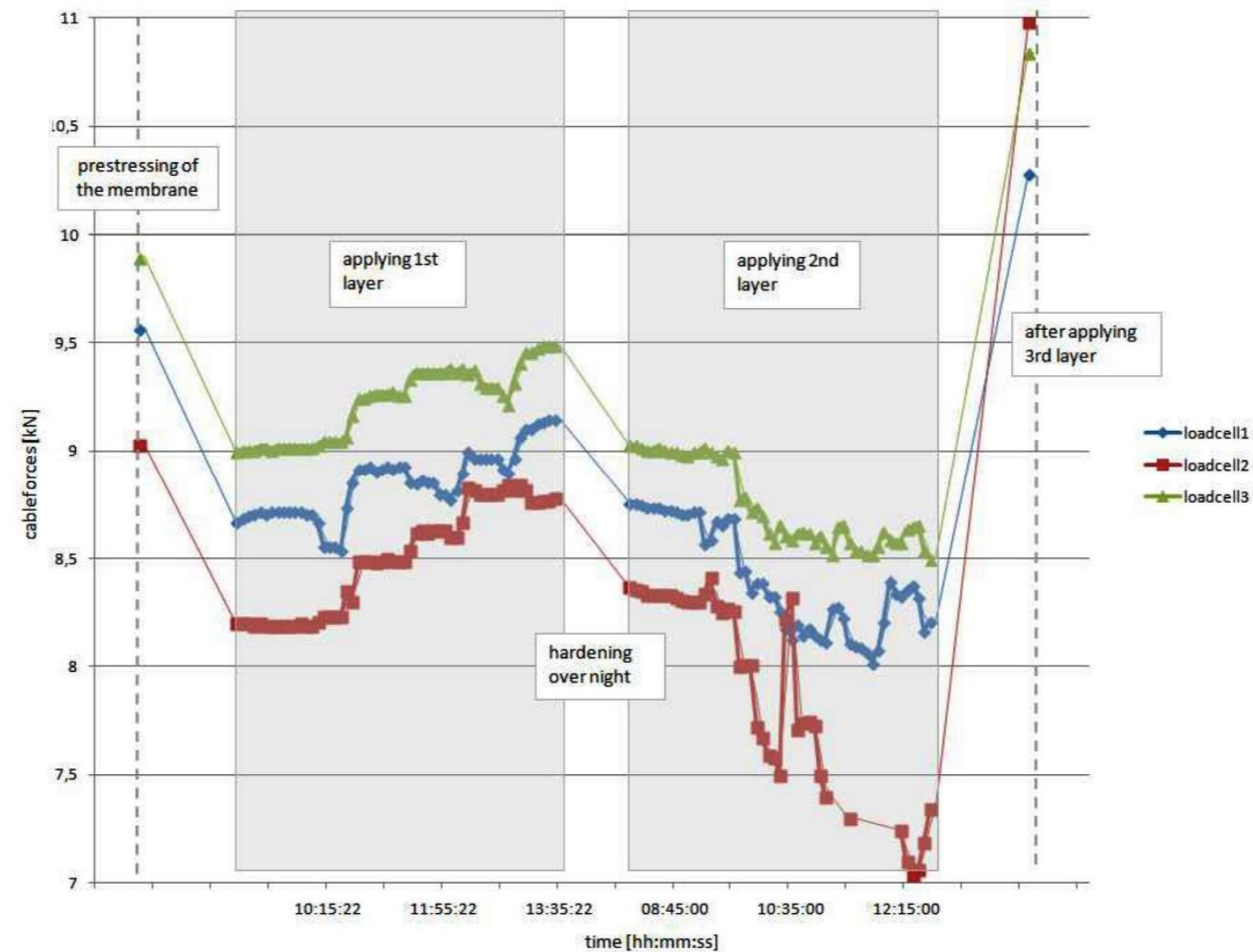


Figure 4.19 – Plot of variation of tie-down cable forces during the application of shotcrete on the membrane surface.

The tie-down cable forces were measured on September 16th of 2013 after the last shotcrete layer was applied to the surface of the membrane.

The tension forces in the tie-down cables were recorded to be: KMD1 = 10.3 kN, KMD2 = 10.8 kN, and KMD3 = 10.9 kN.



Figure 4.20 shows some pictures of the completed prototype structure during the Winter of 2013 and the Spring-Summer of 2014. The structure appears to be in static equilibrium with the tie-down cables straight down to the concrete bases and the steel edge beams in straight position.



Figure 4.20 – Pictures of completed membrane-concrete shell prototype after hardening of shotcrete and finished shell surface.

The final constructed membrane-concrete shell prototype structure was subjected to several large scale load tests to determine its adequacy to support real life external forces. Prior of starting the load tests the tie-down cable forces were measured on May 5 of 2014 to monitor the level of tension forces in the cables.

The tension forces in the tie-down cables were recorded to be: $KMD1 = 6.76 \text{ kN}$, $KMD2 = 6.83 \text{ kN}$, and $KMD3 = 8.44 \text{ kN}$.

The tie-down cable forces have dropped down from the original prestressed forces at the time of membrane installation and final stage of spraying of shotcrete. The following lost of prestress are noted to be: 34.37% at $KMD1$, 36.76% at $KMD2$, and 22.6% at $KMD3$. It is interesting to note that as the entire membrane-concrete shell prototype structure hardens and settles into its position of static equilibrium due to the new loading conditions of additional permanent uniformly distributed selfweight of the membrane-concrete composite structure the internal forces in the members of the structure are redistributed as displacements of the steel frame members take place around the six edges of the prototype.



Two large scale load tests were performed on the completed shell prototype structure. Figure 4.21 shows pictures of the placement of cement bags on the flatter portions of the shell surface for the four different loading increments of the first large scale load test. This first load test was done on June 5, 2014 under the supervision of Henning Dürr, Robert Off, and Kristian Tourneau. For this first large scale load test, the completed prototype structure was loaded with a number of cement bags stacked on the surface of the shell near and around the center point of the prototype where the three ridge cables intersect. Cement bags with individual weights of 25 kg. (~50 lbs.) each were used. For a cement bag of 50 lbs. and approximately 20” (1.67ft.) width and 30” (2.5’) length, a uniformly distributed load of 12 psf can be estimated for one layer of bags evenly distributed over a projected surface.



Load Test I-1 – 13 bags ~ 325 kg. Load Test I-2 – 20 bags ~ 500 kg. Load Test I-3 – 30 bags ~ 750 kg. Load Test I-4 – 33 bags ~ 825 kg.

Figure 4.21 – Pictures of 1st large scale load tests on the top surface of the membrane-concrete shell prototype.

The cement bags were placed around the center of the prototype and mostly over the ridge cables lines having surface areas that will allow the bags to stay on top of the shell and not slide down. For the 1st series of load test the bags were stacked in four groups representing each one different loading increment. The 1st load increment corresponded to 13 bags, ~325 kg. (3.2 kN – 650 lbs.), 2nd load increment to 20 bags, ~500 kg. (5 kN – 1,000 lbs.), 3rd load increment to 30 bags, ~ 750 kg. (7.5 kN – 1,500 lbs.), and 4th load increment to 33 bags, ~825 kg. (8.2 kN – 1,650 lbs.)

It is important to note here that due to the high steep slope of the surface of the finished membrane-concrete shell it was extremely difficult to have a truly uniformly distributed load on the entire surface of the prototype. Figure 4.22 shows the tabulated values of axial tensile forces in the tie-down cables that were recorded during the process of four loading increments of cement bags at 325 kg., 500 kg., 750 kg., and 825 kg.. An additional loading condition at 900 kg. was done and axial forces recorded. After this loading condition the cement bags were removed from the shell surface and a final reading of the axial forces was performed in the tie-down cables for a zero load on the shell surface. The table shown in Figure 4.22 has tabulated values for the numbered load test, time, applied load on the shell surface, and axial tension forces at load cells KMD1, KMD2, and KMD3.



TestNo	Time	load [kg]	cableforce KMD1 [kN]	cableforc KMD2 [kN]	cableforc KMD3 [kN]
1	11:45	0	-6,76	-6,83	-8,44
2	12:00	after trespass	-6,99	-7,05	-8,34
evenly distributed load (sector1, sector2, sector3)					
3	12:12	325	-7,17	-7,23	-8,48
4a	12:16	500	-6,85	-6,97	-8,36
4b	12:20	500	-6,81	-6,94	-8,35
5	12:22	750	-6,89	-7	-8,44
6	12:25	825	-6,91	-7,06	-8,45
7	12:26	825	-6,95	-7,11	-8,49
ridge cables removed					
8	12:39	825	-7,15	-6,96	-8,36
load on sector2					
9a	12:45	825	-6,69	-6,92	-8,3
9b	12:45	825	-6,7	-6,9	-8,29
10	12:48	900	-6,74	-6,94	-8,3
11	12:58	0	-6,37	-6,29	-7,67

Figure 4.22 – Tabulated axial tensile forces recorded at tie-down cables for the four loading increments on the membrane-concrete shell prototype.

After a detailed review of the tabulated values of axial forces at the three tie-down cables supporting the high points of the steel edge frame beams it is noted that there is no virtually any significant change in the magnitude of the axial forces in the tie-down cables, which seems to suggest that after the layers of shotcrete on the tensioned membrane surface have hardened and the entire structure has settled due to the selfweight of the recently hardened concrete then the whole prototype becomes a real composite 3D member having a combined behavior of a membrane-concrete shell structure without significant contribution of the tie-down cable to the stability and strength of the newly formed composite shell structure.



The second series of large scale load tests of the prototype (measurement of cable forces and 3D Laser-Scanning of the shell surface) were performed on July 16th of 2014 by: Cindy Daluge, Henry Foltin, and two helpers under the supervision of Henning Durr and Dr. Robert Off. The tension forces in the tie-down cables prior of the loading test were recorded to be: KMD1 = 7.15 kN, KMD2 = 6.99 kN, and KMD3 = 8.28 kN.



Load Test II-1 – 30 bags ~ 750 kg.

Load Test II-2 – 50 bags ~ 1,250 kg.

Load Test III-1 – 27 bags ~ 675 kg.

Figure 4.23 – Pictures of 2nd and 3rd large scale load tests on the top surface of the membrane-concrete shell prototype.

The loads applied to the prototype for this second series consisted of similar accumulation of cement bags around the center part of the prototype having the flatter portion of the shell surface. The 1st loading condition consisted of 30 bags = 750 kg. (1,500 lbs.) and the 2nd loading condition consisted of 50 bags = 1,250 kg. (2,500 lbs.). Pictures for this second series of load increments are shown in Figure 4.23.

The third large scale load test consisted of the application of a concentrated load of 675 kg. (some 27 bags of cement, 25 kg. each ~1,350 lbs.) at an arbitrary point in one of the sectors of the shell surface at a distance of approximately 0.98 m. from the center point of the shell and at an angle of approximately 48.31° from the line of one of the ridge cables. Figure 4.23 shows the method that was used to hang a wooden pallet with the 27 bags of cement from a localized point on the surface of the membrane-concrete shell. To achieve the concentrated load test, a hole was drilled thru the concrete shell thickness at a relatively flat portion of the shell surface as it is shown in Figure 4.24. A diagram showing the point of application of the concentrated load is also shown in Figure 4.24, a threaded circular eye steel rod was installed with some additional wood blocking plate of approximately 11 cm² of contact surface to distribute the point load on the shell and avoid localized punching failure of the concrete.

At the bottom of the shell a threaded steel hook with some hangers were connected to the threaded steel rod to support the loads from the cement bags stacked on a wooden “europalette” weighting ~650 kg.. A wheel loader was used to very slowly and smoothly bring the loaded wooden palette up with the weights hung by two heavy duty belts attached to a circular steel ring connected to the steel hook and rod from the shell surface. Figures 4.23 and 4.24 shows the hardware and connectors that were used for this third large scale concentrated load test.



Figure 4.24 – Pictures of 3rd load test of concentrated load and detail to hung weights from the membrane-concrete shell prototype.

The results of the 2nd and 3rd large scale load tests are shown in tabulated form in Figure 4.25. The first part of the test consisted on applying a small load of approximately 90 kg. on the flatter part of the shell and record the axial loads in the tie-down cables for zero (0 kg.) load and 90 kg. load, next the load on the shell was increased to 750 kg. and axial loads in the tie-down cables were recorded. It is noted at this point that there is no significant variation in the level of axial tension forces in the tie-down cables from 0 kg. to 750 kg. load on the shell.

At this point of the load test, the three tie-down cable forces were released (cables were loosen up) completely to bring the cable forces to approximately zero tension force and maintaining the applied load on the shell of 750 kg., In the next step of the load test the team proceed to retension all the three tie-down cables to a target tension force of approximately 8 kN at each cable. Next the load on the surface of the shell was increased from 750 kg. to 1,250 kg. and the tension forces in the three tie-down cables were recorded. Observations of the recorded values of axial tension forces in the tie-down cables reveals that there is no significant increase or variation in the level of axial tension forces in the three cables.

Test No	Time	Load [kg]	cableforce KMD1 [kN]	cableforce KMD2 [kN]	cableforce KMD3 [kN]	ScanNr.
reference measurement						
1	11:30	0	-7,15	-6,99	-8,28	M_1
2	12:31	90	-6,95	-6,71	-7,52	
evenly distributed load (sector1,2,3)						
3	12:40	750	-7,08	-6,9	-7,86	M_2
loosening staycables						
ay	12:56	750	-0,02	-6,11	-7,25	
5	12:57	750	-0,01	-5,43	-0,33	
6	13:00	750	0	0,59	-0,32	M_3
retensioning staycables						
7	13:22	750	-8,17	-7,95	-8,1	M_4
8	13:37	1250	-8,3	-8,45	-8,04	M_5
surface load on sector1						
9	13:54	1250	-8,54	-8,45	-8,04	M_6
pointload in sector3						
10	14:25	675	-8,65	-8,07	-8,54	M_7
load removed						
11	14:50	0	-8,33	-8,22	-8,34	

Figure 4.25 – Tabulated axial tensile forces recorded at tie-down cables for the 2nd and 3rd load tests on the membrane-concrete shell prototype.

The 3rd large scale load test consisted on the application of a concentrated load of 650 kg. at a specific point on the shell surface as it is shown in Figure 4.24. For this loading condition the axial forces in the tie-down cables were recorded and the tabulated values of Figure 4.25 reveals that again here for this loading condition there is no significant increase or variation of the axial tension forces in the three tie-down cables. Next the loads were removed completely from the shell surface and axial forces in the tie-down cables were also recorded for 0 kg. load with no significant variations.



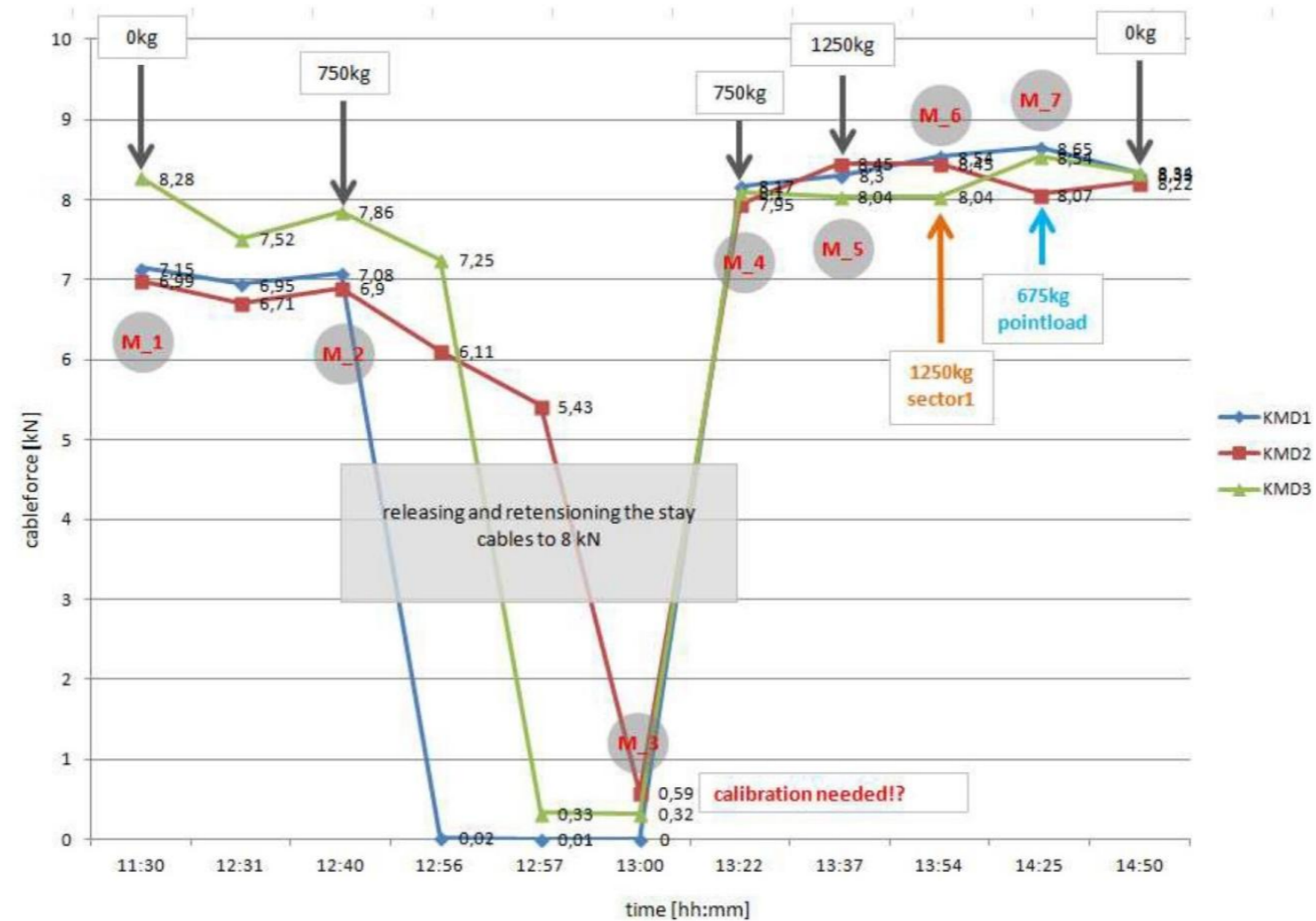


Figure 4.26 – Plot of tabulated axial tensile forces recorded at tie-down cables for the 2nd and 3rd load tests on the membrane-concrete shell prototype.

The tabulated values of axial tensile forces in the tie-down cables for the 2nd and 3rd large scale series of load tests corresponding to the application of distributed surface load and the concentrated load on the prototype membrane shell from start at zero load to end of test back to zero load are shown in Figure 4.26. The variation of the values of axial tension forces are noted for the first applied distributed load of 750 kg., followed by a release of the axial force in the three tie-down cables, re-tensioning of the three cables up to approximately 8 kN maintaining the first distributed load of 750 kg., next step the distributed load on the shell is increased to 1,250 kg., and finally the last part of the test consisted of applying the concentrated force of 675 kg. until the end of the test when the concentrated load was removed and the prototype was left with zero load. Observations of the plotted values of axial tensile forces in the tie-down cables reveals no significant variations on the magnitude of axial tension forces in the cables.

The deflection of the membrane-shell prototype surface under the different loading conditions was approximately determined by using a system of laser scans which was performed simultaneously with the application of the load tests and the measuring of the axial forces in the tie-down cables. Figure 4.27 shows the graphics of the laser scans and Nurbs lines of the shell surface under loading conditions. The first step is to perform a laser scan of the shell surface with no loads other than the selfweight of the membrane-concrete shell to collect a series of points that will be used as the reference points for the initial state of the shell under zero external loads, this step is represented by the Pointcloud M_1.

For each other loading case listed in the table of Figure 4.25, a corresponding laser scan of the shell surface was performed and recorded as scans M_2 to M_7. Next each one of the pointclouds for each loading case M_2 to M_7 was compared to the pointclouds of the initial reference scanned set of pointclouds M_1 to measure the deflection of the shell as the difference between each set of points of M_2 to M_7 and M_1. This process was performed using the Rhino and Grasshopper software which proved to be very efficient to process the amount of data for each loading condition. It is important to note that for each set of pointcloud scanned points, a Nurbs surface was generated for M_1 to M_7.

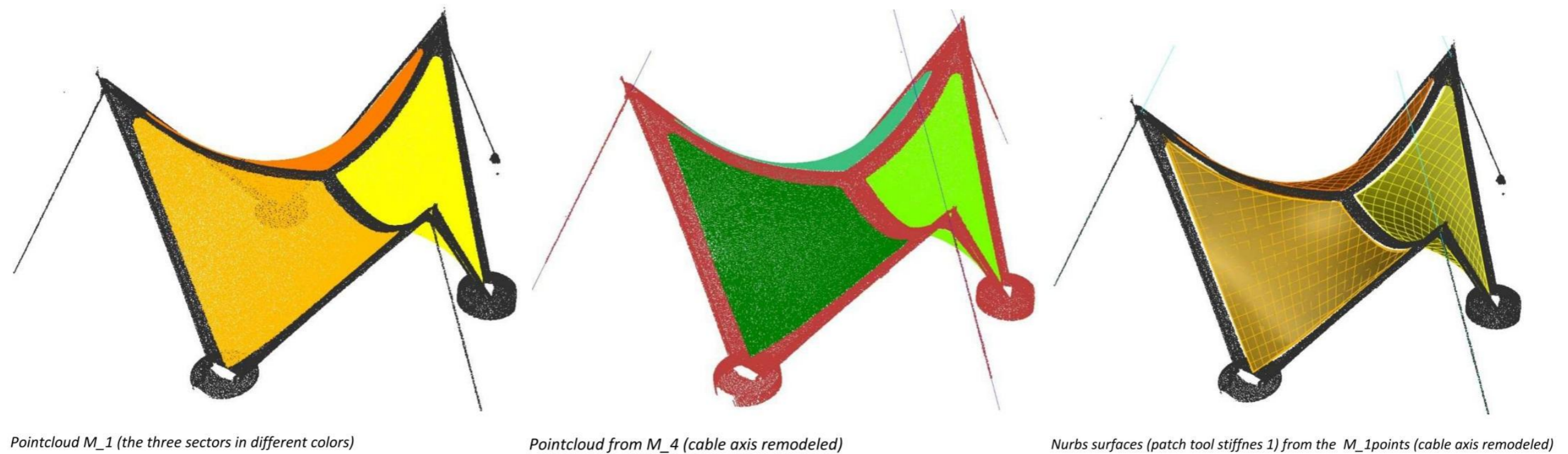


Figure 4.27 – Laser Scan plots and Nurbs lines of the shell prototype surface to determine the deflection of the shell under loads.

The Laser Scan plots of the membrane-concrete shell surface for loading cases M_4, M_5, and M_6 are shown in Figures 4.28 and 4.29. Surface plots of the prototype surface Plan and prototype surface Elevations and Isometric provides a view of the laser scanning performed.

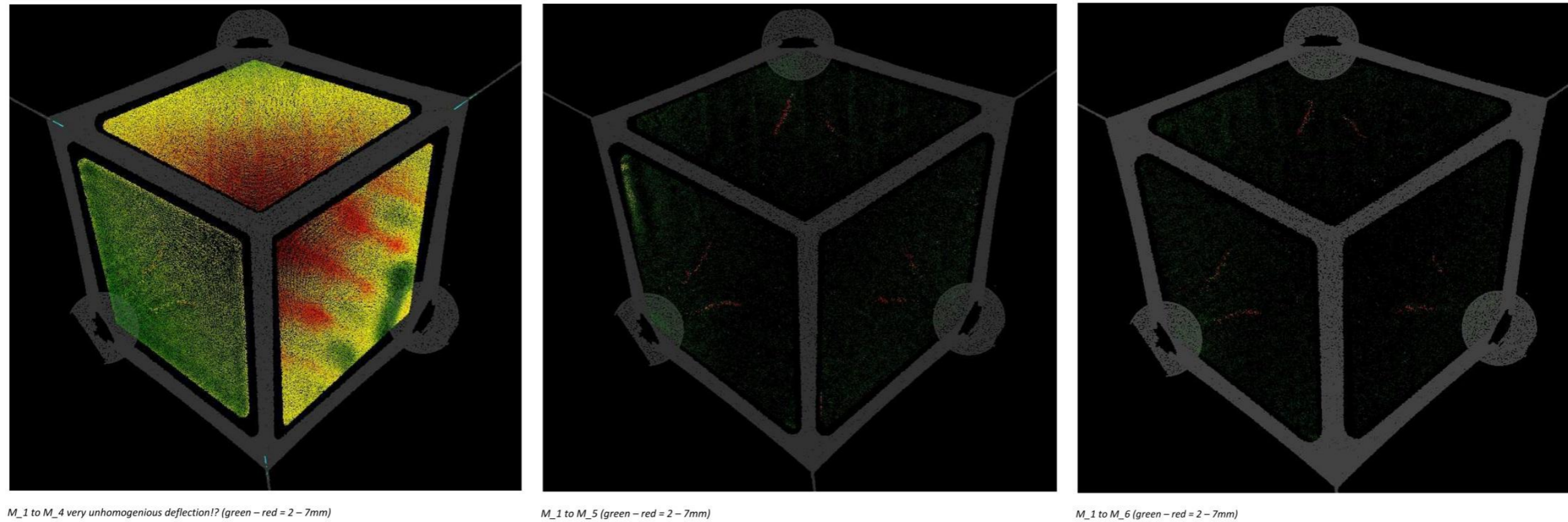


Figure 4.28 – Laser Scan plots of the shell prototype for loading cases M_4, M_5, and M_6 to determine deflection of the shell surface.

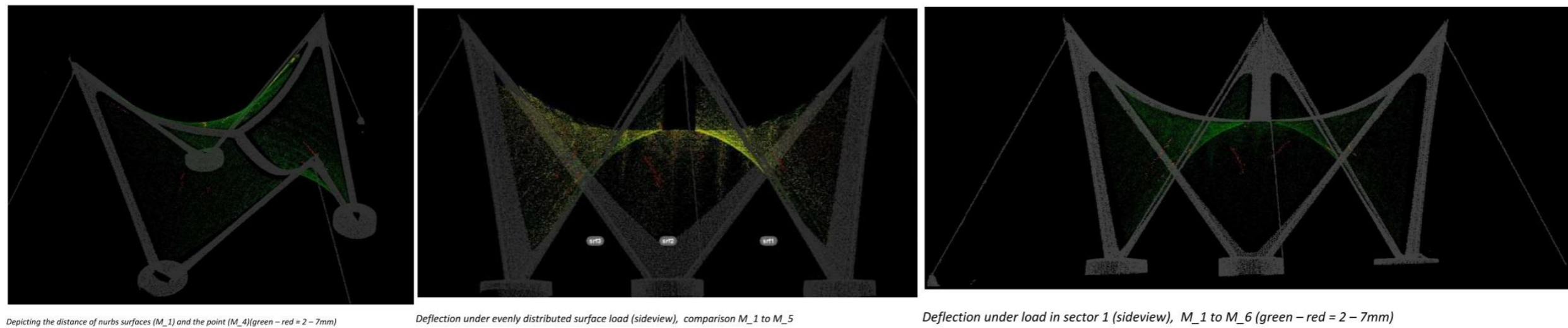
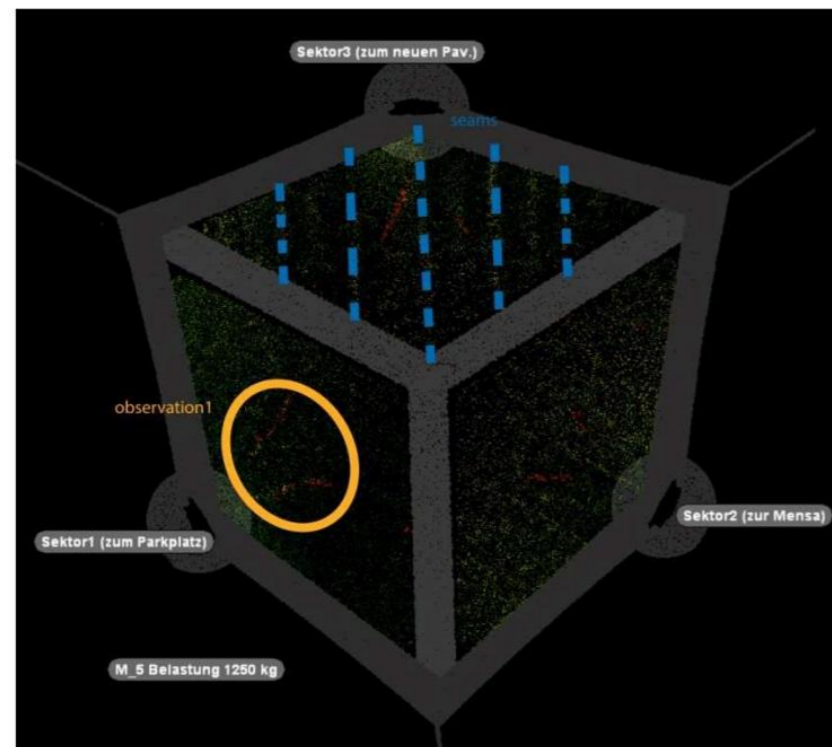
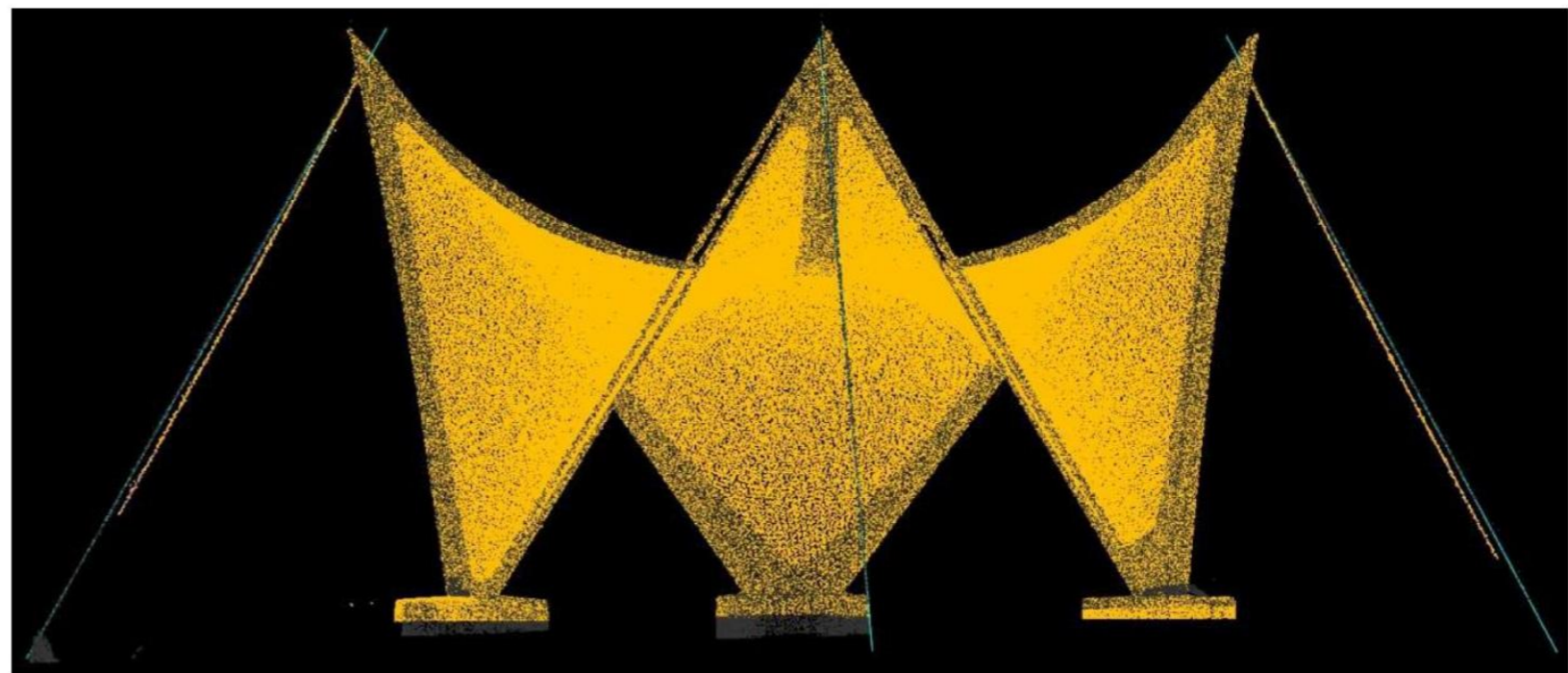


Figure 4.29 – Laser Scan plots and Nurbs surface lines of the shell prototype surface to determine the deflection for M_4, M_5, and M_6.

The review of the results obtained by the laser scan measurements of the reference model M_1 and the other measured models M_2 to M_6 where the deflections are obtained by subtracting the values of the green and red points that are superimposed for each loading case reveals that the maximum deflections measured are in the range from 5 mm. to 10 mm. for load cases M_5 (1,250 kg. distributed load on sectors 1, 2, and 3) and M_6 (1,250 kg. distributed load on sector 1 only) respectively as shown in Figures 4.28 and 4.29. It is noted from the results of the laser scanning shown in Figure 4.30 that there are some major differences of the obtained values of distances of cloud points for similar locations of one sector to another.



Deflection under evenly distributed surface load (topview) M_5



M_1 to M_4 mismatching of the cable axes (M_4 cables not straight = less tension!?)

Figure 4.30 – Laser Scan plots in Plan and Elevation of the shell prototype for loading case M_5, Unusual deflections of surface and cables.

For loading case M_4 the tie-down cables show a slight offset at the bottom sections of the cable, revealing that the cable appears to have a slight curved section rather than a straight configuration as it is shown in Figure 4.30. The laser scan of M_4 was done at the Test step No. 7 which is right after the tie-down cables were re-tensioned to bring them up to an axial tensile force of 8 kN. Therefore it is reasonable to believe that the reaccommodation of the entire membrane-concrete prototype after the cable have been re-tensioned may have induced some type of compression forces into the cables causing the cable to go slack and lose its straight configuration. The entire membrane-concrete shell at this stage is heavy and the three high points at the top of the steel edge beams can have slight movements in space due to unbalanced loading conditions.

The maximum deflection of the membrane-concrete shell prototype for the concentrated load of 675 kg. (loading case M_7, applied on sector 3) was measured to be 8 mm.. The laser scan of the prototype surface together with a comparative plot of the laser scan and the pointcloud diagrams to compare and identify the deflection pattern of the shell surface under the concentrated load of 675 kg. is shown in Figure 4.31. a screenshot of the Grasshopper Script routine that was used to process the series of points for each one of the loading conditions that were scanned during the series of load tests is also shown here in Figure 4.31 to illustrate the automation of the process to obtain the deflections of the shell surface under loads.

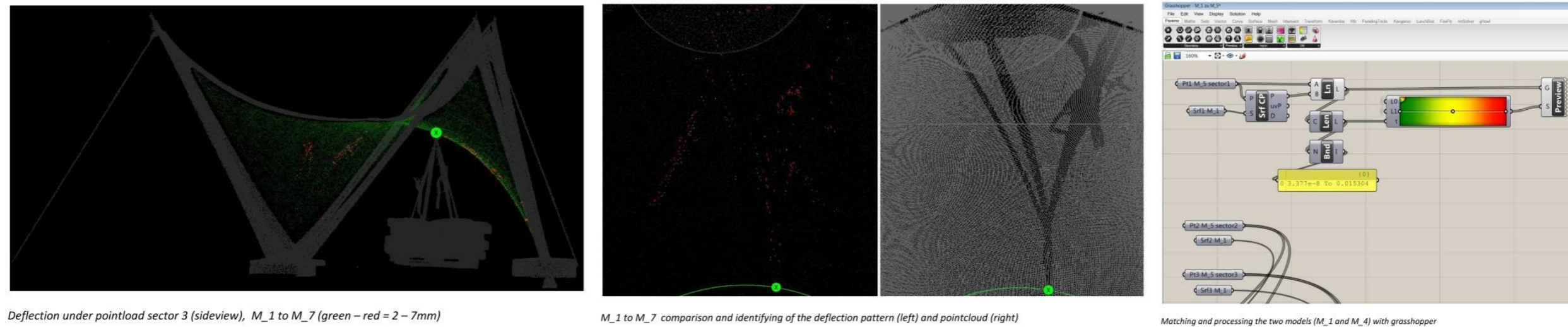


Figure 4.31 – Laser Scan plots and Nurbs surface lines of the shell prototype to determine the deflection from Concentrated Load for M_7.

It is important to note that for all the surveyed models using the laser scans, several straight lines that represent the lines of the seams of the membrane structure were detected. Other unusual curved lines where the values of the deflections of the shell are much larger than in the rest of the shell surface are difficult to explain but were observed during the analysis of the laser scan plots.

To evaluate the actual material properties of the structural components of the membrane-concrete prototype acting in a composite and combined manner during and after completing the construction of the prototype, several concrete specimen samples were taken for laboratory testing. The type of specimen samples are shown in Figure 4.32. Rectangular specimens measuring 20 cm. x 40 cm. were extracted at each one of the three lower sectors of the prototype to test them and evaluate the real composite action behaviour of the combined PES-PVC Ferrari Preconstraint 392 membrane mesh with the mix of sprayed concrete (shotcrete) and steel fibers. Each one of the rectangular (20x40 cm.) specimens was then cut in the concrete workshop of IMS into three smaller “warp” samples and three smaller “weft” samples of approximately 50 mm. height (thickness of shell) and the width and length dimensions shown in Table of Figure 4.33 for the 3-point flexural testing shown in Figure 4.32.

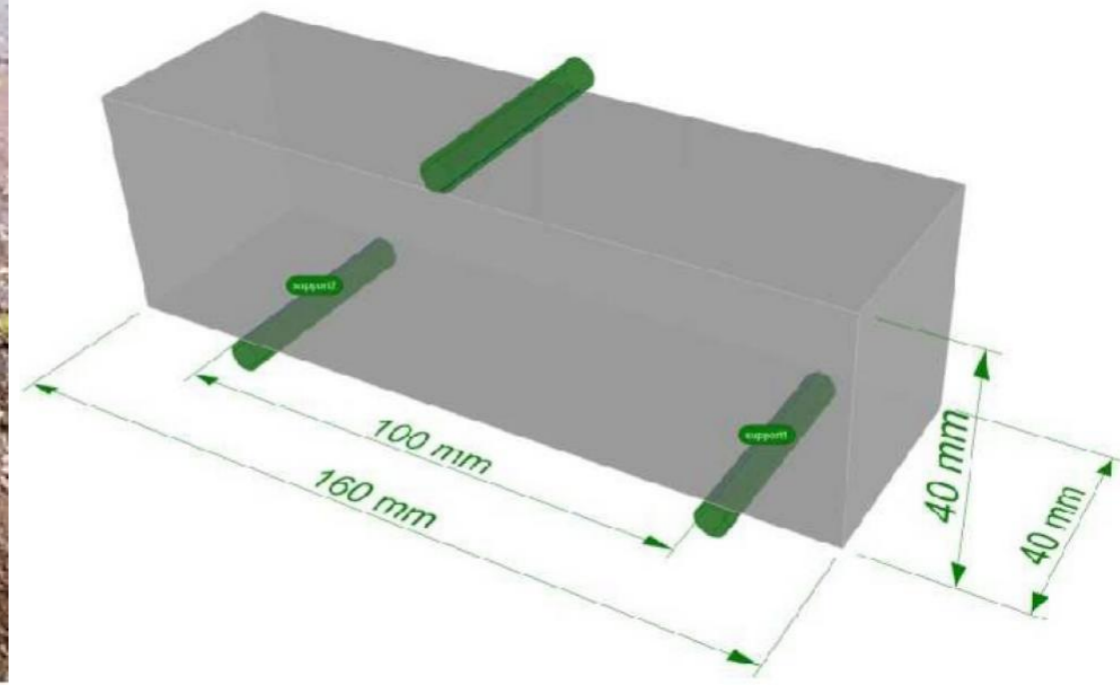




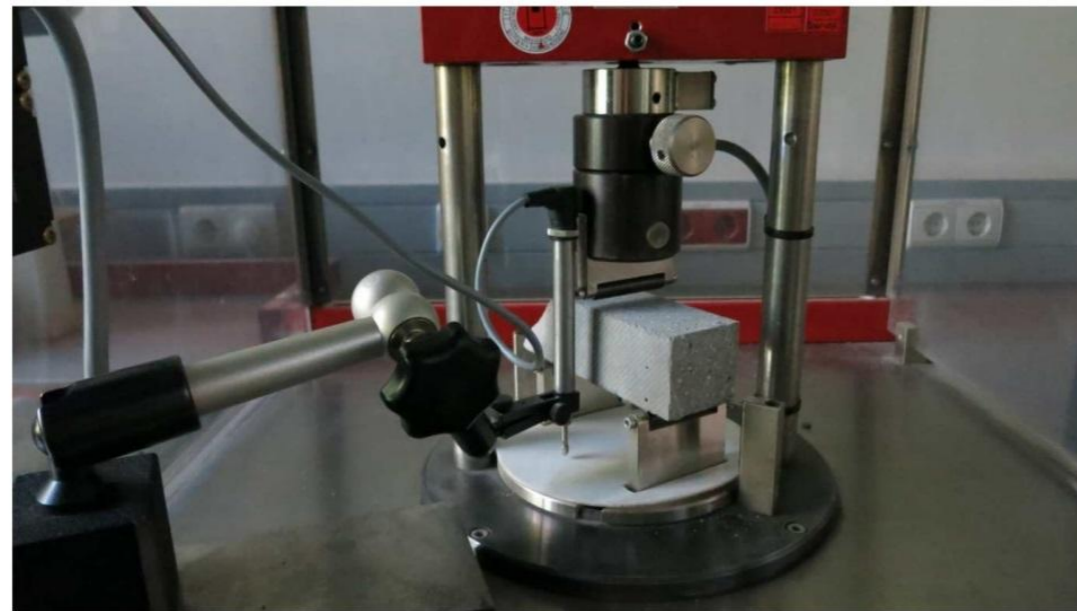
20x40 cm. Specimen from Sector 1



45x45 cm. Square Shotcrete Specimen - "Spritzkissen"



Approximate Geometry of Specimens to be tested – 40 mm. x 40 mm. x160 mm.



Testing rig (3 point flexural testing) with external displacement transducer



Membrane-Concrete Specimen during testing

Figure 4.32 – Membrane-Concrete Specimen Samples, Geometry for testing, Testing Machine setup and Specimen after bending test.



During spraying of shotcrete on the tensioned PES-PVC membrane mesh, square specimens measuring 45 cm. x 45 cm. called “Spritzkissen” were produced to test them in the laboratory to determine the flexural strength of the shotcrete with steel fibers as shown in Figure 4.32. The purpose of having specimens of the prototype with the PES-PVC membrane mesh and without the mesh tested in the laboratory was to compare the difference of the flexural strength of the two type of specimens of the pure concrete material with the steel fibers included and the composite material of shotcrete with steel fibers and the PES-PVC membrane mesh combined.

The 3-point flexural testing of concrete samples with external displacement transducer that were extracted from the constructed membrane-concrete prototype were performed by Mr. Henning Dürr at IMS in September 24th of 2014. All the test samples cut from the prototype specimens and the shotcrete material were tested in the laboratory of IMS using a three-point flexural testing machine equipped with an external displacement transducer. To accommodate the tip of the transducer to record the vertical displacements of the specimen under load, a metal plate was glued to the underside of the specimen as it is shown in Figure 4.32.

During the flexural test of each one of the specimen samples, several values of the external vertical force being applied to the specimen at the top center point and the vertical deformations at the bottom center point of the specimen were recorded. The plots of vertical force (in kN) and the vertical displacements (in mm.) for the prototype shell specimens listed in Figure 4.33 (Spritzkissen samples, “warp” samples, and “weft” samples) are shown in Figure 4.34. The Spritzkissen samples contain only the mix of shotcrete with the steel fibers, without layers of fabric attached to them.

A review of the tabulated values of maximum force (F_{max} in kN) and the calculated stress values supported by the three type of samples under the 3-point flexural testing procedure clearly reveals that the prototype samples having the prestressed fabric attached to the bottom face of the shotcrete with steel fibers attain a high strength value compared to the shotcrete samples with steel fibers but without the fabric attached to the bottom face of the shell samples. There is no significant difference between the strength values of the samples having the prestressed fabric oriented either in the warp or fill direction, but there is certainly a noticeable increase in stiffness of the samples reflected in the decrease of vertical deflection under load of the samples having the fabric attached to it as compared to those samples of Spritzkissen with no fabric at all.

The tabulated values of average bending stresses of the prototype samples reveal a 27.2% increase of average strength of warp samples and 33.3% increase of average strength of fill samples with respect to the Spritzkissen samples without fabric. There is a clearly a significant increase in stiffness of the samples having the prestressed fabric oriented either in the warp or fill direction. Samples with prestressed fabric can sustain a higher applied force with less vertical displacement as can be seen in the plots shown in Figure 4.34.



testing rig	3-point flexural testing with external displacement transducer
test temperature	23°C
code	
date	24.09.2014
person in charge	Henning Dürr
geometry of specimen	prism
Logfile	Maschine 3 mit Verformungsaufnehmer_HD092014_Spritzkissen.ZSE

no.	speciman	width [mm]	height [mm]	length [mm]	direction	Fmax [kN]	stress[N/mm ²]	Average stress (N/mm ²)
1	IV. 1	43	45	147	-	5,16	8,89	
2	IV. 2	44	47	149	-	4,82	7,44	
3	IV. 3	41	44	147	-	3,94	7,45	
4	IV. 4	42	43	147	-	4,68	9,04	7.873
5	IV. 5	40	44	148	-	3,91	7,57	
6	IV. 6	44	44	148	-	3,89	6,85	
7								
8	I. 1	41	49	164	warp	6,36	9,69	
9	I. 2	41	47	165	warp	6,73	11,15	11.077
10	I. 3	43	48	165	warp	8,18	12,39	
11								
12	II. 1	43	58	163	warp	>10	10,37	
13	II. 2	42	57	163	warp	8,72	9,59	9.42
14	II. 3	42	55	163	warp	7,03	8,3	
15								
16	III. 1	39	57	170	warp	8,52	10,09	9.29
17	III. 2	41	58	168	warp	7,81	8,49	
18								
19	I. 4	40	50	178	fill	6,94	10,41	
20	I. 5	40	50	179	fill	6,07	9,11	9.183
21	I. 6	41	50	180	fill	5,49	8,03	
22								
23	II. 4	40	46	182	fill	6,11	10,83	
24	II. 5	42	47	179	fill	7,67	12,4	11.76
25	II. 6	40	50	180	fill	8,03	12,05	
26								
27	III. 4	40	63	182	fill	>10		----
28	III. 4b							
29	III. 5							
30								
31								

axial area moment, rectangle	I		
width beam	b		0,044 m
height beam	h		0,047 m
	$I = b * h^3 / 12$	[m ⁴]	3,8068E-07
axial section modulus	W		
axial area moment	I		3,8068E-07
distance between outer fiber and neutral axis	a _{max}		0,0235 m
	$W = I / a_{max}$	[m ³]	1,6199E-05
bending moment	M _b		
transverse force	F		4820 N
distance between the supports	l		0,1 m
	$M_b = (F * l) / 4$	[Nm]	120,5
bending stresses	σ _b		
bending moment	M _b		120,5
axial section modulus	W		1,6199E-05
	$σ_b = M_b / W$	[N/m ²]	7438577,72
			N/mm² 7,4385777

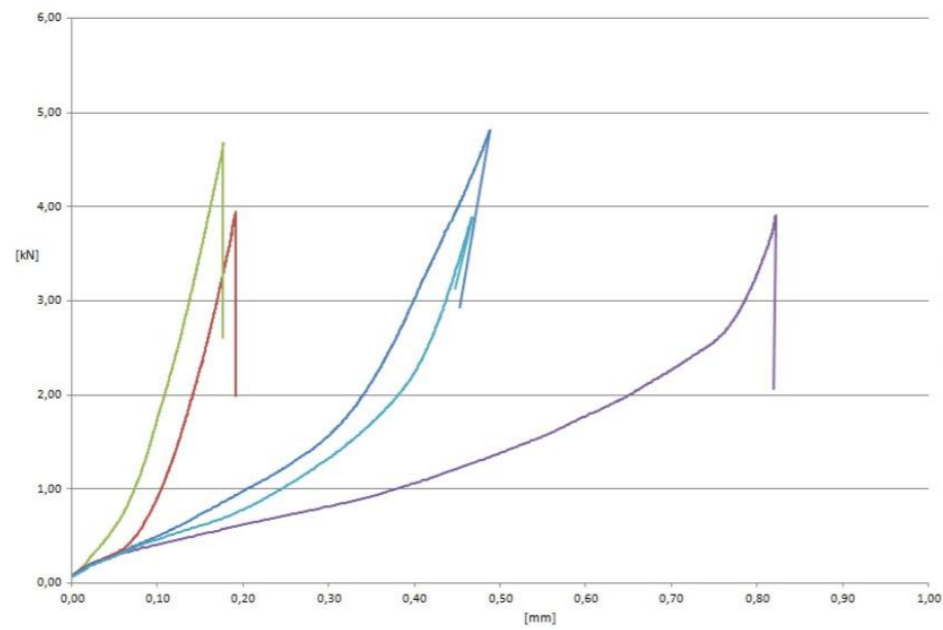
calculation of the bending stresses (example specimen Spritzkissen IV2)

3-Point Flexural Testing Results of Prototype specimens

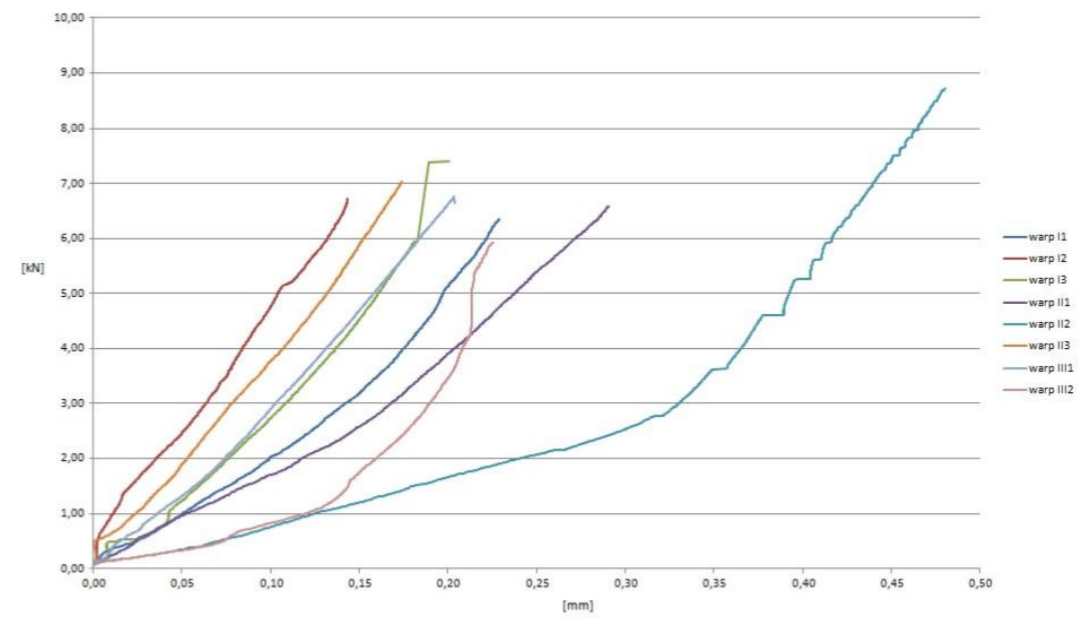
Figure 4.33 – Tabulated bending stress values from 3-point laboratory flexural testing and detailed tabulated stress calculations.

Information on the Prototype materials datasheets are presented in Appendix D for general information and documentation on material properties.

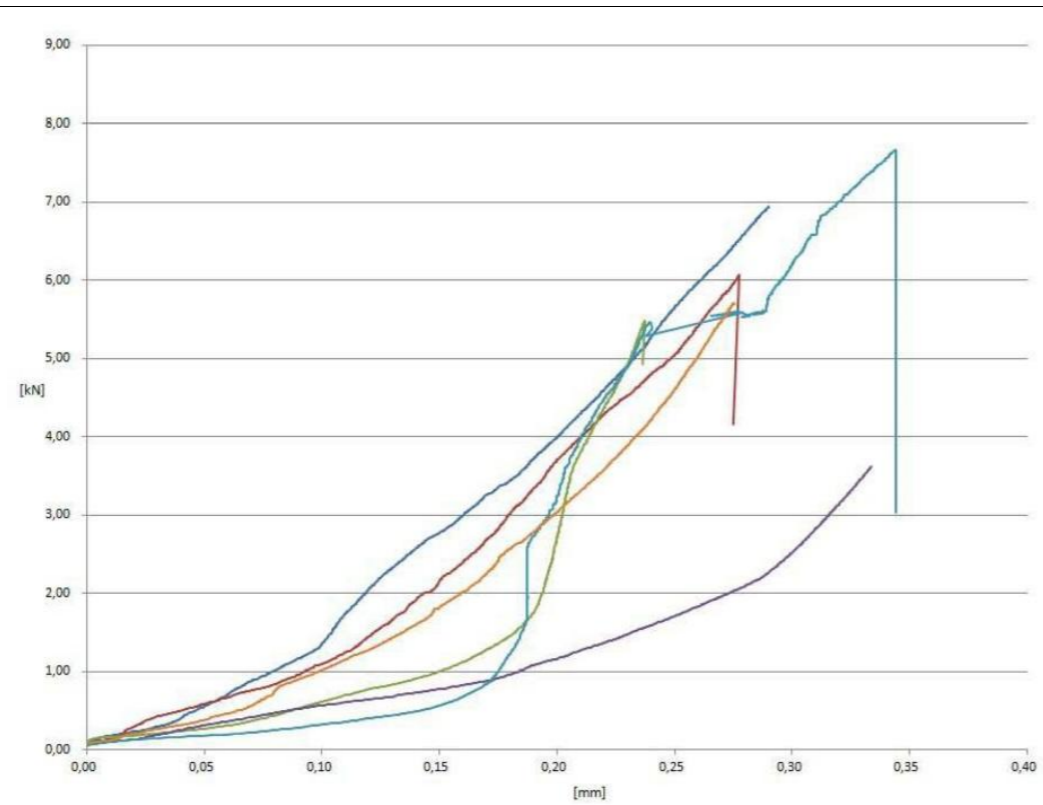




force-deformation-diagram, "spritzkissen"



force-deformation-diagram, "warp"-samples from shell



force-deformation-diagram, "fill"-samples from shell

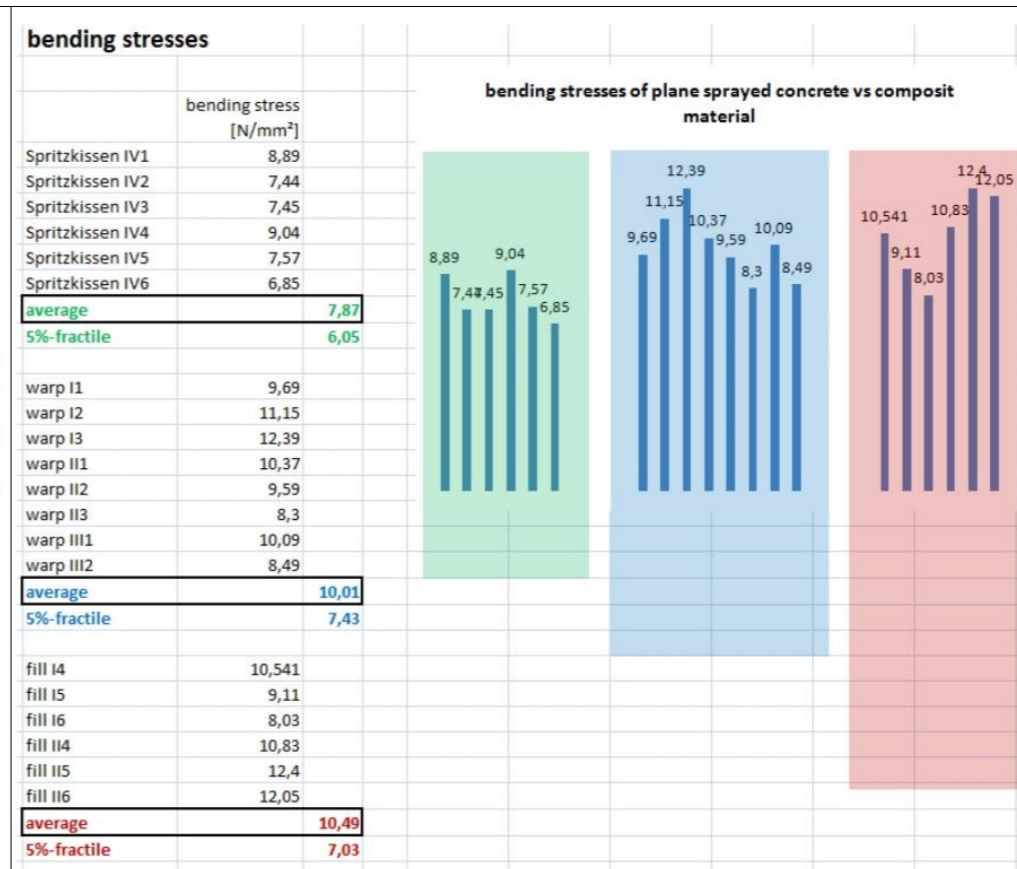


Figure 4.34 – Pictures of 3rd load test of concentrated load and detail to hung weights from the membrane-concrete shell prototype.



The lessons learned from the construction of the membrane-concrete shell prototype can be summarized in the following items:

- a.) The process to monitor the deflection of the finished bottom surface of the membrane-concrete shell can be refined and optimized. The scanning procedure that was used to determine the vertical deflections of the finished concrete surface was not the most efficient and it clearly needs to be refined or changed to another system based upon a photogrammetry approach. Another option to determine the deflection of the concrete shell surface might be to use deflection gauges that are directly embedded into the concrete shell surface and that can be used later to measure the deflections to specific points of the concrete shell surface. This option may be very costly and time consuming; therefore it is apparent that there is some room for improvements in this part of measuring the deflections of the membrane-concrete shell prototype.
- b.) For the material testing of the prototype concrete samples it is also possible here to refine the measuring of the vertical deflections of the samples under the increased applied external vertical load. Instead of using a horizontal metal plate, some metal circular plates can be embedded or glued to the concrete samples to then use some digital dial gages to record the vertical displacements.
- c.) The location, position, and number of fabric layers that can be embedded and used to provide the flexible formwork and to provide internal and external reinforcement of the membrane-concrete shell cross section is important and play a key role in the ultimate axial, shear, and bending strength of the concrete shell cross section. As it was known years ago with Ferrocemento widely used by Pier Luigi Nervi to build amazingly thin concrete shells, the higher and closer number of thin layers of fabric fully bonded with shotcrete mix, the stronger the final concrete shell structure becomes. Therefore this topic of multiple layers of fabric within membrane-concrete shell structures deserves further investigation to determine the effectiveness of bonding of fabric with layers of concrete or shotcrete mix reinforced with steel or carbon fibers.
- d.) The analysis of results of the material testing for the samples of the prototype reveals that the initial biaxial prestressing introduced into the fabric clamped to the steel frame has a strong influence on the final shape of the shell prototype, therefore it is highly recommended to perform further investigation into this topic of initial level of biaxial prestressing of the flexible fabric formwork.

The contents of this Chapter presented in the form of graphics, pictures, diagrams, tables, materials data sheets, thickness measurements and testing plots of materials testing and prototype displacements are entirely the results of the experimental, research, and development work performed by Dr. Robert Off (robert.off@ims-institute.org) and Henning Duerr (he.duerr@ims-institute.org) of the IMS to build the membrane-concrete shell prototype. The Author has simply reorganized and formatted the contents of this chapter to document and provide a summary of the research work and to have this material available for the work of Finite Element Analysis of the prototype to be done in Chapter 5 of this Thesis.



CHAPTER 5 - FINITE ELEMENT ANALYSIS OF IMS SHELL USING Ix-CUBE 4-10 SOFTWARE

The fundamental concepts for the analysis and design of thin concrete shell structures that have been discussed in Chapter 3 covers the basics for the theory of curvilinear surfaces of revolution, translation, and ruled surfaces, classification of shells, the membrane and bending theories with their applications to circular cylindrical shells, shells of revolution of zero curvature (developable shells), positive, and negative Gaussian curvatures, conical shells, shells of double curvature of synclastic and anticlastic shapes, hyperbolic paraboloids, hyperboloids, ellipsoids, elliptic paraboloids, conoids, circular domes, ellipsoids, paraboloids of revolution, hyperboloids (ruled surfaces generated between two parabolic curves at both ends) and some other curvilinear shell forms.

In Section 3.3, the membrane and bending theory analysis methods were briefly discussed. The mathematical differential equations that can be formulated for specific individual cases of shells with regular boundary conditions and some type of axisymmetric loading conditions were identified to produce some type of closed form solutions which are theoretical mathematical solutions for only some specific geometrical configurations. Partial differential equations of high order will need to be solved to arrive to mathematical solutions that could only be applicable to some unique cases of shell structures. Free form shell structures present a big challenge to be solved using purely mathematical differential equations.

The Membrane Theory is a simplified version of the Bending Theory. Due to the complexity of the high order differential equations to be solved for different boundary and loading conditions, it is almost imperative that some type of additional simplifications need to be introduced into the mathematical formulations to arrive to some specific solutions. To achieve the solutions of the high order differential equations the Fourier Series method provides another level of simplifications to solve the partial differential equations. At the end of the process of rigorous mathematical solutions the designers can immediately identify that the solutions obtained are not necessary exact solutions but merely some type of approximate solutions which represent solutions that are directly related to the assumed boundary conditions, assumed applications of external loadings, and assumed support conditions that reflect the degrees of freedom of the structural supports as accurate as possible to the real as-built structural supports.

Other simplified solutions to shell structures that present some type of configurations that can be assimilated to funicular shape forms can be solved using simplified methods of analysis that are based on analogies to the typical solution of funicular parabolic curves that can provide solutions with a reasonable degree of approximation similar to the solutions to the cable supported structures. Experimental tests may need to be done to prove the validity and degree of approximation of the funicular analogy methods of shell analysis.



For all those shell structures where the mathematical differential equations and any other simplified method or analogy type of simplified solution are extremely difficult or impossible to obtain, then the engineer may need to resort to use a Finite Element Analysis (FEA) computer method to establish the 3D model with the appropriate element types, material properties, edge, boundary conditions, and all the appropriate support points to perform a computational analysis using finite element methods which can provide an approximate analytical solution.

In the next sections the Author will present the methodology used to model the membrane-concrete shell IMS prototype structure using the Finite Element Analysis Methods and to perform the analysis using special purpose computer software which will be described as well. Two different computer programs will be used to do the entire finite element analysis of the prototype. The Ix-Cube 4-10 program will be used to do the initial form-finding of the tensioned membrane with the edge steel beams, tie-down cables, and ridge cables supported at three points to concrete bases embedded into the ground and to run the analysis of the membrane-concrete shell structure under loads. General Purpose 3D structural analysis software STAAD-Pro can also be used to perform additional analysis of the shell structure under loads and to verify the accuracy of the results obtained using the Ix-Cube 4-10 software.

5.1 - FINITE ELEMENT ANALYSIS METHODOLOGY

In general reinforced concrete members under loads present a nonlinear behavior which is due to the inherent nonlinear material properties and characteristics of concrete and steel rebars that leads into cracking of the composite material once the tensile stresses in the materials exceed the rupture and yield strength of concrete and steel respectively. Therefore elastic behavior of reinforced concrete shell structures is not strictly applicable and a realistic analysis of a reinforced concrete shell structure under loads must be carried out by the use of applicable nonlinear analysis software that takes into account material and geometrical nonlinearity under selfweight of the structure and external applied loading conditions.

The typical stress-strain plot of concrete appears to be nonlinear right from the initial stages of the compression load testing and continues to be nonlinear all the way up to the crushing point, the stress-strain plot of the reinforcing steel bars also present a nonlinear behavior right after the yield point of the steel is reached, from this point a ductile steel bar undergoes certain degree of nonlinear elongation before it reaches the rupture point. Therefore both concrete and steel reinforcing bars which are part of any reinforced concrete shell structure are to be analyzed by software which is capable to handle the nonlinear behavior of the materials.



The Finite Element Method (FEM) is a computer oriented methodology which is a well suited general purpose computer program based on the stiffness or displacement methods of structural mechanics mainly focused on the discretization procedure to subdivide a 2D or 3D structure into a finite number of structural components linked to each other at specific finite number of nodes (some free nodes and others fixed nodes) that define the overall shape of the structure. The structural components or elements each one has their own specific material properties and geometrical dimensions that will allow the overall behavior of the structure to be in equilibrium and maintain a compatibility of displacements under specific external loading conditions applied and transferred through the nodes.

This finite element method is a general purpose 2D and 3D analysis method for structural framing composed of beams, columns, struts, cables, frames, trusses, plates, shells, and other elements interconnected to each other in a continuous manner and supported at specific points by pinned, fixed, or roller type of supports that will provide equilibrium with the externally applied forces and compatibility of displacements and deformations of the entire structural framing.

Detailed information and extensive literature on the Finite Element Method (FEM) is available in numerous college textbooks and technical papers. The classical textbook of Zienkiewicz, O.C., “The Finite Element Method” listed in the References section of this Thesis presents a detailed study of this method describing the different types of elements such as: straight bars, flat plates, curved, triangular, rectangular, quadrilateral, hexagonal, and other variety of type of finite element members with a variety number of nodal points.

Continued developments on the FEM have led to the creation of several types of shell elements capable of modeling large displacements, rotations around three axis, geometric imperfections, creep, cracking, nonlinear and inelastic material properties, steel reinforcement elements, and other special type of shell elements have been developed. With the appropriate material properties of the elements of the shell structure and the appropriate definitions of the connecting nodes between the finite elements, supports, and boundary conditions then a nonlinear Finite Element Analysis is capable to predict the whole behavior of a shell structure from initial loading up to failure.

Structural systems composed mainly of tensioned fabric/membrane elements in combination with tensioned cables, struts, edge and tie-down cables typically undergo large displacements (translations and rotations) and behave in a highly nonlinear manner. The stress-strain behavior of tensioned fabric/membranes is also highly nonlinear and the overall structure under the application of external loads presents large displacements of the interconnecting nodes which leads to a geometrical nonlinear behavior of the overall structure.



Therefore tensile structures requires of a special type of finite element analysis which is based upon an initial approximation of the starting shape of the tensioned membrane that has been given an initial internal prestress to achieve a shape in equilibrium. Finding a unique shape of the membrane in equilibrium under an initial internal prestress is called: “Form Finding” which is an iterative nonlinear procedure. In this procedure the overall structure is also divided into a finite number of elements of membrane sections, cables, struts, and beams with their corresponding interconnecting nodes which may be free to displace or may have fixed displacements (translations and rotations) at the points of supports of the structure. Then for tensile membrane structures the Finite Element Method (FEM) is also applicable but with a different solution strategy which at the end must provide a solution that will be within specified approximation tolerance to converge to a unique solution that will satisfy the static equilibrium of forces and the compatibility of deformations.

Tensioned Fabric/Membrane structures are commonly modeled using a triangular or quadrilateral type of plate element that is an anisotropic 2D element with different material properties in two perpendicular directions called “warp” and “weft” (also known as “fill”). In some cases where the layout of the tensioned structure requires a mesh of cables or bars is also commonly used to model the 2D or 3D tensile structure.

Four different computational methods for the analysis of tensioned fabric membrane structures have been implemented by university researchers and by individual software developers to obtain the solutions to their nonlinear behavior, they are briefly described below:

A. - Nonlinear Finite Element Stiffness Analysis (FEA) - In this method a set of simultaneous equations is generated to represent the translational displacements and rotational equilibrium at each one of the free nodes of the structure. The static analysis is arranged in matrix form according to the following equation of equilibrium: $\mathbf{P} = \mathbf{K} \mathbf{U}$; where \mathbf{P} is a vector that contains the sum of applied prestress and external applied loads, \mathbf{K} is the stiffness matrix, and \mathbf{U} is the vector of nodal displacements. The stiffness matrix of the structural system includes the material properties of the elements, modulus of elasticity (E), the geometrical cross section member properties (A), and the length of the member (L) among other of the applicable stiffness terms of the structural elements of the tensioned membrane system. The solution sought requires the determination of the geometric compatibility for specific initial values of prestressing, a task which is commonly referred as form-finding. The solution to this problem is basically independent of the stiffness properties of the membrane materials instead it requires that the geometrically nonlinear configuration is solved by an iterative procedure. As the pretensioned membrane structure undergoes displacement of the nodes the deformed shape of the structure is used as the starting geometry for the subsequent analysis until the structural system converges to a stable configuration within the specified tolerances of an acceptable solution.



B. - Dynamic Relaxation (DR) – Is a numerical analysis method, in which a set of simultaneous equations for the geometric nonlinear problem of form finding is solved by equating it to the case of dynamic analysis where the nodal points are assimilated to discrete points with assigned mass and damping characteristics which will respond consistent with the induced vibrations from the dynamic behavior of the system. At each time step of the dynamic analysis the forces at each node are evaluated and any unbalanced internal forces from the mass and acceleration at each location are determined, as the magnitude of the unbalanced forces diminishes then the prestressed structural system come to a state of dynamic equilibrium. This method was originally developed in England by A.S. Day listed in the References section.

C. - Force Density Method (FDM) – Is a numerical analysis method that uses a special analytical technique that linearizes the equations of the tensioned structure to produce a form finding solution of the tension net system. This method can be used to obtain solutions of cable net systems under a given system of applied external loads or it can also be primarily used to obtain a desired membrane shape in equilibrium for a given state of internal prestressing conditions of a membrane system or a cable net system under initial prestress forces. The FDM allows engineers and designers to find forms of tensioned membrane and cable net systems in equilibrium for a given 2D or 3D geometrical configuration of the structure supported at specified points and with members having a given set of force density ratios (tension cable/membrane force divided by its cable/membrane length). The FDM apply to cable/membrane net systems where the elements are connected to each other at the node points and it is relatively independent of the initial geometry and position of the free nodes part of the tensioned cable/membrane net structure. Different initial values of force density ratios produce different final geometries of the tensioned systems in equilibrium. It takes an extensive practical experience in the field of tensioned membrane structures and a good common engineering sense to come up with an initial good approximation to the final desired form in equilibrium.

This Force Density Method is numerically stable and robust to achieve equilibrium forms for determinate, indeterminate, stable, and unstable tensioned cable/membrane structures. Given force densities which are positive produce a system of equations positive, definite, and always produce a specific solution. Once the coordinates of the nodes are found to be in equilibrium then the length and forces in the cable/membrane net elements are determined. The change in length and force in the elements of the system are used to find the unstressed length of the elements provided the stress-strain relationship of the elements are known. The higher the force density ratio, the shorter the elements become under a given constant force, the higher the force density ratio, the larger the force in the elements for a constant length. Force Density Ratio = $fdr = F/L$ (Force divided by Length). When the force densities for all the elements at a given node are equal and uniformly distributed around the node, then we can say that we have obtained a state of minimal surface.



Once the prestressed cable/membrane net structure has attained an equilibrium shape then the deflected forms for different loading conditions other than the initial prestressed loading can be obtained. Every time the external loads change, the equilibrium geometry changes and a new solution in equilibrium must be obtained. The force density method solution for externally applied loads is an iterative procedure to solve the set of nonlinear equations. For each iteration a new constant length of cable is set, the force densities are then adjusted as necessary until equilibrium is achieved within the tolerances set for the accuracy of forces and displacements.

D. - Updated Reference Strategy (URS) - In this method a numerical formulation is developed to do the form finding of minimal surfaces and to find the equilibrium form of prestressed fabric and membrane structures. The URS method is based upon an iterative procedure to regularly update the stiffness matrix of the structural system which can be applied to any structure that can be discretized into a finite number of cable and membrane elements under the initial prestressing of cables and membrane elements, selfweight, lateral pressure, and other external loading conditions. The URS method is very robust, reliable, and efficient to solve tensioned membrane structures. In general terms it is said that the Force Density Method (FDM) is the special case of applying the Updated Reference Strategy (URS) to a cable net system.

5.2 – NON-LINEAR ANALYSIS OF IMS SHELL PROTOTYPE

The IMS membrane-concrete shell prototype will be analyzed following a non-linear analysis procedure that will take into account every step of the construction sequencing starting with a flexible tensioned membrane structure in equilibrium with the tie-down cables and the edge strut beams around the perimeter of the membrane and following with the application of the several layers of shotcrete over the tensioned membrane to achieve a hardened reinforced concrete shell in equilibrium with its selfweight and the remaining portions of the structure which are maintained fully tensioned throughout the entire construction process. It is essential to understand very clearly each one of the stages of construction of the prototype structure to be able to properly select the software tool that will be able to realistically simulate the entire behavior of the structure as close as possible to the actual conditions for each loading situation.

The specific plan geometry, elevations, heights, dimensions, details, materials properties, configuration of supports and steps of the sequencing of construction of the IMS Membrane-Concrete Shell Prototype which is the main subject of this Thesis work have been presented and discussed at length in Chapter 4. Figure 5.1 shows the conceptual 3D Model Plan and Isometric Views of the IMS prototype with the basic dimensions, heights, and structural components.



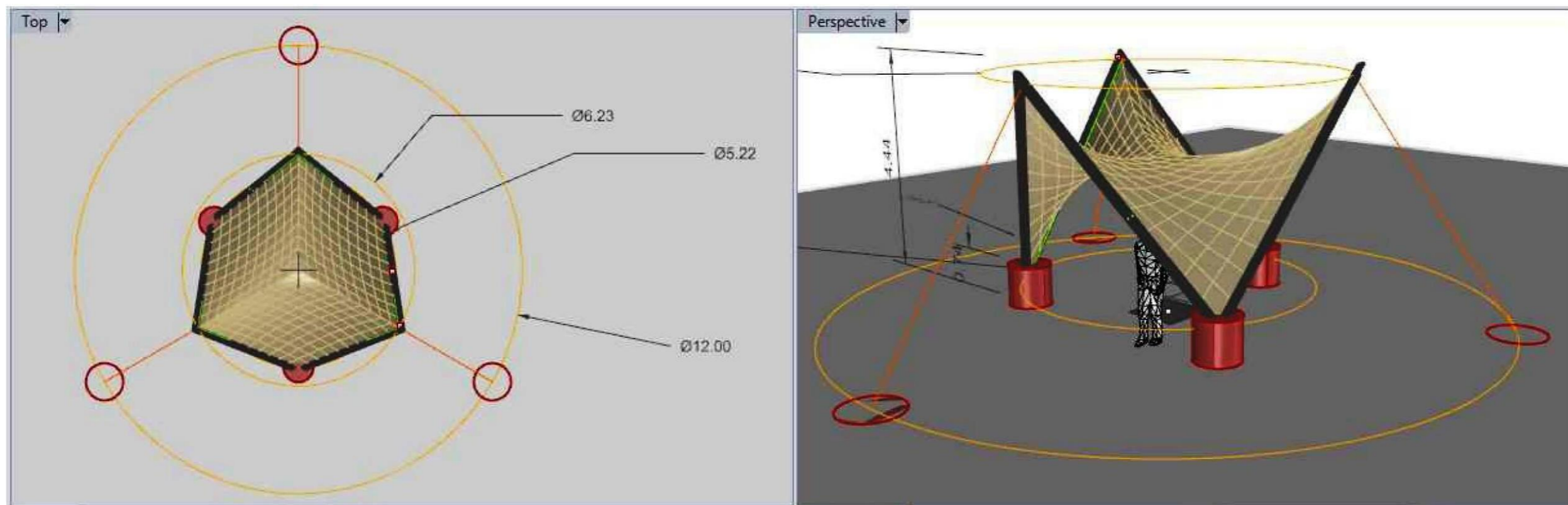


Figure 5.1 – Conceptual 3D Model of the IMS Membrane-Concrete Shell Prototype – Plan and Isometric Views.

The structural drawings for the entire IMS shell prototype and for each one of the components, parts, members, and structural layout with plans, elevations, sections, isometric and with all the dimensions, heights, connections, details, materials specifications, and detailed patterns for the fabrication of the flexible PVC membrane are shown in Appendix C.

The drawings include: the base plate details, lug plates, anchor bolts, reinforcement cages for the concrete bases, weldments for ridge cables, membrane cutting patterns with fabric weldment details, wide flange edge steel beams, aluminum clamping, bolts for clamping to steel beams, end cutting and plate details to connect steel edge beams, base plate details and anchors to concrete bases, , tie-down cable details with the fittings, turnbuckles, and end connections to steel weldment plates. Detailed dimensions of components are shown for precise fabrication and assembly.

The listing of the main components and construction steps involved in the installation process of the IMS prototype can be summarized as follows:

CONCRETE BASES – ANCHORS & PLATES - STEEL FRAME AND WELDMENTS – CABLES – FLEXIBLE MEMBRANE - SHOTCRETE



1. The site is surveyed and staked out to mark the exact location of the six concrete bases that will be embedded into the ground to support the three tie-down cables and the six lower ends of the edge steel beams of the frame that will support the flexible PVC membrane. Three concrete bases are placed 120 degrees apart within an outer circle of 12 m. diameter and set with the top of the base close to the ground level, the other three concrete bases are placed 120 degrees apart within an inner circle of 5.22 m. diameter and set with the top of the base elevated some 0.74 m. above the ground level.
2. Excavation is done at six locations up to a depth of approximately 1m. below exterior grade for three outer holes of approximately 1.00 m. diameter and three inner holes of approximately 0.80 m. diameter which are then filled with concrete around a cage of steel vertical reinforcing bars and circular horizontal steel ties for the full height of the concrete footing bases.
3. Immediately after the concrete is cast for the six footing bases the steel base plates with their anchor bolts are set in the exact position and orientation at the top of the concrete bases and with the top of the base plates at the elevations shown in the structural drawings of Appendix C. The top of the three inner concrete footing bases are left with a recessed down area at the center of the bases around the base plates forming a circular curb around the edges to retain the portions of the shotcrete that will be placed on the tensioned membrane.
4. The flexible assembled PVC membrane that has already being welded together in one single piece and with all the edge details is clamped along the six edges to the bottom flanges of the steel frame beams as it is shown in Figure 5.2.
5. Three steel tie-down cables are attached to the three high points of the steel frame and three ridge cables are also connected to the three high points of the steel frame and joined together at the center point of the prototype right under the flexible membrane. The three tie-down cables and the three ridge cables will work together to maintain equilibrium of the tensioned membrane-frame system during the erection process. The three ridge cables are welded together to a steel plate which serves as a tension ring element to maintain equilibrium of the prototype.
6. The steel frame composed of six straight wide flange steel beams already assembled and connected at their high points together with the clamped membrane is erected, and bolted to the steel base plates at the three low points of the concrete footing bases. At this time all the major components of the IMS prototype consisting of flexible membrane, steel frame, and cables are installed, anchored, and supported on the six reinforced concrete footing bases. All the connections of the steel framing, flexible membrane clamping to the steel beams, bolted connections of the beams to the pinned joints and base plates, and cable connections to the steel beams and base plates are verified for accuracy.



7. After the steel frame, flexible membrane, and cables are installed the entire system is then tensioned by applying prestressing axial forces to the three tie-down cables which in turn brings tensioned membrane forces into the flexible membrane to achieve a uniform field of axial stresses in the system until a state of static equilibrium of the entire system is reached as is shown in Figure 5.2.

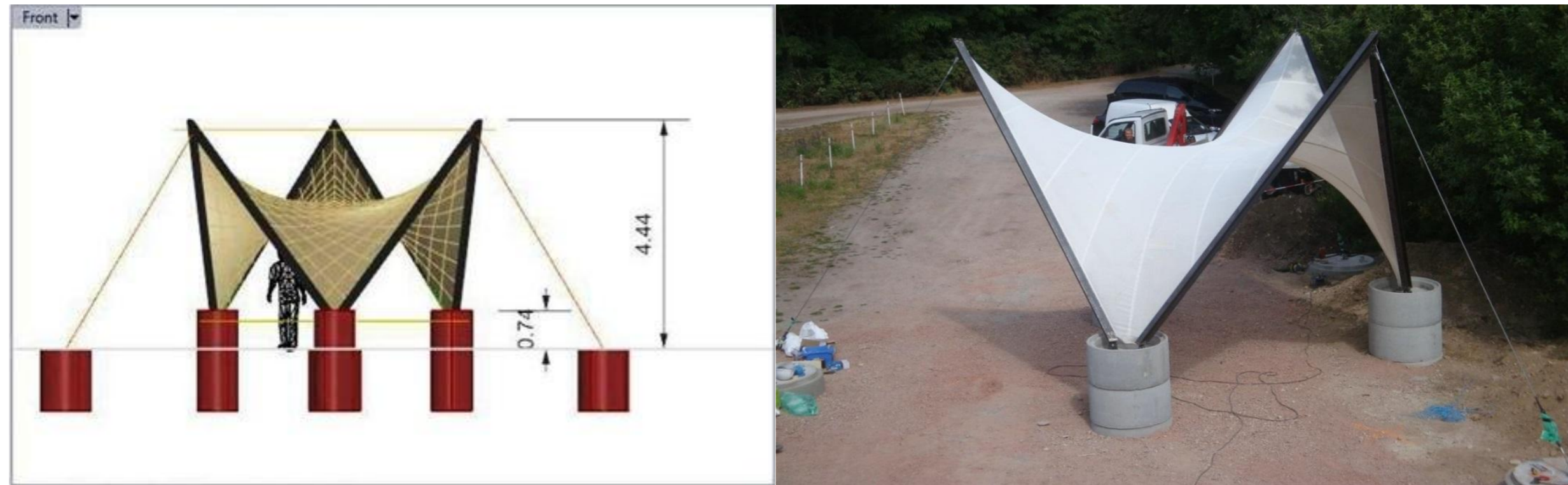


Figure 5.2 – IMS Membrane-Concrete Shell Conceptual Model and Installed Membrane, Frame, Cables, and Concrete Bases.

8. Once the flexible membrane has been fully pretensioned and it is in equilibrium with the steel frame, tie-down cables, and ridge cables, the top surface of the membrane is fully covered with several layers of shotcrete up to the projected thickness of the shell of 50 mm. The bottom surface of the membrane is covered with a layer of shotcrete given a smooth finish. Throughout the whole process of tensioning of the cables and applying shotcrete, digital measurements of the axial forces in the cables are recorded and scanning of the final shell surface is also recorded for further processing and analysis. Figure 5.3 shows some pictures of the constructed membrane-concrete shell prototype.



Figure 5.3 – Pictures of the completed IMS Membrane-Concrete Shell Prototype with the entire shotcrete shell surface installed.

It is very important to identify clearly every single step of the entire construction process of the membrane-concrete shell prototype as it is described in the steps noted above. The completed structure can be considered to be a Hybrid Tensioned Membrane-Concrete Shell which will behave under its selfweight and under the external environmental forces of snow, wind, and seismic as a hybrid composite highly tensioned steel framed cable supported reinforced concrete shell. Its overall behavior under external loading is quite complex and will require the use of sophisticated non-linear analysis structural analysis software.

The main objective of this Thesis is to present the basic analytical procedures and computational steps required to achieve a realistic representation of the entire membrane-concrete shell prototype under selfweight, initial prestressing, and external snow, wind, and seismic design loads and forces. From the construction steps described in items 1 to 8 listed above then TWO major as-built conditions of the prototype structure are identified and shall be selected to be fully analyzed using non-linear finite element analysis software.

FIRST CONDITION OF AS-BUILT PROTOTYPE - The flexible thin membrane which has been patterned, cut, and welded all together into one piece is clamped to the six edge steel beams and is fully tensioned by adjusting the tie-down cables with prestress forces until the entire assembly is brought to equilibrium and to the desired shape of the tensioned flexible membrane which will have to support the layers of shotcrete on the membrane. At this stage the structure looks as it is shown in Figure 5.2.



The tensioned prototype with the flexible membrane, steel beams, and cables is then analyzed by using the special purpose non-linear form-finding analysis software Ix-Cube 4-10 and following the NFDM (non-linear force density method) approach. Ample internal prestress is introduced into the flexible membrane to achieve a form which will be suitable to maintain equilibrium of the prototype for the next stage of applied shotcrete. At this stage the flexible membrane and the three interior ridge cables are fully tensioned and will have a defined shape that can be accurately predicted by modeling the prototype with the Ix-Cube 4-10 software. The structure shown in Figure 5.2 is analyzed and a screenshot is presented in Figure 5.4.

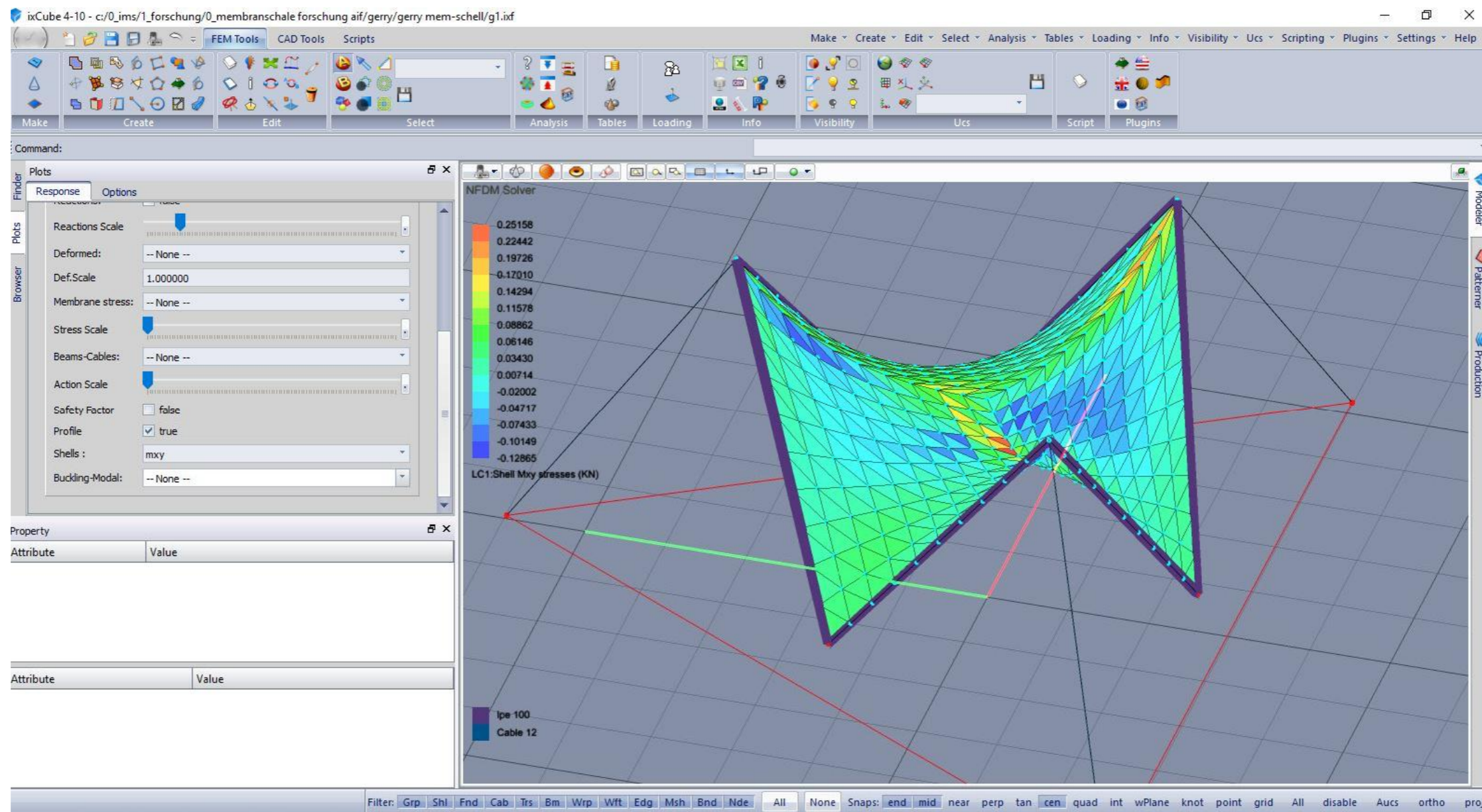


Figure 5.4 – IMS Membrane-Concrete Shell Prototype modeled using Ix-Cube 4-10 software for membrane form-finding and stress analysis.



The non-linear form-finding analysis of the prototype using the Ix-Cube 4-10 NFDM approach will produce all the member forces in the steel beams, axial tensile forces in the tie-down cables, axial tensile forces in the ridge cables, support reactions at the six low points of support of the steel beams on the concrete bases, warp, weft, and von-misses tensile stresses in the flexible membrane, and the displacements of the three high free nodes of the structure for the equilibrium and form-finding conditions of the prototype. All the results are color coded for better visualization of the magnitude of the values being obtained from the non-linear analysis. Once the form-finding analysis has been completed and all the structural members part of the prototype (including the flexible membrane) are in static equilibrium then the structure is ready to be post-processed in the next stage when the shotcrete is applied in layers to the flexible membrane to become a final membrane-concrete shell structure.

At this point all the structural members of the membrane-concrete shell prototype that is shown in Figure 5.2, including tie-down and ridge cables, steel beams, flexible membrane, and clamping connection of membrane to the steel beams are checked for their adequacy (strength, stiffness, and stability) under the initial prestressing conditions of the entire structure. The six edge steel beams are sized and designed to be able to act as a rigid beam fixed at the two end points with all the reaction forces from the tensioned membrane clamped along the length of the steel beams. The system can be considered a highly hybrid structural prestressed composite rigid and flexible membrane and active rigid bending combined system that behaves in a highly non-linear fashion.

The three high points of the prototype structure are free nodes in 3D space that can have large displacements depending on the magnitude of the tension forces in the tie-down and ridge cables to maintain static equilibrium. Considering the fact that there is only one tie-down cable at each one of the three high points then any unbalanced axial forces in the steel beams, cables, and flexible membrane could potentially cause uncontrolled displacements of the three high nodes, making virtually impossible to maintain the three high nodes all at the same exact location as they were originally set during the erection process. The main task at this point of the erection sequencing is to maintain the flexible membrane well tight and fully tensioned to ensure that it will properly support the next phase of shotcreting without going flat or have undesirable areas of ponding when subjected to the layers of fresh shotcrete being applied on top of the membrane.

SECOND CONDITION OF AS-BUILT PROTOTYPE – The process of applying shotcrete to the recently erected tensioned flexible membrane, beams, and cable system is done in several steps. First a very thin layer of shotcrete is applied over the entire tensioned flexible membrane to achieve an initial uniformly surface that will harden into a thin concrete shell. The entire prototype structure starts changing from a flexible lightweight surface into a heavier hardened concrete surface which now has more substantial selfweight than the previous very thin light membrane.



The newly formed thin concrete shell membrane structure will tend to attain a new state of static equilibrium with the entire surface changing shape and the free high nodes undergoing displacements due to the additional selfweight of the thin layer of shotcrete. During the shotcreting process all the cable forces are closely monitored to make sure that the required prestress is maintained during the entire application of shotcrete onto the membrane surface, maintaining the tie-down cable fully tensioned will assure that the membrane will perform properly to support the new weights being added to the tensioned membrane surface. After the application of two more layers of shotcrete and finishing the top and bottom surfaces of the membrane-concrete shell structure the final prototype is complete and looks like it is shown in Figure 5.3.

During the shotcreting process the top and bottom surfaces of the membrane-concrete shell structure is scanned to obtain the approximate thickness of the final concrete shell, it was found that the thickness throughout the entire surface is not exactly the same and it had some variations due to the curvature of the flexible membrane and the variability of the application of the shotcrete over the surface of the membrane. It was found that the approximate average thickness of the concrete shell came up to be 50 mm. +/-.

The non-linear analysis of the newly formed composite structure of the flexible membrane, cables, beam elements, and now the added elements of concrete shell throughout the entire surface of the membrane is performed using the Ix-Cube 4-10 software that has the capability to not only do the form-finding of the flexible membrane but also allows to perform a non-linear analysis of the composite membrane-concrete shell structure. The thickness of the concrete shell elements is defined and input as a new geometrical property, the material properties of the concrete are also defined and input into the model to account for a new type of thicker and strong membrane element. Modulus of Elasticity (E), Poisson Ratio (ν), and Shear Modulus (G) are the main material properties parameters for the concrete shell elements.

The non-linear analysis of the entire membrane-concrete shell structure is then performed with Ix-Cube 4-10 software to obtain the new state of equilibrium of the prototype under the new selfweight conditions of the concrete elements over the entire surface. Cable forces, Beam member forces, and Membrane stresses in the shell elements are produced by the Ix-Cube 4-10 software. The results are then checked to verify that all the cable elements, beam members, and membrane elements forces and stresses are within the allowable and safe stresses and strength of the materials specified for cables, beams, and shell members.

In Ix-Cube 4-10 software the concrete shell elements are defined as FEM-PLATE elements with their corresponding material properties. All the previous results from the form-finding analysis of the flexible membrane, cables, and beam forces are maintained and transferred from the initial analysis onto the extended analysis of the prototype now having the composite section of membrane-concrete shell elements.



5.3 - FINITE ELEMENT ANALYSIS OF IMS SHELL PROTOTYPE

In the previous Sections 5.1 and 5.2 the Finite Element Analysis (FEA) method and the Non-linear Analysis procedure have been discussed and reviewed in relation to their application for the detailed analysis of form-finding, member forces, and element stresses of the hybrid membrane-concrete shell prototype structure which has been modeled, designed, detailed, analyzed, and constructed by a research team of the IMS. In this Section 5.3 the Author will present the basic procedure that was done to recreate and validate the modeling and analysis of the membrane-concrete shell structure.

The Finite Element Analysis was carried out completely using Ix-Cube 4-10 software which allows doing the form-finding of the membrane and the stress analysis of the rigid beam members, cables, and concrete shell elements under the selfweight and the different specified loading conditions. A conceptual 3D model shown in Figure 5.5 was created in Rhino with all the model geometry, dimensions, and member sizes.

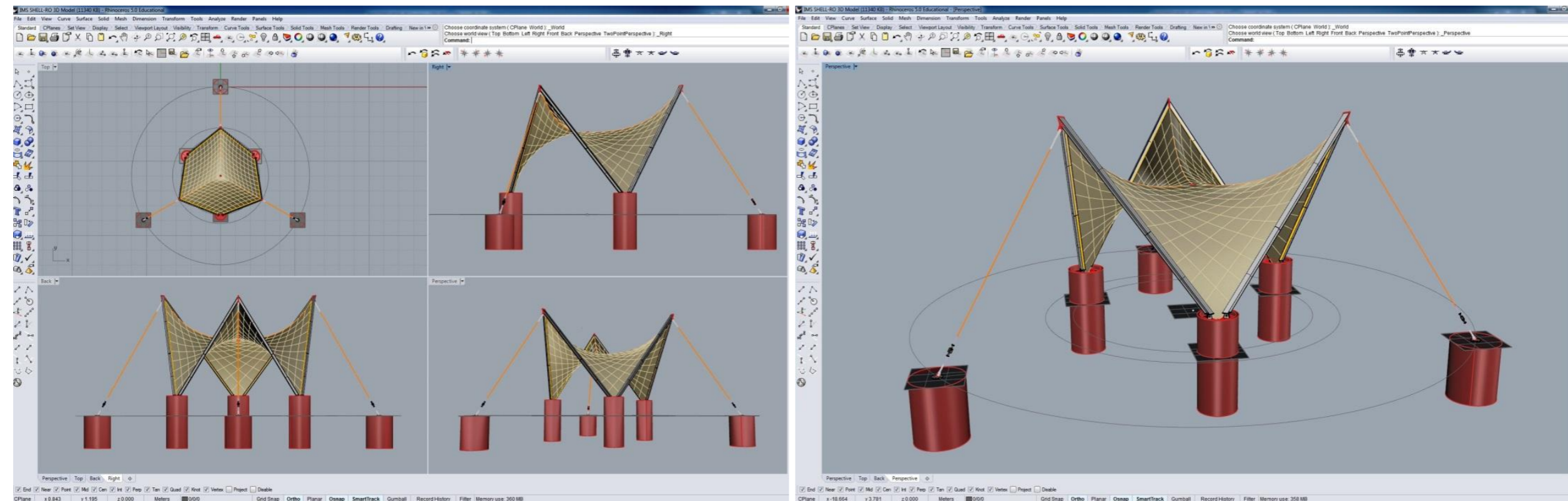


Figure 5.5 – IMS Membrane-Concrete Shell Prototype conceptual 3D Model Plan, Elevations, and Isometric using Rhino software.

The Step by Step procedure to create a 3D model of the IMS membrane-concrete shell prototype in Rhino and then import that model into Ix-Cube 4-10 software for the form-finding and the non-linear finite element analysis will be explained in detail as follows:



STEP 1 – CREATE THE BASIC GEOMETRY OF THE 3D MODEL IN RHINO SOFTWARE.

The first step to initiate the finite element analysis of the membrane-concrete prototype is to generate a 3D CAD model of the structural members using a 3D CAD software such as Rhino, AutoCAD or any other 3D CAD software. The basic geometry can also be generated directly in Ix-Cube 4-10. The tie-down cables, edge beams, and ridge cables can be generated using line elements which will be set up at those points established at the support nodes and at those nodes free in 3D space connecting the high points of the edge beams. The geometry of the 3D CAD model will be based strictly upon the basic points of supports, heights, orientation, and position of the key nodes set up in a circular pattern for the three concrete bases of the tie-downs, the three concrete bases for the low points of the edge beams, and the three high points of the steel beams. The mesh for the membrane can also be generated with Rhino software or it could be left open to be generated next inside Ix-Cube 4-10 software.

Figure 5.6 below shows the basic geometry of the prototype including the lines for tie-down cables, ridge cables, edge beams, and the membrane mesh generated with Rhino. This model is then saved and will later be imported into Ix-Cube 4-10 for further processing. It is very important to have a very well defined geometry of the 3D model which can then later be used for other software such as Ix-Cube 4-10 and Staad-Pro.

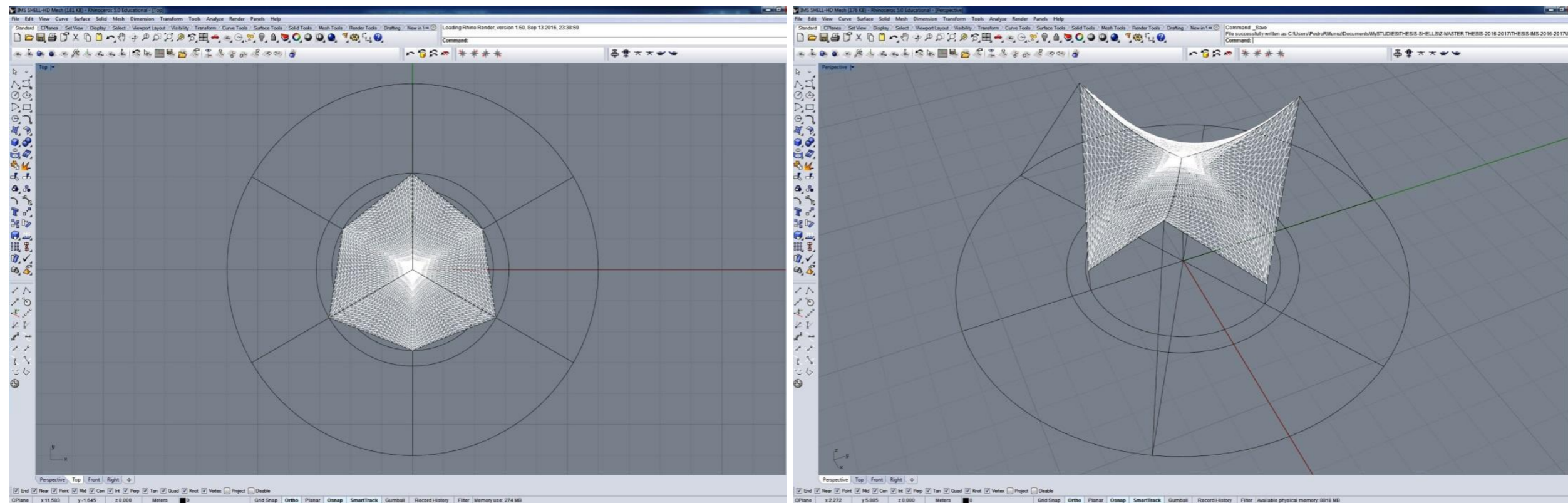


Figure 5.6 – Step 1 – Geometrical 3D Model Plan and Isometric of IMS Membrane-Concrete Shell Prototype using Rhino software.



STEP 2 – IMPORT THE BASIC GEOMETRY OF THE 3D MODEL FROM RHINO INTO IX-CUBE 4-10

The CAD entities of the 3D prototype model generated in Rhino software are imported and brought into IxCube 4-10 software. The tie-down cables, edge steel beams, ridge cables, membrane mesh, and fixed supports at the three high and three low points are set as FEM elements in IxCube 4-10 with their corresponding attributes and properties to then be post-processed for form-finding of the tensioned membrane mesh and non-linear analysis of the membrane-concrete mesh under the specified design loads of selfweight, snow, wind, and seismic effects.

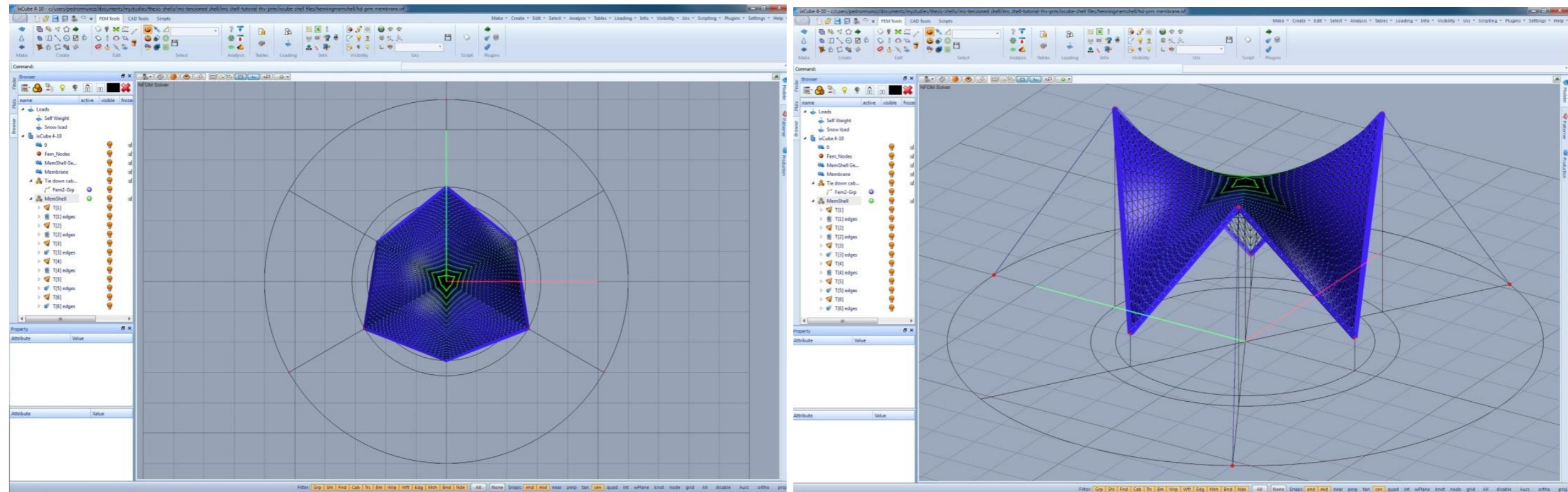


Figure 5.7 – Step 2 – Geometrical 3D Model components of IMS prototype imported from Rhino into IxCube 4-10 software.

The following attributes and properties were assigned to the prototype components of the tensioned membrane structure shown in Figure 5.7 above:

- A. Membrane Mesh: Membrane Prestress Formfinding; Warp = 2 kN/m ; Weft = 2 kN/m; Membrane: Preconstraint 392S-Ferrari.
- B. Tie-Down Cables: Cable 10; Nonlinear, FF-Deformable; Pretension = 10.0 kN.
- C. Ridge Cables: Cable 8; Nonlinear, FF-Deformable; Pretension = 3.0 kN.
- D. Edge Beams: HEA 100; Linear, Stiff-Deformable; Pretension = 0.001 kN.
- E. Shell Surface Areas is estimated to be approximately: 29.186 m².

The tensioned membrane structure is now ready to be processed for form-finding using IxCube 4-10 software.



STEP 3 – PERFORM THE FORM-FINDING OF THE TENSIONED MEMBRANE USING IX-CUBE 4-10

The three high points of the membrane structure are initially set as fixed and restrained from any displacements in the x, y, and z directions and the membrane is clamped to the stiff rigid edge steel beams along the six sides of the membrane. The form-finding of the membrane is performed using IxCube software and the distribution of the warp and weft stresses in the membrane are noted to be fairly evenly distributed over the surface. The results of the form-finding analysis with the three high points fixed are shown in Figure 5.8 below.

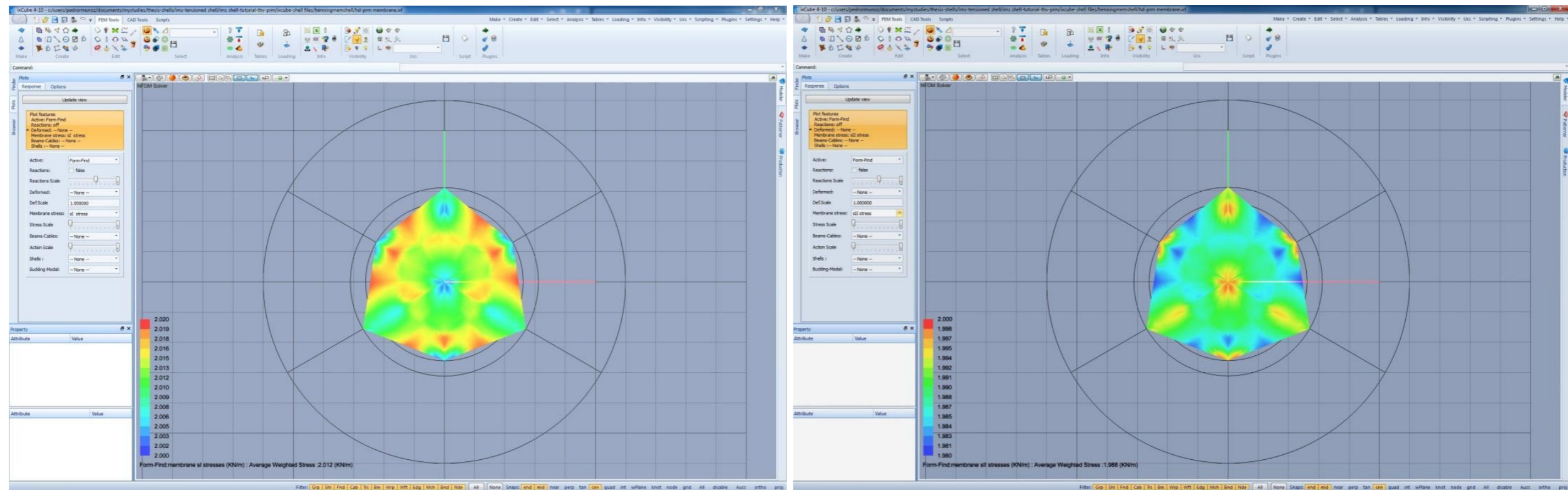


Figure 5.8 – Step 3 – Form-finding of the membrane structure with the three high points fixed and the membrane clamped to the steel edge beams.

The three high points of the tensioned membrane structure are next set free to have displacements in any direction and the three tie-down cables are fixed at their ends with the tensioned membrane remaining clamped to the six edge steel beams. Figure 5.9 below shows the plots of the tensioned membrane structure plan and isometric with free nodes and the results of the form-finding analysis performed with the redistribution of the stresses in the membrane due to the movement of the high points and the free deformation of the rigid steel beams as they deform due to the clamping forces from the membrane attached to the weak axis of the edge steel beams.



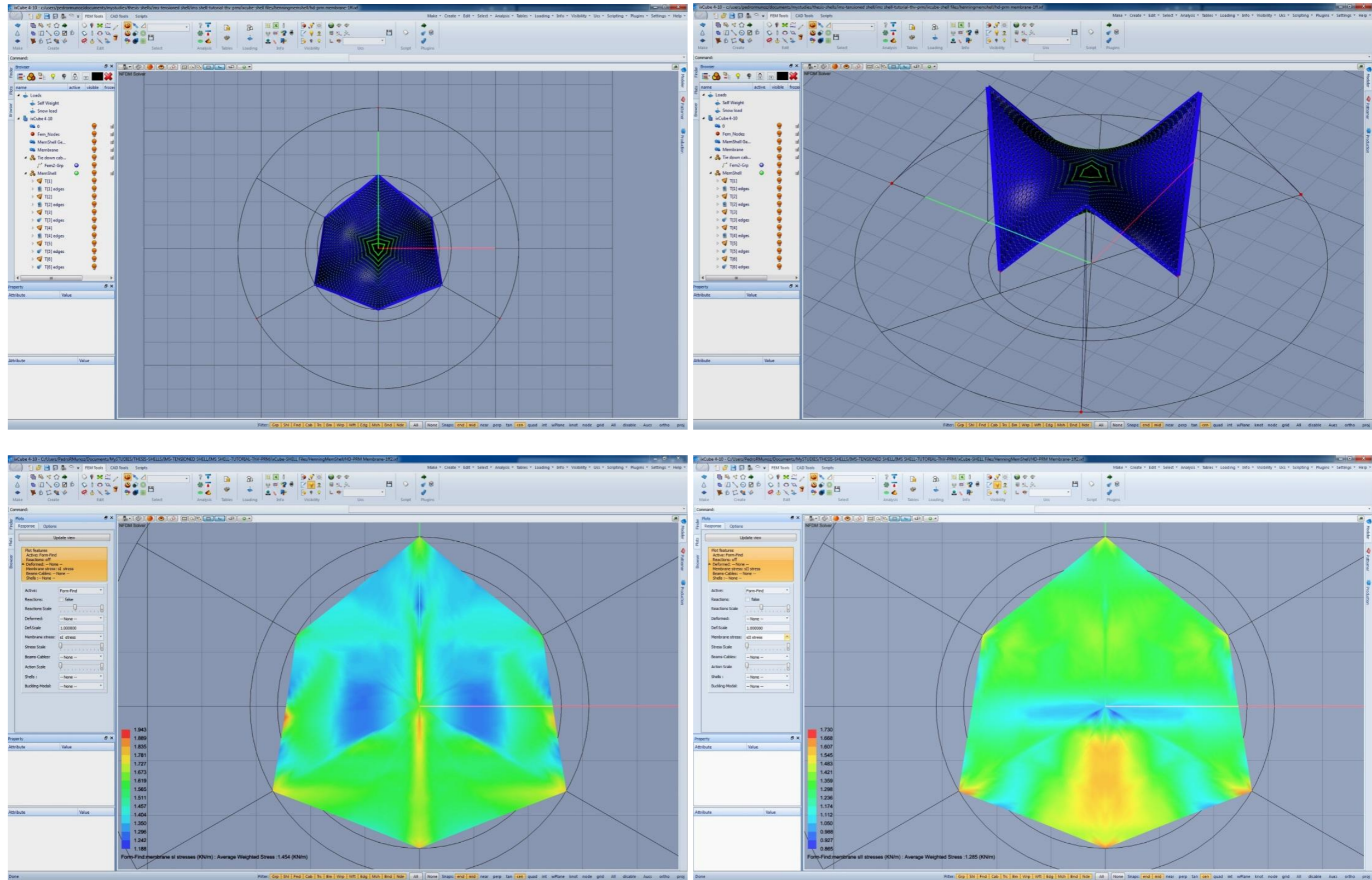


Figure 5.9 – Step 3 – Form-finding of the membrane structure with the three high points free and the membrane clamped to the steel edge beams.



The axial loads in the six edge steel beams, three tie-down cables and the three ridge cables are shown in Figure 5.10 below together with the plots of the reaction forces at the six points of supports of the tensioned membrane structure. Clearly the three tie-down cables are fully under axial tension forces as well as the three ridge cables, and the six edge steel beams are fully under axial compressive forces.

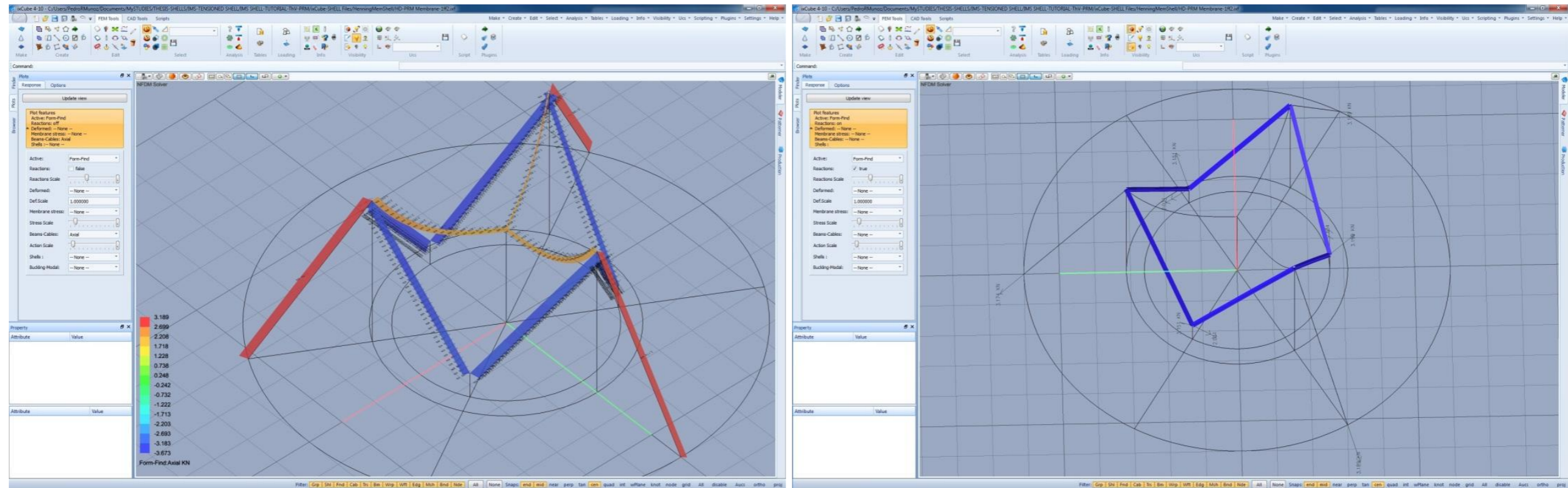


Figure 5.10 – Step 3 – Axial Forces and Reactions at Support points from the Form-finding Analysis of the tensioned membrane structure.

The reaction forces at the six points of supports (the reinforced concrete bases cast at ground level) reveal that the three concrete bases supporting the tie-down cables are under pullup forces and the other three concrete bases are under downward compression forces. The six reinforced concrete bases are designed to properly support the maximum reaction forces during the process of fully tensioning the membrane clamped along the edges of the perimeter steel beams.

At this point we have a tensioned membrane flexible fabric that is clamped to the edge steel beams and is fully in equilibrium with the ridge cables and tie-down cables onto the concrete bases that provide the supports for the entire tensioned structure. The shape of the tensioned membrane can be altered by modifying the initial prestress forces in the flexible membrane and the three ridge cables that are joined all together at the center line of the structure and clamped to the ends of the edge steel beams which in turn are connected to the tie-down cables. This is an iterative process until the final target position of the center line of the structure where the three ridge cables connect is achieved.



STEP 4 – GENERATE THE CONCRETE MEMBRANE-SHELL 3D MODEL FROM THE OBTAINED FORM OF THE MEMBRANE

After the form-finding iterative process of the flexible membrane is completed then the designer shall proceed to generate the concrete shell elements which shall coincide with the generated geometry of the tensioned membrane from the form-finding in equilibrium with the rest of the rigid beams and cables of the structure. It is very important that the geometry of the generated membrane elements and the new generated concrete shell elements match exactly at the nodal points to assure that there will be good behavior of the tensioned membrane and the concrete shell elements.

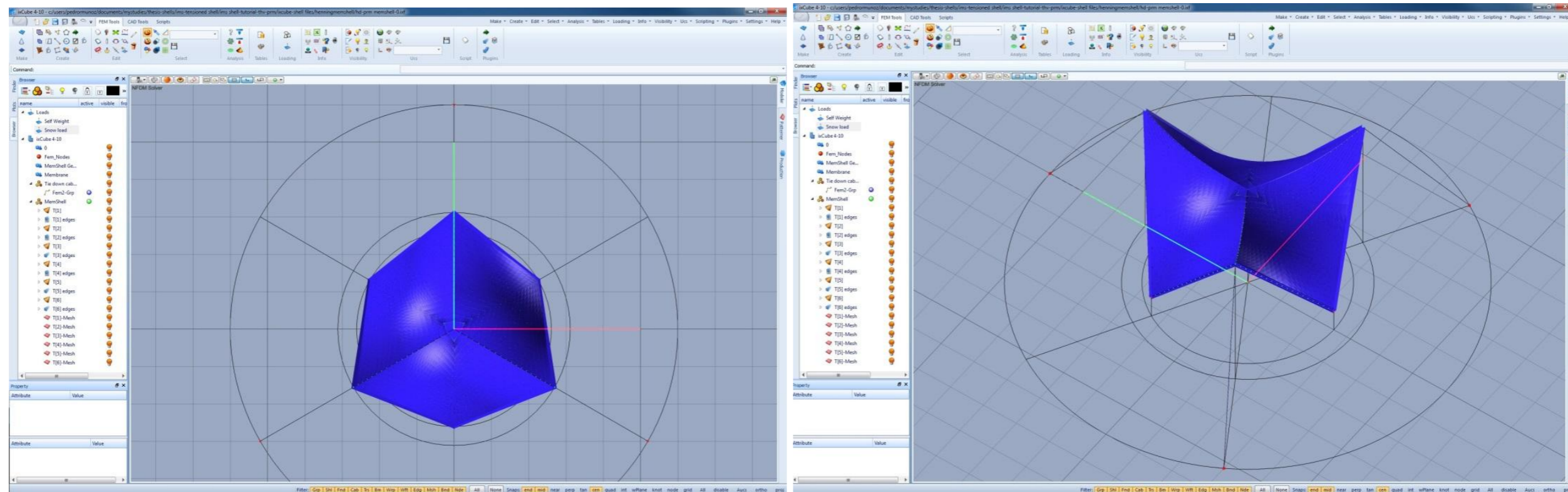


Figure 5.11 – Step 4 – 3D Model of the Membrane-Concrete Shell Structure with Beams, Cables, and Supports inside IxCube 4-10.

There are few steps that are required to be done to get the membrane and concrete shell elements all into IxCube 4-10. First the user creates a new layer for a FEM shell structure. Within the new layer (say MemShell) Drag T[1] Mesh from layer ‘Membrane’ to layer ‘FemShell’ (drag on name MemShell). Next Drag T[1] Edges from layer ‘Membrane’ to layer ‘MemShell’. Inside IxCube 4-10 EXPORT the entire Model to a Rhino CAD file (say Membrane.3dm). Then staying inside IxCube 4-10 IMPORT the just created Rhino Membrane.3dm file into IxCube 4-10 and bring the T[1]-Mesh of the membrane into layer MemShell as ‘FemPlates’. At this point the user should have both ALL the membrane mesh and ALL the concrete shell elements into their corresponding layers inside IxCube 4-10. User then Select the Shell T[1]-Mesh elements to assign the appropriate properties, thickness=50 mm, Deformability: Stiff Deformable, and Material Property: Concrete C28/35, 28MPa for cylinder, 35 MPa for prism.



STEP 5 – DEFINE AND ASSIGN SELFWEIGHT, SNOW, WIND, AND SEISMIC LOADS TO THE 3D MODEL ELEMENTS

After the form-finding process of the tensioned membrane has been completed, the shape of the desired membrane is acceptable, and the concrete shell mesh has been generated and is all together with the shaped membrane, rigid beams, ridge, and tie-down cables, the 3D model is now in equilibrium and ready to be processed for the specified design loads that will be applied to the membrane-concrete shell structure and verify the adequacy of the concrete shell to properly support the design loads within safe and allowable stresses.

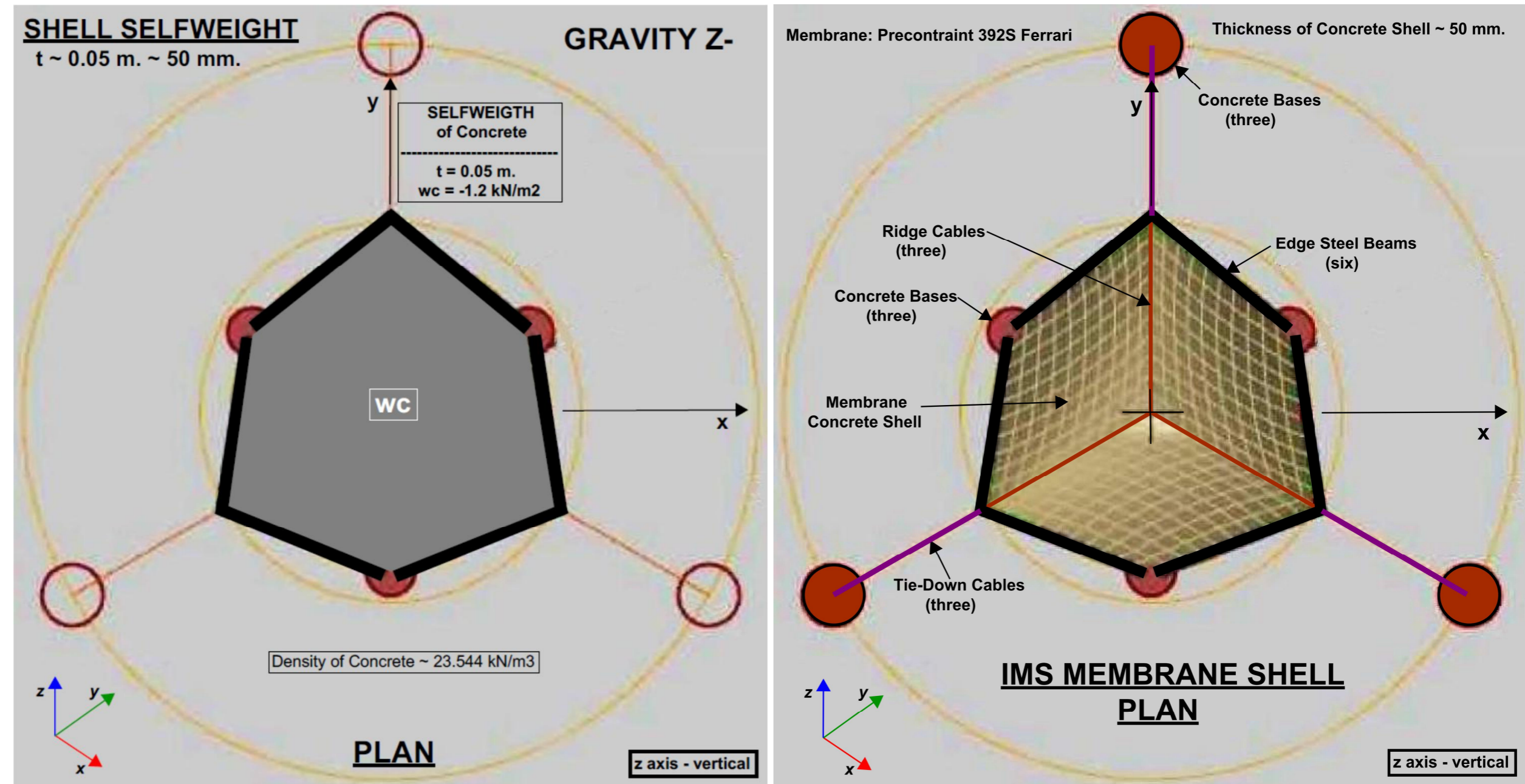


Figure 5.12 – Step 5 – 3D Prototype structure Selfweight Load condition and Membrane Concrete Shell structural components.

PRESTRESS LOAD (PL) – The prestress load effects in the structural components of the membrane-concrete shell prototype structure are mainly due to the internal forces and stresses that are induced in the members from the initial prestressing of the membrane in warp and weft directions and the prestress forces introduced into the tie-down cables during the construction process of the prototype structure. See Figure 5.10.

SELFWEIGHT LOAD (DL) – The selfweight of all the components that form the membrane-concrete shell structure including flexible membrane, edge steel beams, ridge cables, tie-down cables, and concrete shell are considered to be the dead load of the structure. See Figure 5.12. The total selfweight of the concrete shell itself is estimated to be approximately 34.36 kN.

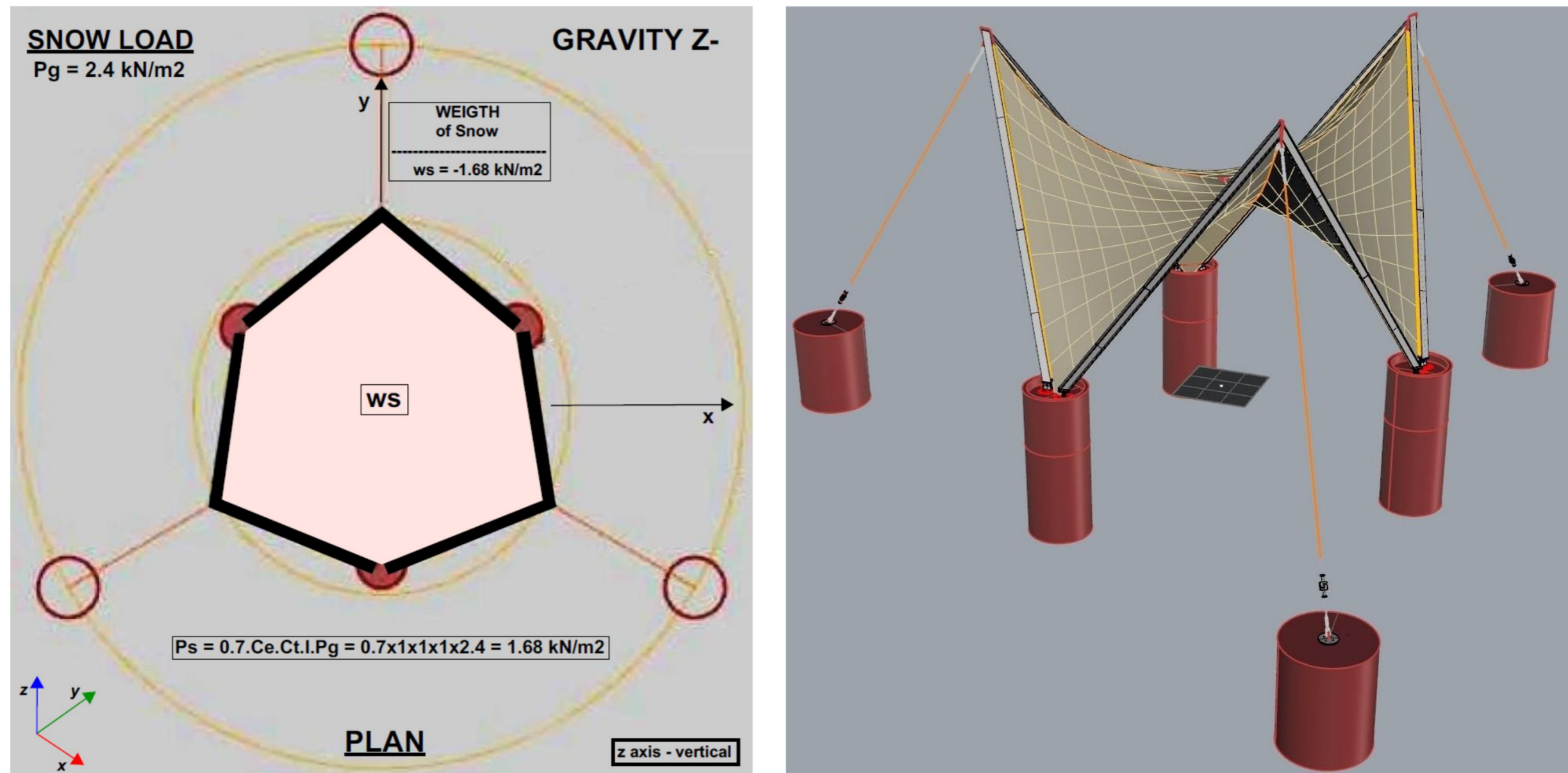


Figure 5.13 – Step 5 – 3D Prototype structure with Snow Load condition and Isometric View of the 3D model.

SNOW LOAD (SL) – The snow load on the top surface of the concrete shell structure is based upon the ground snow load that could fall around the locality where the prototype was built. A relative moderate ground snow load is shown in Figure 5.13 with the corresponding value to be used as a uniformly distributed projected vertical snow load over the entire surface of the shell structure. Total snow load is approximately 49.03 kN.

WIND LOADS ALONG X AND Y AXIS (WLX, WLY) – The wind loads on the structure will be determined based upon a basic horizontal wind pressure produced by moderate winds which will impose a distributed pressure on different sectors of the concrete shell surface.

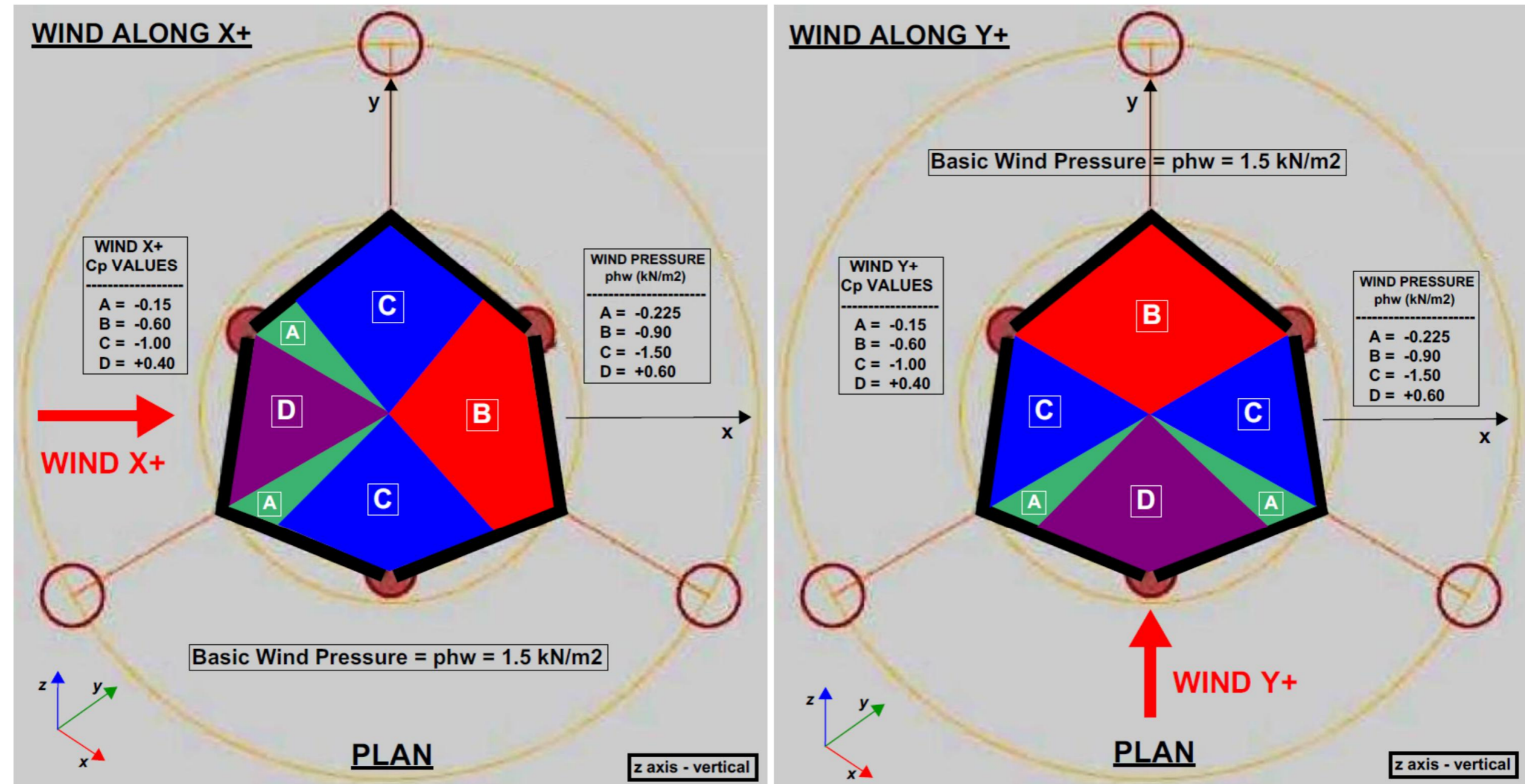


Figure 5.14 – Step 5 – 3D Prototype structure with Wind Loading Condition along X and Y Axis, Cp values for different shell surface regions.

Wind could blow onto the shell structure from any direction, therefore there will be four basic directions which will be considered for the finite element analysis of the shell structure. Figures 5.14 and 5.15 show the wind pressure diagrams for the four directions with the corresponding values of the C_p coefficients of wind pressure depending on the slope of the shell surface facing the direction of the wind. There will be an uplift wind pressure condition that will be considered acting upward along the Z axis as shown in Figure 5.15.

WIND LOADS ALONG V AND Z AXIS (WL_V, WL_Z) -

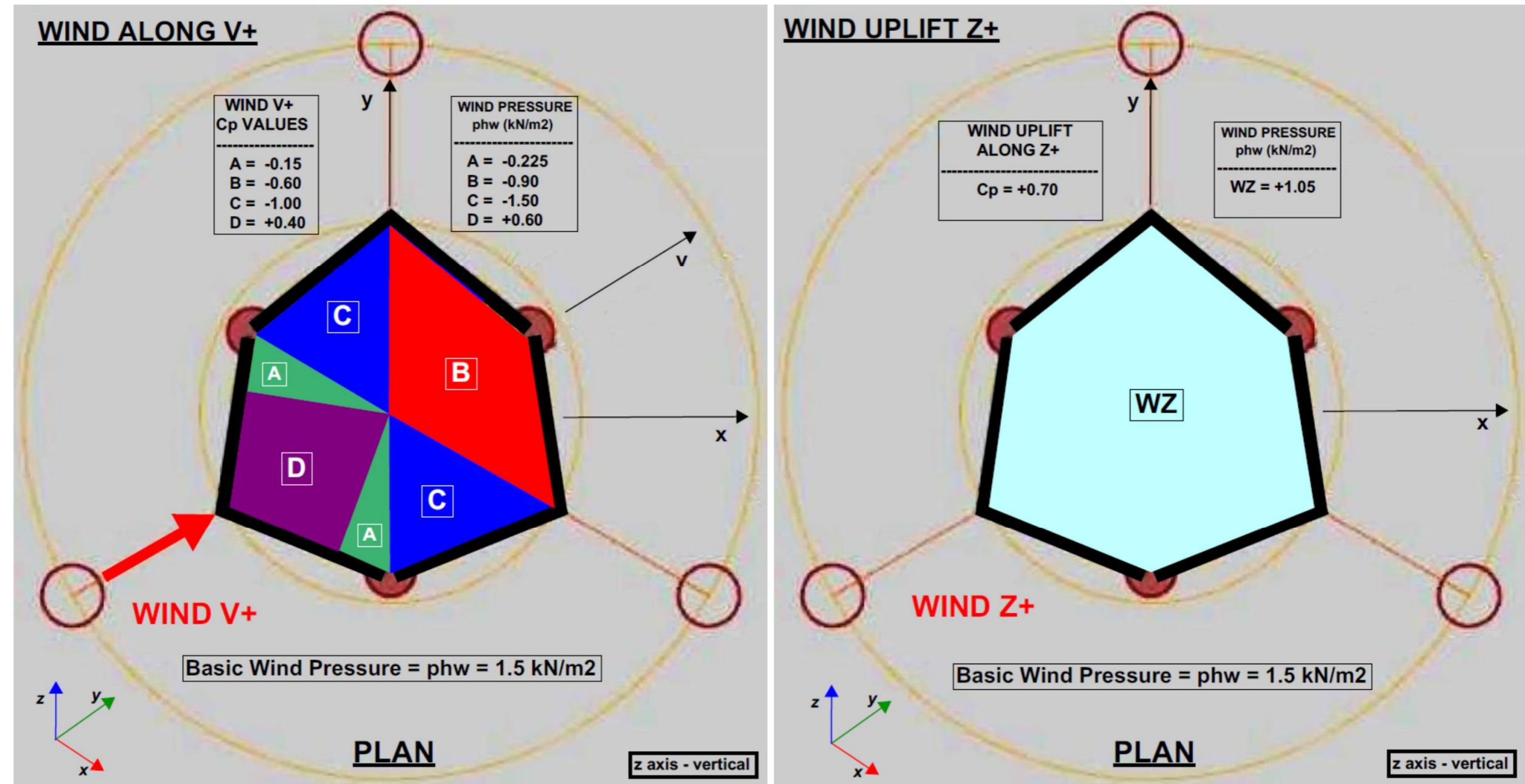


Figure 5.15 – Step 5 – 3D Prototype structure with Wind Loading Condition along V and Z Axis, C_p values for different shell surface regions.

EARTHQUAKE SEISMIC LOADS ALONG X AND Y AXIS (EQX, EQY) – The earthquake seismic loads will be induced into the concrete shell structure when a seismic event occurs near and around the locality of the prototype structure. A moderate earthquake will produce horizontal and vertical forces which are proportional to the selfweight of the structural components of the shell structure. Just like wind forces, seismic forces could also act in any direction and are mainly applied at the center of gravity of the mass of the structural components. See Figures 5.16 and 5.17.

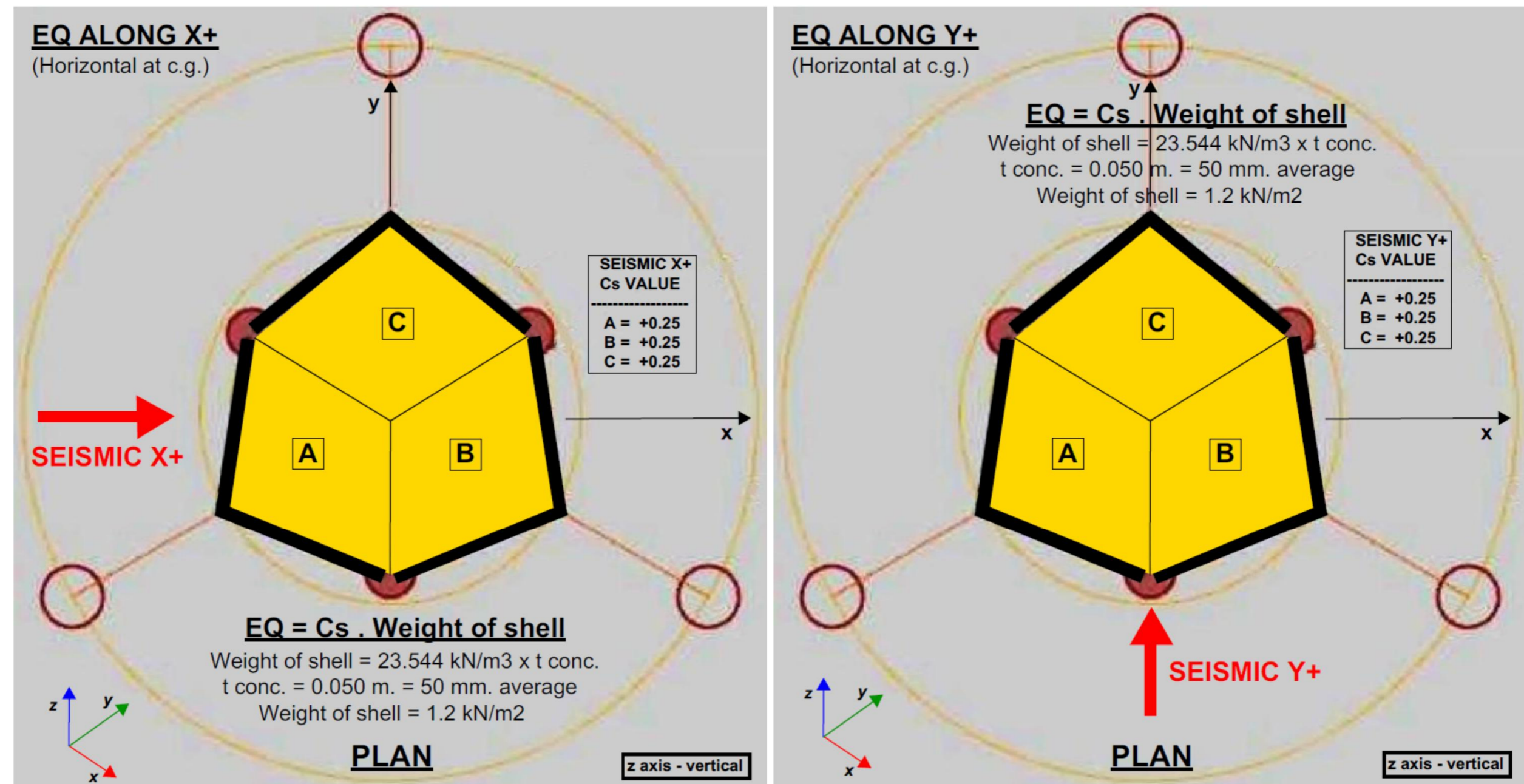


Figure 5.16 – Step 5 – 3D Prototype structure with Seismic Loading Condition along X and Y Axis, Cs values for shell surface regions.

EARTHQUAKE SEISMIC LOADS ALONG V AND Z AXIS (EQV, EQZ) – For the finite element analysis of the membrane-concrete shell prototype structure a horizontal coefficient of 0.25g will be applied to the individual weights of the shell structural components, and a vertical coefficient of 0.025g will be applied at the center of gravity of the components as well. It is important to recognize that together with horizontal forces acting in any direction during seismic events there are also vertical forces that are generated simultaneously. The vertical seismic components will increase the total selfweight of the structure during the earthquake events.

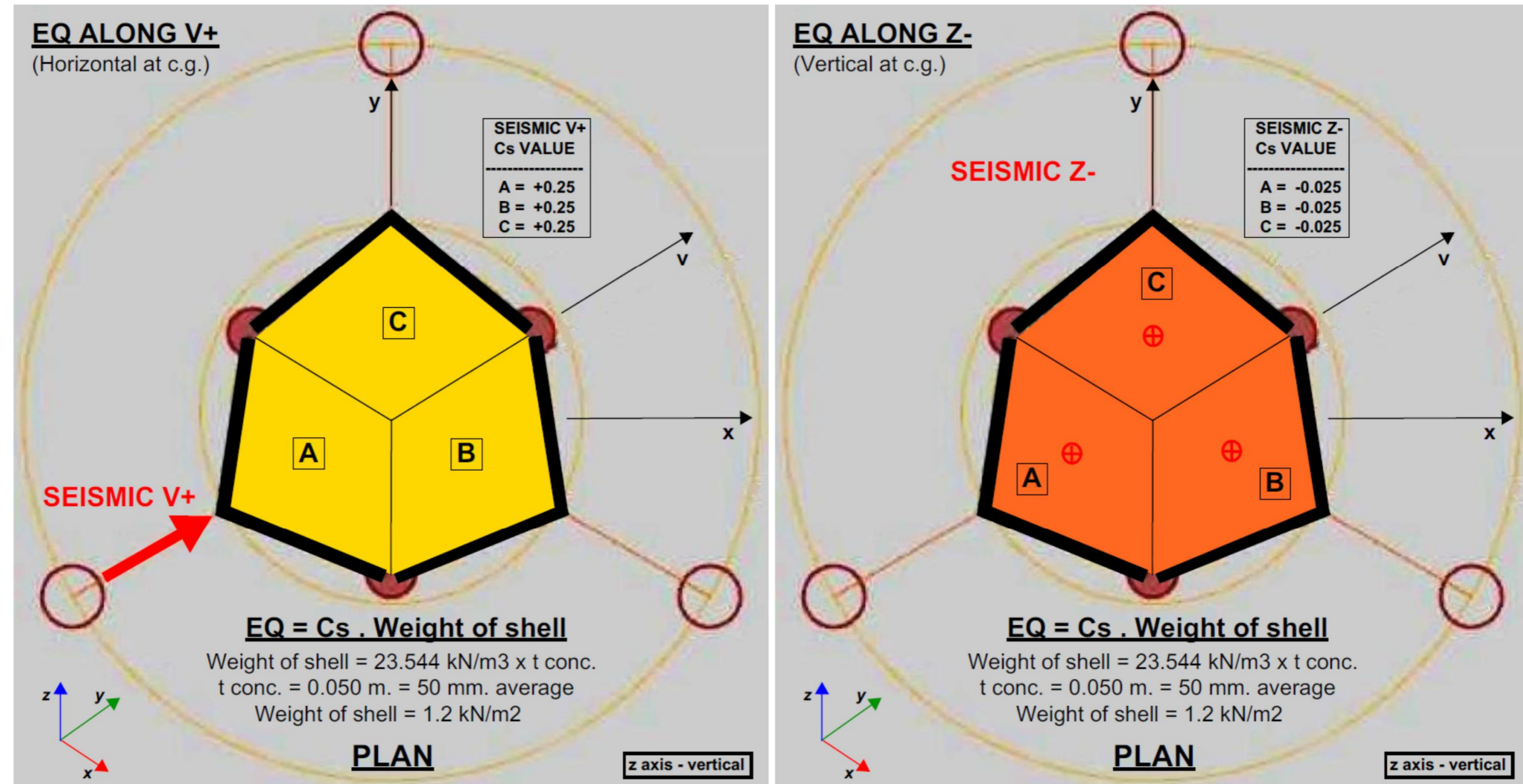


Figure 5.17 – Step 5 – 3D Prototype structure with Seismic Loading Condition along V and Z Axis, Cs values for shell surface regions.

TESTING LOADS (TL) - The Finite Element Analysis of the membrane-concrete shell prototype will also be done for the loading conditions that were performed on the prototype right after the construction of the shell structure was completed and the shotcrete applied on the flexible tensioned membrane has properly cured and hardened. Several loads were applied to the prototype in the form of groups of cement bags each weighting 25 kgs. that were placed over the surface of the hardened shell structure. A complete description of the testing load conditions on the prototype is presented in Chapter 4. Figure 5.18 below shows the graphics of the selfweight load and the evenly distributed load along the ridge cables of the prototype.

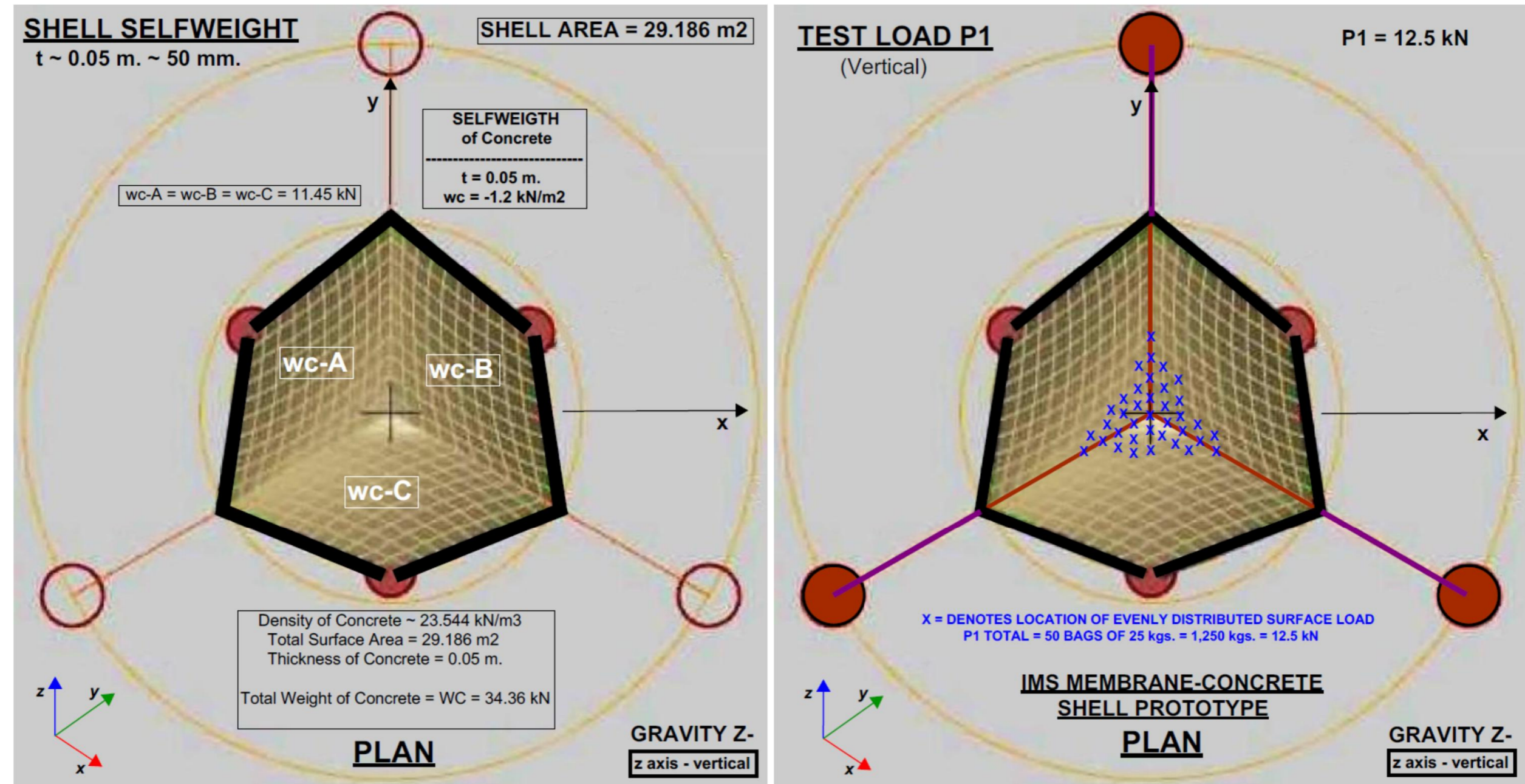


Figure 5.18 – Step 5 – 3D Prototype structure with Selfweight Loading Condition and Evenly Distributed Surface Loads on Shell structure.

The prototype concrete shell structure was tested under several load increments that were applied step by step and under full monitoring of the tie-down cable forces and scanning of the deflected shape of the concrete shell surface under load. The maximum values of the most representative loading conditions will be input into the Finite Element Analysis model to study the behavior of the concrete shell prototype under several loading combinations with its selfweight. Figure 5.19 below shows the unsymmetrical distributed surface load and a concentrated point load on the shell.

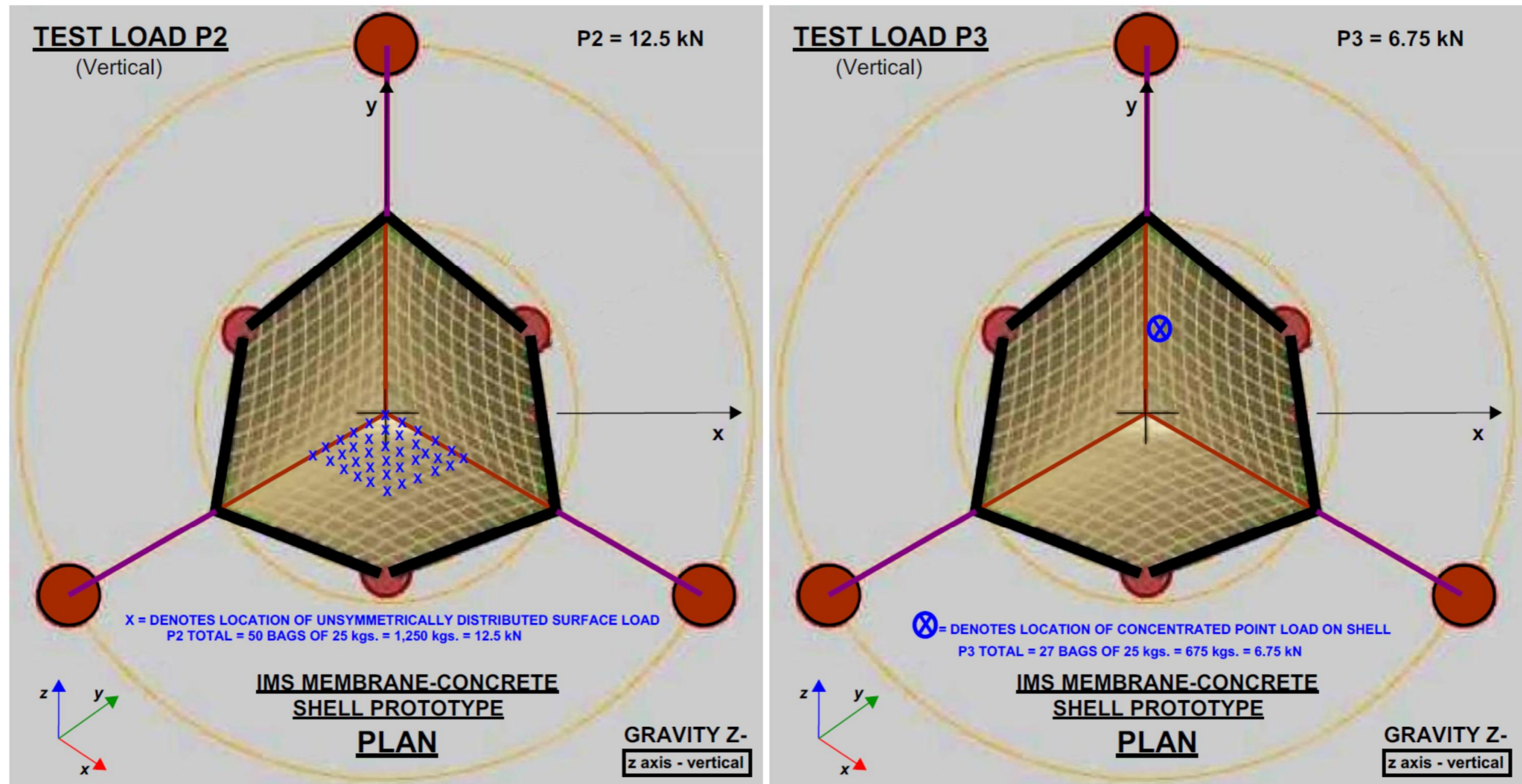


Figure 5.19 – Step 5 – 3D Prototype structure with Unsymmetrical Distributed and Concentrated Point Load on Surface of the Shell structure.



LOADING CONDITIONS AND LOAD COMBINATIONS

The finite element analysis of the IMS prototype experimental structure will be performed for the most commonly and typical load conditions to which the structure will be exposed to during its lifetime, including those loads from the selfweight of all the materials and components and the most commonly environmental loads such as snow, wind, and earthquake. The prototype structure will also be analyzed for those experimental testing load conditions that were applied to the prototype right after the construction has been completed and the shotcrete of the shell had been allowed to cure completely. The total surface area of the membrane-concrete shell structure is estimated to be approximately 29.186 m².

The prototype experimental structure was built with a flexible PVC fabric which has been pretensioned in the warp and weft directions with an initial prestressing force induced into the membrane by prestressing a set three of tie-down cables and three ridge cables connected to a set of six edge rigid wide flange steel beams which are supported on reinforced concrete bases at the ground level providing support for the overall prototype structure. The edges of the flexible PVC membrane are clamped along and to the edges of the six steel beams around the whole perimeter of the structure. This initial state of pretensioning condition constitutes the Prestress Load Condition PL which is one of the main initial load conditions of the prototype structure. At this initial stage the prototype in static equilibrium is subjected to the combined Dead Load DL and Prestress Load PL.

The Basic Load Conditions for the Finite Element Analysis of the membrane-concrete shell prototype structure are presented graphically in Figures 5.10 to 5.19 where the numerical figures of the values of each corresponding load are provided, the basic load conditions are listed below:

1. DL = Dead Load or Selfweight of ALL the structural components.
2. PL = Prestress Load in the membrane, cables, and other structural members.
3. SL = Snow Load
4. WL = Wind Load
5. EQ = Earthquake Seismic Load
6. TL = Testing Load

The prestressing of the flexible membrane and the cables creates a state of internal forces in the rigid steel beams, cables, and flexible membrane which need to be taken into account for the next phase of nonlinear analysis of the composite membrane-concrete shell structure under the service load conditions. After the form-finding analysis is completed the results are saved and the prototype structure with all the internal forces and stresses in the elements is analyzed for the specified design service and environmental load conditions and load combinations to determine the maximum stresses in the concrete shell elements, maximum member forces in the steel beam and cable elements, the total displacements of the concrete shell elements and the three high nodes of connection of steel beams to the tie-down cables.



The membrane-concrete shell prototype structure will be analyzed for the most commonly typical sets of load combinations that are reasonable and expected to occur during its life time. The prototype is considered to be a hybrid membrane, concrete, steel, prestressed cable structure. The Basic Load Combinations for the Finite Element Analysis are mainly based on typical and realistic values of combinations as noted below:

- | | |
|-------------------------------|---|
| 1. DL + PL | - Selfweight + Prestress |
| 2. DL + PL + TL1 | - Selfweight + Prestress + Testing Load P1 |
| 3. DL + PL + TL2 | - Selfweight + Prestress + Testing Load P2 |
| 4. DL + PL + TL3 | - Selfweight + Prestress + Testing Load P3 |
| 5. DL + PL + SL | - Selfweight + Prestress + Snow Load |
| 6. DL + PL + WLX(+) | - Selfweight + Prestress + Wind Load Along X(+) axis |
| 7. DL + PL + WLY(+) | - Selfweight + Prestress + Wind Load Along Y(+) axis |
| 8. DL + PL + WLX(+) | - Selfweight + Prestress + Wind Load Along V(+) axis |
| 9. DL + PL + WLZ(+) | - Selfweight + Prestress + Wind Load Along Z(+) axis, Uplift |
| 10. DL + PL + EQX(+) | - Selfweight + Prestress + Seismic Load Along X(+) axis |
| 11. DL + PL + EQY(+) | - Selfweight + Prestress + Seismic Load Along Y(+) axis |
| 12. DL + PL + EQV(+) | - Selfweight + Prestress + Seismic Load Along V(+) axis |
| 13. DL + PL + EQZ(-) | - Selfweight + Prestress + Seismic Load Along Z(-) axis |
| 14. DL + PL + SL + 0.5.WLX(+) | - Selfweight + Prestress + Snow Load + 0.5.Wind Load Along X(+) axis |
| 15. DL + PL + SL + 0.5.WLY(+) | - Selfweight + Prestress + Snow Load + 0.5.Wind Load Along Y(+) axis |
| 16. DL + PL + SL + 0.5.WLV(+) | - Selfweight + Prestress + Snow Load + 0.5.Wind Load Along V(+) axis |
| 17. DL + PL + SL + 0.5.WLZ(-) | - Selfweight + Prestress + Snow Load + 0.5.Wind Load Along Z(-) axis |
| 18. DL + PL + 0.5.SL + WLX(+) | - Selfweight + Prestress + 0.5.Snow Load + Wind Load Along X(+) axis |
| 19. DL + PL + 0.5.SL + WLY(+) | - Selfweight + Prestress + 0.5.Snow Load + Wind Load Along Y(+) axis |
| 20. DL + PL + 0.5.SL + WLX(+) | - Selfweight + Prestress + 0.5.Snow Load + Wind Load Along V(+) axis |
| 21. DL + PL + 0.5.SL + WLZ(-) | - Selfweight + Prestress + 0.5.Snow Load + Wind Load Along Z(-) axis |
| 22. DL + PL + SL + 0.5.EQX(+) | - Selfweight + Prestress + Snow Load + 0.5.Seismic Load Along X(+) axis |
| 23. DL + PL + SL + 0.5.EQY(+) | - Selfweight + Prestress + Snow Load + 0.5.Seismic Load Along Y(+) axis |
| 24. DL + PL + SL + 0.5.EQV(+) | - Selfweight + Prestress + Snow Load + 0.5.Seismic Load Along V(+) axis |
| 25. DL + PL + SL + 0.5.EQZ(-) | - Selfweight + Prestress + Snow Load + 0.5.Seismic Load Along Z(-) axis |
| 26. DL + PL + 0.5.SL + EQX(+) | - Selfweight + Prestress + 0.5.Snow Load + Seismic Load Along X(+) axis |
| 27. DL + PL + 0.5.SL + EQY(+) | - Selfweight + Prestress + 0.5.Snow Load + Seismic Load Along Y(+) axis |
| 28. DL + PL + 0.5.SL + EQV(+) | - Selfweight + Prestress + 0.5.Snow Load + Seismic Load Along V(+) axis |
| 29. DL + PL + 0.5.SL + EQZ(-) | - Selfweight + Prestress + 0.5.Snow Load + Seismic Load Along Z(-) axis |

The Finite Element Analysis of the prototype for the listed load combinations noted above will be carried out inside IxCube 4-10 software.



STEP 6 – FINITE ELEMENT ANALYSIS OF MEMBRANE-CONCRETE SHELL PROTOTYPE

The finite element analysis of the membrane-concrete shell prototype is performed for the basic load conditions and load combinations listed in the previous Step 5 section using the IxCube 4-10 software. The Author of this Thesis have included in the list of load cases, three basic experimental testing loads that were done some time after the prototype concrete-shell structure has been completed and allowed to cure. The maximum loading cases of cement bags that were placed on the top surface of the concrete shell were selected to the finite element analysis and the intermediate loading increments are considered to be of less effect on the maximum effects that will be produced from the maximum load of the stacked cement bags.

The basic environmental load cases of snow, wind, and seismic have been selected and their values defined for some hypothetical locations where these effects are not either very low or very high, but are relatively of moderate magnitude to have a realistic case for academic analysis and design procedure. The values defined to be input for the finite element analysis are not specifically tied to an American or European Standard, but do represent some realistic values of moderate magnitude of snow, wind, and seismic effects. Some simplifications have been made to define the input values of wind and seismic loads due to the limitations of clear and specific guidelines for the case of this new type of hybrid tensioned membrane-concrete shell structure that could be found in the codes and current literature.

The seismic loads have been defined following the Equivalent Lateral Force Procedure analysis method specified in the ASCE 7-10, Chapter 12, “Seismic Design Requirements for Building Structures”, where the seismic horizontal force in any direction is determined in accordance with the equation: $EQ = C_s \cdot W$, where: EQ is the equivalent horizontal seismic force applied at the center of gravity of the structural components, C_s is the seismic response coefficient factor, and W is the effective seismic weight. The C_s value is a function of the design spectral response acceleration parameter in the short period range of the structure (S_d), the seismic Response Modification Factor of the structure (R), and the seismic importance factor of the structural element (I_e).

It is important to note here that any other seismic analysis and design procedure that has been established and recognized by a legal Building Code of any other country or community can also be used to determine the applicable horizontal and vertical seismic forces that are to be applied to a given structure under evaluation and study of forces and stresses. The finite element analysis performed in this Thesis work is not specifically tied to any single American or European building code and Materials Design Standards but rather based on the basic principles of commonly accepted mechanical behavior of materials and typical responses of structures under normal loading conditions of snow, wind, and seismic effects. The load combinations used for the finite element analysis have also been established based for normal and reasonable service loading conditions.



The membrane-concrete shell prototype structure is mainly a hybrid prestressed composite structure which is built in phases and remains with an internal state of prestressing forces and stresses which are carried internally the entire life time of the structure until the tie-down cables are removed or the structure is altered in one way or another. If any of the tie-down cables is removed or losses part of the initial prestress axial force induced during the construction phase, then the forces in ALL the components of the prototype structure are redistributed and the high point nodes will have changes in the displacements in 3D space.

The scope of the finite element analysis for this Thesis work is limited only to the study of the as-built membrane-concrete shell prototype under the normal service loading conditions listed above in Step 5. Other extreme service conditions of the prototype due to removal of one, two, or the three tie-down cables is outside the scope of this Thesis work, but can certainly be evaluated as another special extreme loading condition which can then be processed using the IxCube 4-10 software or any other general purpose finite element analysis software.

The results of the maximum membrane stresses in the concrete shell elements, maximum axial forces and bending moments in the steel beams, and the maximum axial forces in the tie-down and ridge cables are presented in the graphics shown in Figures 5.## to 5.##.

STEP 7 – TABULATED RESULTS OF CONCRETE SHELL, STEEL BEAMS, AND STEEL CABLES UNDER LOADING CONDITIONS

After the finite element analysis for the different load conditions and load combinations listed in Step 5 is completed using the nonlinear analysis of IxCube 4-10 software, then the results of membrane stresses of the concrete shell elements (axial tension, axial compression, shear, and bending moment), forces and bending moments of edge steel beams, and axial forces in the tie-down and ridge cables are examined and tabulated to determine the maximum forces and stresses in the concrete, steel beams, and cables. The maximum forces and stresses in the prototype components listed above are then compared to the allowable forces and stresses of the different material to determine their adequacy to safely support the design loads and maintain the overall structure within the allowable and tolerable limits of lateral and vertical displacements of the structure.

The finite element analysis was performed for the membrane-concrete shell prototype having a uniform thickness of 50 mm. throughout the entire surface of the shell and with the three high points at the ends of the steel edge beams tied-down with cables to a fixed point at the ground level. The maximum results are tabulated for the concrete shell, steel beams, and cables. Then the three tie-down cables were removed and the three high points were allowed to have free displacements without the tie-down cables. The maximum results are shown below in tabulated form. To study the influence of the thickness of the concrete shell another analysis was done with a reduced thickness of just 10 mm.



MEMBRANE-CONCRETE SHELL PROTOTYPE - SUMMARY OF RESULTS FROM FINITE ELEMENT ANALYSIS

t = 50 mm. = 0.05 m.

LOAD CASE COMB. #	MEMBRANE CONCRETE SHELL				STEEL BEAMS			Cables-TD	Cables-RDG	REACT. TD	REACT. BMS
	Max. Tension (+) (kN/m ²)	Max. Compression(-) (kN/m ²)	Max. Bending (kN-m/m)	Max. Shear (kN/m ²)	Max. Axial (kN)	Max. Bending (kN-m)	Max. Shear (kN)	Max. Axial (kN)	Max. Axial (kN)	Max. Axial (kN)	Max. Axial (kN)
1	16.604	-9.742	0.063	+/- 12.19	-6.054	0.085	+/- 0.409	3.113	2.099	3.103	16.221
2	16.384	-9.698	0.062	+/- 12.085	-12.796	0.161	+/- 0.775	3.083	2.104	3.073	34.441
3	16.391	-9.724	0.062	+/- 12.11	-13.338	0.166	+/- 0.796	3.082	2.104	3.072	35.876
4	16.574	-9.728	0.062	+/- 12.13	-8.386	0.11	+/- 0.535	3.108	2.1	3.098	22.006
5	16.711	-10.952	0.063	+/- 12.22	-14.992	0.199	+/- 0.957	3.064	2.1	3.054	40.546
6	16.575	-9.729	0.063	+/- 11.984	-4.813	0.112	+/- 0.529	3.133	2.098	3.123	12.183
7	16.395	-9.783	0.061	+/- 11.928	-5.077	0.099	+/- 0.48	3.132	2.099	3.122	12.149
8	16.789	-9.78	0.064	+/- 11.979	-5.132	0.086	+/- 0.369	3.136	2.098	3.125	13.117
9	16.164	-9.706	0.061	+/- 11.986	-3.321	0.084	+/- 0.289	3.132	2.099	3.122	8.751
10	17.618	-11.372	0.063	-25.229	-8.781	0.19	+/- 0.888	3.143	2.097	3.133	21.832
11	16.381	-13.856	0.062	-25.967	-8.388	0.206	+/- 0.966	3.134	2.098	3.124	22.552
12	19.771	-9.814	0.062	-19.723	-8.707	0.173	+/- 0.808	3.124	2.097	3.114	20.904
13	16.598	-9.739	0.063	+/- 12.186	-6.274	0.087	+/- 0.422	3.112	2.099	3.102	16.815
14	16.697	-10.652	0.064	18.226	-14.365	0.213	-1.017	3.069	2.10	3.057	38.386
15	16.607	-9.829	0.062	21.067	-14.497	0.207	+/- 0.992	3.073	2.10	3.04	38.416
16	16.804	-10.54	0.064	20.286	-14.531	0.196	+/- 0.939	3.075	2.10	3.065	38.977
17	16.491	-9.843	0.063	19.125	-13.626	0.178	+/- 0.855	3.073	2.10	3.067	36.814
18	16.629	-9.75	0.064	-17.261	-9.28	0.17	+/- 0.883	3.109	2.099	3.099	24.216
19	16.448	-9.804	0.061	14.772	-9.546	0.157	+/- 0.754	3.107	2.098	3.097	24.205
20	16.842	-9.801	0.064	-13.585	-9.601	0.136	+/- 0.645	3.111	2.099	3.101	25.263
21	16.218	-9.727	0.061	+/- 12.001	-7.791	0.099	+/- 0.479	3.107	2.099	3.097	20.917
22	16.803	-12.329	0.064	-25.14	-16.355	0.252	+/- 1.196	3.079	2.099	3.069	43.151
23	16.60	-11.485	0.063	-22.728	-16.153	0.26	+/- 1.236	3.067	2.099	3.057	43.492
24	16.695	-12.312	0.063	-20.768	-16.312	0.244	+/- 1.157	3.069	2.099	3.058	42.652
25	16.708	-11.022	0.063	21.113	-15.102	0.201	+/- 0.964	3.064	2.10	3.053	40.844
26	19.043	-11.668	0.063	-30.276	-13.25	0.248	+/- 1.162	3.119	2.097	3.108	33.815
27	16.435	-14.181	0.062	-29.978	-12.855	0.264	+/- 1.24	3.109	2.10	3.099	34.544
28	21.196	-10.819	0.063	-23.734	-13.174	0.231	+/- 1.082	3.099	2.097	3.089	32.87
29	16.651	-9.76	0.063	14.867	-10.743	0.144	+/- 0.697	3.088	2.10	3.063	28.977
ENVELOPE LOAD #	21.196 28	-14.181 27	0.064 8	-30.276 26	-16.355 22	0.264 27	+/- 1.24 27	3.143 10	2.1 27	3.133 10	43.492 23

Figure 5.20 – Membrane-Concrete Shell Prototype – Summary of Results from Finite Element Analysis – t = 50 mm. – High Points Tied Down.



MEMBRANE-CONCRETE SHELL PROTOTYPE - SUMMARY OF RESULTS FROM FINITE ELEMENT ANALYSIS

t = 10 mm. = 0.01 m.

LOAD CASE COMB. #	MEMBRANE	CONCRETE	SHELL		STEEL BEAMS			Cables-TD	Cables-RDG	REACT. TD	REACT. BMS
	Max. Tension (+) (kN/m ²)	Max. Compression(-) (kN/m ²)	Max. Bending (kN-m/m)	Max. Shear (kN/m ²)	Max. Axial (kN)	Max. Bending (kN-m)	Max. Shear (kN)	Max. Axial (kN)	Max. Axial (kN)	Max. Axial (kN)	Max. Axial (kN)
1	17.772	-9.708	0.005	+/- 12.904	-3.606	0.173	+/- 0.468	3.012	2.121	3.002	6.468
2	16.647	-9.641	0.004	+/- 12.837	-13.333	0.168	+/- 0.579	2.963	2.165	2.953	24.816
3	16.62	-9.671	0.004	20.87	-14.586	0.169	+/- 0.613	2.961	2.168	2.950	27.151
4	17.611	-9.715	0.005	+/- 27.323	-7.468	0.17	+/- 0.461	3.010	2.127	2.999	12.748
5	17.003	-9.831	0.005	+/- 17.759	-16.487	0.195	+/- 0.838	2.911	2.153	2.900	30.903
6	17.828	-9.418	0.008	+/- 13.201	-2.329	0.173	+/- 0.581	3.114	2.11	3.104	-3.374
7	17.64	-9.982	0.006	+/- 12.512	-2.809	0.174	+/- 0.548	3.071	2.118	3.061	-3.238
8	18.041	-9.659	0.007	+/- 13.013	-2.53	0.172	+/- 0.483	3.085	2.109	3.075	-3.848
9	17.39	-9.582	0.005	+/- 12.639	-2.187	0.17	+/- 0.468	3.059	2.110	3.049	-1.027
10	18.011	-12.987	0.007	-15.718	-8.338	0.284	+/- 1.133	3.131	2.097	3.127	12.756
11	17.235	-10.498	0.008	-15.169	-7.241	0.313	+/- 1.255	3.136	2.107	3.126	13.406
12	18.799	-9.635	0.007	-16.166	-8.468	0.250	+/- 0.995	3.097	2.095	3.086	12.008
13	17.739	-9.704	0.005	+/- 12.889	-3.92	0.172	+/- 0.467	3.010	2.122	3.000	7.058
14	17.031	-9.686	0.005	+/- 12.907	-15.811	0.246	+/- 1.026	2.954	2.148	2.944	28.939
15	16.937	-9.969	0.006	+/- 12.562	-15.972	0.22	+/- 0.935	2.940	2.152	2.930	28.712
16	17.138	-9.806	0.005	+/- 12.813	-15.949	0.206	+/- 0.865	2.947	2.148	2.937	29.550
17	16.812	-9.768	0.005	+/- 12.626	-14.525	0.167	+/- 0.700	2.934	2.148	2.924	27.168
18	17.444	-9.479	0.007	+/- 13.128	-8.693	0.224	+/- 0.898	3.063	2.126	3.052	14.898
19	17.256	-10.044	0.006	+/- 12.439	-9.055	0.175	+/- 0.723	3.020	2.134	3.010	14.473
20	17.657	-9.72	0.006	+/- 12.941	-8.97	0.170	+/- 0.576	3.034	2.126	3.024	15.995
21	17.005	-9.644	0.005	+/- 12.567	-6.123	0.168	+/- 0.449	3.008	2.126	2.998	11.207
22	17.122	-9.929	0.008	+/- 13.051	-18.847	0.311	+/- 1.299	2.97	2.142	2.960	33.765
23	16.735	-9.551	0.006	+/- 12.823	-18.305	0.326	+/- 1.363	2.965	2.147	2.955	34.178
24	16.893	-9.701	0.008	+/- 13.013	-18.918	0.295	+/- 1.233	2.946	2.140	2.935	33.285
25	16.986	-9.829	0.005	+/- 12.751	-16.644	0.197	+/- 0.845	2.909	2.154	2.899	31.201
26	17.626	-11.86	0.010	-15.116	-14.780	0.356	+/- 1.450	3.080	2.114	3.070	24.648
27	16.850	-10.564	0.007	-16.67	-13.682	0.385	+/- 1.572	3.085	2.124	3.075	25.410
28	19.925	-10.181	0.009	-14.835	-14.909	0.322	+/- 1.312	3.045	2.111	3.035	23.757
29	17.354	-9.765	0.005	+/- 12.816	-10.361	0.17	+/- 0.536	2.959	2.138	2.949	19.274
ENVELOPE LOAD #	19.925 28	-12.987 10	0.010 26	+/- 27.323 4	-18.847 22	0.385 27	+/- 1.572 27	3.131 10	2.168 3	3.127 10	34.178 23

Figure 5.21 – Membrane-Concrete Shell Prototype – Summary of Results from Finite Element Analysis – t = 10 mm. – High Points Tied Down.



MEMBRANE-CONCRETE SHELL PROTOTYPE - SUMMARY OF RESULTS FROM FINITE ELEMENT ANALYSIS

t = 50 mm. = 0.05 m.

NO TIE-DOWN CABLES

LOAD CASE COMB. #	MEMBRANE	CONCRETE	SHELL		STEEL	BEAMS	Cables-TD	Cables-RDG	REACT. TD	REACT. BMS	
	Max. Tension (+) (kN/m ²)	Max. Compression(-) (kN/m ²)	Max. Bending (kN-m/m)	Max. Shear (kN/m ²)	Max. Axial (kN)	Max. Bending (kN-m)	Max. Shear (kN)	Max. Axial (kN)	Max. Axial (kN)	Max. Axial (kN)	
1	2.704	-4.536	0.009	6.73	-5.068	0.071	+/- 0.346	0	2.092	0	13.532
2	2.763	-5.456	0.009	9.112	-6.675	0.089	+/- 0.434	0	2.093	0	17.873
3	2.804	-3.603	0.009	9.031	-6.911	0.091	+/- 0.444	0	2.094	0	18.481
4	2.651	-5.362	0.009	+/- 13.807	-6.235	0.084	+/- 0.409	0	2.093	0	16.426
5	5.561	-10.255	0.020	19.56	-14.021	0.186	+/- 0.896	0	2.094	0	37.899
6	6.417	-6.919	0.011	-12.504	-3.822	0.099	+/- 0.467	0	2.091	0	9.564
7	0.498	-3.700	0.013	9.68	-4.088	0.086	+/- 0.417	0	2.092	0	9.519
8	6.322	-3.103	0.011	-7.571	-4.145	0.065	+/- 0.309	0	2.091	0	10.438
9	0.283	-2.65	0.006	3.057	-2.329	0.028	+/- 0.141	0	2.091	0	6.048
10	9.97	-5.51	0.011	-14.088	-6.434	0.124	+/- 0.585	0	2.092	0	16.230
11	7.153	-2.849	0.010	-13.962	-6.233	0.132	+/- 0.625	0	2.092	0	16.562
12	11.049	-4.127	0.010	-10.833	-6.392	0.115	+/- 0.546	0	2.091	0	15.733
13	2.739	-2.901	0.009	6.887	-5.178	0.072	+/- 0.353	0	2.092	0	13.830
14	7.418	-6.716	0.019	16.823	-13.39	0.200	+/- 0.956	0	2.093	0	35.731
15	3.119	-7.771	0.014	19.669	-13.525	0.194	+/- 0.931	0	2.093	0	35.766
16	7.37	-7.803	0.020	18.889	-13.56	0.184	+/- 0.877	0	2.093	0	36.328
17	4.351	-7.101	0.019	17.724	-12.652	0.165	+/- 0.793	0	2.093	0	34.159
18	7.846	-3.753	0.017	-16.521	-8.297	0.157	+/- 0.741	0	2.092	0	21.557
19	0.745	-5.342	0.014	13.362	-8.564	0.144	+/- 0.692	0	2.093	0	21.545
20	7.751	-5.526	0.012	-12.625	-8.621	0.123	+/- 0.583	0	2.092	0	22.595
21	1.711	-4.001	0.010	9.472	-6.806	0.086	+/- 0.416	0	2.092	0	18.233
22	9.194	-8.793	0.020	20.708	-14.704	0.213	+/- 1.014	0	2.093	0	39.188
23	7.786	-7.244	0.019	+/- 18.075	-14.596	0.217	+/- 1.035	0	2.093	0	39.328
24	9.734	-8.225	0.019	19.26	-14.675	0.209	+/- 0.995	0	2.093	0	38.906
25	5.579	-7.744	0.020	19.638	-14.076	0.187	+/- 0.899	0	2.094	0	38.048
26	11.399	-7.629	0.013	-19.142	-10.911	0.182	+/- 0.860	0	2.093	0	28.355
27	8.582	-7.931	0.016	-17.979	-10.708	0.190	+/- 0.900	0	2.092	0	28.690
28	12.478	-8.759	0.017	-14.850	-10.866	0.173	+/- 0.821	0	2.092	0	27.85
29	4.168	-7.466	0.011	13.302	-9.654	0.130	+/- 0.628	0	2.093	0	26.012
ENVELOPE LOAD #	12.478 28	-10.255 5	0.020 5	20.708 22	-14.704 22	0.217 23	+/- 1.035 28	0	2.094 3	0	39.328 23

Figure 5.22 – Membrane-Concrete Shell Prototype – Summary of Results from Finite Element Analysis – t = 50 mm. – No Tie Down Cables.



MEMBRANE-CONCRETE SHELL PROTOTYPE - SUMMARY OF RESULTS FROM FINITE ELEMENT ANALYSIS

t = 10 mm. = 0.01 m.

NO TIE-DOWN CABLES

LOAD CASE COMB. #	MEMBRANE	CONCRETE	SHELL		STEEL BEAMS			Cables-TD	Cables-RDG	REACT. TD	REACT. BMS
	Max. Tension (+) (kN/m ²)	Max. Compression(-) (kN/m ²)	Max. Bending (kN-m/m)	Max. Shear (kN/m ²)	Max. Axial (kN)	Max. Bending (kN-m)	Max. Shear (kN)	Max. Axial (kN)	Max. Axial (kN)	Max. Axial (kN)	Max. Axial (kN)
1	1.406	-2.427	0.006	+/- 1.685	-2.216	0.036	+/- 0.136	0	2.074	0	3.855
2	1.245	-2.615	0.005	+/- 2.732	-4.538	0.056	+/- 0.226	0	2.084	0	8.217
3	1.306	-2.624	0.005	+/- 3.574	-5.027	0.059	+/- 0.239	0	2.085	0	9.123
4	1.549	-4.781	0.005	+/- 13.594	-4.152	0.049	+/- 0.198	0	2.077	0	6.995
5	3.67	-3.588	0.005	+/- 4.167	-15.144	0.181	+/- 0.772	0	2.108	0	28.376
6	5.661	-5.952	0.009	-7.770	-1.352	0.138	-0.517	0	2.063	0	-5.262
7	7.511	-5.625	0.007	10.136	-1.69	0.146	+/- 0.619	0	2.071	0	-3.353
8	5.346	-3.412	0.008	-5.964	-1.383	0.109	+/- 0.45	0	2.064	0	-5.145
9	0.165	-3.123	0.005	+/- 1.472	-1.283	0.032	+/- 0.169	0	2.062	0	-3.689
10	8.853	-6.028	0.006	-8.541	-4.608	0.153	0.603	0	2.083	0	6.960
11	6.054	-4.779	0.007	-7.027	-4.065	0.168	+/- 0.663	0	2.068	0	7.282
12	10.021	-5.601	0.007	-8.772	-4.669	0.137	+/- 0.535	0	2.076	0	6.556
13	1.436	-2.437	0.005	+/- 1.692	-2.374	0.038	+/- 0.144	0	2.074	0	4.154
14	5.798	-4.099	0.006	-6.332	-14.476	0.232	-0.963	0	2.103	0	26.417
15	4.195	-3.381	0.006	+/- 6.235	-14.634	0.208	+/- 0.871	0	2.107	0	26.185
16	5.639	-3.648	0.006	-4.476	-14.610	0.192	+/- 0.801	0	2.104	0	27.029
17	2.363	-3.472	0.004	+/- 3.738	-13.172	0.148	+/- 0.635	0	2.102	0	24.621
18	6.793	-6.017	0.009	-9.273	-7.345	0.211	-0.835	0	2.080	0	12.392
19	7.446	-4.494	0.007	8.633	-7.692	0.161	+/- 0.658	0	2.088	0	11.948
20	6.477	-3.810	0.007	-4.631	-7.611	0.131	+/- 0.513	0	2.085	0	13.443
21	0.064	-3.166	0.004	+/- 1.463	-4.735	0.042	+/- 0.179	0	2.079	0	8.594
22	7.392	-4.311	0.006	-5.301	-16.338	0.238	+/- 1.002	0	2.113	0	29.815
23	5.993	-4.206	0.005	-5.961	-16.069	0.247	+/- 1.037	0	2.105	0	30.015
24	7.977	-4.82	0.006	-4.99	-16.371	0.231	+/- 0.972	0	2.109	0	29.554
25	3.685	-3.602	0.004	+/- 4.190	-15.223	0.182	+/- 0.776	0	2.109	0	28.526
26	9.984	-5.135	0.006	-7.689	-11.074	0.225	+/- 0.921	0	2.101	0	19.060
27	7.186	-4.925	0.007	-8.53	-10.529	0.24	+/- 0.984	0	2.085	0	19.452
28	11.152	-6.153	0.005	-7.438	-11.133	0.209	+/- 0.853	0	2.093	0	18.574
29	2.568	-2.894	0.005	+/- 2.395	-8.838	0.11	+/- 0.462	0	2.092	0	16.406
ENVELOPE LOAD #	11.152 28	-6.153 28	0.009 6	10.136 7	-16.338 22	0.24 27	+/- 1.037 23	0	2.109 24	0	30.015 23

Figure 5.23 – Membrane-Concrete Shell Prototype – Summary of Results from Finite Element Analysis – t = 10 mm. – No Tie Down Cables.



A selected number of graphical plots for the Load Case Combinations # 3, 4, 11, 16, 20, 23, and 27 highlighted in yellow in the Table of Figure 5.20 are shown below in Figures 5.24 to 5.30. Mainly the maximum axial compressive, tensile, and shear stresses, maximum bending moment of the concrete shell elements, maximum axial and shear forces, maximum bending moment of the steel edge beams, the maximum axial tensile forces of the ridge and tie-down cables, and the maximum reaction forces at the concrete bases for the selected load combination cases are shown in the figures below.

STEP 8 – GRAPHICAL PLOTS AND INTERPRETATION OF THE FINITE ELEMENT RESULTS

The overall membrane-concrete shell structure under the initial prestressing forces in the flexible membrane and the tie-down cables with the selfweight of the layers of rigid shotcrete shell form a hybrid tensioned structure (due to having the three high points of the structure restrained from displacements by the three tie-down cables) that mainly behaves as a tensile hyper membrane shell structure causing the majority of the shell surface to still remains largely under tensile stresses, very low values of tension but still tension, which is not a desirable condition for any concrete structure.

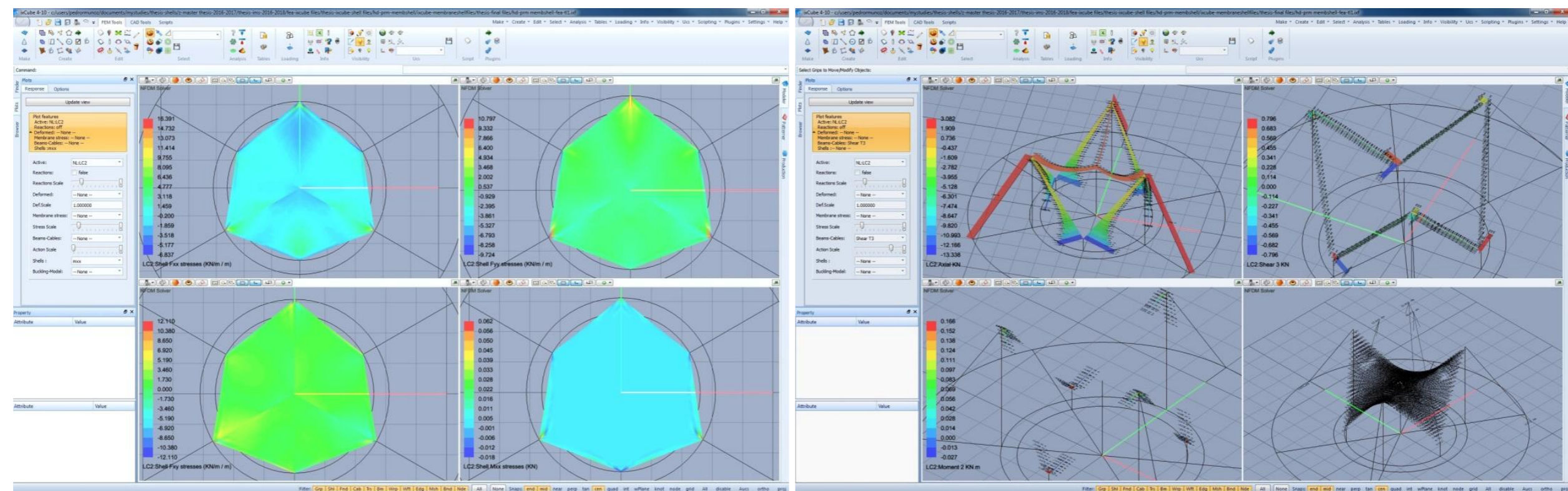


Figure 5.24 – Finite Element Analysis Graphical Results for Testing Load P2 – Load Case Combination #3 – t = 50 mm. – Tie Down Cables.



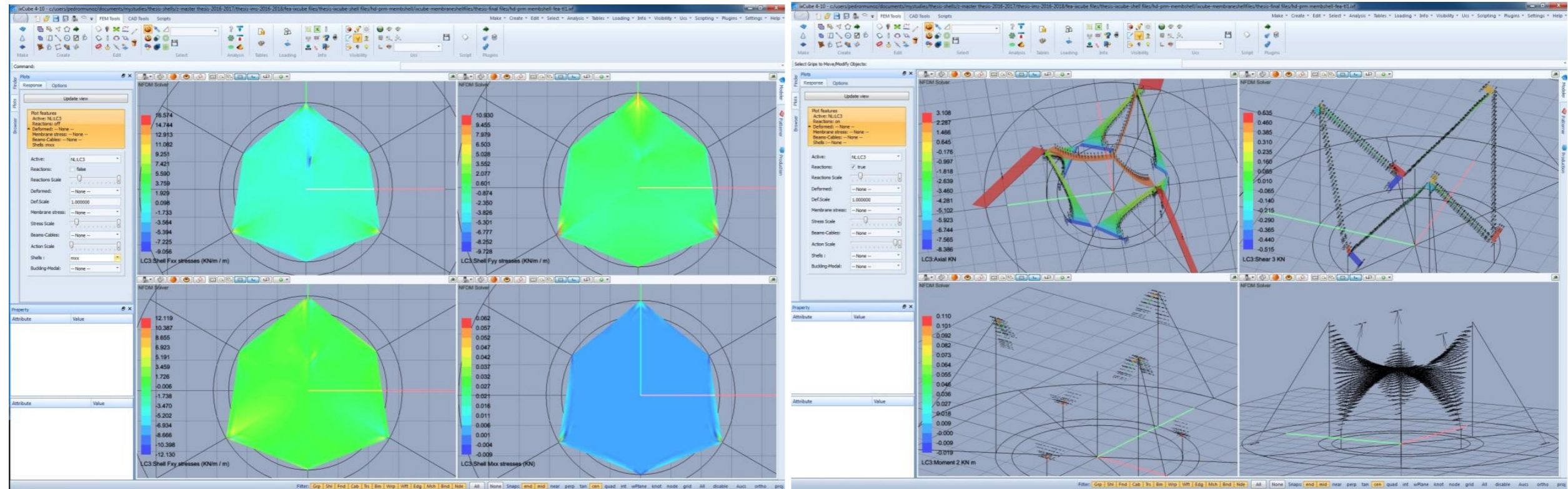


Figure 5.25 – Finite Element Analysis Graphical Results for Testing Load P3 – Load Case Combination #4 – $t = 50$ mm. – Tie Down Cables.

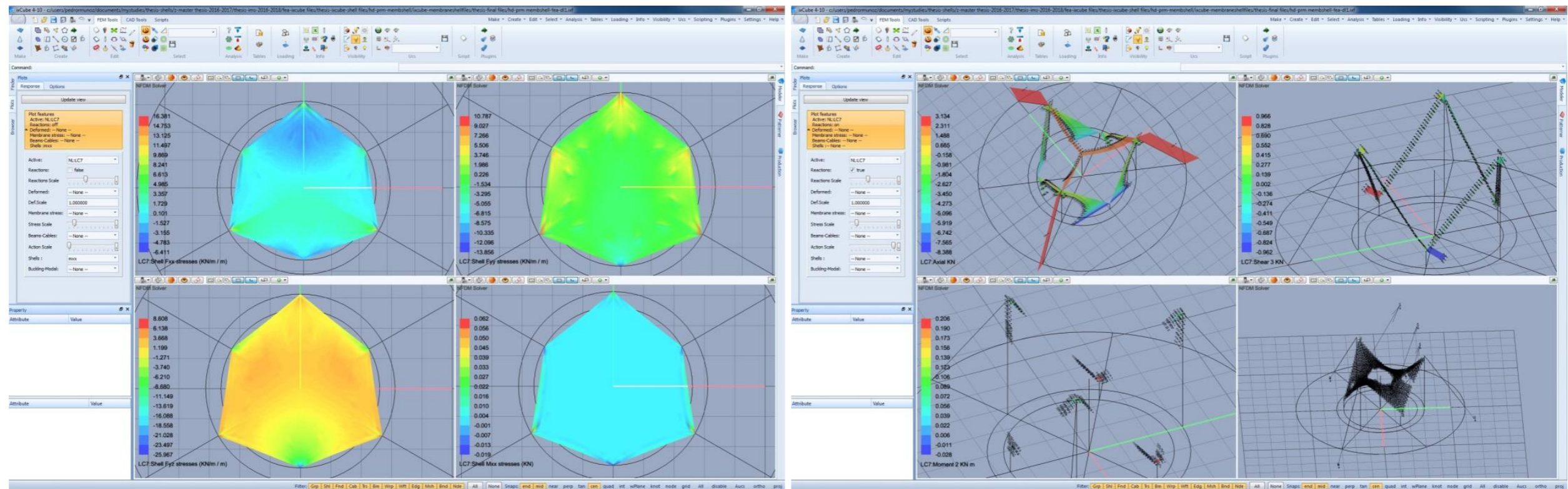


Figure 5.26 – Finite Element Analysis Graphical Results for Seismic Load EQY – Load Case Combination #11 – $t = 50$ mm. – Tie Down Cables.



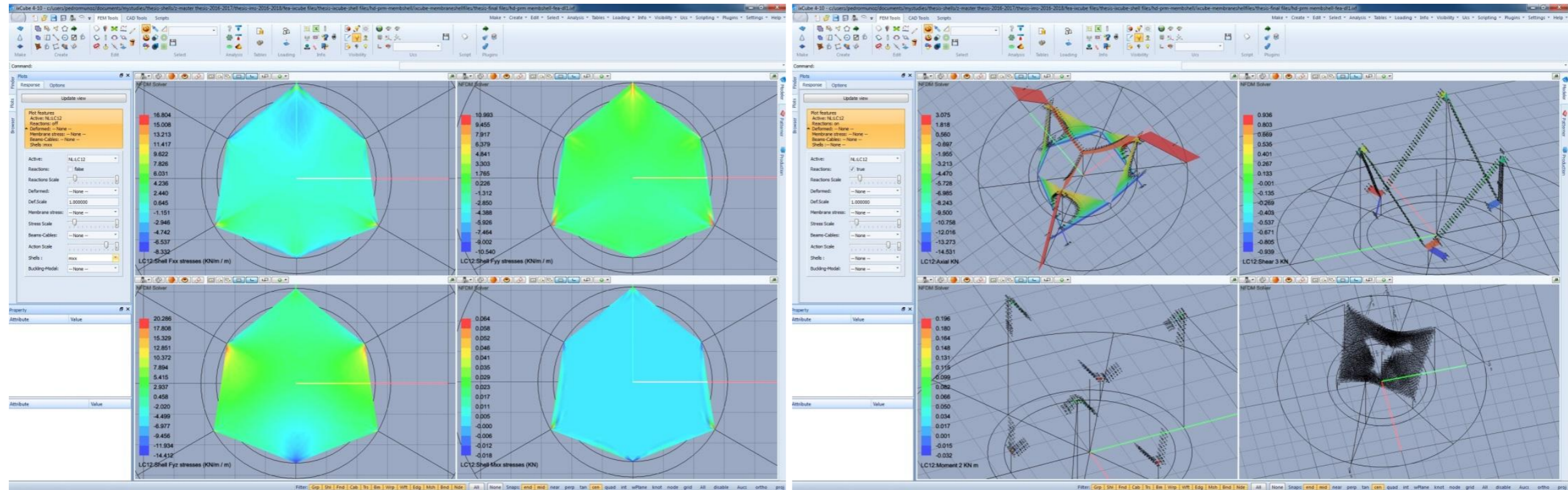


Figure 5.27 – Finite Element Analysis Graphical Results for Snow+1/2 Wind Load V-Load Case Combination #16 – $t = 50$ mm. – Tie Down Cables.

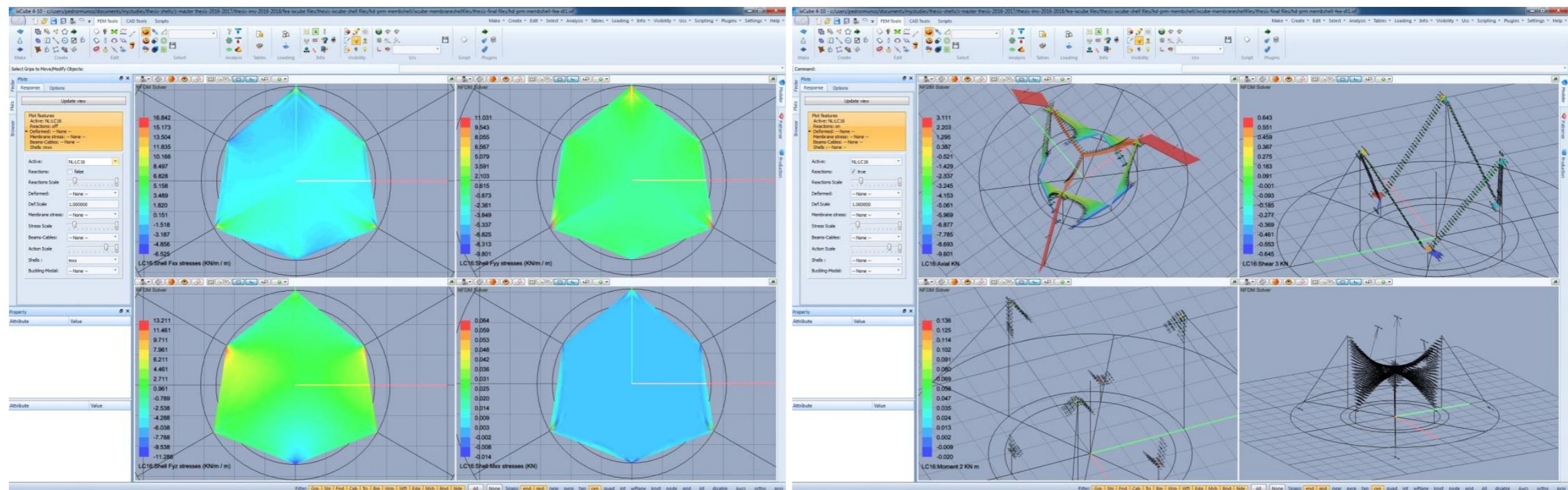


Figure 5.28 – Finite Element Analysis Graphical Results for 1/2Snow+ Wind Load V-Load Case Combination #20 – $t = 50$ mm. – Tie Down Cables.



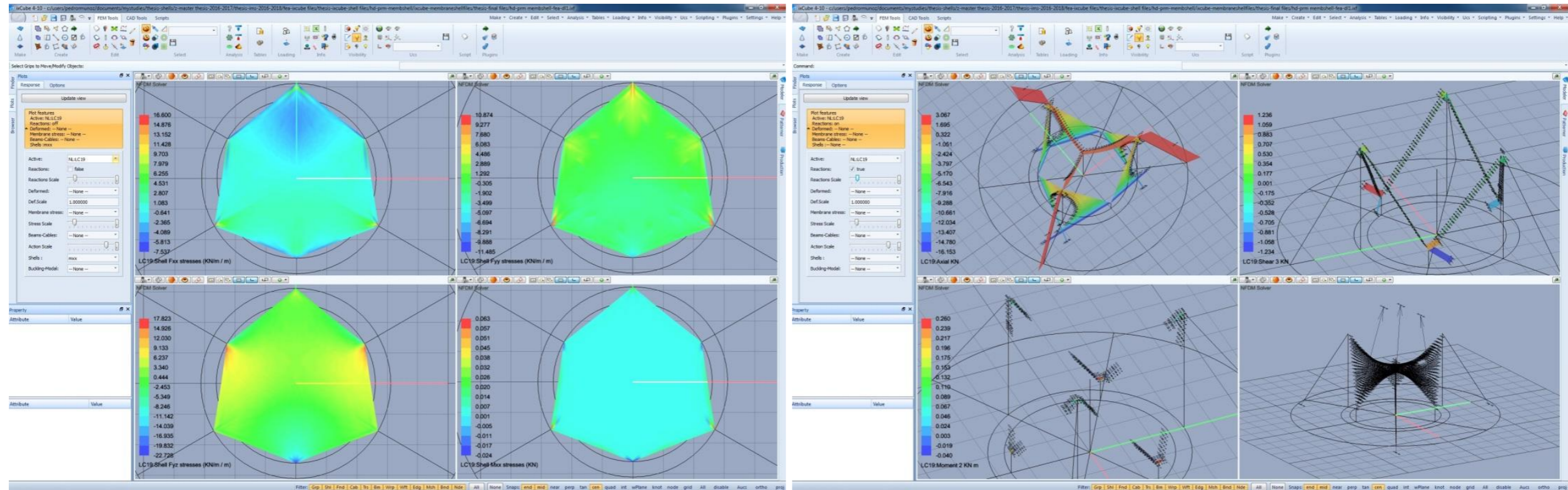


Figure 5.29 – Finite Element Analysis Graphical Results for Snow+ 1/2 Seismic EQY–Load Case Combination #23 – $t = 50$ mm.–Tie Down Cables.

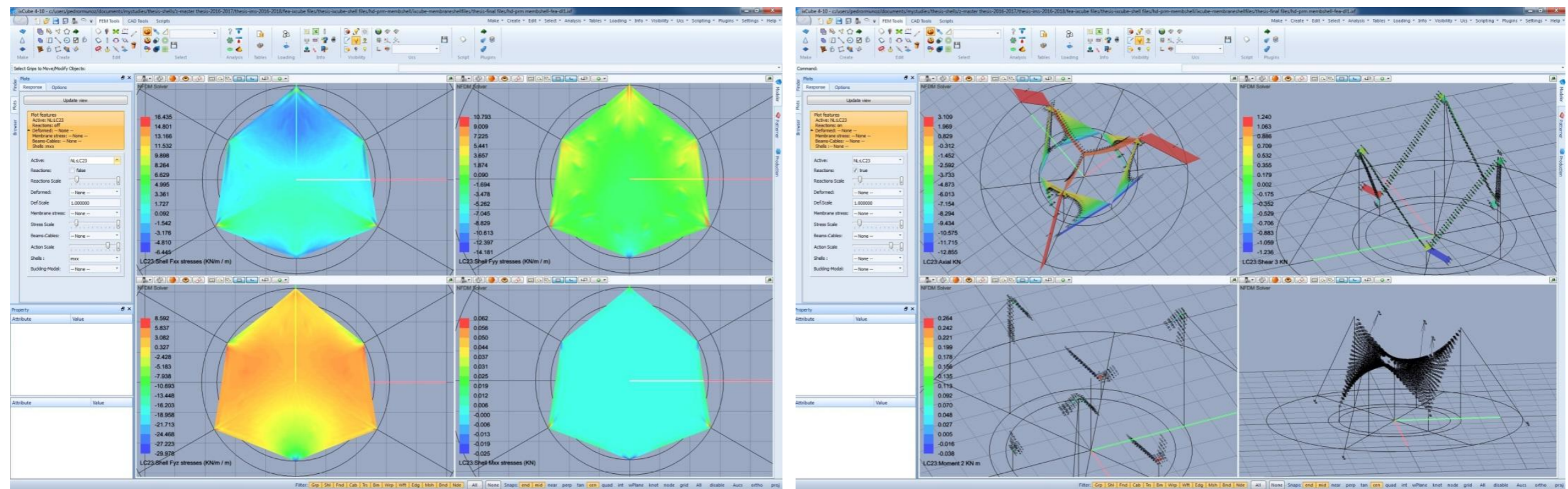


Figure 5.30 – Finite Element Analysis Graphical Results for 1/2 Snow+ Seismic EQY–Load Case Combination #27 – $t = 50$ mm.–Tie Down Cables.



STRUCTURAL ANALYSIS AND DESIGN CHECK OF THE IMS PROTOTYPE MEMBER STRESSES AND INTERNAL FORCES

The next and final step of the finite element analysis of the IMS membrane-concrete shell prototype structure is to verify that the maximum stresses and forces in the concrete shell elements, steel beams, and ridge cables are within the allowable safe stresses for the service loading conditions and load combinations for which the prototype structure has been analyzed. When reading the stresses and member forces from the tabulated values and graphical plots presented in the previous sections the sign convention used indicates that the values given as positive are to be considered as tension and the values given as negative are to be considered to be compression.

The reaction forces at the three points of supports of the edge beams and the three points of support of the tie-down cables indicates that the forces going upward are to be considered compression forces at the top of the concrete bases from the beams and the forces going downward are to be considered tension pullout forces of the tie-down cables at the top of the concrete bases at the ground level. Any forces that come up to be the opposite as it is noted above then are to be considered the opposite way.

The description of the Load Case Combinations listed as # 1 to 29 in Figures 5.20 to 5.24 are given at the end of Step 5, where the selfweight of the membrane-concrete shell with the initial prestress of the flexible membrane serving as formwork for the applied shotcrete is combined with the three different Testing Loads labeled as TL1, TL2, and TL3, with the Snow loads labeled SL, with the Wind along X, Y, Z, and V, and with Earthquake (Seismic) loads along X, Y, Z, and V directions in plan of the prototype. Diagrams of the different load cases noted above are shown in Figures 5.12 to 5.19 of Step 5. A close look of the tabulated values of the finite element analysis shown in Figures 5.20 to 5.23 reveals the following highlights of the maximum element stresses and member forces results, reaction forces, and nodes displacements:

- A. It is clear from the tabulated results that not a single load case or single load case combination produces the maximum stresses and maximum member forces for each one of the elements and members of the prototype in that single load case or load combination, therefore it is very important that the designer of any membrane-concrete shell structure is mindful to consider all the possible external environmental load cases which can take effect at the locality of the shell structure and make provision to analyze the structure for all possible worst case scenarios.
- B. The horizontal (along x, and y axis) and vertical (along z axis) displacements of the three high points where the slopping steel edge beams are connected to the tie-down cables were noted to be very minimal, less than 1 mm. for the cases when the nodes were restrained by the tie-down cables and when the nodes were allowed to have free displacements without tie-down cables. It appears that the membrane-concrete shell structure with and without the tie-down cables is a very stiff and rigid shell structure that redistributes forces around very effectively.



- C. For the 50 mm. membrane-concrete shell structure it appears that the load conditions that produce the maximum element stresses and member forces of the prototype are those that involve the combination of snow with seismic effects. It is very difficult to predict when a locality may have critical environmental conditions where a high magnitude seismic event occurs right in the middle of one of the worst blizzard snow conditions, it could certainly happen, but the probability of occurrence is somewhat less than the maximum combined effects at the same time. Still the shell designers have to be mindful to consider the worst case scenarios that are listed in the Building Codes of the country where the structure will be built.
- D. For the 10 mm. membrane-concrete shell structure it is noted a marked increase in the concrete shell shear stresses and uplift reaction forces at some points of support of the structure under the wind loading conditions. The more we reduce the concrete thickness of a shell structure the more it tends to behave like a tensioned thin membrane fabric structure, where the wind effects control over any other seismic load conditions. If we think of two-way reinforced concrete flat slabs or flat plates we immediately associate them to one of the most critical design conditions which is the shear stresses around the perimeter of the connections of the slab to the supporting beams and columns. Typically some type of special shear reinforcement in the form of shear studs and steel plates are needed to be added to the thin concrete flat plate/slab.
- E. A review of the graphical plots of concrete shell stresses and steel beam member forces and stresses shown in Figures 5.24 to 5.30 for the 50 mm. concrete shell prototype clearly reveals a distribution of stresses with the maximum values occurring at points of the structure with high concentration of stresses at very localized areas, leaving the remaining of the shell under stress values which are much more lower than those occurring at corners of the prototype going from high to low points of supports and at those low points of supports at the ends of the fixed edge beams supporting the prototype. It is important to highlight and recommend here the shell designers that if the distribution of membrane and shear stresses throughout the surface of the shell reveals that portions of the concrete shell will be exposed to stresses that are very low and that can be considered to be negligible then those portions of the concrete shell can be certainly be removed or make much thinner to reduce the overall total weight of the structure and allow for a more uniform distributions of stresses in the shell structure.
- F. At the end a more efficient and lightweight concrete shell structure can be achieved leading into a process of topology optimization and enhancements of the final shell structure with the intention to generate optimized membrane-concrete shell lattice and mixed solid-latticed concrete shell structure which will certainly be lightweight and structurally efficient to handle membrane axial tension and compression and shear stresses. The topology optimization process of the concrete shell structure then will lead into savings in the supporting foundations.



- G. For the edge steel beams the entire perimeter of the membrane-concrete shell elements provide full lateral bracing of the weak axis of the I-beams against global axial buckling and for localized top and bottom buckling of the flanges which are fully restrained by the thickness of the concrete shell. The axial capacity of the steel beams will be mainly controlled by the bending strength of the strong axis of the steel I-beam having both ends restrained for displacements for the K value of approximately 1 for the KL/r slenderness ratio to calculate the allowable stress for axial compression capacity.
- H. The stiffness of the edge steel beams along the six edges of the membrane-concrete shell prototype provides a very efficient system to control the high concentrations of tensile, compression, and shear stresses that will develop along the interface and at the corners of the concrete shell. As the axial compressive forces accumulate along the length of the edge steel beams to connect to the top of the concrete base supports, the steel also provides an efficient way to handle high concentrated stresses in the steel which can be handled by the high tensile strength of the steel beams.
- I. For the tabulated values of the two cases of the membrane-concrete prototype having the three high points free to have displacements and no tie-down cables from the top of the beams to the concrete bases at ground level, it is then noted that the tensile membrane stresses in the concrete shell elements are considerably reduced, making the majority of the concrete shell prototype to go mostly in compression. It clearly appears that once the tie-down cables are released or removed then the membrane-concrete shell prototype behaves mostly as a hyper concrete shell which still have a high stiffness to resist loads due to the doubly curved hyper surface that is created by the configuration of the high and low points of the originally tensioned membrane between the edge beams and ridge cables.

PLAIN AND FIBER REINFORCED CONCRETE MATERIAL PROPERTIES

The stress-strain curves for plain concrete and fiber reinforced concrete samples under axial compressive laboratory testing loads are shown below in Figures 5.31 and 5.32. The maximum values of the axial compressive strength of the concrete samples tested in the laboratory are labeled as the “Ultimate Compressive Strength – f'_c ”. It is noted that there is a marked difference between the plain concrete and the fiber reinforced concrete samples particularly the magnitude of the strain values for given values of axial compressive stress of the concrete samples. The plain concrete samples appear to experience much larger strain values than the fiber reinforced concrete samples for the same level of axial compressive stress, which can be clearly seen in the plots shown below.



For the finite element analysis using IxCube 4-10 the material properties that were input for concrete is C28/35, 28 MPa as the ultimate compressive strength which is equivalent to 28,000 kN/m² or also equivalent to 28 N/mm² (~4,065 psi) .

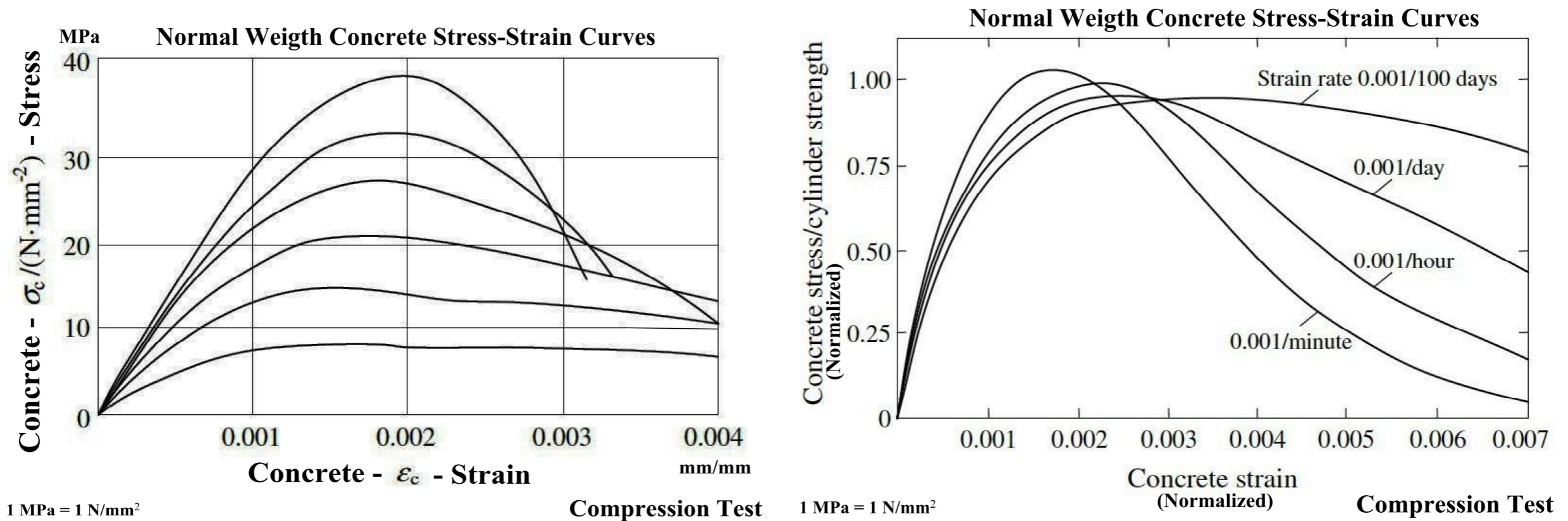


Figure 5.31 – Typical Stress-Strain Curves of Normal Weight Concrete samples under Axial Compressive Test, No Steel Fibers.

The typical stress-strain curves for both plain concrete and fiber reinforced concrete samples clearly shows a well-defined proportional straight line for stress values approximately below half of the ultimate compressive strength, which is an indication that some type of elastic behavior takes place in this range that can be called elastic range. Beyond this point cracking of the concrete under a combination of tensile and shear stresses starts to take place causing the concrete to undergo plastic behavior where the concrete reaches its maximum ultimate compressive stress at its peak point of the curves. Beyond the maximum compressive strength then concrete start to undergo rapid and large strain deformations and start losing strength rapidly until reaches its break point at its maximum strain value when the sample is considered to have failed.

Two typical stress-strain curves for concrete samples with different percentages of fibers volume are shown below in Figure 5.32.

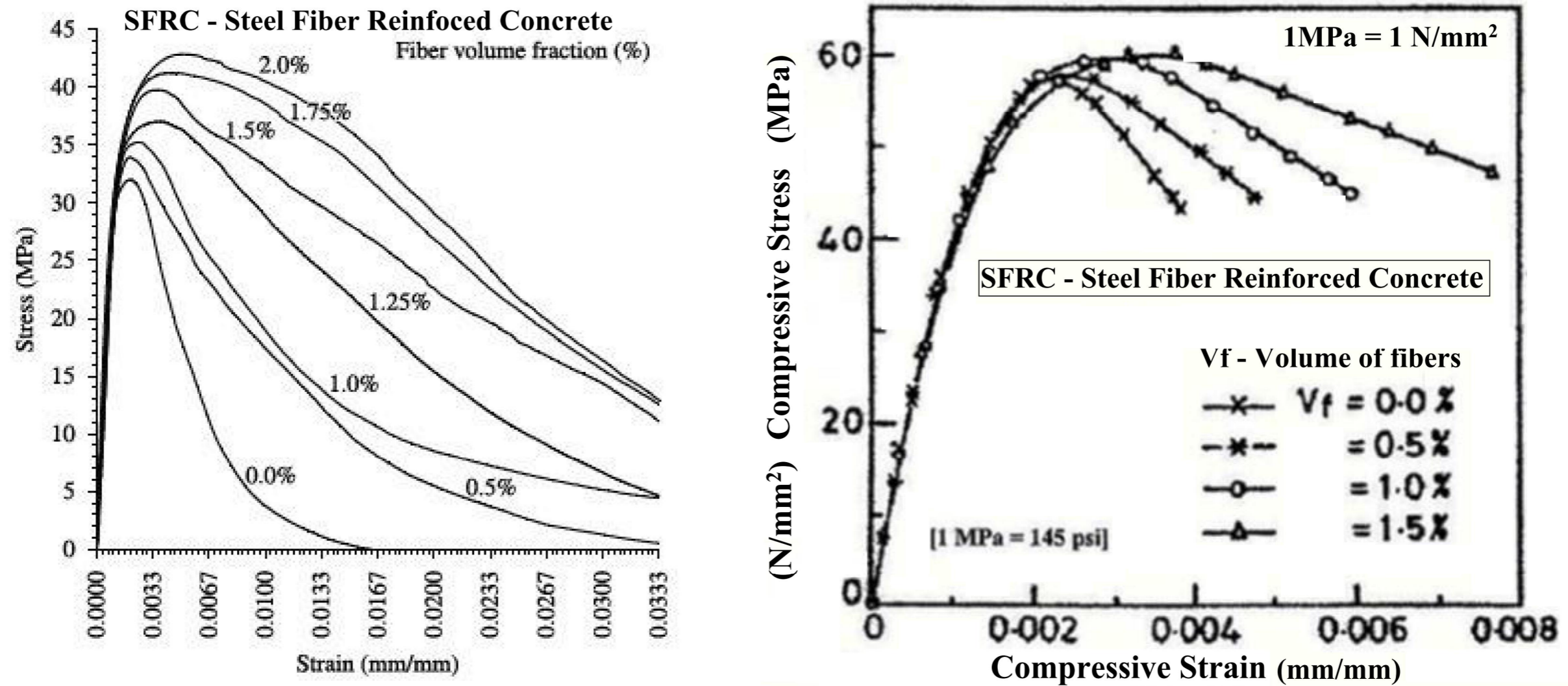


Figure 5.32 – Typical Stress-Strain Curves of Steel Fiber Reinforced Concrete samples under Axial Compressive Test.

CORRELATION BETWEEN TENSILE FLEXURAL STRENGTH AND COMPRESSIVE STRENGTH OF CONCRETE

The initiation of cracking in concrete members is clearly evidenced when the tensile capacity of the concrete under externally applied loads is exceeded. One could say that this initial value of tensile stress when a crack originates and start to propagate in the concrete members can be considered to be the tensile flexural strength value of concrete or the modulus of rupture (MOR) of concrete. Beyond this point the cracked sections of the concrete start to widen and propagate throughout the thickness of the concrete member causing the concrete to undergo nonlinear behaviour.



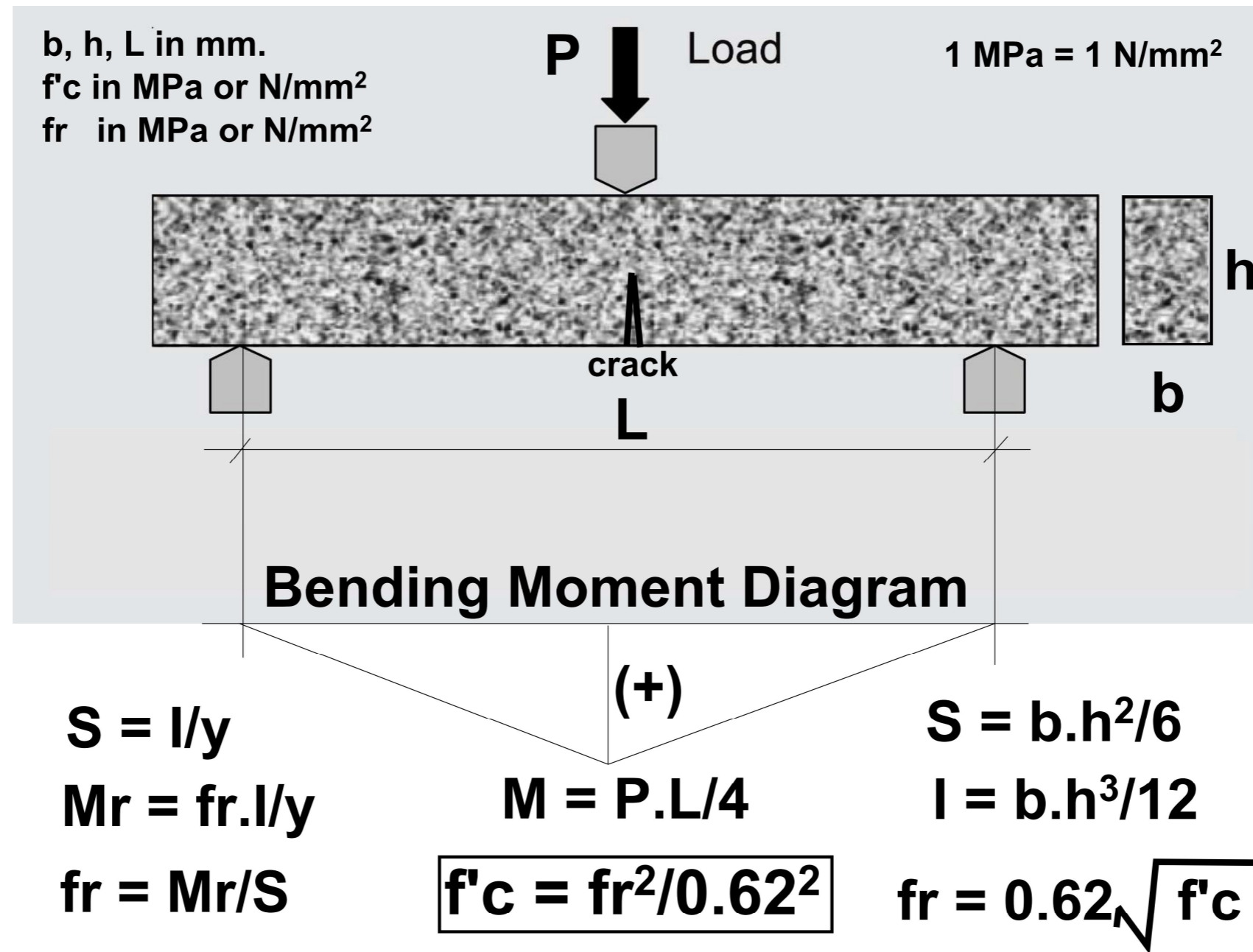


Figure 5.33 – Typical 3-Point set-up of Flexural Testing of Concrete samples with Geometrical Design and Strength Parameters.

The behaviour of cracked concrete members is highly unpredictable in terms of determining their maximum or ultimate capacity to sustain tensile, shear, and compressive stresses in their plastic range. Therefore it is important to limit the capacity of shell structures to those values of strength and capacity of the concrete that could offer safe and reliable performance under service loading conditions. Figure 5.33 above describes the basic geometrical and strength parameters that are involved in the design check process of concrete under tensile stresses.



The empirical correlation between the flexural strength f_r (also known as Modulus of Rupture MOR) and the ultimate compressive strength of plain concrete f'_c has been recommended by various design codes of different countries to facilitate a reasonable relationship between the two parameters. Some tabulated values are presented in the Figure shown below which are based upon extensive academic research performed at each country by different universities and testing laboratories.

Code	Country	Relationship
IS: 456-2000	India	$f_r = 0.7 \sqrt{f_c}$
ACI	USA	$f_r = 0.62 \sqrt{f'_c}$
NZS-3101	New Zealand	$f_r = 0.60 \sqrt{f'_c}$
EC-02	Europe	$f_r = 0.201 f_c$
BS-8110	Britain	$f_r = 0.60 \sqrt{f'_c}$

Figure 5.34 – Tabulated empirical relationships between Flexural Strength and Compressive Strength of plain concrete by Country Building Codes.

In the table shown above, the following parameters are defined as follows:

f_r = modulus of rupture (flexural strength) of plain concrete at 28 days in N/mm^2 .

f_c = cube compressive strength of concrete at 28 days in N/mm^2 , and

f'_c = cylinder compressive strength of concrete at 28 days in N/mm^2 .

It is important to note here that the initiation of cracking from the bottom surface of the concrete beam specimen under testing will provide the basis to determine the value of the load P which will cause the limiting state of initiation of failure of the concrete under tensile flexural stresses.

For concrete C28/35: $f'_c = 28 \text{ MPa (N/mm}^2) = 4,320 \text{ psi}$



From the Test Records of the laboratory material tests shown in Figure 4.33 one could extract from the list of values tabulated for specimens IV.1 to IV.6 an average maximum applied test force P of 4.40 kN. for a concrete specimen having a test span L of 100 mm.. P_{cr} can be safely estimated to be half of the ultimate test load, to be $P_{cr} = 2.2$ kN. Figure 5.35 below shows the experimental test set up used to obtain the value of P .

Calculations of Cracking Moment $M_{cr} = P_{cr} \cdot L / 4$. and tensile stress of concrete $f_r = M_{cr} \cdot y / I = M_{cr} / S$ at cracking moment for: $P_{cr} = 2.2$ kN, $L = 100$ mm., and dimensions of the concrete specimens tested, $b = 44$ mm. and $h = 47$ mm. comes out to be: $M_{cr} = 55,000$ N-mm.

The Section Modulus S of the concrete specimen tested can be calculated to be: $S = I / y = bh^2 / 6 = 16,199.33$ mm³.

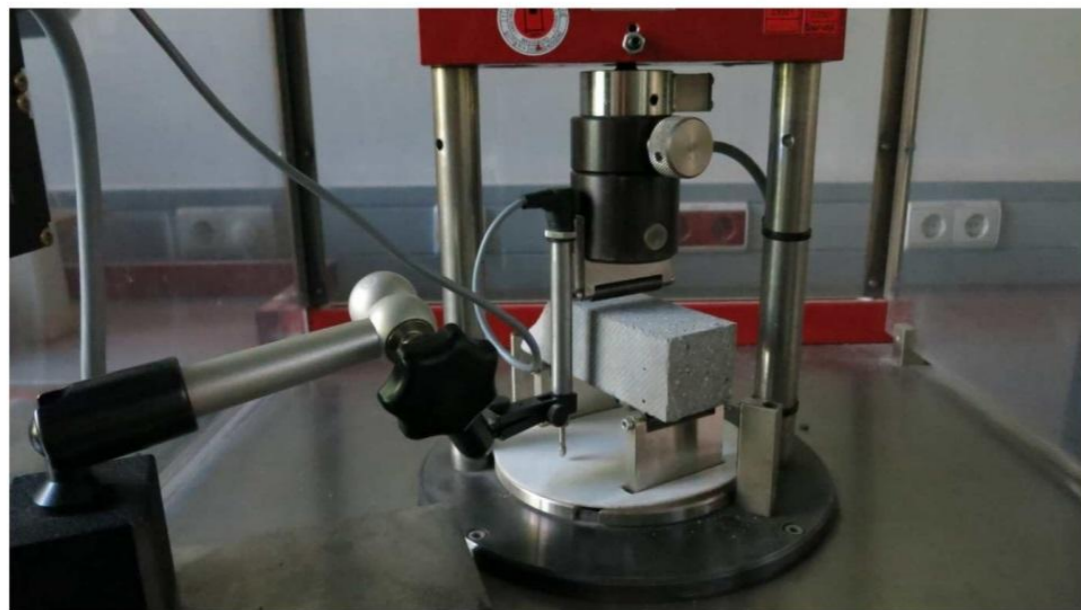
The Tensile Stress f_r at Cracking Moment M_{cr} can be calculated as: $f_r = M_{cr} / S = 55,000 / 16,199.33 = 3.395$ N/mm². = 492.92 psi.

The correlated relationship between the flexural strength of concrete f_r and the ultimate compressive strength of concrete f'_c can be given as:

$$f_r = 0.62 \cdot (f'_c)^{1/2} \quad (f'_c \text{ and } f_r \text{ in MPa}) \quad \text{and} \quad f'_c = f_r^2 / (0.62)^2 \quad (f'_c \text{ and } f_r \text{ in MPa}) \quad \text{with: } 1 \text{ MPa} = 1 \text{ N/mm}^2$$

The calculated value of f'_c from the just obtained value of f_r of 3.395 N/mm² (MPa) comes up to be: $f'_c = 29.98$ N/mm² (MPa) = 4,352.5 psi.

The values of tensile flexural strength of concrete $f_r = 3.395$ N/mm² and compressive strength of concrete $f'_c = 29.98$ N/mm² will be used as the limiting values of tension and compression which will be used to check against the values obtained from the finite element analysis.



Testing rig (3 point flexural testing) with external displacement transducer

Figure 5.35 – Experimental 3-Point set-up of Flexural Testing of Concrete samples of IMS Membrane-Concrete Shell Prototype.

DESIGN CHECKS OF THE MEMBRANE-CONCRETE SHELL ELEMENTS, STEEL BEAMS, AND CABLES.

After the finite element analysis of the membrane-concrete shell prototype structure has been completed we then look at the tabulated values of the maximum stresses in the concrete shell elements and the maximum forces and stresses in the steel beams and cables to determine its adequacy to sustain the effects of the selfweight of the structure combined with the externally applied environmental forces of snow, wind, and seismic effects (established in the local building codes) that could act on the prototype structure along many different directions during its life service loading conditions. The results of the finite element analysis have been tabulated and shown in Figures 5.24 to 5.30 with the maximum envelope of stresses and forces and the corresponding load case condition. The maximum stresses and forces from the tabulated results of the finite element analysis will be checked against the allowable safe stresses of the prototype materials.

EXPERIMENTAL AND ALLOWABLE STRESSES OF CONCRETE FOR DESIGN CHECKS

The allowable tensile, compression, shear, and flexural stresses of the concrete material of the prototype can safely be defined as follows:

FLEXURAL TENSION: $f_t = 0.62 \cdot \sqrt{f'_c}$; From experimental testing, $f_r = f_t = 3.395 \text{ N/mm}^2$

ULTIMATE COMPRESSION: $f'_c = 29.98 \text{ N/mm}^2$; From correlation with $f_r = 3.395 \text{ N/mm}^2$, $f'_c = 29.98 \text{ N/mm}^2$.

ALLOWABLE SHEAR: $f_v = 0.30 \cdot \sqrt{f'_c}$; $f_v = 1.643 \text{ N/mm}^2 \text{ (MPa)}$.

ALLOWABLE COMPRESSION: $f_c = 0.25 \cdot f'_c$; $f_c = 7.495 \text{ N/mm}^2 \text{ (MPa)}$.

A. MEMBRANE-CONCRETE SHELL ELEMENTS – t = 50 mm. – C28/35 – f'c = 28 MPa

Maximum Tensile Stress in the concrete shell elements: $F_t = +21.196 \text{ kN/m}^2 = +0.0212 \text{ N/mm}^2 = +3.08 \text{ psi} < f_t \rightarrow \text{OK}$

Maximum Compressive Stress in the concrete shell element: $F_c = -14.181 \text{ kN/m}^2 = -0.0142 \text{ N/mm}^2 = -2.06 \text{ psi} < f_c \rightarrow \text{OK}$

Maximum Shear Stress in the concrete shell elements: $F_v = +/-30.276 \text{ kN/m}^2 = +/-0.0303 \text{ N/mm}^2 = +/-4.40 \text{ psi} < f_v \rightarrow \text{OK}$

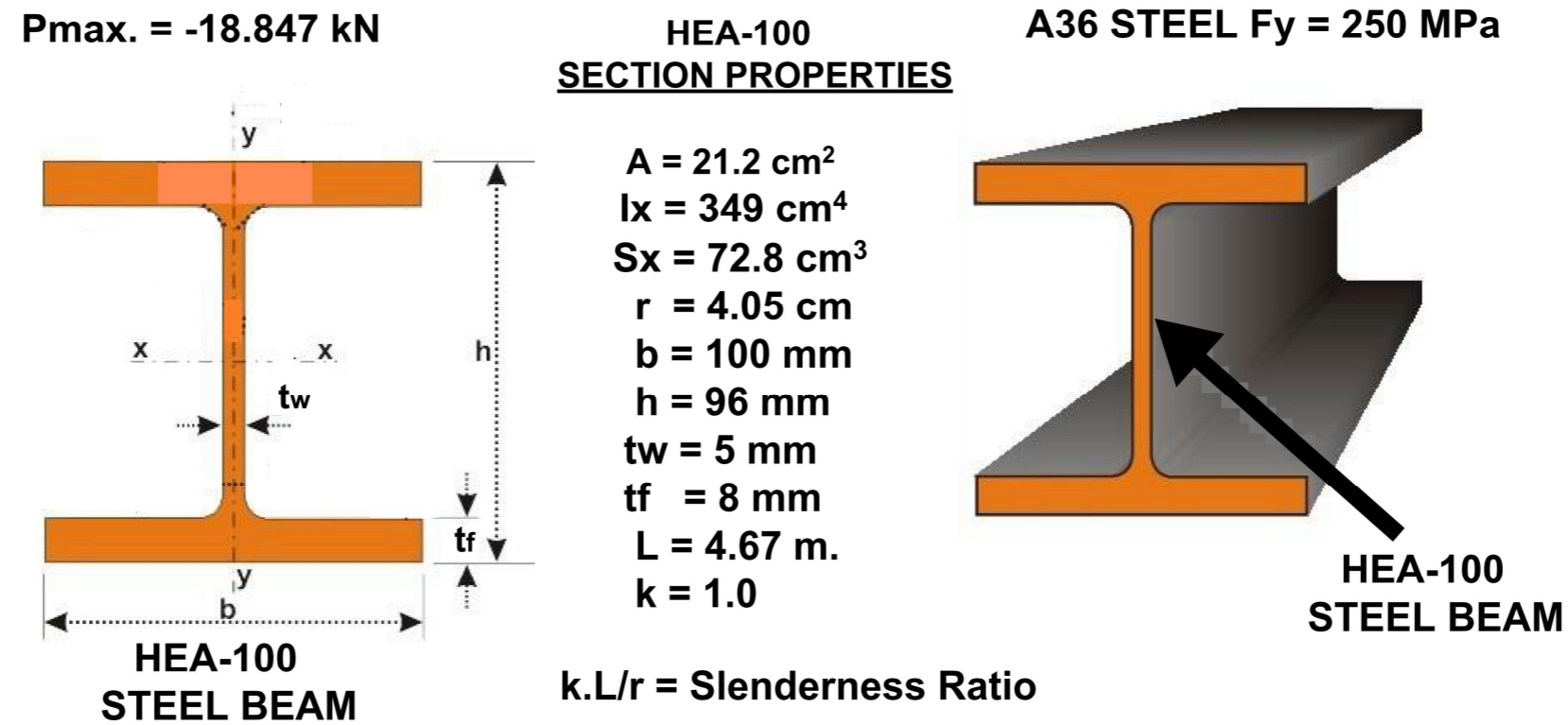
Maximum Bending Moment in the concrete shell elements: $M_b = +/-0.064 \text{ kN-m/m} = +/-0.064 \text{ kN-m/m} = +/-64 \text{ N-mm/mm} < M_{cr} \rightarrow \text{OK}$

Maximum Flexural Strength in the concrete shell elements: $F_b = +/-153.6 \text{ kN/m}^2 = +/-0.1536 \text{ N/mm}^2 = +/-22.3 \text{ psi} < f_r \rightarrow \text{OK}$



B. STEEL BEAM MEMBERS – HEA-100 WIDE FLANGE STEEL I-BEAM

The Maximum Axial Compression Force, Bending Moment, and Shear Force that were calculated by the finite element analysis have been checked against the allowable axial, bending, and shear capacity of the HEA-100 steel beam and were found to be adequate.



CALCULATIONS FOR AXIAL, BENDING, AND SHEAR CAPACITY

<u>AXIAL</u>	<u>BENDING</u>	<u>SHEAR</u>
$k.L/r = 1.0 \times 4,670/40.5 = 115.31$	$M_{max.} = 0.385 \text{ kN-m}$	$V_{max.} = 1.572 \text{ kN}$
$F_y = 250 \text{ N/mm}^2 \text{ (MPa)}$	$S = 72.8 \times 10^3 \text{ mm}^3$	$A = 21.2 \times 10^2 \text{ mm}^2$
$F_a = 75.831 \text{ MPa (N/mm}^2)$	$F_b = 165 \text{ N/mm}^2 \text{ (MPa)}$	$F_v = 112.5 \text{ N/mm}^2 \text{ (MPa)}$
$P_a = 75.831 \times 21.2 \times 100 = 160.76 \text{ kN}$	$f_b = 5.29 \text{ N/mm}^2 \text{ (MPa)}$	$f_v = 5.25 \text{ N/mm}^2 \text{ (MPa)}$

Figure 5.36 – Calculations to check the design and capacity of steel edge beams for axial loads, bending moments, and shear forces.



C. STEEL WIRE ROPES TIE-DOWN AND RIDGE CABLES

Maximum Axial Tensile Force in the Tie-Down Cables = 3.143 kN. < 10.9 kN, Safe Load Capacity of 3/8” cable → OK, say acceptable.

Maximum Axial Tensile Force in the Ridge Cables = 2.168 kN. < 7.56 kN, Safe Load Capacity of 5/16” cable → OK, say acceptable.

Rope Diameter		Minimum Breaking Strength		Safe Load		Weight	
(in)	(mm)	(lb _f)	(kN)	(lb _f)	(kN)	(lb _m /ft)	(kg/m)
1/4	6.4	5480	24,4	1100	4.89	0.11	0.16
5/16 - Ridge Cables	8	8520	37,9	1700	7.56	0.16	0.24
3/8 - Tie-Down Cables	9.5	12200	54,3	2440	10.9	0.24	0.36
7/16	11.5	16540	73,6	3310	14.7	0.32	0.48
1/2	13	21400	95,2	4280	19.0	0.42	0.63
9/16	14.5	27000	120	5400	24.0	0.53	0.79
5/8	16	33400	149	6680	29.7	0.66	0.98
3/4	19	47600	212	9520	42.3	0.95	1.41
7/8	22	64400	286	12900	57.4	1.29	1.92
1	26	83600	372	16700	74.3	1.68	2.50
1 1/8	29	105200	468	21000	93.4	2.13	3.17
1 1/4	32	129200	575	25800	115	2.63	3.91
1 3/8	35	155400	691	31100	138	3.18	4.73
1 1/2	38	184000	818	36800	164	3.78	5.63
1 5/8	42	214000	852	42800	190	4.44	6.61
1 3/4	45	248000	1100	49600	221	5.15	7.66
1 7/8	48	282000	1250	56400	251	5.91	8.80
2	52	320000	1420	64000	285	6.72	10.0

Figure 5.37 – Tabulated Safe Loads and Minimum Breaking Strength of Steel Wire Rope Cables – 6 strand x 19 wires (6x19).

The Maximum Axial Tensile Forces that were calculated by the finite element analysis have been checked against the Allowable Safe Tensile Load of the 8 mm. ridge cables and the 10 mm. tie-down cables and were found to be adequate to support the specified design load combinations.



D. REINFORCED CONCRETE BASES TO SUPPORT STEEL BEAMS AND TIE-DOWN CABLES

The two types of reinforced concrete bases are to be designed to support the maximum forces that will result from the reaction forces at the ends of the steel beams and the tie-down cables that are connected to the top of the concrete bases set into the ground. The three reinforced concrete bases supporting the steel beams (labeled CB-1) are of 0.80 m. diameter and 2.00 m. total height, embedded 1.00 m. into the ground, the other three reinforced concrete bases supporting the tie-down cables (labeled CB-2) are of 1.00 m. diameter and 1.00 m. total height, embedded completely into the ground. Assumed Estimated Allowable Soil Bearing Capacity = 2,000 psf (pounds per square foot).

CONCRETE BASE CB-1 – UNDER DOWNWARD COMPRESSIVE FORCES FROM EDGE STEEL BEAMS – $\varnothing = 0.80$ m. x $h = 2.00$ m.

Diameter of Concrete Base = 0.80 m. = 2.625 ft. - Area of Concrete Base $A = \pi \cdot 2.625^2 / 4 = 5.412$ ft²

Maximum Downward Force $P_{dn} = 43.492$ kN = 9,777 lbs.

Soil Bearing Pressure – $\sigma = P/A = 9,777$ lbs/5.412 ft² = 1,800 psf < 2,000 psf → say OK, Acceptable.

CONCRETE BASE CB-2 – UNDER UPWARD PULLOUT FORCES FROM TIE-DOWN CABLES – $\varnothing = 1.00$ m. x $h = 1.00$ m.

Diameter of Concrete Base = 1.00 m. = 3.28 ft. - Area of Concrete Base $A = \pi \cdot 3.28^2 / 4 = 8.45$ ft²

Height of concrete base $h = 1.00$ m. = 3.28 ft.

Weight of Concrete Base Downward – $W_{conc.} = 150$ pcf . $A \cdot h = 150 \times 8.45' \times 3.28' = 4,157$ lbs.

Maximum Upward Force - $P_{up} = 3.133$ kN = 704.30 lbs. <<< Weight of Concrete Base → say OK, Acceptable

The maximum downward and upward forces that will result to be applied onto the reinforced concrete bases were checked and it was found that the applied soil bearing pressures under the concrete bases CB-1 supporting the steel beams came out to be less than the assumed allowable soil bearing pressure and the pull up forces on the concrete bases CB-2 supporting the tie-down cables were found to properly hold down the upward forces from the cables.

Having checked and verified that the allowable strength and stiffness of the structural materials that form the membrane-concrete shell prototype structure including the membrane, concrete, steel beams, cables, and supporting reinforced concrete bases are within the allowable safe stresses permitted for the materials, the we can say that the prototype membrane-concrete shell structure is acceptable for the design loads.



CONSTRUCTED IMS MEMBRANE-CONCRETE SHELL PROTOTYPE STRUCTURE

The completed as-built constructed membrane-concrete shell structure is shown in Figure 5.38. Both sides of the concrete shell structure are well finished and display a very smooth exposed surface of shotcrete shell. The target heights and overall prototype dimensions were well achieved.



Figure 5.38 – View of completed Membrane-Concrete Shell Structure, edge beams, cables, and concrete bases right after completed construction.



CHAPTER 6 - CONCLUSIONS

The finite element analysis that has been completed to study the membrane-concrete shell prototype experimental structure built by IMS at the Bernburg Campus of the Anhalt University reveals that the selected designed thickness of approximately 50 mm. or 5 cms. (~ 2") has been found adequate for the span, dimensions, and configuration of the tensioned membrane-concrete shell structure built without temporary wooden formwork, but using a flexible PVC lightweight tensioned fabric clamped to a rigid frame of steel beams around the entire perimeter that are tie-down and supported on reinforced concrete bases at the ground level. The tensioned PVC fabric membrane is covered with shotcrete that is placed in thin layers over the entire surface of the tensioned membrane until it hardens to form a stiff and rigid shotcrete shell which has a mix of concrete with an embedded volume of small steel fibers. The PVC membrane, and the steel tie-down, and ridge cables are pretensioned to achieve the shell form.

It has been found that the selected thickness of the concrete shell can be reduced up to five times of the initial designed 50 mm. to a value of 10 mm. for which the stresses and deformations of the membrane-concrete shell prototype structure is still acceptable to support the specified design loads of the selfweight, snow, wind, and seismic load combinations.

The topic of thin shell reinforced concrete structures has gained a lot of attention lately by researchers, architects, engineers, builders, developers, owners, and environmentalists who realize on the great benefits of a strong, durable, and resilient material such as reinforced concrete that can be molded in virtually any type and shape of 2D and 3D curvilinear, folded, developable, synclastic, anticlastic, spherical, cylindrical, vaulted, and free form using either conventional formwork materials or innovative flexible textile, membranes, and high strength fabric materials to serve as temporary or permanent formwork to achieve the final form of the thin shell reinforced concrete structures.

The use of new technologies or adaptive old technologies to achieve the final desired shape and form of thin concrete shells have always been a challenge for designers and builders to create energy efficient shells structures that can serve multiple purposes for the building that they enclose as part of roofs, facades, floors, building envelope, and sculptures. Researchers lately have been using 3D printing, robotics, cable nets, flexible formworks, digitation of shell components, prefabrication and assembling on site precast shell elements, casting of shells using curvilinear EPS blocks that can be moulded to virtually any curved shape.

The discussion on the prospects of seeing more reinforced concrete shell structures into the main stream of building construction has been very active since many years ago. Professor Christian Meyer of Columbia University and Michael H. Sheer in 2005 published an article in the Concrete International magazine of ACI where they raise the question: "Do Concrete Shells Deserve another Look", they indicate that industry professionals



provide mixed opinions on this subject. Robert P. Schmitz in a technical article published in the Concrete Contractor Magazine issue of April 2016 also posted the question: “Is there a future for Fabric-Formed Concrete”.

Recently Adriaenssens and Block as guest editors of the Journal of the International Association for Shells and Spatial Structures (IASS) and as new co-chairs of IASS Working Group 5 (WG5) wrote a Preface to the special issue of WG5 titled: “New Directions for Shell Structures”, where they discuss the new challenges that face designers, architects, engineers, builders, and developers of thin shell reinforced concrete structures to realize the geometry, analysis, design, materials, and its constructability. This special issue of Journal of the IASS, Vol. 58, No. 1 has been published in March of 2017 presents several technical papers on Structural morphology, of plated shells, Flexibly-formed thin reinforced concrete shells, Analysis of shell structures using stress tensors and wire coat hanger analogy, Implementation of slender concrete shells with prefabricated elements, Prototype of GFRP elastic gridshell braced by a fiber-reinforced concrete envelope, Shells made of textile reinforced concrete applications in Germany, Design of hypar roofs built of guadua bamboo, and Optimized high-performance concrete shells for parabolic trough collectors.

As a result of the comprehensive and thorough research work done during the literature review and study of the different topics presented in this Thesis work several important topics have been identified to be of promising and potential practical use and applications in the building and construction industry which are listed below:

- The revival of interest in thin concrete shells and their most recent innovative construction methods can lead to more efficient, economical, sustainable, and resilient designs which can contribute to reduce the carbon footprint in the environment.
- The finite element analysis and design of thin reinforced concrete shells can lead to optimizations that allow for more reductions in total weight of shell structures and allow for more open sections in the shell surface for increased natural light and light weight of total structures which in turn lead into savings of the supporting framing and foundation structures.
- The availability of new design and construction technologies such as 3D printing, robotics, parametric designs, and prefabrication of modular and repetitive building sections may allow for the exploration of more efficient and economical organic forms which can be adaptable to facades, roof, floors, and walls of building systems.
- The complexity of the mathematical analysis of shell structures cannot be an obstacle to limit the use of thin concrete shell structures as a viable and suitable design solution to many different type of building systems for roof, floors, walls, and facades which had already being built many years ago but had been forgotten and felt into limited use at the present time. Several powerful computer programs for nonlinear analysis



and formfinding are now available which allow for the exploration of many different concrete shell geometries and configurations which combined with lightweight infill materials such as ETFE cushions, flexible fabrics, and polycarbonate can lead to very lightweight long span roof, floor, walls, and façade building systems.

- Thin concrete shell structures are certainly a suitable solution for low-cost housing in developing countries where the construction of shell structures can be adaptive and optimized based upon the appropriate local materials and local labor force to build the shell structures. Reinforced concrete grid-shell structures are another promising application for long span roof systems and modular floor systems.
- A variety and diverse pool of applications of thin concrete shell structures can be implemented to be built in areas prone and highly exposed to seismic events where permanent and temporary shelter conditions can be provided for the safety and protection of citizens in areas of high seismic risk. The use of flexible fabric formed concrete shell structures can prove to be very efficient to build rapid deployable structures for shelter or permanent housing.
- Innovative reinforced concrete shell dome and vaulted structures can be used for military and civilian protection, buildings, and housing that may be exposed or subjected to bombings, tornados, hurricanes, flooding, earthquakes and any other extreme environmental effects.

Some of the graphics, pictures, photos, diagrams, plots, schematics, internet links, biographical information of authors and shell designers, software routines and programing scripts, and other similar information presented in this Thesis have been obtained from websites, web links, technical papers, textbooks, academic publications, Journals, Magazines, and research using Google and other internet search engines readily available in the web. The readers are encouraged to expand their knowledge on the fascinating subject of membranes, shells, and flexible formed concrete structures by reading the relevant books, articles, technical papers, and publications listed in the References section of this Thesis.

Efforts have been made to give credit and indicate the sources that produced the original information presented in this Thesis when applicable. In Chapter 7, the section of References lists most of the numerous Textbooks, Publications, Journals, Papers, and Web links to some of the material studied to organize the concepts presented in this Thesis. It is not the intention of the Author to take complete ownership of the information presented in this Thesis but rather make use of it to explain and clarify the basic concepts that underlines the main subject of this Thesis work.

“More work still to be done, let’s maintain three things in mind: INSPIRATION to undertake new challenges, INTUITION to go along the right path, and INNOVATION to come up with something new, safe, practical, useful, feasible, and economical to build.



Chapter 7 - REFERENCES

- Abel, J. F., and Chilton, J.C., “Heinz Isler – 50 Years of New Shapes for Shells”, Journal of the IASS, Vol. 52, No. 3 September n. 169, 2011.
- ACI 318-14, “Building Code Requirements for Structural Concrete (ACI 318-14) and Commentary”; American Concrete Institute, 2014.
- ACI 318.2-14, “Code Requirements for Thin Shells and Commentary (ACI 318.2-14)”, American Concrete Institute, 2014.
- ACI CCS408.CAT, “Shotcrete for the Craftsman”, ACI Concrete Craftsman Series 4, 2008, 85 pp.
- ACI Committee 334, “Concrete Shell Structures – Practice and Commentary (ACI 334.1R-92-2002)”, American Concrete Institute, 1992.
- ACI Guide 506R-16, “Guide to Shotcrete (ACI 506R-16)”, American Concrete Institute, 2016.
- ACI 506.2-13, “Specifications for Shotcrete – ACI 506.2-13”, American Concrete Institute, 2013.
- ACI Guide 506.1R-08, “Guide to Fiber Reinforced Shotcrete (ACI 506.1R-08)”, American Concrete Institute, 2008, 12 pp.
- ACI Report 334.3R-05, “Construction of Concrete Shells Using Inflated Forms (ACI 334.3R-05)”, American Concrete Institute, 2005, 13 pp.
- ACI Report SP-28, “Concrete Thin Shells,”; American Concrete Institute, Farmington Hills, MI, 1971, 424 pp.
- ACI Report SP-67, “Concrete Shell Buckling,”; American Concrete Institute, Farmington Hills, MI, 1981, 234 pp.
- ACI Report SP-110, “Hyperbolic Paraboloid Shells, State of the Art Report”; American Concrete Institute, Farmington Hills, MI, 1988, 184 pp.
- ACI Report SP-244, “Thin Fiber and Textile Reinforced Cementitious Systems”.
- ACI Report SP-250, “Textile Reinforced Concrete”.
- ACI Report SP-251, “Design and Applications of Textile-Reinforced Concrete”.
- ACI Specification 506.2-95, “Specification for Shotcrete (ACI 506.2-95)”, American Concrete Institute, 1995.
- Adams, D.O., “Can flexure testing provide estimates of composite strength properties?”, Composites World Magazine, October 2017, pp. 10-11.



- Adriaenssens, S, et. al., “Shell Structures for Architecture – Form Finding and Optimization,”; Routledge, Taylor & Francis Group, New York, 2014.
- Adriaenssens, S., and Block, P., “New Directions for Shell Structures”, Preface to the Special Issue of WG5 of the IASS. Journal of the International Association of Shell and Spatial Structures, 2017, Vol. 58, No. 1, March n. 191, pp. 5.
- Allen, E., “Form and Forces, Designing Efficient Expressive Structures”, John Wiley & Sons, 2010.
- Andersen, T.J., Leal, W.R., Thrane, L.N., “Lessons from the TailorCrete Project”, Concrete International, No. 3, March 2016, pp. 54-61.
- Anhalt University, “Anhalt University of Applied Sciences, Dessau, Germany”, www.hs-anhalt.com, 2017.
- ANSI/NFPA 102, “American National Standard for Grandstands, Folding and Telescopic Seating, Tents, and Membrane Structures“, NFPA 2016.
- ASA, “American Shotcrete Association“, www.shotcrete.org.
- ASCE 17-2016, “ASCE Standard on Air-Supported Structures“, American Society of Civil Engineers, ASCE 2016.
- ASCE Manual of Engineering Practice No. 31, “Design of Cylindrical Concrete Shell Roofs“, ASCE, New York, 1952.
- ASCE/SEI 55-16, “ASCE Standard of Tensile Membrane Structures“, American Society of Civil Engineers, ASCE 2016, pp. 50.
- AutoCAD®, “AutoCAD 2000i User’s Guide”, Autodesk, Inc., May 26, 2000.
- Balck, L., “ACI Guide to Shotcrete, Key Changes to New Version of ACI 506“, ACI Concrete International Magazine, February 2017, pp. 35-37.
- Bamforth, P., Chisholm, D., Gibbs, J., and Harrison, T., “Properties of Concrete for use in Eurocode 2“, The Concrete Centre, 2008, pp. 53.
- Bayrak O., “Strut-and-Tie Model, A Professor’s Perspective, Concrete Bridge Design“, ASPIRE Magazine, pp. 42-43, Spring 2017.
- Bedford, A., and Fowler, W., “Engineering Mechanics, Statics”, Fifth Edition, Pearson-Prentice Hall, Upper Saddle River, NJ, 2008.
- Billington, D. P., “Thin Shell Concrete Structures”, 2nd Edition, McGraw-Hill, New York, 1982.
- Billington, D. P., “Thin Shell Structures”, Structural Engineering Handbook, Gaylord and Gaylord, Editors, McGraw-Hill, NY, 1990, pp. 24.1-24.57.
- Billington, D.P., “The Art of Structural Design: A Swiss Legacy, Chapter 5, Heinz Isler: Structural Art in Thin-Shell Concrete”, Princeton, NJ, 2003.



- Bletzinger, K.U., and Ramm, E., “A General Finite Element Approach to the form Finding of Tensile Structures by the Updated Reference Strategy”, *Journal of the International Association for Shell and Spatial Structures, J. IASS*, 1999, No. 14, pp. 131-145.
- Block, P., “Block Research Group (BRG), <http://www.block.arch.ethz.ch/>, Institute of Technology in Architecture at ETH, Zurich, 2017.
- Block, P., and Ochsendorf, J., “Thrust Network Analysis: A new methodology for three-dimensional equilibrium, *Journal of the International Association for Shell and Spatial Structures, J. IASS*, 2007, Vol. 48, No. 3, pp. 1-7.
- Block, P., and Van Mele, T., “Novel Form Finding Method for fabric formwork for concrete shells”, *Journal of IASS*, 2011, Vol. 52(4), pp. 217-224.
- Brand, M., and Tailor, T., “Not Just Another Dome Idea”, *Structure Magazine*, November 2014, pp. 34-36.
- Brown, N., “Form, Use, and Sustainability: A Geometric and Structural Feasibility Study of Hypar Shells,” *Department of Civil and Environmental Engineering, Princeton University*, April 2012, 191 pp.
- Brush, D. O., and Almroth, B. O., “Buckling of Bars, Plates, and Shells”, International Student Edition, McGraw-Hill Kogakusha, Ltd. 1975.
- Burger N., and Billington, D.P., “Felix Candela, Elegance and Endurance: An Examination of the Xochimilco Shell”, *Journal of IASS*, V47, 2006.
- Calladine, C.R., “Theory of Shell Structures”, Cambridge University Press, UK, 1988, 763 pp.
- Candela, F., “Simple Concrete Shell Structures”, *ACI Journal*, V. 23, No. 4, December. 1951, pp. 321-332.
- Candela, F., “Structural applications of hyperbolic paraboloidal shells”, *ACI Journal*, V. 26, No. 5, January 1955, pp. 397-416.
- Candela, F., “General Formulas for Membrane Stresses in Hyperbolic Paraboloidal Shells”, *Journal of the ACI*, October 1960.
- Carlton, W. S., “Material Behavior of Latex-Modified Concrete in Thin Hyperbolic Paraboloid Shells”, University of Oklahoma, Graduate College of School of Civil Engineering and Environmental Science, Norman, Oklahoma, Master’s Thesis, 2013, pp. 139.
- Cassinello, P., “75th Anniversary of the innovative system design for shell structures of Ildefonso Sanchez del Rio”, *Journal of the IASS*, 2016, V57, No. 3, September No. 189, pp. 219-226.
- Chilton, J., “Form-finding and fabric forming in the work of Heinz Isler”, Orr, J., Evernden, M., Darby, A. & Ibell, T. (Editors), *ICFF 2012: Proceedings of the Second International Conference on Flexible Formwork, ICFF 2012, 27-29 June 2012, Bath, UK., 2012*, pp. 84-91.



- Chilton, J., "The Engineer's Contribution to Contemporary Architecture – Heinz Isler", Thomas Telford Publication, London, 2000.
- Chinn, J., "Cylindrical Shell Analysis Simplified by the Beam Method", Journal of ACI, 55, May 1959.
- Concrete International, ACI, "Concrete Visually Transmuted in Monolithic Sculpture", Concrete International, No. 3, March 2016, pp. 35-39.
- Cuvilliers, P., Douthe, C., Peloux, L., and Le Roy, R., "Hybrid Structural Skin: Prototype of a GFRP Elastic Gridshell Braced by a Fiber-Reinforced Concrete Envelope", J. of IASS, Vol. 58, No.1, No. 191, March 2017, pp. 65-78.
- Davis, W., "HyparActive, A Design Exploration Tool for Multi-segment Hyperbolic Paraboloid Shells", Master's Thesis, University of Washington, Department of Architecture, 2016, pp. 47.
- Day, A.S., "An Introduction to Dynamic Relaxation", The Engineer, January 1965.
- D'Anza G., "IxCube 4-10, "Advanced Form Finding, Modeling, Analysis, and Patterning Software for Tensile Structures", www.ixray-ltd.com, 2014.
- Dean, D.L., and Strode W., "Design, Construction, and Testing of a Plywood Hyperbolic Paraboloid Lattice Structure", The Bulletin of Engineering and Architecture, 41, Lawrence: University of Kansas Publications, 1958.
- Downs, J.W., "Practical Conic Sections, Dover Publications
- Du Bois, A.J., "The elements of Graphical Statics and their application to framed structures", Reprint University of Michigan Library, 2010.
- Dürr, H., and Off, R., "From Membrane Form to Rigid Shell", Tensinews NR. 27, September 2014, pp. 14-16.
- Dürr, H., and Off, R., "Report on the Research Activities on the Membrane-Concrete Shell Prototype at Bernburg Campus", IMS, 2017.
- Eisenbach, P., and Grohmann, M., "Structural Implementation of Slender Concrete Shells with Prefabricated Elements", J. of IASS, Vol. 58, No. 1, No. 191, March 2017, pp. 51-64.
- Ekkehard R. and Eberhard S., "Heinz Isler, Schalen", Die Deutsche Bibliothek, 2002.
- EUROCODE 2 (EC2), "BS EN 1992, Eurocode2: Design of Concrete Structures", www.eurocode2.info – www.concretecentre.com/eurocode2.
- Farshad, M., "Design and Analysis of Shell Structures", Springer, 1st. Edition, Kluwer Academic, 1992.



- Gaylord, E.H. and Gaylord C.N., “Structural Engineering Handbook”, McGraw-Hill Book Company, New York, 1968 and 1990.
- Gibson, J.E., “Computer Analysis of Cylindrical Shells”, E. and F.N. Spon Ltd. London, 1961.
- Gould, L.S., “Optimizing Automotive Lightweighting”, AD&P Magazine, www.ADandP.media.com, pp. 34-36, January 2016.
- Grasshopper®, “Algorithmic Modeling for Rhino by David Rutten”, www.grasshopper3d.com, Grasshopper 2017.
- Graybeal, B.A., “Ultra-High-Performance Concrete Connections-FHWA”, Technical Article, Aspire Magazine, Summer 2004, pp. 32-33.
- Greco, C., “The FERRO-CEMENTO of Pier Luigi Nervi, the new material and the first experimental building”, Spatial Structures: Heritage, Present, and Future, University of Rome, “TOR VERGATA”, Italy, 1994.
- Hanskat, C.S., “Shotcrete Placed in Multiple Layers does NOT Create Cold Joints”, Concrete International Magazine, December 2014, pp. 46-47.
- Hibbeler, R.C., “Mechanics of Materials, Seventh Edition, Pearson Prentice Hall, Upper Saddle River, NJ, 2008.
- IASS Working Group No. 5, “Recommendations for Reinforced Concrete Shells and Folded Plates,”; International Association for Shell and Spatial Structures, Madrid, Spain, 1979, 66 pp.
- IMS e.V., “Institute of Membranes and Shell Structures, Anhalt University”, www.ims-institute.org, Dessau, Germany, 2017.
- Indian Standards Institution (ISI), “Code of Practice for Construction of Reinforced Concrete Shell Roofs”, IS 2204-1962, New Delhi, 1962.
- Indian Standards Institution (ISI), “Criteria for the Design of Reinforced Concrete Structures and Folded Plates”, IS 2210-1962, New Delhi, 1963.
- Isler, H., “The Stability of Thin Concrete Shells, Buckling of Shells”, Ramm, E. (ed.), Springer, Berlin, 1982, pp.644-672.
- ISOFF, “International Society of Fabric Forming - ISOFF”, www.fabricforming.org.
- IxCube 4-10, “Advanced Form Finding, Modeling, Analysis, and Patterning Software for Tensile Structures”, www.ixray-ltd.com, Ix Ray ltd. 2014.
- JCI, Japan Concrete Institute, “Guidelines, Conference Proceedings and Standards”, www.jci-net.or.jp, Tokyo, Japan.
- Jasiczak, J., Majchrzak, W., and Czajka W., “Construction of Undulating Walls Using Dry-Mix Shotcrete”, ACI Concrete International Magazine, June 2015, pp. 31-35.



- Killian, A. and Ochsendorf J., “Particle-Spring Systems for Structural Form Finding”, Journal of IASS, Vol. 46, n. 147, 2005.
- Kelkar, V.S. and Sewell, R.T., “Fundamentals of the Analysis and Design of Shell Structures”, Prentice –Hall, Inc., Englewood Cliffs, NJ, 1987.
- Lepencies, I., et al., “Modeling of Load Transfer Behavior of AR-Glass-Rovings in Textile Reinforced Concrete”, SP-244-7.
- Levens, A.S., “Graphics, Analysis and Conceptual Design”, Second Edition, John Wiley & Sons, Inc. New York, NY, 1968.
- Li, Qingpeng, Borgart, A., and Wu, Yue, “How to Understand ‘Structural Morphology’”, J. of IASS, Vol 57, No. 2, No. 188, June 2016, pp. 145-158.
- Madeo, F. and Novi, F., “Architectural Research through to Practice”, 48th International Conference of the Architectural Science Association, 2014.
- Medwadowski, S., “Multidirectional Membrane Reinforcement”, ACI Structural Journal, V. 86, No. 5, Sept.-Oct. 1989, pp.563-569.
- Melaragno, M., “An Introduction to Shell Structures, The Art and Science of Vaulting”, Van Nostrand Reinhold, New York, 1991.
- Meyer, C., “Do Concrete Shells Deserve Another Look?”, Concrete International, No. 10, October 2005, pp. 43-50.
- Meyers G., “TSC Global Showcases ‘Roofs for the World’ Demo”, Greenbuilding Elements (GBE) Newsletter, July 23rd, 2010.
- Modi, S., “Advanced Building Construction of Shells,” Published by LinkedIn Share Education, March 5, 2014.
- Moore, F., “Understanding Structures”, McGraw-Hill Co., NY, 1999,
- Neff, W., “Building Construction”, U.S. Pat. 2,270,229, 1941.
- Nervi, P.L., “Structures”, Translated by Giuseppina and Mario Salvadori, F.W. Dodge Corp., New York, 1956, pp. 118.
- Nez, G., Knott, A., and Barrett, M., “Design and Construction of Acrylic Concrete Structures”, 2003.
- Novak, L., “The Practicing Engineer’s Guide to Designing by Strut and Tie Modeling (ACI 318-14)”, PCA Seminar Presentation, March 2017.
- Off, R., and Dürr, H., “From Membrane Form to Rigid Shell”, Tensinews NR. 27, September 2014, pp. 14-16.
- Orr, J.J., Derby, P.D., Ibell, T.J., Evernden, M.C., and Otlet, M., “Concrete structures using fabric formwork”, Department of Architecture and Civil Engineering, University of Bath, The Structural Engineer, Vol. 89, 2011, pp 97-105.



- Parme, A. L., “Elementary Analysis of Hyperbolic Paraboloid Shells”, IASS Bulletin No. 4. 1960.
- Parme, A. L., and Conner, H.W., “Tables for Multibarrel Circular Shells without Edge Beams”, Journal of ACI, Dec. 1959, pp. 1584.
- PCA Portland Cement Association, “Elementary Analysis of Hyperbolic Paraboloid Shells”, Publication No. ISO85.01dD, Skokie, IL, 1960.
- PCA Portland Cement Association, “Coefficients for Design of Cylindrical Concrete Shell Roofs”, PCA, Skokie, IL, 1959.
- Pedreshi, R., “Rethinking Concrete Formwork”, Technical Article, ESALA, Edinburgh School of Architecture and Landscape Architecture, 2017.
- Peerdeman, B., “Analysis of Thin Concrete Shells Revisited: Opportunities due to Innovations in Materials and Analysis Methods”, Master’s Thesis, Delft University of Technology, Faculty of Civil Engineering and Geosciences, June 2008
- Princeton University, Civil Engineering Department, “Evolution of German Shells, Efficiency in Forms”, <http://shells.princeton.edu/works.html>.
- Ramsay, A., and Maunder, E., “Equilibrium Finite Elements for RC Slab Design”, STRUCTURE Magazine, July 2017, pp. 31-33.
- Ramirez, H. D., Scordelis, A.C., and Ngo, D., “Membrane Stresses in Hyperbolic Paraboloid Shells Having a Parallelogram Shape in Plan”, ACI Journal Proceedings, V. 66, No. 12, December 1969, pp. 944-1000.
- Rhinoceros®, “NURBS Modeling for Windows, Version 5.0 User’s Guide”, www.rhino3d.com, Robert McNeel & Associates, 2014.
- RhinoVAULT, “Funicular Form Finding Software”, App for Rhino, by Matthias Rippmann, www.food4rhino.com/app/rhinovault. 2014.
- Rippmann, M., “RhinoVAULT”, Food4Rhino App for Rhino and Grasshopper, Thrust-Network-Approach from Graphic Statics, 2014.
- Scheerer, S., Chudoba, R., Garibaldi, M.P., Curbach, M., “Shells Made of Textile Reinforced Concrete – Applications in Germany”, J. of IASS, Vol. 58, No. 1, No. 191, March 2017, pp.79-93.
- Schmitz, R. P., “Fabric Formed Concrete Panel Design”, Master’s Thesis, Milwaukee School of Engineering, Milwaukee, Wisconsin, 2004.
- Schmitz, R. P., “Is there a Future for Fabric-Formed Concrete”, Concrete Contractor Magazine, www.forconstructionpros.com/article, April 2016.
- Schmitz R. P., “Fabric-Formed Concrete Panel Design”, Charney, F.A. & Grierson, D.E. & Hoit, M. (Editors), ASCE Proceedings of the 17th Analysis and Computation Specialty Conference, 2006 Structures Congress, 18-21 May 2006, St. Louis, Missouri, 2006.



- Segal, E., “The thin concrete shells of Jack Christiansen”, Proceedings of the IASS Symposium at Universidad Politecnica de Valencia, Spain, 2009.
- Scordelis, A. C., Ramirez, H.D., and Ngo, D., “Membrane Stresses in Hyperbolic Paraboloid Shells having an arbitrary quadrilateral shape in plan”, ACI Journal Proceedings, V. 67, No. 1, January 1970, pp. 36-44.
- Shaeffer, R.E., “Tensioned Fabric Structures – A Practical Introduction”, Published by ASCE Task Committee on Tensioned Fabric Structures, 1996.
- Shah, S.P., and Konsta-G, M.S., “Uncoupling Modulus of Elasticity and Strength”, Concrete International Magazine, November 2017, pp.37-41.
- Sobek, W., “Auf Pneumatisch Gestützten Schalungen Hergestellte Betonschalen”, PhD Dissertation, University of Stuttgart, Germany, 1987.
- Sondericker, J., “Graphic Statics, With Applications to Trusses, Beams, and Arches”, First Edition, John Wiley & Sons, New York, 1904.
- Soranakom C., and Mobasher B., “Flexural Analysis and Design of Textile Reinforced Concrete”, Arizona State University (CTRS4), 2009.
- STAAD.Pro, “3D Structural and Finite Element Analysis Software, Technical Reference Manual”, Research Engineers International, Bentley, 2004.
- Sturgeon, K., Holzwart, C., and Raczkowski K., “Dezeen: Book of Ideas, Fatty-Shell (v.01)”, University of Michigan, 2010.
- Tedesko, A., “Construction Aspects of Thin Shell Structures,”; ACI Journal, Proceedings V.49, No. 6, Feb. 1953, pp. 505-520.
- Teknologisk Institut, “State of the Art Report, Best Practice in Formwork Manufacturing”, NICE Fremtidens Nordiske Betonarkitektur, May 2010.
- Timoshenko, S. P., and Gere, J. M., “Theory of Elastic Stability,” 2nd Ed., McGraw-Hill, New York, 1961.
- Timoshenko, S.P., and Woinowsky-Krieger, S.; “Theory of Plates and Shells”, McGraw-Hill, 2nd Ed., New York, 1959.
- Varghese, P.C., “Design of Reinforced Concrete Shells and Folded Plates”, PHI Learning Private Limited, Delhi-110092, 2014.
- Veenendaal, D., Bakker, J., and Block, P., “Structural Design of the flexible formed mesh-reinforced concrete sandwich shell roof of NEST HiLo”, Journal of IASS, 2017, Vol. 58, No. 1, March n. 191, pp. 23-38.
- Veenendaal, D., and Block, P., “Design process for prototype concrete shells using a hybrid cable-net and fabric formwork”, Journal of Engineering Structures 75, 2014, pp. 39-50, Elsevier.



Veenendaal, D., West M., Block, P., “History and overview of fabric formwork: using fabrics for concrete casting”, Ernst & Sohn, Verlag für Architektur und technische Wissenschaften GmbH & Co. KG, Berlin · Structural Concrete 12 (2011), No. 3., pp. 164-177.

Velimirovic, L., Radivojevic, G., and Kostic, D., “Analysis of Hyperbolic Paraboloids at small deformations”, University of Nis, Journal of Architecture and Civil Engineering, Vol. 1, No. 5, 1998, pp. 627-636.

West, M., “The Fabric Formwork Book: Methods for Building New Architectural and Structural Forms in Concrete”, 1st Edition, 2016.

West, M., “Fabric-Formed Concrete Members, Formwork allows flexibility, efficiency in design”, ACI Concrete International October 2003, p. 55.

West, M., Abdelgar, H. S., Gorski, J.: ‘State of the art report on fabric formwork’, Concrete: Construction, Sept 4-6, 2007, The International Conference on Construction and Building Technology 2008 (ICCBT 2008), Volume: ICCBT 2008 - B - (08) – pp. 93-106.

Wilby, C.B., “Design Graphs for Concrete Shell Roofs”, Applied Science Publishers Ltd., Barking, Essex, England, 1980.

Wolfe, W.S., “Graphical Analysis, A Text Book on Graphic Statics”, First Edition, McGraw-Hill Book Company, Inc. New York, NY, 1921.

Zalewski, W., and Allen, E., “Shaping Structures: Statics”, John Wiley & Sons, Inc., New York, NY, 1998.

Zienkiewicz, O.C., “The Finite Element Method”, 3rd Edition, McGraw-Hill Book Company, New York, 1977.



CHAPTER 8 - APPENDICES

APPENDIX A - NOTATION

Symbol	Description	Symbol	Description
<i>2D</i>	two dimensional	<i>C_p</i>	coefficient of wind pressure
<i>3D</i>	three dimensional	<i>C_s</i>	coefficient of seismic force
<i>3DGS</i>	three dimensional graphic statics	<i>C_t</i>	coefficient for snow temperature
<i>a</i>	length of major axis of ellipse adjustment coefficient of parabolic cable length	<i>I</i>	snow importance factor
<i>A</i>	cross-sectional area of member	<i>cosh</i>	trigonometric hyperbolic cosine
<i>ACI</i>	American Concrete Institute	<i>d</i>	height of parabola at top of inscribed circle depth of wide flange steel section
<i>AiF</i>	German Federation of Industrial Research	<i>dx</i>	unit with of shell element along x axis
<i>AMP</i>	additive manufacturing process	<i>dy</i>	unit with of shell element along y axis
<i>App</i>	laptop or mobile phone software application	<i>dz</i>	unit thickness of shell element along z axis
<i>AR</i>	alkali resistant	<i>DFE</i>	discrete flexible formwork
<i>ASCE</i>	American Society of Civil Engineers	<i>DL</i>	dead load/selfweight
<i>AutoCAD</i>	3D CAD software	<i>DR</i>	dynamic relaxation
<i>b</i>	width of minor axis of ellipse width of beam width of wide flange steel section	<i>DTI</i>	Danish Technological Institute
<i>BMS</i>	beams	<i>E</i>	modulus of elasticity
<i>BRG</i>	Block Research Group	<i>EC</i>	Eurocode
<i>BSt</i>	British Standard	<i>EQ</i>	seismic earthquake load/force
<i>c</i>	ratio of height to square width of hyperparabola width of parabola at top of inscribed circle constant ratio that defines the shape of hyperbola	<i>EPS</i>	expanded polystyrene
<i>c.g.</i>	center of gravity	<i>ETFE</i>	Ethylene Tetrafluoroethylene
<i>C++</i>	computer programming language	<i>ETH</i>	Eidgenössische Technische Hochschule Swiss Federal Institute of Technology
<i>CAD</i>	computer aided design	<i>ft.</i>	feet (')
<i>CI</i>	concrete international	<i>F</i>	axial Force in structural members applied force on beam cross section
<i>CLT</i>	cross laminated timber	<i>F_a</i>	allowable axial stress of steel sections
<i>COMB.</i>	combination	<i>F_y</i>	yield stress of steel
<i>C28/35</i>	compressive strength of concrete cylinder and prism	<i>FDM</i>	force density method
<i>C_e</i>	coefficient for snow exposure type	<i>FEA</i>	finite element analysis
		<i>FEM</i>	finite element method
		<i>FHWA</i>	Federal Highway Administration



<i>FRC</i>	ferrocemento	<i>ln</i>	natural logarithmic function
<i>fb</i>	allowable bending stress of steel section	<i>l_p</i>	length of parabolic curve of cable from end to end
<i>fdr</i>	force density ratio (force divided by length)	<i>L</i>	length of member or span of shell
<i>fc</i>	allowable compressive stress of concrete		horizontal projected span of parabolic cable
<i>f^c</i>	ultimate compressive strength of concrete	<i>LISP</i>	programming scripting routine for AutoCAD
<i>fr</i>	tensile stress of concrete at cracking moment	<i>L_{cable}</i>	total length of cable along curve from end to end
<i>ft</i>	allowable tensile stress of concrete	<i>m.</i>	meters, unit of length
<i>fv</i>	allowable shear stress of concrete	<i>m²</i>	square meter
<i>g</i>	gravity force	<i>mm.</i>	millimeters, unit of length
<i>G</i>	gaussian curvature	<i>M_{max.}</i>	maximum bending moment of steel section
<i>GAM</i>	graphical analysis method	<i>Max.</i>	maximum
<i>GFRP</i>	glass fiber reinforced plastics	<i>MIT</i>	Massachusetts Institute of Technology
<i>GSM</i>	graphic statics method	<i>M_b</i>	bending moment of cross section
<i>h</i>	height of hyperbolic paraboloid	<i>M_{cr}</i>	cracking moment of concrete
	height of beam	<i>MOR</i>	modulus of rupture
<i>H</i>	horizontal reaction force at end of cable in equilibrium	<i>M_x</i>	internal bending moment around x in shell element
<i>HEA</i>	European wide flange steel beam section	<i>M_y</i>	internal bending moment around y in shell element
<i>HPGS</i>	hyperbolic paraboloid grid shell	<i>M_{xy}</i>	internal torsional moment around x in shell element
<i>Hypar</i>	hyperbolic paraboloid	<i>M_{yx}</i>	internal torsional-moment around y in shell element
<i>in.</i>	inches (“)	<i>n</i>	ratio of sag to span length of parabolic cable
<i>I</i>	moment of inertia of cross section	<i>NFDM</i>	non-linear form density method
<i>I_e</i>	seismic importance factor of structural element	<i>N_x</i>	internal axial force along x in shell element
<i>I_s</i>	importance factor for snow loads	<i>N_y</i>	internal axial force along y in shell element
<i>IASS</i>	international association of shells and spatial structures	<i>N_{xy}</i>	internal shear-torsion force around x in shell element
<i>IMS</i>	institute of membranes and shell technologies	<i>N_{yx}</i>	internal shear-torsion force around y in shell element
<i>ISI</i>	Indian Standards Institution		
<i>ISOFF</i>	international society of fabric formwork	<i>p</i>	distance from focus to directriz of parabola
<i>Ix-Cube</i>	form finding analysis software program		focal length of parabola from focus to vertex
<i>JCI</i>	Japan Concrete Institute		external pressure applied on the shell surface
<i>kg</i>	kilograms, unit of weight	<i>phw</i>	horizontal wind pressure
<i>ksi</i>	kips per square inch	<i>psi</i>	pounds per square inch
<i>kN</i>	kiloNewtons	<i>P</i>	forces applied to members
K	stiffness matrix of structural system	<i>P1,P2,P3</i>	testing loads P1, P2, and P3 applied to prototype
<i>k</i>	slenderness coefficient	P	vector of applied prestress forces
<i>l</i>	length or span of structure	<i>Pa</i>	allowable axial compression force of steel section
<i>lbs.</i>	pounds, unit of weight	<i>PCA</i>	Portland Cement Association



<i>PES</i>	polyester	<i>T</i>	tensile force
<i>PL</i>	prestress load	<i>TAM</i>	truss analogy method
<i>PTFE</i>	Polytetrafluoroethylene	<i>TFRC</i>	textile fibre reinforced concrete
<i>PVC</i>	Polyvinyl Chloride	<i>TD</i>	tie downs
<i>Python</i>	programming scripting language for Rhino	<i>TL</i>	testing load
<i>P_{cr}</i>	test load <i>P</i> at cracking moment <i>M_{cr}</i> .	<i>TNA</i>	thrust network approach
<i>P_g</i>	ground snow load	<i>TRC</i>	textile reinforced concrete
<i>P_s</i>	snow load on surface of shell structure	<i>TSC</i>	thin shell composite
<i>Q_x</i>	internal shear force along x in shell element	<i>T_o</i>	axial horizontal tension at cable in equilibrium
<i>Q_y</i>	internal shear force along y in shell element	<i>T_{max}</i>	maximum axial tension at cable end in equilibrium
<i>r</i>	radius of circle, radius of curvature of shell	<i>U</i>	vector of nodal displacements
	radius of curvature of shell surface	<i>USA</i>	United States of America
	radius of gyration of cross section	<i>UHPC</i>	ultra high performance concrete
<i>r_x</i>	radius of curvature of shell around x axis	<i>UK</i>	United Kingdom
<i>r_y</i>	radius of curvature of shell around y axis	<i>URS</i>	updated reference strategy
<i>r-θ-z</i>	polar coordinate system	<i>u</i>	poisson's ratio
<i>R</i>	radius of circle	<i>V_{max}</i>	maximum shear force of steel section
	radius of curvature of parabola	<i>W</i>	weight of structure/effective seismic weight
	vertical reaction force at end of cable in equilibrium	<i>WC</i>	total weight of concrete shell
	seismic response modification factor	<i>WG5</i>	working group 5 of IASS
<i>RDG</i>	ridge	<i>WL</i>	wind load
<i>REACT.</i>	reactions	<i>WZ</i>	uplift wind pressure along z axis
<i>Rhino</i>	3D CAD software	<i>w</i>	width of hyperbolic paraboloid
<i>R₁</i>	radius of curvature of shell around x axis		uniformly distributed load on shell
<i>R₂</i>	radius of curvature of shell around y axis	<i>w_c</i>	weight of concrete
<i>s</i>	sag of cable at mid-span	<i>w_s</i>	weight of snow
<i>S</i>	section modulus of cross section	<i>www</i>	world wide web
<i>S_{ds}</i>	design spectral response acceleration parameter	<i>x</i>	x axes of the x-y-x coordinate system
<i>SL</i>	snow load	<i>y</i>	y axes of the x-y-x coordinate system
<i>STAAD</i>	structural analysis software program	<i>z</i>	z axes of the x-y-x coordinate system
<i>STM</i>	strut-and-tie model	<i>x-y-z</i>	Cartesian rectangular coordinate system
<i>t</i>	thickness of concrete shell	<i>σ</i>	membrane stresses in shell thickness
<i>tf</i>	thickness of flange of steel section	<i>σ_b</i>	bending moment stress of cross section
<i>tw</i>	thickness of web of steel section	<i>θ</i>	angle of radial coordinate system
<i>tconc.</i>	thickness of concrete	<i>∅</i>	diameter



APPENDIX B – AUTOCAD LISP AND RHINO PHYTON SCRIPTS

AUTOCAD LISP SCRIPT TO GENERATE 2D SEGMENTAL PARABOLIC CURVES – IN AUTOCAD RUN AS PAR

```
(defun C:par( / pt1 pt2 pt3 pt_a pt_b dx x y x_start x_end num_pts a b c
ret_list ocmd oblip sset ent1)

(setq ocmd (getvar "cmdecho") oblip (getvar "blipmode"))
(setvar "cmdecho" 0)
(setvar "blipmode" 0)

(initget 7)
(setq pt1 (getpoint "\nSelect first point on parabola:"))
(setq pt2 (getpoint "\nSelect second point on parabola:"))
(setq pt3 (getpoint "\nSelect third point on parabola:"))

(setq num_pts (getint "\nNumber of points to use:"))

(setq ret_list (get_coeff pt1 pt2 pt3))

(setq a (nth 0 ret_list)
b (nth 1 ret_list)
c (nth 2 ret_list)
x_start (nth 3 ret_list)
x_end (nth 4 ret_list)
)

(setq dx (/ (- x_end x_start) (float num_pts) ))
(setq x x_start)
(setq y (fpoly a b c x))
(setq pt_a (list x y 0.0))
(setq x (+ x_start dx))
(setq sset(ssadd))

(repeat num_pts
(setq y (fpoly a b c x))
(setq pt_b (list x y 0.0))
(command "_pline" pt_a pt_b "")
(command "_point" pt_a pt_b "")
(setq sset (ssadd (entlast) sset))

(setq pt_a pt_b x (+ x dx) )
)

(command "_point" pt_a pt_b "")
(command "_pedit" "L" "J" sset "" "")
(setvar "cmdecho" ocmd)
(setvar "blipmode" oblip)
)

(defun get_coeff(pt1 pt2 pt3 / x1 x2 y1 y2 x3 y3 x1sq x2sq x3sq
a b c ret_list)

(setq x1 (car pt1) y1 (cadr pt1) x1sq (* x1 x1) )
(setq x2 (car pt2) y2 (cadr pt2) x2sq (* x2 x2) )
(setq x3 (car pt3) y3 (cadr pt3) x3sq (* x3 x3) )
(setq x_start (min x1 x2 x3) x_end (max x1 x2 x3))
(setq det1 (det x1sq x2sq x3sq x1 x2 x3 1.0 1.0 1.0))
(setq a(/ (det y1 y2 y3 x1 x2 x3 1.0 1.0 1.0) det1))
(setq b(/ (det x1sq x2sq x3sq y1 y2 y3 1.0 1.0 1.0) det1))
(setq c(/ (det x1sq x2sq x3sq x1 x2 x3 y1 y2 y3 ) det1))
(setq ret_list (list a b c x_start x_end))
)

(defun fpoly(a b c x / y)
(setq y (+ (* a x x) (* b x) c) )
)

(defun det(a1 a2 a3 b1 b2 b3 c1 c2 c3 / ret_val)
(setq ret_val (+
(* a1 (- (* b2 c3) (* b3 c2) ))
(* b1 (- (* c2 a3) (* c3 a2) ))
(* c1 (- (* a2 b3) (* a3 b2) ))
)
)
)
)
```



RHINO PYTHON SCRIPT TO GENERATE 2D SEGMENTAL PARABOLIC CURVES - IN RHINO RUN AS parabola_half2_anyplane

```
import rhinoscriptsyntax as rs

def fpoly(a, b, c, x):
    y = (a*x*x)+(b*x)+c
    return y;

def det(a1, a2, a3, b1, b2, b3, c1, c2, c3):
    ret_val = (a1*((b2*c3)-(b3*c2)))+(b1*((c2*a3)-(c3*a2)))+(c1*((a2*b3)-(a3*b2)))
    return ret_val;

def get_coeff(pt1, pt2, pt3):
    x1 = pt1[0]
    y1 = pt1[1]
    x1sq = x1*x1
    x2 = pt2[0]
    y2 = pt2[1]
    x2sq = x2*x2
    x3 = pt3[0]
    y3 = pt3[1]
    x3sq = x3*x3

    x_start = min(x1, x2, x3)
    x_end = max(x1, x2, x3)
    det1 = det(x1sq, x2sq, x3sq, x1, x2, x3, 1.0, 1.0, 1.0)
    a = det(y1, y2, y3, x1, x2, x3, 1.0, 1.0, 1.0)/det1
    b = det(x1sq, x2sq, x3sq, y1, y2, y3, 1.0, 1.0, 1.0)/det1
    c = det(x1sq, x2sq, x3sq, x1, x2, x3, y1, y2, y3)/det1
    return (a, b, c, x_start, x_end);

#start of main routine
def par():
    cpt1 = rs.GetPoint("Select first point-Start X of parabola:")
    cpt2 = rs.GetPoint("Select second point-End X of parabola:", cpt1)
    cpt3 = rs.GetPoint("Select third point-Vertex or Any point on parabola:", cpt1)

    planemaster = rs.PlaneFromPoints(cpt1, cpt2, cpt3)

# cplane1 = rs.PlaneFromFrame(pt1, pt2-pt1, pt3-pt1)
xform = rs.XformRotation1(planemaster, rs.WorldXYPlane())

pt1 = rs.PointTransform(cpt1, xform)
pt2 = rs.PointTransform(cpt2, xform)
pt3 = rs.PointTransform(cpt3, xform)

num_pts = rs.GetInteger("Number of points to use:")

vec1 = pt2 - pt1
pt2 = pt1 + (2 * vec1)
num_pts = 2 * num_pts
ret_list = get_coeff(pt1, pt2, pt3)

a = ret_list[0]
b = ret_list[1]
c = ret_list[2]
x_start = ret_list[3]
x_end = ret_list[4]

dx = (x_end - x_start)/num_pts
x = x_start
y = fpoly(a,b,c,x)
pt_a = [x, y, 0.0]
x=x+dx

ixform = rs.XformInverse(xform)

for i in xrange(num_pts/2):
    y = fpoly(a,b,c,x)
    pt_b = [x, y, 0.0]
    cpt_a = rs.PointTransform(pt_a, ixform)
    cpt_b = rs.PointTransform(pt_b, ixform)
    rs.AddLine(cpt_a, cpt_b)
    rs.AddPoint(cpt_a)
    rs.AddPoint(cpt_b)
    pt_a = pt_b
    x=x+dx

# Check to see if this file is being executed as the "Main" python
# script instead of being used as a module by some other python script
# This allows us to use the module whichever way we want.
if __name__ == '__main__': par()
```



APPENDIX C – DRAWINGS OF MEMBRANE-CONCRETE PROTOTYPE

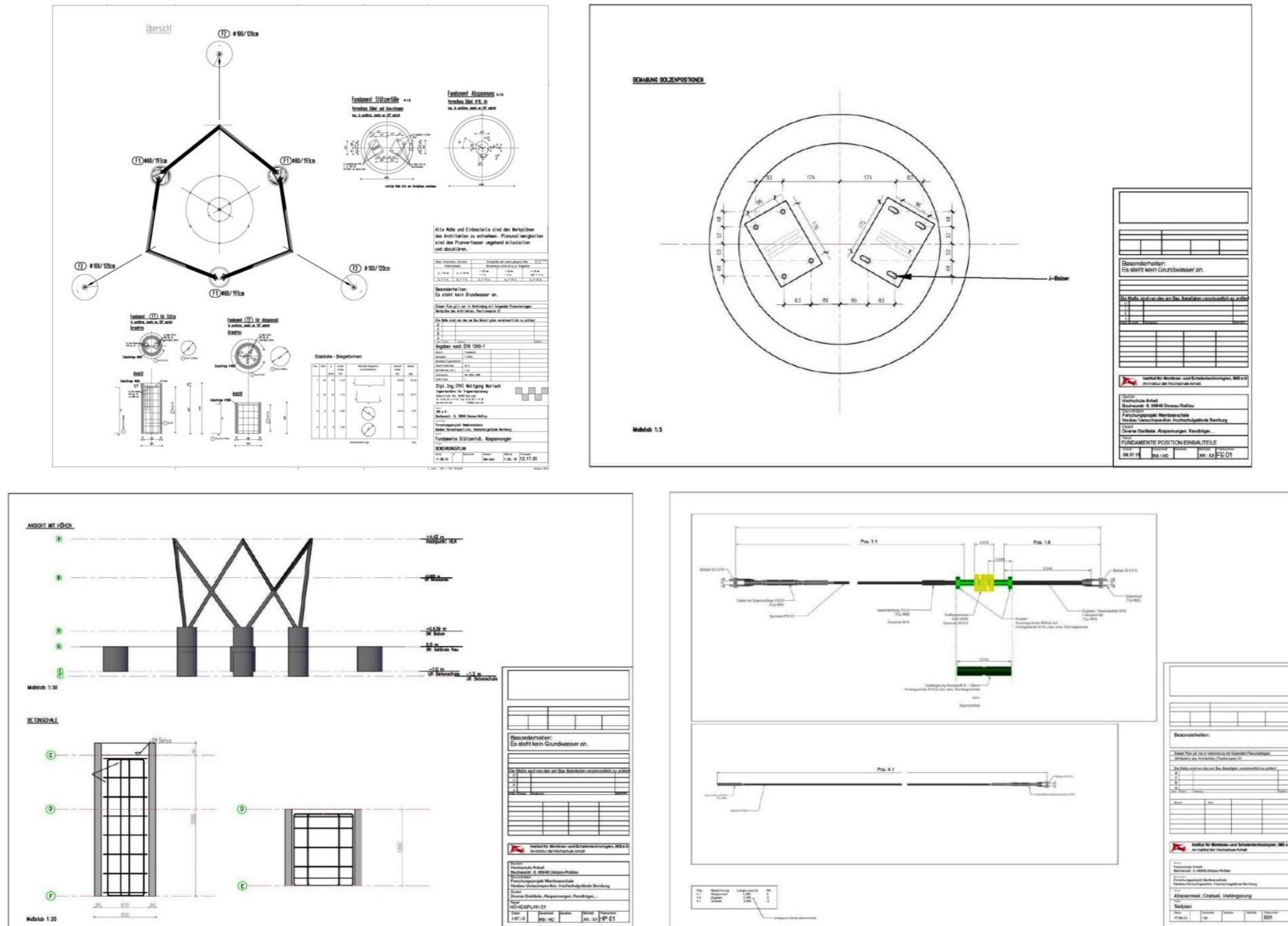


Figure C.1 – Plan Layout of Concrete Footings, Elevations, Base Plates with Anchor Bolts, Rebar Details and Cables.



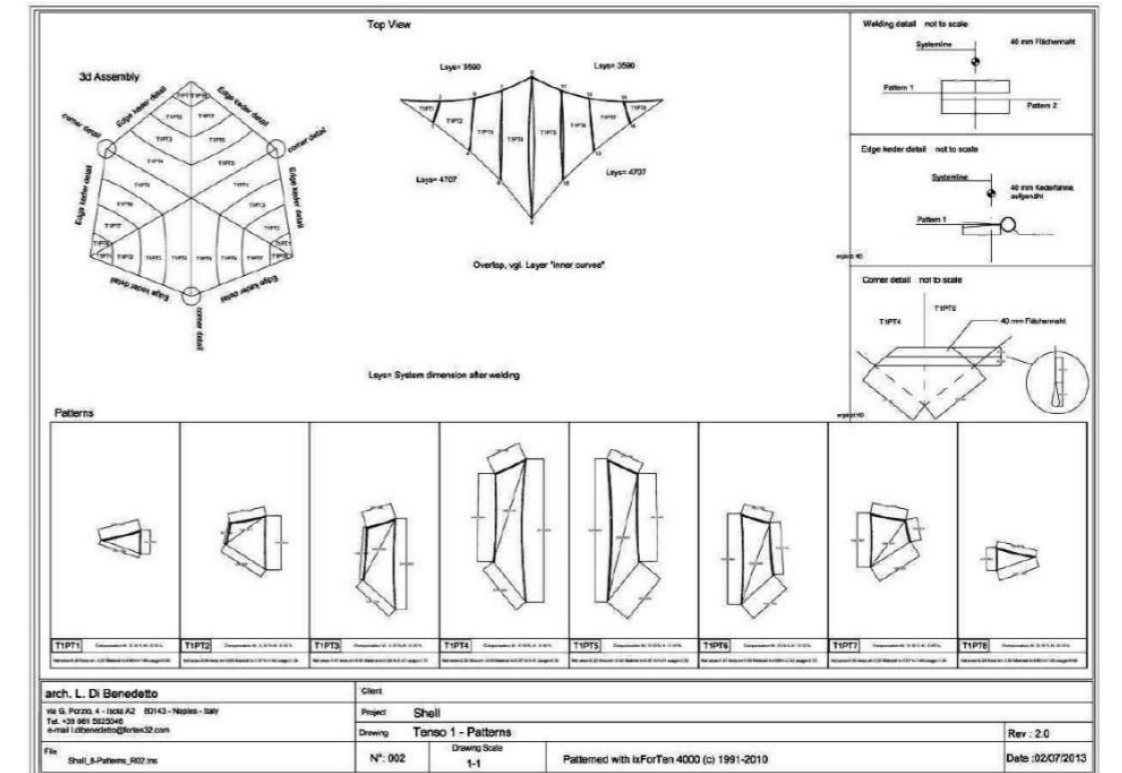
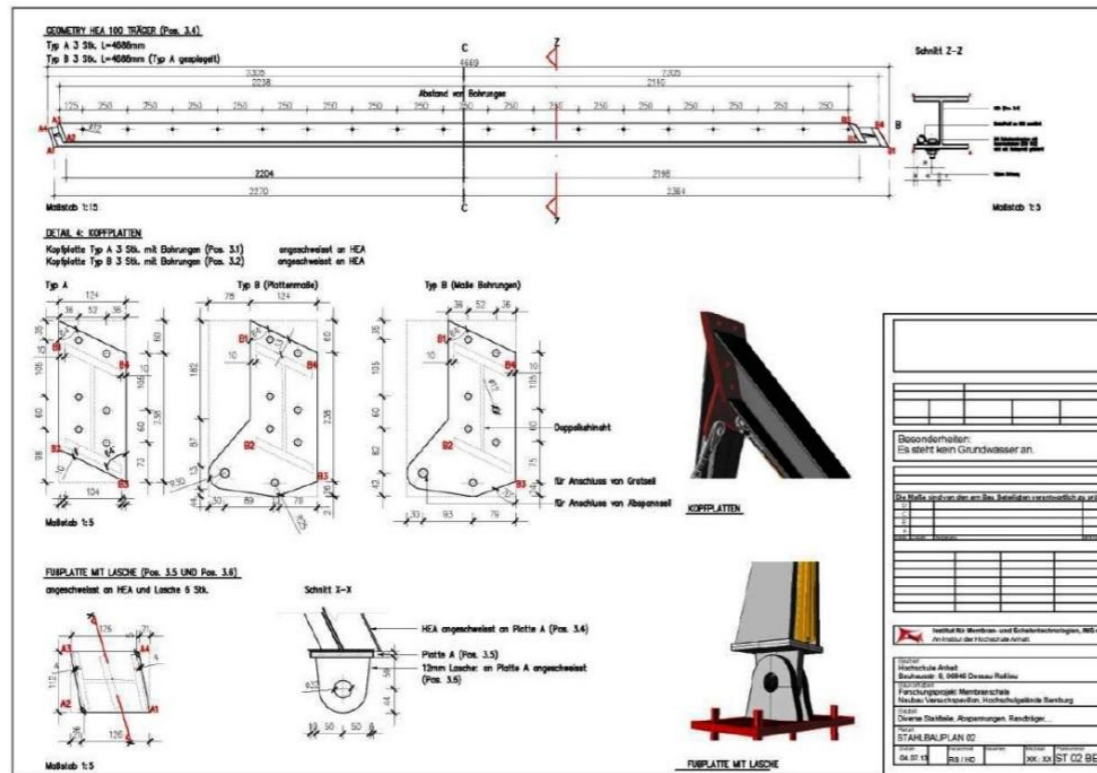
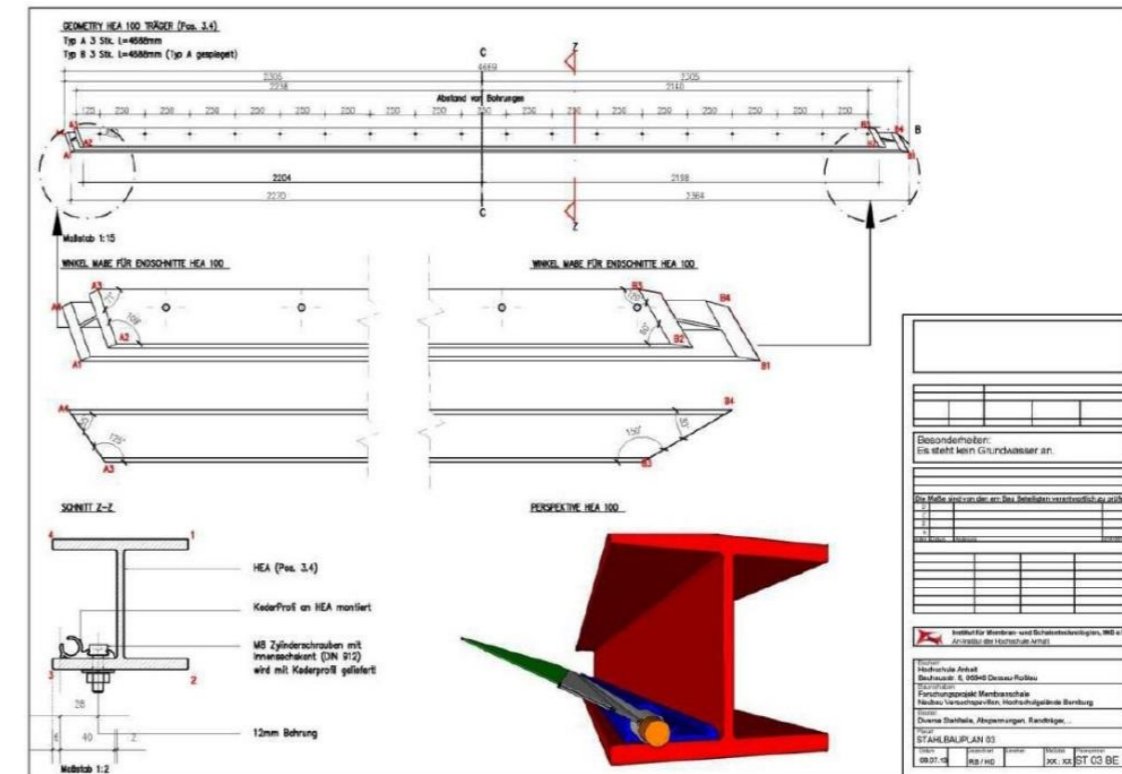
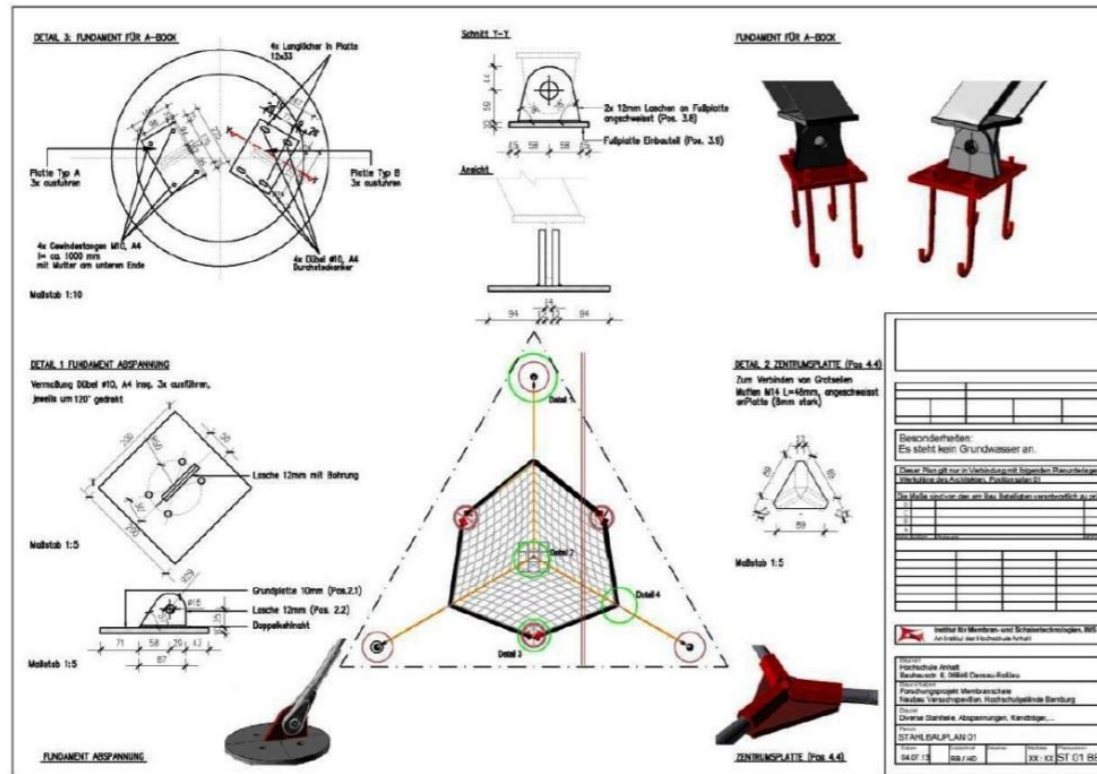


Figure C.2 - General Arrangement, Base Plates, Membrane, Steel Edge Members, and Steel Connection Details.



APPENDIX D – DATASHEETS OF MATERIALS TO BUILD THE IMS PROTOTYPE

D.1 – FABRIC: Ferrari Precontraint 392 S2 - MESH





PRECONTRAI
392 S2



▶ MAJOR ADVANTAGES


- Durability conserved:
 - > High coating thickness at yarn peak height
 - > S2 treatment for better cleanability (white colour)
- Excellent weldability
- Excellent resistance to climatic damage
- Exceptional dimensional stability



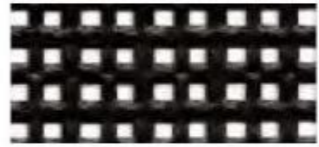
TECHNICAL SPECIFICATIONS		
	Précontraint 392 S2	Standards
Yarn	1100 dtex PES HT	TERBUISSE
Weight	820 g/m ²	EN ISO 2286-2
Width	180 cm	
Standard format length/jumbo rolls*	± 50 lm	
Tensile strength (warp/weft)	300/300 daN/5 cm	EN ISO 1421
Tear strength (warp/weft)	60/60 daN	DIN 53.363
Adhesion	8/8 daN/5 cm	EN ISO 2411
Finish	Formula S2 (only on white 100S2) / fluorinated varnish weldable	
Porosity	± 27%	
Windefficiency	81%	XPG 39-100-3 ¹⁾
Flame retardancy	M2/NFP 92-507 • Method 2/NFPA 701 • CSFM T19 • B1/DIN 4102-1 • 01/GOST 30244-94 • M2/UNE 23.727-90 • VKF 5.3/SN 198898 • Schwerbrennbar Q1-Tr1/ONORM A3800	
Cold resistance	- 30°C	
Heat resistance	+ 70°C	
Quality management system		ISO 9001

*1) Measurements carried out at the CMEFE in Geneva, sample 25 x 35 cm

COLOURS & REFERENCES



392-100S2



392-1075

D.2 – SHOTCRETE - Concrete SAKRET SSM4P

TECHNICAL DATA SHEET



SAKRET Silica Spritzmörtel SSM 4 P

SSM 4 P

silica spray mortar
hydraulically hardening, silica modified, cementitious factory-mix dry mortar
acc. to EN 14487 / DIN 18551, EN 206 / DIN 1045, DV GW 300 and 347

- application areas:**
- mixture for creation of spray mortar for concrete repairs with a special suitability for the drinking water area.
 - for pneumatic delivery in dry spraying method
 - For reinforcing concrete and reinforced concrete.
 - For tunnel construction and civil engineering.

- Suitability:**
- for wall and floor
 - for interior and exterior use

- Properties:**
- extremely dense texture
 - normal setting
 - slight rebound
 - building material class A 1, non-combustible

- Material Basis:**
- cement - DIN EN 197
 - standardized grain size DIN EN 12620
 - additives and admixtures to improve workability (processing) properties

TECHNICAL DATA SHEET



SAKRET Silica Spritzmörtel SSM 4 P

SSM 4 P

Technical Data:		
in layer thicknesses of		15 - 40 mm applicable with one layer
grain size		4 mm
working temperature		+ 5 °C bis + 30 °C
compressive strength		C35 / 45
bulk density of hardened concrete		approx. 2,2 kg/dm ³
corrosion of the reinforcement by carbonation		XC1 XC2 XC3 XC4
reinforcement corrosion through chlorides		XD1 XD2 XD3
corrosion of the reinforcement by chlorides from seawater		XS1 XS2 XS3
corrosion of concrete by frost attack		XF1 XF2 XF3
corrosion of concrete by chemical attack		XA1 XA2 XA3
corrosion of concrete by stress of abrasive wear		XM1 XM2
concrete corrosion caused by an alkali-silica reaction		WO WF WA
water penetration depth		≥ 15 mm
fire classification		A 1 DIN EN 13501 - 1 (not flammable)

- Substrate Pre-Treatment:**
- adhesion strength of the absorbing substrate has to be $\geq 1,5 \text{ N / mm}^2$, secured by a suitable pre-treatment method.
 - remove dust, loose parts, efflorescences, sinter layers and other separating agents from the substrate.
 - the substrate has to be adequately removed (e.g. sandblasting with SAKRESIV) in a way that convex coarse stone grains are visible.
 - The substrate has to be pre-wetted at least 24 hours prior to application of shotcrete; the concrete underlay should be dim-moist prior to application of shotcrete.



TECHNICAL DATA SHEET



SAKRET Silica Spritzmörtel SSM 4 P

SSM 4 P

Processing:

- for pneumatic delivery in dry spraying method (g unite).
- suitable for all dry spraying machines as e.g. Aliva, Meynadier, Mader, Clever and similar; indications of machine producer as to water-, air and current supply should be considered.
- Working with a nozzle-distance of approx. 1 m and a spraying angle of 90 degrees secures an optimum spraying result (slight rebound, high compaction).
- The following guidelines must be followed during execution of sprayed concrete works:
 - DIN 14487 / 18551 spray concrete
 - guideline for protection and repair of concrete elements, German committee for reinforced concrete
 - ATV DIN 18314, spray concrete works
 - ATV DIN 18349, concrete maintenance works
 - ZTV-ING
- The rebound quantity depends - among others - on substrate condition, on injection angle, spraying distance and method.
- if in doubt arrange for test surfaces.

Post Treatment:

- to be protected (e.g. with ventilated foils or jute bags) against weather influences like sun, wind, driving rain and frost as well as against too fast drying.
- duration of after-treatment acc. to weather-conditions and relative prescriptions, e.g. after-treatment guideline of German concrete association, Rili SIB and ZTV-ING.

Storage:

- Weather protected, cool and dry on timber mats
- sealed bundles for 12 months from date of manufacture.
- less chlorate acc. to guideline 2003 / 53 / EG, GISCODE ZP1.
- Seal open bundles at once and process within a short period of time

Waste Management:

- hardened product remainders to be wasted as common rubble under code no. 17 09 04.

Remarks:

- technical data refer to +20 °C and 50 % relative air moisture
- lower temperatures prolong, higher temperatures shorten indicated values.
- may only be smoothed and abraded as 2. layer, not as single layer.
- the setting material has to be sheltered from sun, draught, frost and too high (> 30°C) and too low (< 5°C) temperatures
- SAKRET concrete - repair systems are in bags from 40 t quantity and as Sacks full pallets in stock!
- keep away from children
- further remarks: see safety data sheet and in the Internet under <http://www.sakret.de>

TECHNICAL DATA SHEET



SAKRET Silica Spritzmörtel SSM 4 P

SSM 4 P

Certificates / Certificate of Approval:

- DV GW 300, 347, 270
- subject to permanent internal and external control.

During execution of work the relevant recommendations and guidelines, rules and standards, relevant technical instruction leaflets as well as the acknowledged rules of architecture and engineering have to be regarded. We do not have any influence on different weather / substrate and object conditions. Our written and spoken application / technological recommendations handed out to customers and craftsmen respectively are without obligation and do not constitute any contractual legal relationship and no lateral duty of a sales contract. All indications and recommendations of technical data sheets refer to standard purpose of use. With the publication of this technical instruction sheet the previous ones loose their validity.

Delivery Form Silica Spritzmörtel SSM 4 P:

Concrete Quality acc. to DIN 1045	Consumption without rebound	Order Unit bundle	Delivery Unit quantity	EAN
C35 / 45	approx. 2,2 t/m ³	40 kg bag	30 pc./pallet	-650288
C35 / 45	approx. 2,2 t/m ³	1 t loose	1 t (in silo)	-663530



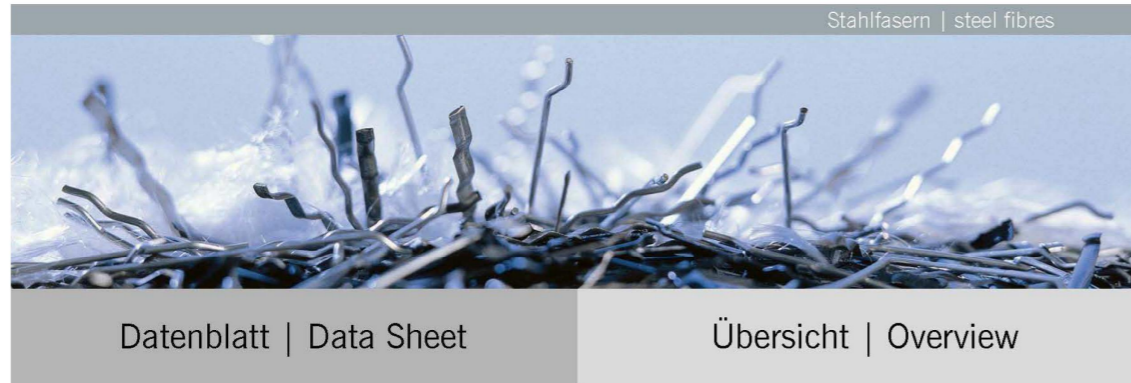
STANDARD VALUES FOR DIFFERENT CONCRETE CLASSES FOR USE WITH EUROCODE 2

28 Days-Compressive Strength (MPa)						
Concrete Class (cyl/cube)	Cylinder (150 mm dia, 300 mm height)			Cube 150 mm		
	Minimum Characteristic Compressive Strength (Fck)	Average Compressive Strength (Fcm)	Any Single Minimum Compressive strength Test Result (Fci)	Minimum Characteristic Compressive Strength (Fck)	Average Compressive Strength (Fcm)	Any Single Minimum Compressive strength Test Result (Fci)
C8/10	8	12	4	10	14	6
C12/15	12	16	8	15	19	11
C16/20	16	20	12	20	24	16
C20/25	20	24	16	25	29	21
C25/30	25	29	21	30	34	26
C30/37	30	34	26	37	41	33
C35/45	35	39	31	45	49	41
C40/50	40	44	36	50	54	46

Mix designation	C12/16	C16/20	C20/25	C25/30	C30/37	C35/45	C40/50	C45/55	C50/60	C55/67	C60/75	C70/85	C80/95	C90/105
Characteristic cylinder strength f_{ck}	12	16	20	25	30	35	40	45	50	55	60	70	80	90
Target mean cylinder strength f_{cm}	20	24	28	33	38	43	48	53	58	63	68	78	88	98
Characteristic cube strength $f_{ck,cube}$	16	20	25	30	37	45	50	55	60	67	75	85	95	105
Target mean cube strength $f_{cm,cube}$	26	30	35	40	47	55	60	65	70	77	85	95	105	115



D.3– STEEL WIRE FIBRES WITH HOOKED ENDS - KrampeHarex



Datenblatt | Data Sheet

Übersicht | Overview

KrampeHarex® Stahldrahtfaser mit Endverankerung | steel wire fibre with hooked ends

Bei der Herstellung von Drahtfasern werden Drähte verschiedener Durchmesser und Festigkeiten, je nach gewünschtem Stahlfasertyp, durch zwei gegenläufige Walzen geführt. Hierbei werden je nach verwendetem Segment auf den Walzen die Drähte in ihre spezielle Form gebogen und auf Länge geschnitten. KrampeHarex Stahldrahtfasern werden standardmäßig in 30 mm, 45 mm, 50 mm und 60 mm Länge hergestellt. Die Drahtdurchmesser liegen zwischen 0,5 mm und 1,2 mm. Zur Verankerung in der Betonmatrix besitzen sie entweder Endhaken oder sind über die gesamte Länge gewellt. Die Wahl der jeweiligen Fasertypen wird durch den Anwendungsfall bestimmt. Es gilt jedoch je länger und dünner Drahtfasern sind, desto schwerer sind sie zu dosieren und zu verarbeiten. Da Schlankheiten (Länge/Durchmesser) von mehr als 60 nur mit zusätzlichen Maßnahmen, wie zum Beispiel Einblasgeräten zu dosieren sind, haben sich im üblichen Industriebodenbau und Wohnungsbau die Fasertypen DE 50/1,0 N und DE 60/1,0 N bewährt. Bei höheren Betongütern müssen auch die Festigkeiten der Stahlfasern erhöht werden. Hier können mittelfeste (z.B. DE 60/1,0 M) oder hochfeste Fasern eingesetzt werden (z.B. DE 60/1,0 H) werden. Drahtfasern sind in der Lage Risse zu überbrücken und so Kräfte von Rissufer zu Rissufer zu übertragen. Der Stahlfaserbeton mit Drahtfasern ist duktil und kann im gerissenen Zustand noch Kräfte aufnehmen.



For manufacturing wire fibres, wires of different diameters and strengths according to the desired type of steel fibre are passed through two rollers working in opposite direction. Depending on the segment used on the rollers, the wires are bent to their specific form and cut to length in the course of this operation. KrampeHarex steel wire fibres are normally manufactured in lengths of 30 mm, 45 mm, 50 mm and 60 mm. The wire diameters range from 0,5 mm to 1,2 mm. For anchorage in the concrete matrix, they either possess hooked ends or are corrugated over the whole length. The selection of the respective type of fibre depends on the case of application. However, the longer and thinner the wire fibres, the more difficult they are to be dosed and worked. As aspect ratios (length/diameter) over 60 may only be dosed by means of additional measures, such as injection devices, the fibre types DE 50/1,0 N and DE 60/1,0 N have proved successful in conventional industrial flooring and house building. When using superior concrete grades, also the strengths of the steel fibres should be increased. In this case, fibres of medium strength (e.g. DE 60/1,0 M) or high strength (e.g. DE 60/1,0 H) may be used. Wire fibres are able to bridge cracks, and thus to transmit forces from one crack edge to the other. Concrete reinforced by wire fibres is characterised by ductility and may even accept forces after cracking.



KrampeHarex® GmbH & Co. KG · Pferdekamp 6-8 · 59075 Hamm · Germany
Phone +49 (0)23 81 · 977 977 · Fax +49 (0) 23 81 · 977 955 · www.krampeharex.com · info@krampeharex.com

KrampeHarex® CZ spol. s.r.o. · Osvobocení 234 · 664 81 Ostrovačice · Czech Republic
Phone +42 (0) 549 · 245 064 · Fax +42 (0) 0549 · 245 065 · www.krampeharex.cz · info@krampeharex.cz

KrampeHarex® Fibrin Gesellschaft mbH & Co. KG · Lindengasse 20 · 4040 Linz · Austria
Phone +43 (0) 732 731 011 · Fax +43 (0) 732 · 731 011 73 · www.krampefibrin.com · info@krampefibrin.com



Bezeichnung Name	Länge Length (mm)	Durchmesser Diameter (mm)	Querschnitt Cross section	Form Shape	Material Material	Werkstoff-Nr. Material-No.	Zugfestigkeit Tensile strength (N/mm ²)
DE 60/1,0 N	60 ±10%	1,00 ±10%	rund round		C7D	1.0313	1100 ±15%
DE 60/1,0 M					C9D	1.0304	1400 ±15%
DE 60/1,0 H					C38D	1.0516	2400 ±15%
DE 60/0,8 N	60 ±10%	0,80 ±10%	rund round		C7D	1.0313	1200 ±15%
DE 60/0,8 M					C9D	1.0304	1550 ±15%
DE 60/0,8 H					C38D	1.0516	2400 ±15%
DE 60/0,6 N	60 ±10%	0,60 ±10%	rund round		C7D	1.0313	1250 ±15%
DE 60/0,6 M					C9D	1.0304	1550 ±15%
DE 60/0,6 H					C38D	1.0516	2400 ±15%
DE 50/1,0 N	50 ±10%	1,00 ±10%	rund round		C7D	1.0313	1100 ±15%
DE 50/1,0 M					C9D	1.0304	1400 ±15%
DE 50/1,0 H					C38D	1.0516	2400 ±15%
DE 50/0,8 N	50 ±10%	0,80 ±10%	rund round		C7D	1.0313	1200 ±15%
DE 50/0,8 M					C9D	1.0304	1550 ±15%
DE 50/0,8 H					C38D	1.0516	2400 ±15%
DE 50/0,6 N	50 ±10%	0,60 ±10%	rund round		C7D	1.0313	1250 ±15%
DE 50/0,6 M					C9D	1.0304	1550 ±15%
DE 50/0,6 H					C38D	1.0516	2400 ±15%
DE 45/1,0 N	45 ±10%	1,00 ±10%	rund round		C7D	1.0313	1100 ±15%
DE 45/1,0 M					C9D	1.0304	1400 ±15%
DE 45/1,0 H					C38D	1.0516	2400 ±15%
DE 45/0,8 N	45 ±10%	0,80 ±10%	rund round		C7D	1.0313	1200 ±15%
DE 45/0,8 M					C9D	1.0304	1550 ±15%
DE 45/0,8 H					C38D	1.0516	2400 ±15%
DE 35/0,8 N	35 ±10%	0,80 ±10%	rund round		C7D	1.0313	1200 ±15%
DE 35/0,8 M					C9D	1.0304	1550 ±15%
DE 35/0,8 H					C38D	1.0516	2400 ±15%
DE 35/0,6 N	35 ±10%	0,60 ±10%	rund round		C7D	1.0313	1250 ±15%
DE 35/0,6 M					C9D	1.0304	1550 ±15%
DE 35/0,6 H					C38D	1.0516	2400 ±15%
DE 35/0,5 N	35 ±10%	0,50 ±10%	rund round		C7D	1.0313	1250 ±15%
DE 35/0,5 M					C9D	1.0304	1550 ±15%
DE 35/0,5 H					C38D	1.0516	2400 ±15%
DE 30/0,8 N	30 ±10%	0,80 ±10%	rund round		C7D	1.0313	1200 ±15%
DE 30/0,8 M					C9D	1.0304	1550 ±15%
DE 30/0,8 H					C38D	1.0516	2400 ±15%
DE 30/0,6 N	30 ±10%	0,60 ±10%	rund round		C7D	1.0313	1250 ±15%
DE 30/0,6 M					C9D	1.0304	1550 ±15%
DE 30/0,6 H					C38D	1.0516	2400 ±15%

KrampeHarex® GmbH & Co. KG · Pferdekamp 6-8 · 59075 Hamm · Germany
Phone +49 (0)23 81 · 977 977 · Fax +49 (0) 23 81 · 977 955 · www.krampeharex.com · info@krampeharex.com

KrampeHarex® CZ spol. s.r.o. · Osvobocení 234 · 664 81 Ostrovačice · Czech Republic
Phone +42 (0) 549 · 245 064 · Fax +42 (0) 0549 · 245 065 · www.krampeharex.cz · info@krampeharex.cz

KrampeHarex® Fibrin Gesellschaft mbH & Co. KG · Lindengasse 20 · 4040 Linz · Austria
Phone +43 (0) 732 731 011 · Fax +43 (0) 732 · 731 011 73 · www.krampefibrin.com · info@krampefibrin.com

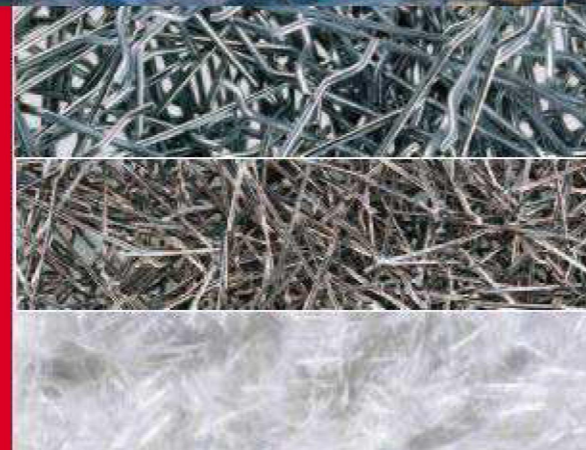


Stahlfasern steel fibres



KrampeHarex®-Fasern
für Spritzbeton

KrampeHarex® fibres
for shotcrete



Kleine Helfer – ganz groß
Great support from small fibres



KrampeHarex®-Fasern für den Stahlfaserspritzbeton ermöglichen vielfältige Anwendungen, auch unter schwierigsten Bedingungen. Im Nass- wie im Trockenspritzverfahren lassen sie sich mit handelsüblichen Spritzmaschinen verarbeiten. Gerade im Tunnelbau werden heute Stahlfasern verwendet, die dafür sorgen, dass der Beton selbst im gerissenen Zustand noch Zugspannung aufnehmen kann. Hier überzeugen die KrampeHarex®-Drahtfasern. Für geringere An-

forderungen stellen die KrampeHarex®-Kaltbandfasern die ideale, weil leicht zu verarbeitende und wirtschaftliche Lösung dar. Zur Verbesserung des Brandschutzverhaltens sind Kombinationen mit KrampeFibrin®-PP-Fasern empfehlenswert.

KrampeHarex® fibres for steel fibre shotcrete can be used in all kinds of ways and in the most difficult circumstances. They can be used in standard shotcrete machines, in both wet-mix and

dry-mix shotcrete. Nowadays, steel fibres are particularly used in tunnel construction, where they ensure that the concrete can still absorb tensile stress even when it has cracked. The performance of KrampeHarex® wire fibres is especially impressive here. For less demanding situations, KrampeHarex® slit steel fibres offer the ideal solution, because they are easy to work with and economical. To improve their behaviour in fire, it is recommended that they are combined with KrampeFibrin® PP-fibres.

Starke Typen für alle Fälle. The right strength for all situations.

<p>KrampeHarex® Drahtfasern KrampeHarex® wire fibres Typ. DE 25/0,5 N Typ. DE 30/0,5 N Typ. DE 30/0,6 N Typ. DE 30/0,8 N</p>	<p>KrampeHarex® Kaltbandfasern KrampeHarex® slit steel fibres Typ. KE 25/0,65 N Typ. KE 30/0,7 N</p>	<p>KrampeFibrin® Kunststofffasern KrampeHarex® polypropylene fibres Typ. PM Typ. PF</p>
<p>Höchste Leistungsfähigkeit für hohe technische Anforderungen. The ultimate performance in the toughest technical conditions.</p>	<p>Leicht und schnell verarbeitet – für durchschnittliche Anforderungen. Quick and easy to use – for average conditions.</p>	<p>Zur Verbesserung des Brandschutzes und zur Vermeidung von Schwindrisiken. To improve fire protection and avoid shrinkage cracks.</p>

Vielfältiger Einsatz Many different uses

- Vorübergehende Sicherung
Temporary scouring
- Endgültiger Ausbau
Final lining
- Baugrubenerbau
Lining foundation trenches

Technische Vorteile Technical benefits

- Besseres Verformungsverhalten
Better deformation behaviour
- Erhöhung der Biegezug- und Spaltzugfestigkeit
Increased bending and splitting tensile strength
- Homogene Stahlfaserverstärkung über die gesamte Querschnittsfläche
Uniform steel fibre reinforcement over the whole sectional surface
- Keine Spritzschatten
No spraying shadow

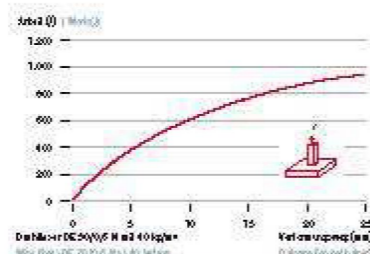
Wirtschaftliches Plus Economic benefits

- Verzicht auf aufwändige Bewehrungsarbeiten
No need for time-consuming reinforcement work
- Betoneinreparatur
Saves concrete
- Weniger Felsabbruch
Less rock breakthrough
- Bauzeitverkürzung
Shorter construction times

Überdurchschnittliche Ergebnisse
Ausgeszeichneter Nachbruch- und Verformungsverhalten dokumentieren die Plattenprüfungen nach Schweizer Richtlinie (SN 352) und Prüfungen an Biegebalken nach dem DBV Merkblatt.

Above average results:
Excellent post-failure and deformation behaviour was demonstrated in slab testing under Swiss guidelines (SN 352) and testing on a bending beam in accordance with the DBV information sheet.

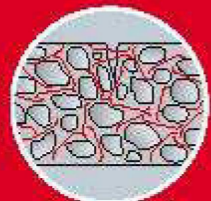
Plattenbiegeversuch gemäß SNCF:
SNCF slab bending test



Lastverformungskurve gemäß Merkblatt des DBV:
Load deformation curve in accordance with the relevant information sheet of the (DBV)



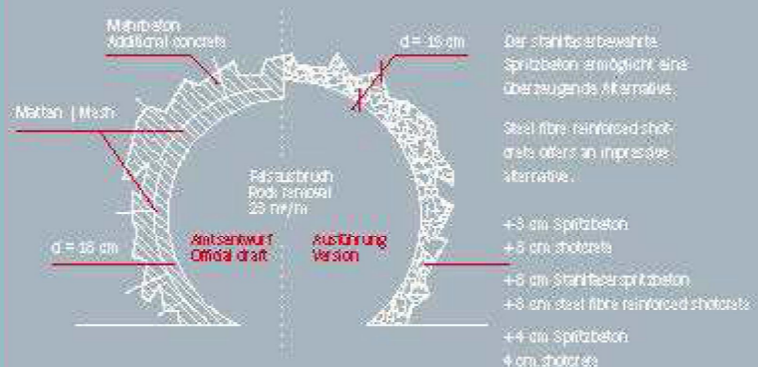
Überzeugend. Impressive.



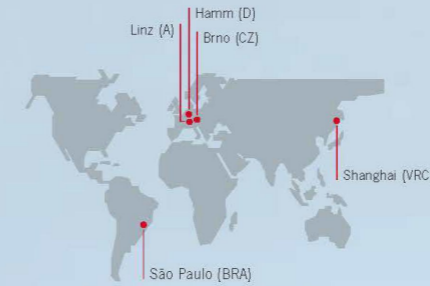
Mit Hilfe der Endhaken „verriegelt“ die Stahlfaser den Riss.

The steel fibre has hooked ends to “stitch up” the cracks.

Sicherheit in nur 1 Arbeitsgang. Safety in a single operation.



Stahlfasern steel fibres



KrampeHarex® entwickelt, produziert und vertreibt Stahlfasern für die unterschiedlichsten Aufgaben und Erfordernisse der Bauindustrie. Höchste internationale Qualitätsstandards, bester Service und die kontinuierliche Erprobung und Weiterentwicklung der gesamten Produktpalette haben bis heute Auftraggeber aus mehr als 40 Nationen und allen Bereichen des Hoch-, Tief- und Ingenieurbaus überzeugt.

KrampeHarex® develops, produces and sells steel fibres for all kinds of jobs and requirements in the construction industry. Extremely high international quality standards, excellent service and continuous testing and development of the entire product range have already convinced customers from over 40 countries and all fields of structural and civil engineering of our capabilities.



Hochwertiges Rohmaterial, eigen- und fremdüberwachte Fertigung
High-quality raw material, self-monitored and externally-monitored production

Zugelassene Produkte
Approved products

Qualifizierte Beratung
Qualified advice

Statische Bemessung
Static dimensioning

Kontinuierliche Prüfung und Forschung
Continuous testing and research

KrampeHarex® GmbH & Co. KG · Pferdemark 6-8 · 59075 Hamm · Germany
Phone +49 (0) 23 81. 977 977 · Fax +49 (0) 23 81. 977 955 · www.krampeharex.com · info@krampeharex.com

KrampeHarex® CZ s.r.o. · Blatného 12 · 61600 Brno · Czech Republic
Phone +42 (0) 541. 247 773 · Fax +42 (0) 541. 247 817 · www.krampeharex.cz · info@krampeharex.cz

KrampeHarex® FIBRIN Gesellschaft mbH · Lindengasse 20 · 4040 Linz · Austria
Phone +43 (0) 732. 731 011 · Fax +43 (0) 732. 731 011 73 · www.krampefibrin.com · info@krampefibrin.com

APPENDIX E – UNITS CONVERSION TABLE

1 inch. =	25.4 mm.	1 KIP =	10 ³ lbs.	1 kPa =	10 ³ N/m ²
1 inch. =	2.54 cm.	1 KIP =	4.4484 kN	1 kPa =	20.885 lbs./ft ² (psf)
1 inch. =	0.0254 m.	1 lb. =	4.4484 N	1 MPa =	10 ⁶ Pa = 10 ³ KPa = 1000 KPa
1 inch, =	0.0833 ft.	1 lb. =	0.0044484 kN	1 MPa =	1 N/mm ² = 145.18 psi
1 ft. =	12 inch.	1 N/m =	0.06852 lbs./ft. (plf)	1 MPa =	1,000 kN/m ²
1 ft. =	0.3048 m.	1 kN/m =	68.519 lbs./ft. (plf)	1 GPa =	10 ³ MPa = 145.18 ksi
1 ft. =	30.48 cm.	1 kN/m =	5.71 lbs./inch. (pli)	1 KSI =	1 kip/in ² (ksi) = 10 ³ psi
1 ft. =	0.3333 Yd.	1 lb./ft. =	14.595 N/m = 0.01459 kN/m	1 KSI =	6.895x10 ³ KPa = 6.895 MPa
1 m. =	1000 mm.	1 lb./inch =	1 pli	1 lbs./in ² =	6.895x10 ⁻³ N/mm ²
1 m. =	3.28084 ft.	1 lb./inch =	17.86 kg/m = 0.01786 ton/m	1 lbs./in ² =	6.895 kN/ m ² = 6,895 N/m ²
1 m. =	39.37008 inch.	1 lb./inch =	0.17513 N/mm.	1 lbs./in ² =	1 PSI = 1 psi
1 cm. =	0.032808 ft.	1 pli =	1 lb./inch	1 psi =	1 PSI = 1 lbs./in ²
1 mm. =	0.03937 inch.	1 kg./m =	9.809 N/m.	1 psi =	1 lbs./in ² = 1 psi
1 Yd. =	3 ft.	1 kg./m =	9.809x10 ⁻³ N/mm.	1 psi =	6.895 KPa = 6.895 kN/m ²
1 Yd ² =	9 ft ²	1 MPa =	1,000 kN/m ²	1 psi =	144 PSF
1 ft ² =	0.1111 Yd ²	1 Pa =	1 N/m ²	1 psf =	1 psf = 1 lbs./ft ²
1 m ² =	10.76391 ft ²	1 N/m ² =	1 Pa	1 lbs./ft ² =	47.882 N/m ²
1 kg. =	2.20462 lbs.	1 N/m ² =	10 ⁻⁶ N/mm ²	1 kg/cm ² =	14.223 lbs./in ² (psi)
1 kg. =	9.809 N	1 N/m ² =	0.020885 lbs./ft ² (psf)	1 kg/cm ² =	2,048.21 lbs./ft ² (psf)
1 TON =	10 ³ kg.	1 N/mm ² =	10 ⁶ N/m ² = 10 ³ kN/m ²	1 ton/m ³ =	62.43 lbs./ft ³ (pcf)
1 TON =	9.809 kN	1 N/mm ² =	1 MPa = 1,000 kN/m ²	1 oz./Yd ² =	0.007 lbs./ft ² (psf)
1 lb. =	0.45359 kg. = 453.592 gr.	1 N/mm ² =	145.03 lbs./in ² (psi)	1 g =	9.80665 m/s ²
1 oz. =	0.0625 lbs.	1 kN/m ² =	1 kPa = 0.001 N/mm ²	1 m/s =	2.232 mph
1 N =	0.2248 lbs.	1 kN/m ² =	20.885 lbs./ft ² (psf)	1 km/h =	0.62 mph
1 N =	0.1019 kg.	1 kN/m ² =	0.14518 lbs./in ² (psi)	1 mph =	0.448 m/s
1 kN =	224.8 lbs.	1 kN/m ² =	0.001 MPa = 10 ⁻³ MPa	1 lb./in ³ =	1,728 lb./ft ³
1 kN =	0.2248 Kips	1 kPa =	1 kN/m ² = 0.14518 psi	1 lb./in ³ =	27,680 kg./m ³
1 kN =	10 ³ N	1 kPa =	10 ³ Pa = 1 KN/m ²		
1kN =	101.9368 kg,	1 kPa =	0.145 lbs./in ² (psi)		

The Unit Conversion Values tabulated above can be useful to the reader, the values are provided as a guideline and are expected to be checked for accuracy before using or implementing them in real projects. The Author has made a good faith effort to calculate the values but does not guarantee the complete accuracy of each one of them. The reader is encouraged to double check them before using those values in actual and real projects.

